University of Nottingham
UK | CHINA | MALAYSIA

Numerical simulation of random Dirac operators

Thesis submitted to the University of Nottingham for the degree of

Doctor of Philosophy, March 2022.

Mauro D'Arcangelo
14302771

Supervised by

John W. Barrett
Sven Gnutzmann

Signature _____

Date _____ / _____ / _____

Abstract

A Euclidean path integral over matrix Dirac operators associated to fuzzy spaces is investigated using analytical and numerical tools of random matrix theory. A numerical library for handling Monte Carlo integration of fuzzy Dirac operators is written and tested. The random matrix theory arising from the simplest class of fuzzy Dirac operators is solved exactly using the theory of Riemann-Hilbert problems, and the results are confirmed numerically. For higher classes of Dirac operators, where integration is extended over many Hermitian matrices, various local minima of the action are found by solving the equations of motion. Among others, $su(2)$ solutions are shown to exist, and strong evidence is given of their realization in the asymptotic regime of the random model. Numerical data is collected in the vicinity of phase transitions occurring in various models, and it is shown how in certain cases they can be interpreted as transitions between a commutative and a non-commutative regime. Finally, a link is established between the action of fuzzy Dirac operators and Yang-Mills matrix models.

Acknowledgements

First and foremost I would like to thank my supervisor, John Barrett, for introducing me to non-commutative geometry, for his continued guidance, and for enabling me to explore the subject freely.
I would also like to thank my second supervisor, Sven Gnutzmann, for his mentorship on everything related to random matrix theory, which makes up most of the content of this thesis.
Special thanks go to L Glaser for encouraging me and being always available to exchange ideas and results, and to Denjoe O'Connor for the highest ratio of useful comments to total number of interactions.

There are two places in Nottingham that I would like to mention. The David Ross Sports Village for hosting my first awkward attempts at bouldering, and Portland Coffee Co for acting as my de facto office.

To the friends I have made along the way I want to say that although we were always meant to scatter across the globe eventually, the moments we shared are still close to my heart.
To my friends and family back home I want to say thank you for making a long distance feel shorter whenever I needed it to.

The completion of this thesis took place in dire times, times that cast a shadow on our future. For this reason I wish to dedicate this work to my nieces and nephew. May you grow up as free as I was to chase your dreams and find your way.

Contents

Introduction

The primary focus of this thesis is the numerical simulation of certain random matrix models arising from the Dirac operators of fuzzy spaces.
Fuzzy spaces are physically-motivated objects rooted in Alain Connes' theory of non-commutative geometry [1]. The general idea behind fuzzy spaces is that, just as non-commutativity between position and momentum marks the separation between classical and quantum mechanics, extending non-commutativity to space-time itself might help achieving a fundamental theory of quantum gravity that has general relativity as its commutative limit.
The details of the mathematical structure of fuzzy spaces and the applications of non-commutative geometry to physics are left for Chapter 1. To help the discussion one could take a physics-agnostic approach at first and regard the study just as a collection of random multi-matrix models.
Following this philosophy, consider a random matrix model for a Hermitian finite-dimensional operator D, called Dirac operator, defined by the partition function:

$$Z \propto \int e^{-S[D]}\, dD \tag{1}$$

where $S[D]$ is an action functional of D. Throughout this thesis, $S[D]$ is taken to be:

$$S[D] = \operatorname{Tr} D^4 + g_2 \operatorname{Tr} D^2 \tag{2}$$

for $g_2 < 0$. If D were a free, unconstrained Hermitian matrix, an exact solution to the model would be already available in the famous work by Brezin, Itzykson, Parisi and Zuber [2]. Importantly however, D has a very precise structure (to be specified later on) in terms of a certain number of arbitrary Hermitian submatrices that will be collectively denoted $\{M_i\}$. The exact number of these free submatrices depends on a choice of integer pair (p, q), which in the rest of this thesis will serve as a proxy for referring to the various models object of study.
The partition function can then be rewritten as:

$$Z \propto \int e^{-S[M_i]} \prod_i dM_i \tag{3}$$

where dM_i this time is the usual measure on Hermitian matrices:

$$dM_i = \prod_{a<b} d\operatorname{Re}(M_i)_{ab}\; d\operatorname{Im}(M_i)_{ab} \prod_a d\operatorname{Re}(M_i)_{aa} \tag{4}$$

and $S[M_i]$ is in general a double-trace potential with quadratic and quartic terms:

$$S[M_i] = \sum_{i,j,k,l} \Big[a \,\mathrm{Tr}\, M_i M_j M_k M_l + b(\mathrm{Tr}\, M_i)(\mathrm{Tr}\, M_j M_k M_l) + c(\mathrm{Tr}\, M_i M_j)(\mathrm{Tr}\, M_k M_l) \Big] + g_2 \sum_i \Big[d \,\mathrm{Tr}\, M_i M_i + e(\mathrm{Tr}\, M_i)(\mathrm{Tr}\, M_i) \Big] \tag{5}$$

for some constants a, b, c, d, e.
To the author's knowledge there is no literature to date for solving these models exactly, except for the simplest ones with $(p, q) = (1, 0)$ and $(0, 1)$. With D (and hence M_i) being finite-dimensional, however, numerical integration using Markov chain Monte Carlo is possible. Given an observable $f(D)$, the aim of the program is to calculate numerically expectation values of the form:

$$\langle f \rangle = \frac{1}{Z} \int f(D) e^{-S[D]} \, dD \tag{6}$$

via their Monte Carlo estimate:

$$\langle f \rangle = \frac{1}{Z} \int f(D) e^{-S[D]} \, dD \approx \frac{1}{N} \sum_{i=1}^{N} f(D_i) \tag{7}$$

where D_i are Dirac operators sampled from the measure:

$$\frac{1}{Z} e^{-S[D]} \, dD. \tag{8}$$

This should be seen as the simplest way to define a Euclidean path integral over fuzzy spaces and study them non-perturbatively. Approaches to quantum gravity involving numerical integration over fluctuating geometries have been attempted before: notable examples are causal dynamical triangulations [3] [4] and causal sets [5] [6]. The idea to do so for fuzzy spaces is more recent and only a few such studies are available at the moment of writing. A brief overview of them is presented next.

Previous art

The idea to define a Euclidean path integral for fuzzy Dirac operators was put forward by Barrett and Glaser in [7], where the first such numerical study appears. The authors start from the axiomatic classification of type (p, q) Dirac operators introduced in [8] to properly define a random matrix model based on fuzzy Dirac operators. They observe that the Connes-Chamseddine spectral action (see Chapter 1) is not suited for the model because the eigenvalues would just drift off to infinity, and propose to explore a different action given by the trace of even powers of the Dirac operator. The first and simplest choice for the action is:

$$S[D] = \mathrm{Tr}\, D^2 \tag{9}$$

where the eigenvalues feel a parabolic potential. The eigenvalue density of the $(1, 0)$ and $(0, 1)$ Dirac operators, which are random matrix models involving just

one Hermitian matrix, is solved for analytically, and the results are confirmed by Metropolis Monte Carlo simulations. Higher types of Dirac operators give rise to multi-matrix models, and even though all the matrices are decoupled from each other and follow a Wigner semicircle law [9], the eigenvalue density of the Dirac operator could not be solved for exactly. The obstruction to that can be seen from the related problem that, given the eigenvalues of two Hermitian matrices, only a certain set of inequalities in known for their sum [10]. Monte Carlo simulations therefore remain the only tool available for the study of higher types even for the simple quadratic potential. However, the quadratic potential alone does not appear to be rich enough for the Dirac operators to display some Weyl-law-like eigenvalue growth [11].
The more interesting case is when a quartic term is included:

$$S[D] = \operatorname{Tr} D^4 + g_2 \operatorname{Tr} D^2 \tag{10}$$

and the coupling g_2 is negative. The potential then has a symmetry-breaking shape and all the matrices interact non-trivially in fourth order terms. A phase transition is observed in some of the models, and the spectrum of the Dirac operator at the phase transition is compared with that of a fuzzy sphere highlighting their similarity. The paper focuses mostly on the spectrum of the Dirac operator as a whole, which is the object that carries physical information and therefore the natural place where physical intuition can guide the exploration. However, the trace part of some of the submatrices is already identified as the relevant order parameter for the transitions.
Subsequent work [12] looked in more detail at the $(1,1)$, $(2,0)$ and $(1,3)$ models, with more precise Monte Carlo data. The $(2,0)$ model is the simplest one with a very prominent phase transition, and for that reason it is a good starting point for understanding higher types, while the $(1,3)$ model has an intriguing combination of features: the random model displays a phase transition, and it is the natural host for a fuzzy sphere of (KO-)dimension 2. Evidence is collected that the phase transitions are at least second order for matrices of size up to 10×10.
One of the key observations of the original study was that, by analogy with the spectrum of commutative Dirac operators, random fuzzy models around phase transitions might acquire some manifold-like properties. The reason has to do with the particular scaling of the eigenvalues, whose growth encodes information about the dimension of the space. This line of thought is pursued in [13], where tools are developed to make sense of the usual notions of dimension and volume in the case of fuzzy spaces. The spectral variance is introduced, a variation of the concept of spectral dimension [14]. The spectral variance is an energy-dependent measure of the dimension of a space, and it is shown to give reasonable estimates of the dimension of the fuzzy sphere and fuzzy torus [15].
Alongside these numerical studies, the first fully analytical treatment of the simplest Dirac operator in the quadratic plus quartic potential appeared in the work of Khalkhali and Pagliaroli [16]. Using the theory outlined in [17], the authors are able to solve for the density of states of the $(1,0)$ and $(0,1)$ Dirac operators. The method, which will be described in detail in Chapter 4, casts the problem of finding the equilibrium measure of a random matrix model into solving a Riemann-Hilbert problem. The theory is generalized to the interacting potential of the quartic ac-

tion by supplementing the treatment with a saddle point calculation. Ultimately, the $(1,0)$ and $(0,1)$ Dirac operators are shown to behave identically, including undergoing a phase transition at $g_2 = -5\sqrt{2}/2$. The resulting eigenvalue densities are plotted for various values of the coupling constant, but a numerical study to support the calculation is not provided.

Structure of the thesis

The objective of this thesis is to develop numerical tools to perform Markov chain Monte Carlo simulations of fuzzy spaces systematically and efficiently. A wide range of models is studied, and random matrix theoretical methods are used whenever possible to predict or analyze the results. Much emphasis is put on the submatrices M_i rather than the Dirac operator. Most parts should be generally accessible to the random matrix theory community, as the physical background is not necessary to follow the discussion, but the findings are hopefully of some interest in numerical quantum gravity. Chapters 3 to 6 are original contributions, as well as the second half of Chapter 2.
What follows is a summary of the content of each chapter.

Chapter 1: Non-commutative Geometry

The first part of Chapter 1 briefly sketches the historical development of non-commutative geometry and its application to the action of the standard model. Some technical details are given when necessary, but a more detailed overview of the subject would be outside the scope of this work. Most of the material is taken from the comprehensive book by Walter van Suijlekom [18], the original spectral action paper by Alain Connes and Ali Chamseddine [19], and the review by Daniel Kastler [20]. See also [21], written in anticipation of the spectral action paper, [22] for the inclusion of neutrinos, and [23] for a modern treatment in the context of quantum field theory.
The second half of the chapter is devoted to the definition of fuzzy spaces in terms of finite real spectral triples as in [8]. The discussion is aimed at giving the general form of a type (p,q) fuzzy Dirac operator, which is the central object of this thesis. Every subsequent piece of calculation can be traced back to equation (1.15), which should be kept in mind at all times.

Chapter 2: Markov chain Monte Carlo

Chapter 2 gives an introduction to Markov chains and the ergodic theorem. Markov chains are the pillars on which most of the literature in importance sampling Monte Carlo integration is based, spanning from classical subjects such as non-perturbative quantum field theory [24] and random matrix models [25], all the way to modern quantum gravity proposals. The discussion follows closely [26], which was chosen for its clarity of exposition.
The two relevant Markov chain Monte Carlo algorithms for this thesis, Metropolis [27] [28] and Hamiltonian [29] Monte Carlo, are first described in general terms and then adapted to the special case of fuzzy spaces in the second part of the chapter.

For Metropolis this involves working out formulas for action differences of the type $S[D]-S[D']$, where D and D' are Dirac operators that differ by a single matrix entry. Hamiltonian Monte Carlo instead requires a formula for calculating the whole action, i.e. powers of traces of the Dirac operator, and for matrix derivatives of the action.
Terms in the action higher than quadratic order couple together all the degrees of freedom of the Dirac operator, making the calculation non-trivial. Formulas for actions with terms of order higher than four are not worked out explicitly, but a general procedure for doing so is outlined.

Chapter 3: The RFL library

RFL (Random Fuzzy Library), an open source C++ library, was written in order to facilitate the process of collecting Monte Carlo data for fuzzy Dirac operators. It collects tools to automatically generate (p, q) Clifford modules and Dirac operators, and all the Monte Carlo formulas mentioned in the previous chapter.
Chapter 3 introduces the library with small code samples to showcase its functionalities and a description of some algorithmic choices that were made. Hopefully, researchers interested in pursuing this line of research in the future will find it a useful guide.
As the complexity of a library increases it becomes harder and harder to avoid bugs in the code. However, unit tests can be designed to ensure that the numerics respect certain theoretical expectations and consequently minimize the risk of unwanted behavior. The results of such tests are reported in the second half of the chapter, the most important being sanity checks regarding the calculation of the action, action difference, and error scaling in Hamiltonian integration.

Chapter 4: One-matrix models

Type $(1, 0)$ and $(0, 1)$ fuzzy Dirac operators involve a single Hermitian matrix, but the random matrix theory they give rise to is not a simple one and it had not been studied analytically until very recently, when Khalkhali and Pagliaroli [16] found a clever way of solving the models exactly using the theory of Riemann-Hilbert problems [17].
In Chapter 4 Monte Carlo simulations of the models are performed in order to check the agreement with the expected theoretical results. Although RFL is capable of handling these models, it would have introduced a certain avoidable overhead which is the price to pay for its generality. For this reason, a simpler Metropolis code was written specifically for this study.
The Monte Carlo simulations are shown to be in disagreement with the results of [16], more so for the $(1, 0)$ model than the $(0, 1)$. The rest of the chapter is dedicated to the reconciliation of theory and numerics, which are then shown to agree to an excellent extent.

Chapter 5: Two-matrix models

Dirac operators with $p + q = 2$ are studied in Chapter 5. These give rise to two-matrix models for which an exact analytical solution is not known, nor is

a general way of achieving it. The leading contribution to solutions with large negative coupling constant, however, can be found with a relatively straightforward stationary analysis. Imposing that first order variations of the action vanish results in a system of scalar and matrix equations that can be solved in particular cases. All solutions to the stationary equations involving involutory matrices are classified in the first part of the chapter, and they are shown to be enough to explain the Monte Carlo data of the $(0, 2)$ and $(1, 1)$ models. The remaining $(2, 0)$ model is then analyzed more in detail, as the data suggests that the stationary solutions alone do not account for the full picture.
The first interesting feature of the $(2, 0)$ model is the presence of a phase transition. What is even more striking, however, is that a secondary phase transition sprouts from the first one for large enough matrices. Arguments are then given for the order of the two phase transitions, and a finite-size scaling analysis is attempted.

Chapter 6: Four-matrix models

A step further in complexity, the four distinct four-matrix models coming from Dirac operators with $p + q = 3$ are the subject Chapter 6. Finding exact solutions does not get any easier in this case, and therefore a stationary equation analysis is once again the only tool available.
These models have an incredibly rich landscape of stationary solutions. Some simple scalar solutions are found, as well as solutions involving involutory commuting matrices. The most interesting aspect, however, is the existence of solutions where the free matrices arrange themselves into n-dimensional irreducible representations of $su(2)$, a property shared by the Dirac operator of a fuzzy sphere.
Numerical data is shown for all four models, and the $(0, 3)$ and $(3, 0)$ types are then analysed in more detail. The $(0, 3)$ model is simulated up to very large negative values of the coupling constant, where it shows clear signs of being in a $su(2)$ phase. The $(3, 0)$ model instead undergoes a phase transition which is marked by scalar and matrix variables trading importance. Arguments are given for the order of the transition and a finite-size scaling analysis is attempted.

Chapter 7: Miscellaneous topics

Chapter 7 deals with more speculative matters: ideas that were not explored in detail but have the potential to become future lines of research.
A connection between the action of fuzzy Dirac operators and the action of Yang-Mills matrix models is discussed, bridging the gap between two apparently unrelated matrix models for quantum gravity.
The concept of dual pair is introduced, which captures the way a Dirac operator with fewer degrees of freedom can help understand the behavior of a more complex one. This is related to the way the asymptotics of the $(0, 2)$ and $(0, 3)$ give information on the small g_2 behavior of the $(2, 0)$ and $(3, 0)$ respectively. The idea is then applied to the $(3, 1)$ and $(1, 3)$ models, which are shown to fit the description of a dual pair at least partially.

Chapter 1

Non-Commutative Geometry

1.1 Early days of non-commutative geometry

The birth and development of non-commutative geometry was strongly influenced by the standard model of particle physics. The critical observation was that the information on the geodesic distance between two points on a manifold is entirely contained in a differential operator D. This differential operator is a generalization of the $\not{\partial} = \gamma^\mu \partial_\mu$ that appears in the Dirac equation for relativistic fermions, and it is therefore known today as the Dirac operator.
More precisely, given a Riemannian spin manifold M with Dirac operator D_M, the distance between two points x and y is given by:

$$d(x,y) = \sup_{a \in C^\infty(M)} \Big[|a(x) - a(y)| : \ ||[D_M, a]|| \leq 1 \Big].$$

Another intriguing fact is that the dimensionality of the manifold is recovered from the asymptotic growth of the eigenvalues of D_M.
Looking at D_M in local coordinates

$$D_M = -i\gamma^\mu \left(\partial_\mu - \frac{1}{4} \Gamma^b_{\mu a} \gamma^a \gamma_b \right)$$

one can see that many common objects of differential geometry are involved in the structure of a Dirac operator on a manifold. A standard way to build D_M given a manifold is to define the Levi-Civita connection, lift it to a connection on the spinor bundle, and compose it with Clifford multiplication [18].
The focal point of non-commutative geometry is to abstract away the fundamental properties of a Dirac operator in order to build it from first principles rather than known differential-geometric constructs. The axiomatization of Dirac operators on manifolds culminated in a reconstruction theorem [30] establishing a complete equivalence between compact Riemannian spin manifolds and an object known as a commutative spectral triple. A commutative spectral triple is composed of a commutative algebra $\mathcal{A}$, which is the algebra of smooth functions on the manifold, a Hilbert space $\mathcal{H}$ that carries a representation of $\mathcal{A}$, and a self-adjoint operator D in $\mathcal{H}$ that acts on the elements of $\mathcal{A}$ as a derivation.
This line of thought has proven extremely fruitful in that it allows a straightforward generalization (which actually predates the full reconstruction theorem)

with deep implications for the standard model. One can allow the algebra $\mathcal{A}$ to be non-commutative, thus defining a new kind of space that preserves all the usual geometric data encoded in the Dirac operator, but that has no analogue as a manifold. Moreover, the formalism easily accommodates composite objects formed by products of spectral triples. Nowadays, it is generally accepted that the geometric structure of the standard model of particle physics is to be understood within the non-commutative-geometric framework as an almost-commutative manifold: a product between an underlying (commutative) space-time manifold and a finite non-commutative internal space that gives rise to the whole Yang-Mills sector.
Historically the development of non-commutative geometry used the standard model itself as a guide rather than the familiar setting of commutative manifolds. Consider the following simple spectral triple:

$$\begin{aligned} \mathcal{A} &= \mathbb{C} \oplus \mathbb{C} \\ \mathcal{H} &= \mathbb{C}^n \oplus \mathbb{C}^n \\ D &= \begin{pmatrix} 0 & M^* \\ M & 0 \end{pmatrix} \end{aligned} \tag{1.1}$$

where M is a $n \times n$ matrix and an element $(u, v) \in \mathcal{A}$ acts in $\mathcal{H}$ as $\mathbb{1}u \otimes \mathbb{1}v$. One can write down a Yang-Mills-type action for the spectral triple which turns out to be $(|\phi|^2 - 1)^2$, where ϕ is a complex scalar. Recognizing this as the typical double well potential of the Higgs field opened up the possibility of deriving the bosonic sector of the standard model on geometrical grounds.
Indeed early attempts in this direction brought Connes and Lott to a prescription [31] where the full electroweak plus Higgs sector of the standard model was derived from the algebra $\mathbb{C} \oplus \mathbb{H}$, with $\mathbb{H}$ being the quaternions. The procedure, however, produced the wrong $U(1)$ hypercharges for the fermions. Rather remarkably, the problem was solved by appending the chromodynamics sector in the form of tensoring the previous electroweak algebra with $\mathbb{C} \oplus M_3(\mathbb{C})$ [20]. The Connes-Lott model already contained most of the ingredients of modern non-commutative geometry. A later addition was the introduction of a real structure J, an anti-linear operator that gives $\mathcal{H}$ the structure of a $\mathcal{A}$-bimodule. Physically, the real structure represents the charge conjugation operator.
Eventually, the Connes-Lott model would be superseded by a new prescription, giving jointly the standard model and general relativity: the spectral action principle.

1.2 The spectral action

The spectral action principle follows the time-honored tradition of deriving physical laws from symmetries. General relativity is built around the concept of invariance under coordinate transformations, or diffeomorphism invariance, while the standard model is defined by local invariance under the group $SU(3) \times SU(2) \times U(1)$. Insofar as a theory of particle physics on curved space-time is consistent, its group of invariance is the semi-direct product:

$$G = \mathcal{U} \rtimes \mathrm{Diff(M)} \tag{1.2}$$

where $\mathcal{U} = C^\infty(M, SU(3) \times SU(2) \times U(1))$. In the language of non-commutative geometry and spectral triples, these symmetries find a unified description in terms of algebra automorphisms $\mathrm{Aut}(\mathcal{A})$, which seamlessly encompass both diffeomorphism invariance and gauge invariance.
The way to obtain jointly gravitation and the standard model is reminiscent of a Kaluza-Klein theory. One takes the product between a commutative spectral triple (describing the underlying manifold) and a finite non-commutative internal space (that carries the Yang-Mills sector). This construction is called an almost-commutative manifold. For a suitable choice of the almost-commutative manifold, it is possible to write an action functional that depends on the spectrum of the Dirac operator and that matches exactly with the Einstein-Hilbert plus Yang-Mills action in a certain asymptotic limit. To better understand the construction it is first necessary to introduce the concept of gauge group of the spectral triple (with the related notion of inner automorphisms) and Morita self-equivalences.
The gauge group of the spectral triple is defined from the normal subgroup $\mathrm{Int}(\mathcal{A}) \subset \mathrm{Aut}(\mathcal{A})$ of inner automorphisms of the algebra, which are automorphisms α_u of the type $\alpha_u(a) = uau^*$, with $uu^* = u^*u = 1$. Under an inner automorphism, a Dirac operator D transforms as:

$$D \mapsto UDU^* \tag{1.3}$$

where $U = uJuJ^{-1}$ are identified with the elements of the gauge group. Inner automorphisms are a purely non-commuative feature, as they are trivial for commutative algebras. The correct internal non-commutative algebra whose inner automorphisms give the standard model gauge group is:

$$\mathcal{A}_F = \mathbb{C} \oplus \mathbb{H} \oplus M_3(\mathbb{C}) \tag{1.4}$$

although a further restriction on the sign of the determinant for the action of the gauge group in the Hilbert space (the unimodular condition) is necessary to get the $SU(3)$ part right. The algebra $\mathcal{A}$ of the almost-commutative manifold describing the standard model on curved space-time is then the tensor product between the algebra of smooth functions $\mathcal{A}_M$ and the finite internal algebra $\mathcal{A}_F$:

$$\mathcal{A} = \mathcal{A}_M \otimes \mathcal{A}_F = C^\infty(M) \otimes \big(\mathbb{C} \oplus \mathbb{H} \oplus M_3(\mathbb{C})\big). \tag{1.5}$$

From (1.3) one can introduce a notion of unitary equivalence between spectral triples, but in fact it proves useful to consider a generalization of this called Morita self-equivalence [18]. Under Morita self-equivalences, a Dirac operator D transforms as:

$$D \mapsto D_\omega = D + \omega + J\omega J^{-1} \tag{1.6}$$

where ω is of the form $\omega = \sum_i a_i[D, b_i]$, with $a_i, b_i \in \mathcal{A}$. This is a generalization of unitary equivalence because putting $\omega = u[D, u^*]$ gives back (1.3).
The spectral action principle requires the physical laws to be a spectral invariant, i.e. to depend only on the spectrum of the Dirac operator. In this sense unitary transformations of the type (1.3) describe the same physics. But the relevant Dirac operator is the more general D_ω of (1.6) obtained by perturbing D with Morita self-equivalences.
It is possible to write both bosonic and fermionic invariants. The simplest bosonic

invariant is the trace of some function of the Dirac operator:

$$S_b = \mathrm{Tr}\, f\left(\frac{D_\omega}{\Lambda}\right) \tag{1.7}$$

where Λ is a cutoff parameter that plays the role of a Planck's length. The first terms of the heath kernel expansion [32] of (1.7) give the Einstein-Hilbert action and the action for the Yang-Mills bosons [19], higher terms being suppressed as inverse powers of Λ. The bosons are identified with the inner perturbations of (1.6), hence the importance of taking into account Morita self-equivalences. The couplings between bosons and fermions are given instead by the following fermionic spectral invariant:

$$S_f = \langle J\psi, D_\omega \psi \rangle. \tag{1.8}$$

It should be noted that the action is written in the Euclidean, as the formalism makes use of a Hilbert space and therefore it does not accommodate indefinite inner products. See [33] for a construction that addresses this issue.
Arguably, getting to write (1.7) and (1.8) requires some rather sophisticated mathematical machinery whose main features were only just outlined here. What should be clear, however, is that it all follows from a few simple principles. This indicates that non-commutative geometry is at the very least close to the real mathematical structure governing high energy physics.

1.3 Finite real spectral triples and fuzzy spaces

Despite the remarkable success of non-commutative geometry in reproducing the action of the standard model and gravitation, the framework does not add fundamental new physics. It does imply some relations between the coupling constants (which led to a prediction, albeit inaccurate, of the Higgs' mass [34]) and it imposes restrictions on physics beyond the standard model, but field quantization is carried out only after the spectral action is unraveled, and the fundamental issues of quantized gravity are still present. As it often happens, however, looking at a problem from a different perspective might indicate the way forward.
A striking feature of the spectral triple of the almost-commutative manifold described above is the very different nature of the two tensored algebras: the infinite-dimensional algebra of smooth functions $\mathcal{A}_M$ on one side, and the finite internal algebra $\mathcal{A}_F$ on the other. A possibility worth exploring is to replace the functions on the manifold with a non-commutative analogue. Such spaces are generally referred to as fuzzy spaces, of which the fuzzy sphere is the most notable example [35]. The idea is that the almost-commutative manifold would emerge as an effective description when integrating out high energies in a purely non-commutative and finite theory.
The spectral triples associated to fuzzy spaces have been worked out in [8] from the axioms of non-commutative geometry. Fuzzy spaces are a particular case of the more general class of finite real spectral triples, whose definition is reported here.

Definition 1. A finite real spectral triple $(\mathcal{A}, \mathcal{H}, D; \Gamma, J)$ consists of:

1. An integer s modulo 8 called the KO-dimension

s	0	1	2	3	4	5	6	7
ϵ	1	1	-1	-1	-1	-1	1	1
ϵ'	1	-1	1	1	1	-1	1	1
ϵ''	1	1	-1	1	1	1	-1	1

Table 1.1: Signs appearing in the definition of a real spectral triple for each KO-dimension.

2. A finite dimensional Hilbert space $\mathcal{H}$
3. A $*$-algebra $\mathcal{A}$ over $\mathbb{R}$ with a faithful representation $(\mathcal{H}, \pi)$
4. A Hermitian operator $D : \mathcal{H} \to \mathcal{H}$ called the Dirac operator
5. A Hermitian operator $\Gamma : \mathcal{H} \to \mathcal{H}$ such that $\Gamma^2 = 1$ called the chirality operator
6. An anti-unitary operator $J : \mathcal{H} \to \mathcal{H}$ called the real structure

In addition, the above data must satisfy:

1. $\Gamma\pi(a) = \pi(a)\Gamma$ for all $a \in \mathcal{A}$
2. $D\Gamma = -\Gamma D$ if s is even, $D\Gamma = \Gamma D$ if s is odd
3. $J^2 = \epsilon, \;\; JD = \epsilon' DJ, \;\; J\Gamma = \epsilon''\Gamma J$ with $\epsilon, \epsilon', \epsilon''$ given in Table 1.1
4. $[\pi(a), J\pi(b)J^{-1}] = 0$ for all $a, b \in \mathcal{A}$
5. $[[D, \pi(a)], J\pi(b)J^{-1}] = 0$ for all $a, b \in \mathcal{A}$

This axiomatic structure imposes some restrictions on the general form a Dirac operator can take, but there is still considerable freedom in a finite real spectral triple. The specialization to fuzzy spaces is guided by the example of the fuzzy sphere, for which a Dirac operator was proposed in [36]. The two main requirements are for $\mathcal{A}$ to be an algebra of matrices, like $M_n(\mathbb{R})$, $M_n(\mathbb{C})$ or $M_{\frac{n}{2}}(\mathbb{H})$, and that there is the action of a Clifford algebra on spinors. The Hilbert space is then of the form $V \otimes M_n(\mathbb{C})$, where V is the spinor space and $\mathcal{A}$ acts as matrix multiplication in $M_n(\mathbb{C})$.
Clifford algebras, and in particular their representation in terms of gamma matrices, will be used extensively throughout. When an action will be built for fuzzy Dirac operators, its structure will be entirely determined by trivial products of gamma matrices (see Chapter 2, 5 and 6). Following the conventions of [8], consider a diagonal matrix η with p occurrences of $+1$ and q occurrences of -1 on the diagonal, and dimension $p + q$. A (p, q) Clifford module for η is a set of matrices $\gamma_1, \ldots, \gamma_{p+q}$ satisfying:

$$\gamma_a\gamma_b + \gamma_b\gamma_a = 2\eta_{ab}. \tag{1.9}$$

This implies that p gamma matrices square to $+1$, q gamma matrices square to -1, and different gamma matrices anti-commute with each other. The most common gamma matrices in the physics literature are the ones with $p + q = 4$ appearing in

the Dirac equation, where an extra matrix γ_5 is defined as the ordered product of γ_1 to γ_4. The equivalent of γ_5 for a general (p, q) Clifford module is the chirality operator γ, defined as:

$$\gamma = i^{\frac{s(s+1)}{2}} \gamma_1 \dots \gamma_{p+q} \tag{1.10}$$

where $s = (q - p) \mod 8$.
When $V \simeq \mathbb{C}^k$ as a vector space is equipped with the standard Hermitian inner product $(\cdot, \cdot)$, one can define a real structure for the Clifford Module as an anti-linear operator $C : V \to V$ such that:

1. $C^2 = \epsilon$
2. $(Cv, Cw) = (w, v)$
3. $C\gamma_a = \epsilon' \gamma_a C$

for the same signs ϵ, ϵ' of Table 1.1.
The stage is now set to give the formal definition of fuzzy space.

Definition 2. Consider a type (p, q) Clifford module V with chirality operator γ, Hermitian inner product $(\cdot, \cdot)$ and real structure C. A type (p, q) fuzzy space is a finite real spectral triple such that:

1. $s = (q - p) \mod 8$
2. $\mathcal{A} = M_n(\mathbb{R})$, $M_n(\mathbb{C})$ or $M_{\frac{n}{2}}(\mathbb{H})$
3. $\mathcal{H} = V \otimes M_n(\mathbb{C})$ with inner product $\langle v \otimes m, v' \otimes m' \rangle := (v, v') \operatorname{Tr} m^* m'$
4. $\pi(a)(v \otimes m) = v \otimes am$
5. $\Gamma(v \otimes m) = \gamma v \otimes m$
6. $J(v \otimes m) = Cv \otimes m^*$

Notice that the algebra acts naturally as matrix multiplication on the left. The right action is instead defined using the real structure:

$$(v \otimes m) \triangleleft a := J\pi(a)^* J^{-1}(v \otimes m) = v \otimes ma. \tag{1.11}$$

The axioms for a real spectral triple impose constraints on the form a fuzzy Dirac operator can take. In general the Dirac operator can be written as:

$$D = \theta + \epsilon' J\theta J^{-1} \tag{1.12}$$

with $\theta \in \operatorname{End}(V) \otimes \operatorname{End}(M_n(\mathbb{C}))$ of the form:

$$\theta = \sum_i \omega_i \otimes X_i \tag{1.13}$$

the ω_i being unordered odd products of gamma matrices. Using the commutation relations between C and the gamma matrices, it follows that D acts on the elements of $\mathcal{H}$ as:

$$D(v \otimes m) = \sum_i \omega_i v \otimes (X_i m + m X_i^*). \tag{1.14}$$

Since D is self-adjoint, ω_i and X_i are either both Hermitian or both anti-Hermitian. Therefore the Hermitian X_i act as anti-commutators, while the anti-Hermitian X_i act as commutators. The most general Dirac operator for a fuzzy space then can be written as:

$$D = \sum_i \alpha_i \otimes \{H_i, \cdot\} + \sum_j \tau_j \otimes [L_j, \cdot] \tag{1.15}$$

where α_i are Hermitian odd products of gamma matrices, τ_j are anti-Hermitian odd products of gamma matrices, H_i are Hermitian $n \times n$ matrices and L_j are anti-Hermitian $n \times n$ matrices.

Chapter 2

Markov chain Monte Carlo

2.1 Introduction

Markov chains are a powerful tool for sampling from arbitrarily complicated probability distributions.
The present work is concerned with the numerical study of random fuzzy spaces, which boils down to the calculation of expectation values of observables over ensembles of Dirac operators:

$$\langle f \rangle = \frac{1}{Z} \int f(D) e^{-S[D]} \, dD \tag{2.1}$$

where f is an observable, Z is a normalization constant such that $\langle 1 \rangle = 1$, dD is the Lebesgue measure on the vector space of Dirac operators, and $S[D]$ is an action functional. Throughout this work, the action will be taken to be:

$$S[D] = g_2 \operatorname{Tr} D^2 + \operatorname{Tr} D^4 \tag{2.2}$$

where $g_2 \in \mathbb{R}$ is a coupling constant. Markov chains enter the picture when (2.1) is replaced by its Monte Carlo estimate:

$$\langle f \rangle = \frac{1}{Z} \int f(D) e^{-S[D]} \, dD = \frac{1}{N} \sum_{i=1}^{N} f(D_i) + O\left(\frac{1}{\sqrt{N}}\right) \tag{2.3}$$

where D_i are Dirac operators sampled (using a Markov chain) from the measure:

$$\frac{1}{Z} e^{-S[D]} \, dD. \tag{2.4}$$

In this chapter a rapid overview of the general theory of Markov chains is presented, together with two notable Markov chain Monte Carlo algorithms and their implementation for fuzzy spaces.

2.2 General theory of Markov chains

In the language of Markov chains, we have a system that can be in one of many possible states E_k (Dirac operators in this case). At each step of the chain, the

system makes a transition from a state E_j to a state E_k with probability p_{jk}. If the initial state of the system is E_{k_0} with probability a_{k_0}, then to a chain $E_{k_0} \to E_{k_1} \to \ldots \to E_{k_n}$ one can associate the probability:

$$P(E_{k_0} \to E_{k_1} \to \ldots \to E_{k_n}) = a_{k_0}\ p_{k_0 k_1} \ldots p_{k_{n-1} k_n}. \tag{2.5}$$

This is a good definition of probability provided that:

1. $a_k \geq 0\ \forall k,\ \ p_{jk} \geq 0\ \forall j, k$;
2. $\sum_k a_k = 1$ (it is always possible to start in some state);
3. $\sum_k p_{jk} = 1\ \forall j$ (it is always possible to move from one state to some other state).

In order to state and interpret the main theorem on which the theory of Markov chains is based, it is useful to introduce the following notation:

1. the probability of making a transition from state E_j to state E_k in exactly n steps will be denoted $p_{jk}^{(n)}$;
2. the probability of the n-th state of the chain being E_k will be denoted $a_k^{(n)}$. Note that $a_k^{(n)} = \sum_j a_j p_{jk}^{(n)}$ and it does not depend on the initial state j.

The following two definitions are also required.

Definition 3. A Markov chain is called *irreducible* if every state can be reached from every other state, not necessarily in one step.

Definition 4. A state E_k is called *periodic* if it exists a positive integer $t > 1$ (the period) such that $p_{kk}^{(n)} = 0$ unless n is a multiple of t. The state is called *aperiodic* otherwise

The importance of Markov chains relies on the following theorem, a proof of which can be found in [26]:

Theorem 1. *Consider an irreducible and aperiodic Markov chain, defined by its transition probabilities p_{jk} and initial probabilities a_j. If there exist $u_k \geq 0$ such that $\sum_k u_k = 1$ and $u_k = \sum_j u_j p_{jk}\ \forall k$, then:*

$$u_k = \lim_{n \to \infty} p_{jk}^{(n)} \quad \forall k. \tag{2.6}$$

The set u_k forms a discrete probability distribution called the *invariant distribution*. The importance of this theorem comes from the following consideration. The probability of making a transition to a state E_k at the n-th step is $a_k^{(n)}$. But, according to (2.6):

$$a_k^{(n)} = \sum_j a_j p_{jk}^{(n)} \to \sum_j a_j u_k = u_k. \tag{2.7}$$

Therefore, for n large enough, the system will find itself in state E_k with probability u_k, regardless of the initial state of the chain.
In importance sampling the invariant distribution u_k is known (equation (2.4) in

this case), and suitable transition probabilities p_{jk} need to be chosen so that u_k is reached. The common strategy is to rewrite the condition $u_k = \sum_j u_j p_{jk}$ in the equivalent way:

$$\sum_j u_k p_{kj} = \sum_j u_j p_{jk} \quad \forall k \tag{2.8}$$

and satisfy a stronger version called detailed balance:

$$u_k p_{kj} = u_j p_{jk} \quad \forall j, k. \tag{2.9}$$

Now factorize the transition probabilities into a proposal part t_{jk} and an accept/reject part c_{jk}:

$$p_{jk} = t_{jk} c_{jk} \tag{2.10}$$

where t_{jk} is the probability of proposing a transition from E_j to E_k, and c_{jk} is the probability of accepting that transition. If the proposal probabilities are chosen such that $t_{jk} = t_{kj}$ (there is equal probability of proposing a transition and its inverse), then the t_{jk} cancel out in the detailed balance equation, which reads:

$$\frac{u_k}{u_j} = \frac{c_{jk}}{c_{kj}} \quad \forall j, k. \tag{2.11}$$

The two Markov chain Monte Carlo algorithms presented below (Metropolis and Hamiltonian) are characterized by the same acceptance probability:

$$c_{jk} = \min\left[1, \frac{u_k}{u_j}\right] \tag{2.12}$$

but they differ in how transitions are proposed.

2.3 The Metropolis algorithm

For concreteness, imagine that the states are parametrized by a finite number of real parameters $(q_1, \ldots, q_N) = \mathbf{q}$. This will be the case for the matrix models considered in this thesis, where the parameters are real and imaginary part of matrix entries. Fix a scale $s \in \mathbb{R}$. The proposal part of the Metropolis algorithm works as follows:

1. pick a parameter q_i uniformly at random
2. shift q_i by $q_i + \delta_s$, where δ_s is chosen uniformly at random in $[-s, s]$.

Since both q_i and δ_s are picked uniformly and the interval $[-s, s]$ is symmetric around zero, there is an equal probability of proposing a move or its inverse. Therefore, in the language of the previous section, $t_{jk} = t_{kj}$. If the target invariant distribution is $u = u(q_1, \ldots, q_N)$, then the accept/reject probability is given by:

$$\min\left[1, \frac{u(\ldots q_i + \delta_s \ldots)}{u(\ldots q_i \ldots)}\right]. \tag{2.13}$$

The Metropolis algorithm works for a wide variety of problems, and it is the algorithm of choice in most exploratory works for its simplicity. However, when

the parameters are continuous quantities, the Hamiltonian Monte Carlo algorithm presented next generally performs better.

2.4 The Hamiltonian Monte Carlo algorithm

The first step in Hamiltonian Monte Carlo is to enlarge parameter space by introducing a "conjugate momentum" p_i to each parameter q_i. The invariant distribution is extended to include the new variables $u(\mathbf{q}) \to u(\mathbf{q}, \mathbf{p})$. By defining the "Hamiltonian" $H(\mathbf{q}, \mathbf{p}) := -\log u(\mathbf{q}, \mathbf{p})$, a state is then evolved along a Hamiltonian trajectory by integrating Hamilton's equations:

$$\frac{dq_i}{dt} = \frac{\partial H}{\partial p_i} \tag{2.14}$$

$$\frac{dp_i}{dt} = -\frac{\partial H}{\partial q_i} \tag{2.15}$$

where t denotes a fictitious evolution time. This specifies a transition $(\mathbf{q}(0), \mathbf{p}(0)) \to (\mathbf{q}(t), \mathbf{p}(t))$ from an initial configuration to a new one. The new configuration is then accepted with probability:

$$\min[1, \exp(H(0) - H(t))] \tag{2.16}$$

Note that energy is conserved in Hamiltonian dynamics, therefore $H(t) = H(0)$ and $\min[1, \exp(H(0) - H(t))] = 1$. However, numerical integration of Hamilton's equations is a non-trivial matter that introduces small errors, therefore in any concrete implementation $H(t)$ will differ from $H(0)$ by a quantity that depends on the time discretization parameter of the numerical integrator.
Even taking into account these small deviations, the trajectory of the system in phase space will nonetheless be fluctuating around hypersurfaces of equal energy. To correct for this behaviour, the momenta are randomized at the beginning of each Monte Carlo iteration. If the extended invariant distribution $u(\mathbf{q}, \mathbf{p})$ is chosen such that it factorizes as $u(\mathbf{q})v(\mathbf{p})$, and the momenta are sampled from their distribution v, then the initial randomization step does not affect the marginal over $\mathbf{q}$.
The complete algorithm goes as follows:

1. sample momenta randomly from $v(\mathbf{p})$;
2. integrate Hamilton's equations for a time t: $(\mathbf{p}(0), \mathbf{q}(0)) \to (\mathbf{p}(t), \mathbf{q}(t))$;
3. accept the new configuration with probability $\min[1, \exp(H(0) - H(t))]$.

Compared to Metropolis, which depends on just one external parameter s, Hamiltonian Monte Carlo has at least two, both related to the integration step: the time discretization ϵ and the total integration time t. More parameters might enter through the kinetic energy term $K(\mathbf{p}) := -\log v(\mathbf{p})$, but in the remainder of this work the kinetic energy will be assumed to be simply $K(\mathbf{p}) = \sum_i p_i^2/2$, which translates to a Gaussian probability distribution.
The numerical integrator of choice for Hamiltonian dynamics is the leapfrog integrator [**betan**] [37], which will be discussed briefly here. Together with the kinetic energy term defined above, consider the potential energy term $S(\mathbf{q}) := -\log u(\mathbf{q})$,

so that the Hamiltonian reads $H(\mathbf{q}, \mathbf{p}) = S(\mathbf{q}) + K(\mathbf{p})$. Discretize the total integration time t in small intervals of duration ϵ. The evolution from time τ to $\tau + \epsilon$ reads:

$$
\begin{aligned}
p_i(\tau + \epsilon/2) &= p_i(\tau) - \frac{\epsilon}{2}\frac{\partial S(\tau)}{\partial q_i} \\
q_i(\tau + \epsilon) &= q_i(\tau) + \epsilon p_i(\tau + \epsilon/2) \\
p_i(\tau + \epsilon) &= p_i(\tau + \epsilon/2) - \frac{\epsilon}{2}\frac{\partial S(\tau + \epsilon)}{\partial q_i}
\end{aligned}
$$

Therefore the momenta are updated by a half-step, followed by a full update of the positions, and then another half-step update on the momenta. The procedure is repeated from $\tau = 0$ to $\tau = t$. The expensive part of the algorithm resides in the calculation of the gradients $\partial S/\partial q$.
In the next section, two issues regarding Markov chains will be discussed, providing a qualitative argument as to why Hamiltonian Monte Carlo generally performs better than Metropolis.

2.5 Thermalization and correlation

Theorem 1, which provides the theoretical foundation of Markov chains, states that the correct invariant distribution is reached asymptotically in the limit of an infinite number of iterations. How fast the Markov chain reaches a reasonably good approximation of the invariant distribution is a problem known as thermalization, in analogy with physical systems reaching a state of thermal equilibrium. This concept is formalized in terms of the mixing time, defined as the number of iterations needed so that the invariant distribution and the approximate distribution are less than $1/4$ apart in total variation distance [38].
A related issue is that of correlation. Two states of a Markov chain which are close in Monte Carlo time are correlated to each other. This is evident in the case of Metropolis by looking at the algorithm itself. From one iteration to the next, the two states differ at most by a small shift in one of the parameters. A measure of how far apart two states need to be in order for them to be uncorrelated is given by the autocorrelation time [39].
Because of the way move proposals are built, Hamiltonian Monte Carlo mixes faster and has less correlation compared to Metropolis. A Hamiltonian trajectory will transport a state along an orbit in phase space, and all the physical parameters of the model will be updated at once in a non-trivial way. However small, correlation is nevertheless still present in Hamiltonian Monte Carlo and needs to be addressed. This issue will be explored further in Chapter 3.

2.6 Dual averaging

As already mentioned, both Metropolis and Hamiltonian Monte Carlo depend on a choice of parameters: the scale s for Metropolis and the integration length L and discretization ϵ for Hamiltonian Monte Carlo. An optimal choice of parameters plays a crucial role in the performance of the algorithm. Take the Metropolis scale

s as an example: too large a scale will result in big jumps with little to no chance of being accepted, while a scale which is too small will make the system's random walk very slow. Ultimately, regardless of the algorithm, the relevant quantity that links free parameters and performance is the acceptance rate, calculated as the fraction of moves that are accepted. Parameter tuning should therefore result in the optimal acceptance rate for the algorithm. This was found to be around 0.23 under rather general assumptions for Metropolis [40] and 0.65 for Hamiltonian Monte Carlo [37].
Dual averaging [41] is a very efficient algorithm to adaptively tune the Monte Carlo parameters so that the optimal acceptance rate is reached. It is based on stochastic optimization with vanishing adaptation [42], and it is a generalization of an earlier proposal [43].
Suppose $x \in \mathbb{R}$ is a tunable parameter of a Monte Carlo algorithm (for example $x = \log(s)$ in Metropolis), and J_t describes a statistics at Monte Carlo time t that one wants to be vanishing (for example J_t can be the difference between the acceptance rate at time t and the optimal acceptance rate). Consider the expectation:

$$j := \lim_{T\to\infty} \frac{1}{T} \sum_{t=1}^{T} \mathbb{E}[J_t(x_t)]. \tag{2.17}$$

Dual averaging defines an updating procedure $x_t \to x_{t+1}$ after each Monte Carlo step in such a way as to ensure that $j \to 0$. The updating rule is split in two steps (hence the name) by means of an intermediate parameter $\tilde{x}_t$:

$$\begin{aligned} \tilde{x}_{t+1} &= \mu - \frac{\sqrt{t}}{\gamma} \frac{1}{t+t_0} \sum_{i=1}^{t} J_i \\ x_{t+1} &= \frac{1}{t^\kappa} \tilde{x}_{t+1} + \left(1 - \frac{1}{t^\kappa}\right) x_t \end{aligned} \tag{2.18}$$

where μ, γ, t_0 and κ are free parameters of the algorithm, and x_1 is set to be $\tilde{x}_1$. The authors in [41] suggest to fix the free parameters in the following way:

$$\mu = \log(10) + x_{\text{ini}}, \quad \gamma = 0.05, \quad t_0 = 10, \quad \kappa = 0.75. \tag{2.19}$$

where x_{ini} is a reasonable initial guess for the parameter (although any value would work).

2.7 Metropolis for fuzzy spaces

The rather general notation adopted so far needs now to be specialized to the case of fuzzy Dirac operators.
Equation (2.4) represents the invariant distribution and Dirac operators are states of the system.
An explicit parametrization of Dirac operators is the following:

$$D = \sum_i \omega_i \otimes (M_i \otimes \mathbb{1} + \epsilon_i \mathbb{1} \otimes M_i^T) \tag{2.20}$$

where ω_i are fixed matrices, ϵ_i are fixed signs, and the free parameters are the $n \times n$ Hermitian matrices M_i. For Metropolis, it will be convenient to take each independent matrix entry as the set of coordinates $\mathbf{q}$, so that the proposed moves are as local as possible. Once a scale $s \in \mathbb{R}$ is fixed, the Metropolis algorithm reads:

1. pick uniformly at random a matrix M_x;
2. pick uniformly at random a matrix entry $(M_x)_{IJ}$;
3. sample uniformly at random a complex number z such that $\mathrm{Re}\, z \in [-s, s]$, $\mathrm{Im}\, z \in [-s, s]$, and then set $\mathrm{Im}\, z = 0$ if $I = J$;
4. propose the move $(M_x)_{IJ} \to (M_x)_{IJ} + z$ and $(M_x)_{JI} \to (M_x)_{JI} + z^*$;
5. accept the move with probability $\min\left[1, e^{-\Delta S}\right]$, where ΔS is the difference between the new action (the one calculated with the updated matrix entry) and the old one.

Starting from an arbitrary Dirac operator and repeating this procedure many times, one is guaranteed to eventually generate Dirac operators correctly distributed according to (2.4).
The speed of the algorithm plays a crucial role in the possibility of investigating higher matrix sizes and obtain enough uncorrelated samples. The Metropolis algorithm requires an evaluation of the difference $S[D'] - S[D]$ at each step, where D is the current Dirac operator and $D' := D + \delta D$ is the proposed move from D. Evaluating this difference is by far the operation that takes up most of the computational time. In previous implementations [7] [12] the values of $S[D']$ and $S[D]$ were computed independently, and then subtracted. But if D' and D differ only slightly, much simplification can be achieved by computing the difference using only the relevant data. As the action contains traces of powers of D, the problem reduces to finding a closed formula for terms of the type $\mathrm{Tr}[(D')^p - D^p]$. A formula for a generic power p can be written, but several drawbacks will be pointed out that make it of limited use. Since only quadratic and quartic terms appear in the action considered here, the cases $p = 2$ and 4 will then be treated separately, and very computationally efficient formulas will be written for evaluating ΔS.

2.7.1 A closed formula for generic p

If $D' = D + \delta D$, then $(D')^p$ is formally a sum of all the possible strings of length p of symbols D and δD. As an example, for $p = 2$:

$$(D')^2 = (D + \delta D)^2 = DD + D\delta D + \delta D D + \delta D \delta D. \tag{2.21}$$

Therefore $(D')^p - D^p$ is a sum of strings of length p with at least one δD. A string containing s occurrences of δD is then viewed as a certain number of clusters $\delta D ... \delta D$, the j-th cluster having length $k_j \geq 0$, followed by a single D. The

difference $(D')^p - D^p$ then can be written as:

$$(D')^p - D^p = \sum_{s=1}^{p} \sum_{\substack{k_1,..,k_{p-s}=0 \\ \sum k_j \leq s}}^{s} [(\delta D)^{k_1} D]\ [(\delta D)^{k_2} D]...[(\delta D)^{k_{p-s}} D](\delta D)^{(s-\sum k_j)}. \tag{2.22}$$

Now, using Eq.(2.20) for the general form of a Dirac operator:

$$D = \sum_{i \in I} \omega_i \otimes [M_i, \cdot]_{\epsilon_i} := \sum_{i \in I} A_i \tag{2.23}$$

Eq.(2.22) can be written as:

$$\sum_{s=1}^{p} \sum_{\substack{k_1,..,k_{p-s}=0 \\ \sum k_j \leq s}}^{s} \sum_{i_1,..,i_{p-s} \in I} (\delta D)^{k_1} A_{i_1} ... (\delta D)^{k_{p-s}} A_{i_{p-s}} (\delta D)^{(s-\sum k_j)}. \tag{2.24}$$

Writing Eq.(2.24) in terms of the submatrices of D is then a matter of keeping track of the indices. The final formula is given in Appendix A.1.
This formula, although appealing for its generality, is somewhat unsatisfactory in a numerical implementation:

1. It contains a variable number of indices on which to sum (1 to $p - s$). This corresponds to a variable number of `for` loops in the code, something which is not easily obtainable.

2. It hides the structure of the terms, making it hard to understand why taking the trace yields a real number. This forces the use of complex numbers instead of real numbers throughout the whole computation, wasting memory and computational power.

3. It is hard to exploit the properties of gamma matrices, which make many terms vanish. As a result, a large number of terms is computed just to obtain zero, again wasting computational power and introducing small errors (vanishing terms are only approximately zero on a computer).

4. In general, the resulting code is completely obscure, even to the person writing it.

In the next section, specific formulas for the case $p = 2$ and $p = 4$ are presented. These formulas are much better suited for an actual implementation.

2.7.2 The case $p = 2, 4$

As the action in (2.2) contains only the second and fourth power of D, these two cases have been worked out explicitly in order to obtain a simpler formula.
First notice that the quantity of interest is a trace, therefore the cyclicity property can be used to write:

$$\mathrm{Tr}[(D')^2 - D^2] = \mathrm{Tr}[\ 2D\delta D + (\delta D)^2\ ] \tag{2.25}$$

$$\begin{aligned}\mathrm{Tr}[(D')^4 - D^4] = \mathrm{Tr}[\ & 4D^3\delta D + 4D^2(\delta D)^2 + \\ & + 2D\delta D D\delta D + 4D(\delta D)^3 + (\delta D)^4\ ].\end{aligned} \tag{2.26}$$

In the following, as an example, the term $\mathrm{Tr}\, D^3\delta D$ will be computed explicitly. All the other terms are similar but simpler to compute.
Write D^3 and δD in terms of the submatrices ω_i and M_i:

$$\delta D = \omega_x \otimes (m_x \otimes \mathbb{1} + \epsilon_x \mathbb{1} \otimes m_x^T) \tag{2.27}$$

$$\begin{aligned} D^3 = \sum_{i_1,i_2,i_3} & \omega_{i_1}\omega_{i_2}\omega_{i_3} \otimes \\ & \otimes (\ M_{i_1}M_{i_2}M_{i_3} \otimes \mathbb{1} + \epsilon_{i_1}\epsilon_{i_2}\epsilon_{i_3}\mathbb{1} \otimes M_{i_1}^T M_{i_2}^T M_{i_3}^T + \\ & \epsilon_{i_1}\epsilon_{i_2}M_{i_3} \otimes M_{i_1}^T M_{i_2}^T + \epsilon_{i_3}M_{i_1}M_{i_2} \otimes M_{i_3}^T + \\ & \epsilon_{i_2}M_{i_1}M_{i_3} \otimes M_{i_2}^T + \epsilon_{i_2}\epsilon_{i_3}M_{i_1} \otimes M_{i_2}^T M_{i_3}^T + \\ & \epsilon_{i_1}M_{i_2}M_{i_3} \otimes M_{i_1}^T + \epsilon_{i_1}\epsilon_{i_3}M_{i_2} \otimes M_{i_1}^T M_{i_3}^T\ ). \end{aligned} \tag{2.28}$$

Multiplying them together and taking the trace yields:

$$\begin{aligned} \mathrm{Tr}\, D^3\delta D = \sum_{i_1,i_2,i_3} & \mathrm{Tr}(\omega_{i_1}\omega_{i_2}\omega_{i_3}\omega_x)\cdot \\ & \cdot(\ n[1 + \epsilon_{i_1}\epsilon_{i_2}\epsilon_{i_3}\epsilon_x *]\,\mathrm{Tr}(M_{i_1}M_{i_2}M_{i_3}m_x)\ + \\ & [\epsilon_{i_3} + \epsilon_{i_1}\epsilon_{i_2}\epsilon_x *]\,\mathrm{Tr}(M_{i_1}M_{i_2}m_x)\,\mathrm{Tr}\, M_{i_3}\ + \\ & [\epsilon_{i_1}\epsilon_{i_2} + \epsilon_{i_3}\epsilon_x *]\,\mathrm{Tr}(M_{i_1}M_{i_2})\,\mathrm{Tr}(M_{i_3}m_x)\ + \\ & [\epsilon_{i_1}\epsilon_{i_2}\epsilon_{i_3} + \epsilon_x *]\,\mathrm{Tr}(M_{i_1}M_{i_2}M_{i_3})\,\mathrm{Tr}\, m_x\ + \\ & [\epsilon_{i_2} + \epsilon_{i_1}\epsilon_{i_3}\epsilon_x *]\,\mathrm{Tr}(M_{i_1}M_{i_3}m_x)\,\mathrm{Tr}\, M_{i_2}\ + \\ & [\epsilon_{i_2}\epsilon_{i_3} + \epsilon_{i_1}\epsilon_x *]\,\mathrm{Tr}(M_{i_1}m_x)\,\mathrm{Tr}(M_{i_2}M_{i_3})\ + \\ & [\epsilon_{i_1} + \epsilon_{i_2}\epsilon_{i_3}\epsilon_x *]\,\mathrm{Tr}(M_{i_2}M_{i_3}m_x)\,\mathrm{Tr}\, M_{i_1}\ + \\ & [\epsilon_{i_1}\epsilon_{i_3} + \epsilon_{i_2}\epsilon_x *]\,\mathrm{Tr}(M_{i_1}M_{i_3})\,\mathrm{Tr}(M_{i_2}m_x)\ ) \end{aligned} \tag{2.29}$$

where $*$ denotes complex conjugation of everything that appears on the right, and the relation $M^T = M^*$ has been used.
To simplify this expression, notice the following:

1. exchanging the indices $i_1 \leftrightarrow i_3$ in Eq.(2.29) is equivalent to taking the complex conjugate of the whole expression
   $\Longrightarrow$ it is possible to limit the sum to $i_1 < i_3$ and take twice the real part;

2. if two indices are the same, say i_1 and i_3, then $i_2 = x$ due to the properties of the Clifford module: $\mathrm{Tr}(\omega_{i_1}\omega_{i_2}\omega_{i_1}\omega_x) \sim \mathrm{Tr}(\omega_{i_2}\omega_x) = 0$ if $i_2 \neq x$
   $\Longrightarrow$ the only case which is not accounted for in the previous point is $i_1 = i_3, i_2 = x$;

3. when $i_1 = i_3$ and $i_2 = x$, each term in Eq.(2.29) is real.

Therefore Eq.(2.29) becomes:

$$\mathrm{Tr}\, D^3\delta D = \sum_{\substack{i_1<i_3 \\ i_2}} 2\,\mathrm{Re}\,\mathrm{Tr}(\ldots) + \sum_{\substack{i_1=i_3 \\ i_2=x}} \mathrm{Re}\,\mathrm{Tr}(\ldots). \tag{2.30}$$

This formula already adresses many of the practical problems listed in the previous section. Further simplification can be achieved if the Metropolis move is local. The simplest case is when m_x has only one non-zero entry (and the one across the diagonal for hermiticity), in which case m_x is written in components as:

$$(m_x)_{ij} = z\delta_{iI}\delta_{jJ} + z^*\delta_{iJ}\delta_{jI} \tag{2.31}$$

where z is a complex number, δ_{ij} is the Kronecker delta, and I, J are the indices of the only non-vanishing entries: $(m_x)_{IJ} = (m_x)^*_{JI} = z \neq 0$.
The final formulas for $p = 2$ and $p = 4$ when m_x has the form of Eq.(2.31) are given in Appendix A.2.

2.8 Hamiltonian Monte Carlo for fuzzy spaces

It is convenient in this case to take the dynamical variables to be the $n \times n$ Hermitian matrices M_i instead of individual matrix entries. The conjugate momenta therefore will be themselves $n \times n$ Hermitian matrices belonging to a Gaussian ensemble. The proposed move coming from Hamiltonian evolution will in general involve an update of every single matrix entry. Therefore, unlike in Metropolis with local updates, the entire Hamiltonian needs to be recomputed in the accept/reject step. Moreover, the leapfrog integrator requires to calculate matrix derivatives of the form:

$$\frac{\partial \operatorname{Tr} D^p}{\partial M_k} =: \partial_k \operatorname{Tr} D^p \tag{2.32}$$

which need to be defined. Let $A \in M_n(\mathbb{C})$ and $f : M_n(\mathbb{C}) \to \mathbb{C}$. For the purposes of this work, the derivative of f with respect to A is defined in components as the $n \times n$ matrix:

$$\left(\frac{\partial f}{\partial A}\right)_{lm} := \frac{\partial f}{\partial A_{ml}}. \tag{2.33}$$

A special case of interest here is:

$$\frac{\partial \operatorname{Tr} AB}{\partial A} = B \tag{2.34}$$

which also allows to calculate:

$$\frac{\partial \operatorname{Tr} A^j B}{\partial A} = A^{j-1}B + A^{j-2}BA + \ldots + BA^{j-1} \tag{2.35}$$

using a simple heuristic rule: differentiate with respect to each A matrix after bringing it to the front by cycling the others to the other side of the trace.
In the following, formulas for $\partial_k \operatorname{Tr} D^2$ and $\partial_k \operatorname{Tr} D^4$ are worked out.

2.8.1 The case $\operatorname{Tr} D^2$

In the quadratic term the M_i matrices are decoupled:

$$\operatorname{Tr} D^2 = \sum_i \operatorname{Tr} \omega_i^2 (2n \operatorname{Tr} M_i^2 + 2\epsilon_i (\operatorname{Tr} M_i)^2). \tag{2.36}$$

Taking a derivative with respect to M_k yields:

$$\begin{aligned}\frac{\partial}{\partial M_k}\left(\sum_i \operatorname{Tr}\omega_i^2(2n\operatorname{Tr}M_i^2+2\epsilon_i(\operatorname{Tr}M_i)^2)\right)\\ =\sum_i \delta_{ik}\operatorname{Tr}\omega_i^2\left(4nM_i+4\epsilon_i(\operatorname{Tr}M_i)\mathbb{1}\right)\\ =4C\left(nM_k+\epsilon_k(\operatorname{Tr}M_k)\mathbb{1}\right)\end{aligned} \tag{2.37}$$

where $C := \operatorname{Tr}\omega_i^2$ is the dimension of the gamma matrices.

2.8.2 The case $\operatorname{Tr} D^4$

First expand $\operatorname{Tr} D^4$:

$$\begin{aligned}\operatorname{Tr}D^4 = \sum_{i_1,i_2,i_3,i_4}\operatorname{Tr}(\omega_{i_1}\omega_{i_2}\omega_{i_3}\omega_{i_4})\cdot\\ \Big(\ n[1+\epsilon\ *]\operatorname{Tr}(M_{i_1}M_{i_2}M_{i_3}M_{i_4})\ \ +\\ \epsilon_{i_1}\operatorname{Tr}M_{i_1}[1+\epsilon\ *]\operatorname{Tr}(M_{i_2}M_{i_3}M_{i_4})\ \ +\\ \epsilon_{i_2}\operatorname{Tr}M_{i_2}[1+\epsilon\ *]\operatorname{Tr}(M_{i_1}M_{i_3}M_{i_4})\ \ +\\ \epsilon_{i_3}\operatorname{Tr}M_{i_3}[1+\epsilon\ *]\operatorname{Tr}(M_{i_1}M_{i_2}M_{i_4})\ \ +\\ \epsilon_{i_4}\operatorname{Tr}M_{i_4}[1+\epsilon\ *]\operatorname{Tr}(M_{i_1}M_{i_2}M_{i_3})\ \ +\\ \epsilon_{i_1}\epsilon_{i_2}[1+\epsilon]\operatorname{Tr}(M_{i_1}M_{i_2})\operatorname{Tr}(M_{i_3}M_{i_4})\ \ +\\ \epsilon_{i_1}\epsilon_{i_3}[1+\epsilon]\operatorname{Tr}(M_{i_1}M_{i_3})\operatorname{Tr}(M_{i_2}M_{i_4})\ \ +\\ \epsilon_{i_1}\epsilon_{i_4}[1+\epsilon]\operatorname{Tr}(M_{i_1}M_{i_4})\operatorname{Tr}(M_{i_2}M_{i_3})\ \Big)\end{aligned} \tag{2.38}$$

where $*$ denotes complex conjugation of everything that appears on the right, ϵ is defined as the product $\epsilon \equiv \epsilon_{i_1}\epsilon_{i_2}\epsilon_{i_3}\epsilon_{i_4}$, and the relation $M^T = M^*$ has been used. Taking a matrix derivative with respect to M_k results in non-vanishing contributions when $k = i_1, k = i_2, k = i_3$ or $k = i_4$:

$$\begin{aligned}\frac{\partial}{\partial M_k}\operatorname{Tr}D^4 = \sum_{i_1,i_2,i_3,i_4}\operatorname{Tr}(\omega_{i_1}\omega_{i_2}\omega_{i_3}\omega_{i_4})\cdot\\ \Big(\delta_{ki_1}A(i_1,i_2,i_3,i_4)+\delta_{ki_2}A(i_2,i_3,i_4,i_1)+\\ \delta_{ki_3}A(i_3,i_4,i_1,i_2)+\delta_{ki_4}A(i_4,i_1,i_2,i_3)\Big)\end{aligned} \tag{2.39}$$

where $A(a,b,c,d)$ is the following $n \times n$ matrix:

$$\begin{aligned} A(a,b,c,d) \equiv\ & n[1+\epsilon\ \dagger]M_bM_cM_d+ \\ & \epsilon_a \mathbb{1}[1+\epsilon\ *]\ \mathrm{Tr}\ M_bM_cM_d+ \\ & \epsilon_b\ \mathrm{Tr}\ M_b[1+\epsilon\ \dagger]M_cM_d+ \\ & \epsilon_c\ \mathrm{Tr}\ M_c[1+\epsilon\ \dagger]M_bM_d+ \\ & \epsilon_d\ \mathrm{Tr}\ M_d[1+\epsilon\ \dagger]M_bM_c+ \\ & \epsilon_a\epsilon_bM_b[1+\epsilon]\ \mathrm{Tr}\ M_cM_d+ \\ & \epsilon_a\epsilon_cM_c[1+\epsilon]\ \mathrm{Tr}\ M_bM_d+ \\ & \epsilon_a\epsilon_dM_d[1+\epsilon]\ \mathrm{Tr}\ M_bM_c \end{aligned} \tag{2.40}$$

and $\dagger$ denotes Hermitian conjugation of everything that appears on the right. Upon relabeling the indices and cycling the ω matrices in the trace, the equation becomes:

$$\begin{aligned} \frac{\partial}{\partial M_k}\ \mathrm{Tr}\ D^4 &= 4 \sum_{i_1,i_2,i_3,i_4} \delta_{ki_1}\ \mathrm{Tr}(\omega_{i_1}\omega_{i_2}\omega_{i_3}\omega_{i_4})A(i_1,i_2,i_3,i_4) \\ &= 4 \sum_{i_1,i_2,i_3} \mathrm{Tr}(\omega_k\omega_{i_1}\omega_{i_2}\omega_{i_3})A(k,i_1,i_2,i_3) =: 4 \sum_{i_1,i_2,i_3} \mathcal{A}_k(i_1,i_2,i_3) \end{aligned} \tag{2.41}$$

with $\mathcal{A}_k(a,b,c)$ defined as the product $\mathrm{Tr}(\omega_k\omega_{i_1}\omega_{i_2}\omega_{i_3})A(k,i_1,i_2,i_3)$.
The sum can be considerably simplified by grouping together terms based on how many indices coincide.
First consider the case where all indices are different:

$$\sum_{\substack{i_1,i_2,i_3 \\ i_a \neq i_b}} \mathcal{A}_k(i_1,i_2,i_3). \tag{2.42}$$

A convenient way to rewrite it is to constrain the indices to be in increasing order $i_1 < i_2 < i_3$ and write explicitly the permutations that generate the whole sum:

$$\begin{aligned} \sum_{i_1<i_2<i_3} \Big(& \mathcal{A}_k(i_1,i_2,i_3) + \mathcal{A}_k(i_2,i_1,i_3) + \mathcal{A}_k(i_3,i_2,i_1) \\ & + \mathcal{A}_k(i_1,i_3,i_2) + \mathcal{A}_k(i_3,i_1,i_2) + \mathcal{A}_k(i_2,i_3,i_1) \Big). \end{aligned} \tag{2.43}$$

Notice that an exchange of indices $i_1 \leftrightarrow i_3$ is equivalent to taking the Hermitian conjugate:

$$\mathcal{A}_k(i_1,i_2,i_3)^\dagger = \mathcal{A}_k(i_3,i_2,i_1) \tag{2.44}$$

therefore (2.43) becomes:

$$\sum_{i_1<i_2<i_3} [1+\dagger]\Big(\mathcal{A}_k(i_1,i_2,i_3) + \mathcal{A}_k(i_1,i_3,i_2) + \mathcal{A}_k(i_2,i_1,i_3) \Big). \tag{2.45}$$

Finally, notice that if $i_a = k$ then the trace over the ω matrices vanishes, therefore the contribution when all indices are different takes the final form:

$$\sum_{\substack{i_1<i_2<i_3\\ i_a\neq k}} [1+\dagger]\Big(\mathcal{A}_k(i_1,i_2,i_3)+\mathcal{A}_k(i_1,i_3,i_2)+\mathcal{A}_k(i_2,i_1,i_3)\Big). \tag{2.46}$$

Before moving on, let us introduce an algorithm to arrive at (2.45) immediately by means of a group-theoretical argument that will readily generalize to higher powers of the Dirac operator. Suppose one has the generic sum of matrices:

$$\sum_{i_a\neq i_b} A(i_1,\dots i_n) \tag{2.47}$$

and suppose that some index exchange $i_a \leftrightarrow i_b$ amounts to a known map (for example taking the Hermitian conjugate). Denote this map $\bullet$. Consider now the symmetric group S_n acting on the indices $i_1,\dots,i_n$. If the permutations corresponding to the index exchanges that induce $\bullet$ (plus the identical permutation) form a subgroup H of S_4, one can calculate the (left or right) cosets and choose a representative σ from each. The sum (2.47) can then be written:

$$\sum_{i_1<\dots<i_n} [1+\bullet]\Big(\sum_{\sigma\in S_n/H} A(\sigma(i_1),\dots,\sigma(i_n))\Big). \tag{2.48}$$

In the explicit case above, $n=3$, $\bullet=\dagger$, $H=\{(),(13)\}$ and $S_3/H=\{(),(23),(12)\}$. Notice that the map does not need to be Hermitian conjugation, as long as the corresponding permutations form a subgroup of the whole permutation group.
Going back to Eq.(2.41), what is left are terms in which at least two indices are equal. These are:

$$\sum_{i_1\neq i_2}\Big(\mathcal{A}_k(i_1,i_1,i_2)+\mathcal{A}_k(i_2,i_1,i_1)+\mathcal{A}_k(i_1,i_2,i_1)\Big)+\sum_i \mathcal{A}_k(i,i,i). \tag{2.49}$$

Or more simply, using the properties of the ω matrices and the index exchange symmetry:

$$\sum_{i\neq k}\Big([1+\dagger]\mathcal{A}_k(i,i,k)+\mathcal{A}_k(i,k,i)\Big)+\mathcal{A}_k(k,k,k). \tag{2.50}$$

Putting together (2.41), (2.46) and (2.50), the final formula for $\partial_k \operatorname{Tr} D^4$ reads:

$$\begin{aligned}\frac{\partial}{\partial M_k}\operatorname{Tr} D^4 = 4\Bigg[&\sum_{\substack{i_1<i_2<i_3\\ i_a\neq k}} [1+\dagger]\Big(\mathcal{A}_k(i_1,i_2,i_3)+\mathcal{A}_k(i_1,i_3,i_2)+\mathcal{A}_k(i_2,i_1,i_3)\Big)\\ &+\sum_{i\neq k}\Big([1+\dagger]\mathcal{A}_k(i,i,k)+\mathcal{A}_k(i,k,i)\Big)+\mathcal{A}_k(k,k,k)\Bigg].\end{aligned} \tag{2.51}$$

The simplified formulas for $\mathcal{A}_k(i,i,k)$, $\mathcal{A}_k(i,k,i)$ and $\mathcal{A}_k(k,k,k)$ are given in Appendix B.

2.9 Calculating the action

In the course of the Monte Carlo routines one needs to repeatedly calculate the value of the action in the accept/reject step. This is especially true for the Hamiltonian method, where the degrees of freedom are updated globally and the new value of the Hamiltonian needs to be recomputed after every trajectory.
Using the same arguments that lead to efficient formulas for $\partial_k \operatorname{Tr} D^2$ and $\partial_k \operatorname{Tr} D^4$, one can write down a formula for S that only involves the M_i matrices. The performance gain in using such a formula instead of calculating S naively from the full Dirac operator will be evident in the next chapter when benchmarking the actual numerical implementation.
The formula (2.36) for $\operatorname{Tr} D^2$ is already simplified. For $\operatorname{Tr} D^4$, expand it as in (2.38) and call the generic term in the sum $\mathcal{B}$:

$$\operatorname{Tr} D^4 = \sum_{i_1,i_2,i_3,i_4} \mathcal{B}(i_1,i_2,i_3,i_4). \tag{2.52}$$

As before, splitting the terms based on how many indices coincide and using the properties of the ω matrices, the sum reads:

$$\begin{aligned}\operatorname{Tr} D^4 = &\sum_{i_a \neq i_b} \mathcal{B}(i_1,i_2,i_3,i_4) + 2\sum_{i_1<i_2}\Big[2\mathcal{B}(i_1,i_1,i_2,i_2) + \mathcal{B}(i_1,i_2,i_1,i_2)\Big] \\ &+ \sum_i \mathcal{B}(i,i,i,i).\end{aligned} \tag{2.53}$$

The group-theoretical argument used in the previous section allows to simplify the sum where no index is the same. Consider the symmetric group S_4 acting on the set of indices $\{i_1,i_2,i_3,i_4\}$. The subgroup of S_4 corresponding to the symmetries of $\mathcal{B}$ is $D_8 = \langle (1,2,3,4),(1,3)\rangle$, i.e. 4 cyclic permutations (that leave $\mathcal{B}$ invariant) and 4 anti-cyclic permutations (that give the complex conjugate of $\mathcal{B}$). Quotient out the action of D_8 by introducing the prefactor $4[1+*]$ (i.e. $8\operatorname{Re}$) and constrain the sum to $i_1<i_2<i_3<i_4$. The terms left out by this procedure are the terms obtained by acting on $\{i_1,i_2,i_3,i_4\}$ with a representative from each (left or right) coset in S_4/D_8. One choice of representatives is $(), (3,4)$ and $(2,3)$, which gives:

$$\begin{aligned}&\sum_{i_a \neq i_b} \mathcal{B}(i_1,i_2,i_3,i_4) = \\ &\qquad \sum_{i_1<i_2<i_3<i_4} 8\operatorname{Re}\Big[\mathcal{B}(i_1,i_2,i_3,i_4) + \mathcal{B}(i_1,i_2,i_4,i_3) + \mathcal{B}(i_1,i_3,i_2,i_4)\Big].\end{aligned} \tag{2.54}$$

The final, computationally efficient formula for $\operatorname{Tr} D^4$ thus reads:

$$\begin{aligned}\operatorname{Tr} D^4 = &\sum_{i_1<i_2<i_3<i_4} 8\operatorname{Re}\Big[\mathcal{B}(i_1,i_2,i_3,i_4) + \mathcal{B}(i_1,i_2,i_4,i_3) + \mathcal{B}(i_1,i_3,i_2,i_4)\Big] \\ &+ 2\sum_{i_1<i_2}\Big[2\mathcal{B}(i_1,i_1,i_2,i_2) + \mathcal{B}(i_1,i_2,i_1,i_2)\Big] \\ &+ \sum_i \mathcal{B}(i,i,i,i).\end{aligned} \tag{2.55}$$

Chapter 3

The RFL library

3.1 Overview

The Random Fuzzy Library (RFL) was written in order to simplify the process of performing Monte Carlo integration of the random matrix models arising from Dirac operators of fuzzy spectral triples. The library is written in C++ and relies on Armadillo [44] for linear algebra operations and GSL [45] for random number generation.
The main features of the library are:

1. automated generation of Clifford gamma matrices and Dirac operators given a (p, q) signature;
2. efficient implementation of both Metropolis and Hamiltonian Monte Carlo;
3. automated parameter tuning based on the dual averaging method [41].

The next few sections will expand on the technical details of each of these points. Although considerable improvements are possible from a software design point of view, the current state of the library should facilitate the academic study of random fuzzy spaces. The library is freely available on GitHub at

`https://github.com/darcangelomauro/RFL.git`

3.2 Clifford modules

Recall from Chapter 1 that given a pair of integers (p, q), a Clifford module is determined by p Hermitian matrices squaring to $+1$

$$\left(\gamma^i\right)^2 = +\mathbb{1}, \quad i = 1, \dots, p$$

and q anti-Hermitian matrices squaring to -1

$$\left(\gamma^j\right)^2 = -\mathbb{1}, \quad j = p+1, \dots, p+q$$

often referred to as gamma matrices. The KO-dimension is defined as

$$s = q - p \mod 8$$

and the chirality operator is

$$\gamma = i^{\frac{1}{2}s(s+1)}\gamma^1 \dots \gamma^{p+q}.$$

Following [8], it is possible to generate an arbitrary Clifford module by taking products of simpler ones. Given a Clifford module (p_1, q_1) with even KO-dimension s_1, gamma matrices $\{\gamma_1^a\}$ and chirality operator γ_1, and another Clifford module (p_2, q_2) with gamma matrices $\{\gamma_2^a\}$, then the following are gamma matrices for a $(p_1 + p_2, q_1 + q_2)$ Clifford module:

$$\gamma_1^1 \otimes \mathbb{1},\ \dots,\ \gamma_1^{p_1+q_1} \otimes \mathbb{1},\ \gamma_1 \otimes \gamma_2^1,\ \dots, \gamma_1 \otimes \gamma_2^{p_2+q_2}$$

and the product is irreducible if the two modules are. It follows that any (p, q) can be generated by multiplying enough copies of the $(2, 0)$, $(1, 1)$, $(0, 2)$, $(1, 0)$ and $(0, 1)$ (with the $(1, 0)$ and $(0, 1)$ on the right, since their KO-dimension is odd). Based on the construction outlined above, the class `Cliff` in RFL automatically builds, given p and q, the corresponding gamma matrices. The following sample code generates a $(3, 2)$ Clifford module and outputs matrix dimension, gamma matrices and chirality operator.

```
#include <iostream>
#include <armadillo>
#include "clifford.hpp"

int main()
{
    int p = 3;
    int q = 2;

    // Create Clifford module C
    Cliff C(p,q);

    // Print dimension of gamma matrices
    std::cout << C.get_dim_gamma() << std::endl;

    // Print gamma matrices
    for(int i=0; i<p+q; ++i)
        std::cout << C.get_gamma(i) << std::endl;

    // Print chirality operator
    std::cout << C.get_chiral() << std::endl;
}
```

The gamma matrices are stored as complex matrices of type `arma::cx_mat` defined in Armadillo. The way the library constructs Clifford modules is by finding the decomposition in terms of $(2, 0)$, $(1, 1)$, $(0, 2)$, $(1, 0)$ and $(0, 1)$ modules, and then multiply them together via overloaded `*` and `*=` operators. Therefore `C1` and `C2` in the code below are the same Clifford module.

```
#include <armadillo>
```

```
#include "clifford.hpp"

int main()
{
    // Create a (4,4) Clifford module via constructor
    Cliff C1(4,4);

    // Create a (4,4) Clifford module via overloaded product
    Cliff B(2,2);
    Cliff C2 = B*B;
}
```

3.3 Dirac operators

The class `Cliff` is used as a base for Dirac operators. Recall that given a (p, q) signature, the corresponding Dirac operator has the form:

$$D = \sum_i \alpha_i \otimes \{H_i, \cdot\} + \sum_j \tau_j \otimes [L_j, \cdot] \tag{3.1}$$

where α_i and H_i are Hermitian, τ_j and L_j are anti-Hermitian, and $\{\alpha_i, \tau_j\}$ form a basis for the algebra generated by the (p, q) gamma matrices. In order to build the Dirac operator from p and q it is therefore necessary to find all linearly independent products of gamma matrices, which will form the sets $\{\alpha_i\}$ and $\{\tau_j\}$ based on Hermiticity. As noted in [8], linearly independent products can be taken to be all odd (unordered) products of length less or equal to $p + q$ of distinct gamma matrices.
Normally, to produce these combinations one would use a series of nested `for` loops. For example, the code to produce all products of three distinct gamma matrices would look like the following

for $i \leftarrow 1, p+q$ **do**
  for $j \leftarrow i+1, p+q$ **do**
    for $k \leftarrow j+1, p+q$ **do**
      $\gamma^{ijk} \leftarrow \gamma^i \gamma^j \gamma^k$
    end for
  end for
end for

If $p + q = 3$ or 4, only products of three distinct gamma matrices need to be generated. If $p + q = 5$ or 6, products of five gamma matrices also need to be generated, and so on. This means that the number of nested `for` loops depends on $p+q$. But in RFL p and q are parameters chosen by the user at runtime, while `for` loops are hard-coded. Since there is no way of knowing how many nested loops one will need beforehand, the nested loops method could not be used (unless one is willing to impose a restriction on the maximum $p+q$, which is also a viable option).
The way RFL generates all linearly independent products of gamma matrices is by using an equivalent formulation of the problem: given an alphabet with $p + q$ letters, produce all unordered strings of odd length $k \leq p + q$ with no repetitions.

Unordered means that two strings are identical if one can be obtained from the other upon commuting the letters. If the odd length requirement is dropped, then such strings are in one-to-one correspondence with binary strings of length $p+q$. For example, if the alphabet is $\{a, b, c, d, e\}$, the string abe corresponds to 11001 via the following identification:

$$\begin{array}{c} a\ b\ c\ d\ e \\ 1\ 1\ 0\ 0\ 1 \end{array}$$

The strategy RFL uses to produce the needed products is then to look at the binary representation of numbers from 0 to 2^{p+q}, pick out those with an odd number of 1s, and then multiply together the gamma matrices whose index corresponds to the position of the 1s in the binary string. Therefore in a set of 5 gamma matrices, the product $\gamma^1\gamma^3\gamma^4$ is identified with the binary string 10110 (or 22 in decimal). Once all odd products are generated this way, the Hermitian and anti-Hermitian ones are counted to know how many H and L matrices are there in the model.
Looking at (3.1), it is clear that a factor of i can be moved from an L_j to the corresponding τ_j, making both Hermitian. Having to deal with only Hermitian objects is considerably more convenient from a programming point of view, and therefore this is the way Dirac operators are represented in RFL. One still needs to keep track of the fact that what was originally an L (H) matrix appears inside a commutator (anti-commutator). Representing commutators and anti-commutators as linear operators in $M_n(\mathbb{C})$, i.e. elements of $M_n(\mathbb{C}) \otimes M_n(\mathbb{C})$, shows how the difference between an L and an H matrix can be stored in a sign:

$$[M, \cdot] = M \otimes \mathbb{1} - \mathbb{1} \otimes M^T \tag{3.2}$$

$$\{M, \cdot\} = M \otimes \mathbb{1} + \mathbb{1} \otimes M^T. \tag{3.3}$$

Ultimately, this leads to (2.20) as a general formula for a Dirac operator:

$$D = \sum_i \omega_i \otimes (M_i \otimes \mathbb{1} + \epsilon_i \mathbb{1} \otimes M_i^T) \tag{3.4}$$

where ω_i and M_i are Hermitian, and $\epsilon_i = \pm 1$ differentiate between commutators and anti-commutators. The ω_i denote collectively what in (3.1) were α or τ matrices.

3.4 The class `Geom24`

The rules described so far are implemented in the RFL class `Geom24`. The class handles all aspects of the numerical simulation, from the creation of the Dirac operator to the Monte Carlo algorithms.
The class constructor requires a choice of Clifford module (p, q), the dimension of the M_i matrices, and a value for the coupling constant g_2. The idea is that the class represents a static picture of the Monte Carlo evolution of the Dirac operator under the usual action:

$$S = g_2 \operatorname{Tr} D^2 + \operatorname{Tr} D^4. \tag{3.5}$$

In the following example, a $(2,0)$ geometry with 32×32 matrices is instantiated at the coupling constant value $g_2 = -3$. A Monte Carlo evolution of 10^4 steps using the Metropolis algorithm is started, and the value of the action is printed every 100 steps to the standard output stream.

```
#include <iostream>
#include <gsl/gsl_rng.h>
#include <ctime>
#include <armadillo>
#include "geometry.hpp"

int main()
{
    // Initialize the random number generator
    gsl_rng* engine = gsl_rng_alloc(gsl_rng_ranlxd1);
    gsl_rng_set(engine, time(NULL));

    // Clifford module parameters
    int p = 2;
    int q = 0;

    // Matrix algebra dimension
    int n = 32;

    // Coupling constant value
    double g2 = -3;

    // Metropolis scale factor
    double scale = 0.05;

    // Create the Dirac operator
    Geom24 G(p, q, n, g2);

    // Metropolis simulation
    for(int i=0; i<100; ++i)
    {
        // Metropolis evolution for 100 steps
        G.MMC(scale, 100, engine);

        // Print the value of the action
        G.print_S(std::cout);
    }
}
```

This rather simple example does not take into account a number of subtleties. From a programming perspective, one would really want a more convenient way of constructing the class, perhaps taking the input data from a configuration file. Moreover, in a real simulation there would be a tuning phase, where the optimal values of parameters like the Metropolis scale factor are found, and a thermaliza-

tion phase where the geometry reaches equilibrium. The following more complete example shows how methods within the class itself allow to address these issues.

```
#include <iostream>
#include <fstream>
#include <ctime>
#include <armadillo>
#include <gsl/gsl_rng.h>
#include "geometry.hpp"

using namespace std;
using namespace arma;

int main()
{
    // Initialize the random number generator
    gsl_rng* engine = gsl_rng_alloc(gsl_rng_ranlxd1);
    gsl_rng_set(engine, time(NULL));


    // Open input file
    ifstream input;
    input.open("input.txt");

    // Create geometry from input file
    Geom24 G(input);
    input.close();


    // Open output files
    ofstream out_S("example_S.txt");
    ofstream out_HL("example_HL.txt");


    // Tuning with dual averaging
    double tgt = 0.8; // Target acceptance rate
    double dt = 0.001; // Initial guess for dt

    G.HMC_duav(10, dt, 10000, engine, tgt, "leapfrog");
    cout << "dual averaging complete" << endl;
    cout << "dual averaged dt: " << dt << endl;


    // Thermalization
    double acc_rate = G.HMC(10, dt, 10000, engine, "leapfrog");
    cout << "thermalization complete" << endl;
    cout << "acceptance rate: " << acc_rate << endl;
```

```
    // Hamiltonian Monte Carlo simulation
    for(int i=1; i<1000; ++i)
    {
        G.HMC(10, dt, 1000, engine, "leapfrog");
        G.print_S(out_S);
        G.print_HL(out_HL);
    }

    out_S.close();
    out_HL.close();
}
```

In this example the class was created from an input file using a specialized constructor:

```
Geom24(std::istream&);
```

which works with any input stream containing the following data in order: p, q, n, g_2.
The tuning phase uses the dual averaging routine to find the optimal value of the Hamiltonian Monte Carlo parameter dt given a target acceptance rate tgt. The prototype is:

```
void HMC_duav(const int& Nt, double& dt, const int& iter,
   gsl_rng* engine, const double& tgt,
   const std::string& integrator);
```

where the arguments are: number of integration steps N_t (int), integration step dt (double), total number of iterations (int), random number generator engine (gsl_rng*), target acceptance rate (double), integration method (string).
The dual averaging routine returns void, but the actual simulation routine has the acceptance rate as a return value:

```
// Thermalization
double acc_rate = G.HMC(10, dt, 10000, engine, "leapfrog");
cout << "thermalization complete" << endl;
cout << "acceptance rate: " << acc_rate << endl;
```

This is a useful sanity check to confirm the correct functioning of the dual averaging procedure. The prototype of the simulation routine is:

```
double HMC(const int& Nt, const double& dt, const int& iter,
gsl_rng* engine, const std::string& integrator);
```

Notice how, compared to `HMC_duav`, the integration step dt is now declared constant (the dual averaging routine has to change dt to find the optimal one, but during the actual simulation dt is fixed).
Finally, the simulation phase shows how the current value of the action and the H and L matrices can be printed to any valid output stream:

```
ofstream out_S("test_S.txt");
ofstream out_HL("test_HL.txt");
```

```
[...]

G.print_S(out_S);
G.print_HL(out_HL);
```

3.5 Benchmarks

This section presents the results of various tests performed on the implementation to check the correct functioning and the performance of the algorithms.

3.5.1 The action

There are two ways of calculating the action, both implemented in RFL. The first one is to build the full Dirac operator and simply calculate $g_2 \operatorname{Tr} D^2 + \operatorname{Tr} D^4$. This method will be referred to as brute-force. The second one uses the efficient formulas (2.36) and (2.55). The brute-force method is by far the easiest to implement numerically, but the computational overhead is large enough to make it completely impractical.
If S_{eff} denotes the value of the action given by (2.36) and (2.55) and S_{bf} denotes the brute-force value[1], a first test aimed at verifying the correct implementation of the formulas is to compare the two. More precisely, the following relative difference was averaged over 100 random Dirac operators:

$$T_1 := \frac{|S_{\text{eff}} - S_{\text{bf}}|}{S_{\text{eff}}}. \tag{3.6}$$

Since the calculation of S_{bf} and S_{eff} involve completely different operations, the test also indirectly verifies that (2.36) and (2.55) themselves are correct.
The test was conducted for matrix dimension 4, 8, 16 and 32 on (2,0), (3,0) and (4,0) Dirac operators. The results are shown in Table 3.1. The scaling of T_1 with n is found to be $O(n^2)$, with no difference across the tested (p, q) types. For completeness, the average order of magnitude of S_{eff} is given in Table 3.2.

	$n = 4$	$n = 8$	$n = 16$	$n = 32$
(2,0)	$1.2 \cdot 10^{-15}$	$4.8 \cdot 10^{-15}$	$2.0 \cdot 10^{-14}$	$8.3 \cdot 10^{-14}$
(3,0)	$9.0 \cdot 10^{-16}$	$3.1 \cdot 10^{-15}$	$1.4 \cdot 10^{-14}$	$5.7 \cdot 10^{-14}$
(4,0)	$2.2 \cdot 10^{-15}$	$9.7 \cdot 10^{-15}$	$3.5 \cdot 10^{-14}$	$1.5 \cdot 10^{-13}$

Table 3.1: Value of T_1 averaged over 100 random Dirac operators for various (p, q) types and matrix sizes.

The second test is aimed at comparing the performance of the two methods by measuring their raw speed and scaling. The total computation time in milliseconds of S_{bf} and S_{eff} for 10 random instances of Dirac operators is shown in Table 3.3 and Table 3.4 respectively. The test was conducted on the same system under similar conditions. The matrix multiplication and tensor product routines are the ones

[1] These two values are mathematically equal, but machine precision introduces small numerical discrepancies between them

	$n=4$	$n=8$	$n=16$	$n=32$
(2,0)	10^4	10^5	10^6	10^7
(3,0)	10^4	10^6	10^7	10^8
(4,0)	10^5	10^6	10^8	10^9

Table 3.2: Average order of magnitude of S_{eff} (and S_{bf}) for Dirac operators of various (p, q) types and matrix sizes.

provided by the Armadillo library, without modifications. For Dirac operators with $p + q = 4$ and 32×32 matrices, the brute-force method takes around 80 seconds to compute the action 10 times. Collecting enough samples in a Monte Carlo simulation would therefore be impossible without implementing S_{eff}. This is due mainly to the scaling in n: S_{bf} scales as $O(n^4)$ while S_{eff} scales as $O(n^2)$ (the scalings are given by tensor product and matrix multiplication complexity respectively).

	$n=4$	$n=8$	$n=16$	$n=32$
(2,0)	5	52	375	9282
(3,0)	9	61	631	13756
(4,0)	41	193	3343	80688

Table 3.3: Raw computing time of S_{bf} in milliseconds for 10 random Dirac operators of various (p, q) types and matrix sizes. The scaling in n is approximately $O(n^4)$.

	$n=4$	$n=8$	$n=16$	$n=32$
(2,0)	0.8	0.9	3	11
(3,0)	2	2	7	29
(4,0)	3	8	27	105

Table 3.4: Raw computing time of S_{eff} in milliseconds for 10 random Dirac operators of various (p, q) types and matrix sizes. The scaling in n is approximately $O(n^2)$.

3.5.2 Action difference in Metropolis

The difference in the action when a single entry is updated in one of the matrices can be calculated efficiently using the formulas given in Appendix A.2. This represents an important performance gain in Metropolis, where such differences need to be calculated repeatedly and take up most of the computational time.
Similarly as in the previous section, the action difference ΔS_{eff} calculated with the formulas of Appendix A.2 was compared numerically with ΔS_{bf}, the action difference calculated by computing the action from scratch before and after the update. Note that the efficient way of computing the whole action was used in ΔS_{bf}.

Table 3.5 shows the relative difference:

$$T_2 := \frac{|\Delta S_{\text{eff}} - \Delta S_{\text{bf}}|}{\Delta S_{\text{eff}}} \tag{3.7}$$

providing numerical validation to the formulas of Appendix A.2. As before, the order of magnitude of ΔS is also reported in Table 3.6.

	$n = 4$	$n = 8$	$n = 16$	$n = 32$
(2,0)	$2.2 \cdot 10^{-14}$	$4.9 \cdot 10^{-14}$	$1.9 \cdot 10^{-13}$	$1.5 \cdot 10^{-12}$
(3,0)	$5.9 \cdot 10^{-14}$	$8.4 \cdot 10^{-14}$	$2.2 \cdot 10^{-13}$	$4.6 \cdot 10^{-12}$
(4,0)	$5.6 \cdot 10^{-14}$	$9.6 \cdot 10^{-14}$	$1.1 \cdot 10^{-12}$	$6.0 \cdot 10^{-12}$

Table 3.5: Value of T_2 averaged over 100 random Dirac operators for various (p, q) types and matrix sizes.

	$n = 4$	$n = 8$	$n = 16$	$n = 32$
(2,0)	10^2	10^2	10^3	10^4
(3,0)	10^2	10^3	10^4	10^4
(4,0)	10^3	10^3	10^4	10^4

Table 3.6: Average order of magnitude of ΔS_{eff} (and ΔS_{bf}) for Dirac operators of various (p, q) types and matrix sizes.

The raw speed of the two methods is shown in Table 3.7 and 3.8. The scaling is $O(n^2)$ for both. That is to be expected, as their complexity is given only by matrix multiplication. However, ΔS_{eff} is several times faster to compute. For instance, for Dirac operators with $p + q = 3$ it is roughly 1.7 times faster, and more than 3.5 times faster for $p + q = 4$. Such a speedup could be the difference between a simulation that runs for a week and a simulation that runs for a month.

	$n = 16$	$n = 32$	$n = 64$	$n = 128$
(2,0)	64	128	562	2166
(3,0)	96	417	1676	6802
(4,0)	463	1775	8626	35183

Table 3.7: Raw computing time of ΔS_{bf} in milliseconds for 100 random Dirac operators of various (p, q) types and matrix sizes. The scaling in n is approximately $O(n^2)$.

3.5.3 Leapfrog

The integration algorithm of choice for Hamiltonian dynamics is the leapfrog integrator, described in Section 2.4. The reason leapfrog works better than other integrators (like Euler's method for example) is that it respects important properties of Hamiltonian dynamics: reversibility and phase space volume preservation. As shown in [46], if dt is the time discretization step, reversible integrators preserve the Hamiltonian up to an error that scales as an even power of dt. For leapfrog

	$n = 16$	$n = 32$	$n = 64$	$n = 128$
(2,0)	25	103	443	1812
(3,0)	56	218	961	3853
(4,0)	124	491	2222	9050

Table 3.8: Raw computing time of ΔS_{eff} in milliseconds for 100 random Dirac operators of various (p, q) types and matrix sizes. The scaling in n is approximately $O(n^2)$.

the error bound scales as dt^2.
Provided that the routine for calculating the Hamiltonian is correct, the best way to verify that the gradients in the leapfrog have been implemented correctly is to check that the theoretical error bound is respected. The test was conducted on Dirac operators of type (2,0), (3,0) and (4,0) and matrix size 8×8. The average energy violation was calculated over 10^4 Hamiltonian trajectories of fixed total length $L = dt \cdot N_t = 0.01$. To have more control over the simulation time, the total number of steps N_t was used as a variable instead of dt. One then expects the energy violation to scale as N_t^{-2}. Figure 3.1 shows the test results with logarithmic variables. The linear fit gives a slope of -2.02(1), -2.02(1) and -2.07(3) for (2,0), (3,0) and (4,0) respectively, compatible with the expected quadratic scaling.

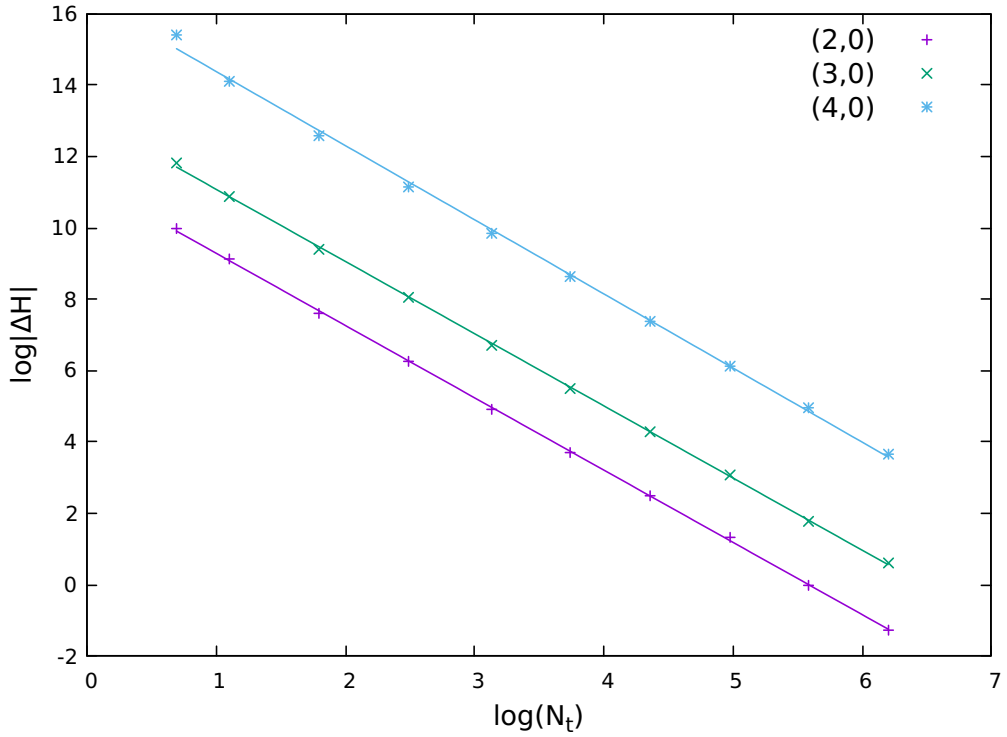

Figure 3.1: Plot of $\log|\Delta H|$ vs $\log N_t$ for (2,0), (3,0) and (4,0) Dirac operators. The linear fit gives a slope of -2.02(1), -2.02(1) and -2.07(3) respectively. The energy violation was averaged over 10^4 trajectories of fixed length $L = 0.01$.

3.5.4 Dual averaging

The tests presented so far gave evidence that the main components of the Monte Carlo routines in RFL are correctly implemented. The only piece missing before moving on to actual simulation benchmarks is to verify that the dual averaging algorithm presented in Section 2.6 works as intended.
A test was conducted on (2,0), (3,0) and (4,0) Dirac operators and matrix size 8×8 to check convergency of the Hamiltonian Monte Carlo acceptance rate towards a target value arbitrarily set at 0.6. The test is comprised of the following steps:

1. a Dirac operator is initialized in a random configuration;
2. the initial value of dt is set to 10^{-6}, small enough to ensure an acceptance rate of 1;
3. a certain number of dual averaging iterations are performed, updating the step size dt;
4. after dual averaging has ended yielding an optimal value for dt, 10^4 full Hamiltonian Monte Carlo iterations are performed and the average acceptance rate is measured.

Figure 3.2 shows how, even for the more complex (4,0) type, just a few thousand iterations of the algorithm are sufficient to output a dt that induces an acceptance rate close to the target one.

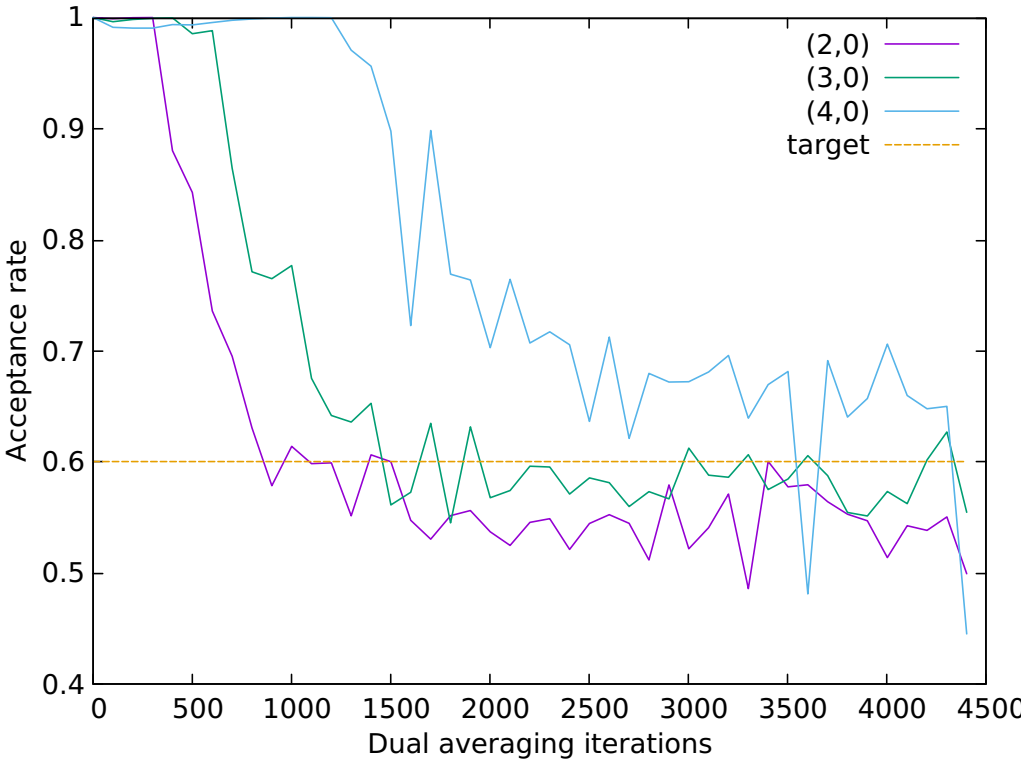

Figure 3.2: Plot of the acceptance rate as a function of the number of dual averaging iterations on dt for (2,0), (3,0) and (4,0) Dirac operators.

3.5.5 Benchmarking against an exact result

Although not many analytical results are available for the matrix integrals considered here, there is a non-trivial observable whose expectation value is known exactly for any geometry and any action polynomial in D. Computing this observable therefore is a good test for the numerical implementation.
Consider the following integral:

$$\int \sum_{ij} \frac{\partial}{\partial D_{ij}} \left(D_{ij} e^{-S[D]} \right) dD \tag{3.8}$$

where the sum is extended over all independent degrees of freedom of the Dirac operator and $S[D]$ is in general a sum of terms like $g_p \operatorname{Tr} D^p$. Since the integral is a total divergence, its value is given by the boundary contributions which vanish because of the exponential.
An explicit calculation of the right-hand side of Eq.(3.8) gives:

$$0 = \int \sum_{ij} \left(1 - \sum_p g_p D_{ij} \frac{\partial}{\partial D_{ij}} \operatorname{Tr} D^p \right) e^{-S[D]} dD \tag{3.9}$$

dividing by the partition function and rearranging the terms:

$$\sum_{ij} 1 = \frac{1}{\int e^{-S[D]}} \int \sum_{ij} \left(\sum_p g_p D_{ij} \frac{\partial}{\partial D_{ij}} \operatorname{Tr} D^p \right) e^{-S[D]} dD. \tag{3.10}$$

The LHS is then the number of degrees of freedom of the Dirac operator, while the RHS is rewritten using an identity proven in Appendix C:

$$\#\text{d.o.f.}(D) = \frac{1}{\int e^{-S[D]}} \int \left(\sum_p g_p \; p \operatorname{Tr} D^p \right) e^{-S[D]} dD = \left\langle \sum_p g_p \; p \;\; \operatorname{Tr} D^p \right\rangle . \tag{3.11}$$

To estimate the number of degrees of freedom recall that in the decomposition (2.20) the M_i matrices are all Hermitian, but the ones associated to an $\epsilon_i = -1$ are traceless. Therefore $\#\text{d.o.f.}(D) = n^2 m - m'$ where n is the dimension of the matrices, m is the total number of M_i matrices and m' is the number of traceless matrices. For the action considered in this work, the observable reads:

$$\#\text{d.o.f.}(D) = 2g_2 \left\langle \operatorname{Tr} D^2 \right\rangle + 4 \left\langle \operatorname{Tr} D^4 \right\rangle =: 2g_2 \left\langle S_2 \right\rangle + 4 \left\langle S_4 \right\rangle . \tag{3.12}$$

Numerical tests of HMC and Metropolis agree with the prediction (3.12) as shown in Table 3.9 for (2,0), (3,0) and (4,0) Dirac operators with 22×22 matrices.

3.5.6 Correlation time

Two samples s_1 and s_2 extracted with a Markov chain present a certain amount of correlation, *i.e.* denoting $P(s_2)$ the probability of extracting s_2 and $P(s_2 \mid s_1)$ the conditional probability of extracting s_2 given that at an earlier step s_1 was extracted, one has $P(s_2 \mid s_1) \neq P(s_2)$. The performance of a Monte Carlo algorithm is crucially dependent on the ability to extract as many uncorrelated

	Exact	Hamiltonian	Metropolis
(2,0)	968	969(2)	968(2)
(3,0)	1935	1934(2)	1931(2)
(4,0)	3868	3869(3)	3868(3)

Table 3.9: Expectation value $2g_2 \langle S_2 \rangle + 4 \langle S_4 \rangle$ calculated for (2,0), (3,0) and (4,0) Dirac operators and 22×22 matrices with Hamiltonian and Metropolis. The exact value is reported on the first column.

samples as possible. Taking the Metropolis algorithm as an example, the difference between two subsequent samples is at most a small displacement in one of the matrix entries. The two samples will therefore be rather redundant, not adding much information in the estimation of expectation values.
The concept of correlation can be formalized in the following way. Given an observable f, define the time-displaced autocorrelation function [39]:

$$\chi(t) = \int dt' \Big(f(t') - \langle f \rangle \Big) \Big(f(t'+t) - \langle f \rangle \Big). \tag{3.13}$$

On general grounds, $\chi(t)$ is expected to decay exponentially:

$$\chi(t) \sim e^{-\frac{t}{\tau}} \tag{3.14}$$

where τ is a typical timescale called the correlation time.
One should consider two samples to be uncorrelated when they are at least 2τ apart. One way to justify this is to look at the formula for the standard deviation of the mean. If N uncorrelated samples are collected, the error on an observable f is:

$$\sigma = \sqrt{\frac{1}{N-1} \Big[\langle f^2 \rangle - \langle f \rangle^2 \Big]} \sim \sqrt{\frac{1}{N} \Big[\langle f^2 \rangle - \langle f \rangle^2 \Big]} \tag{3.15}$$

for large N. In the presence of correlation between samples, the adjusted formula reads:

$$\sigma = \sqrt{\frac{2\tau}{N} \Big[\langle f^2 \rangle - \langle f \rangle^2 \Big]} \tag{3.16}$$

which is to say, the effective number of uncorrelated samples is $N/2\tau$.
The correlation time can be estimated by using a discretized version of (3.13). If the simulation is comprised of T Monte Carlo steps, then:

$$\chi(t) = \frac{1}{T-t} \left[\sum_{t'=0}^{T-t} f(t) f(t+t') \right] - \frac{1}{(T-t)^2} \left[\sum_{t'=0}^{T-t} f(t') \right] \left[\sum_{t'=0}^{T-t} f(t+t') \right] \tag{3.17}$$

and τ is estimated by fitting the exponential (3.14). Since the sums are taken up to $T-t$, the estimation of χ becomes more and more noisy as t approaches T. For this reason, one should take T large enough so that the exponential character is clearly visible over the noise threshold.
A first calculation of the correlation time for Metropolis and Hamiltonian Monte Carlo algorithms in RFL was performed on $(4,0)$ Dirac operators with 8×8 matrices and $g_2 = -4$. The acceptance rate was tuned at 0.8 and 0.2 for Hamiltonian

and Metropolis respectively. The results are shown in Table 3.10.

	τ	Time per move
Hamiltonian	1.20(3)	47 ms
Metropolis	1448(4)	0.18 ms

Table 3.10: Correlation time and time per move in milliseconds in Hamiltonian and Metropolis Monte Carlo for (4,0) Dirac operators with 8×8 matrices and $g_2 = -4$.

As expected two consecutive samples in Metropolis are much more correlated, but take less time to compute. Even then, the estimated time to collect two uncorrelated samples is 112 ms for Hamiltonian and 521 ms for Metropolis, almost a five-fold performance increase in favour of the Hamiltonian algorithm.
The difference is even more impressive in the presence of critical points. Type (2,0) Dirac operators with 32×32 matrices undergo a second order phase transition at around $g_2 = -2.75$. In this case the Hamiltonian algorithm collects uncorrelated samples almost 16 times faster than Metropolis. The results are shown in Table 3.11.

	τ	Time per move
Hamiltonian	1.0(1)	5.7 ms
Metropolis	901(4)	0.1 ms

Table 3.11: Correlation time and time per move in milliseconds in Hamiltonian and Metropolis Monte Carlo for (2,0) Dirac operators with 32×32 matrices and $g_2 = -2.75$, where a second order phase transition occurs.

3.5.7 Error analysis

Given N correlated measurements $f_1, \ldots, f_N$ of an observable f, the error on $\langle f \rangle$ can be estimated with the formula (3.16) which assumes knowledge (via fitting) of the autocorrelation time of f. However, if the measurements are grouped in bins of size n, one could compute N/n separate estimates $\langle f \rangle_1, \ldots, \langle f \rangle_{N/n}$ which will form a set of uncorrelated measurements for large enough n.
The main computational resource used for the numerical simulations of this thesis was the University of Nottingham on-premise HPC facility, Augusta. Thanks to the many CPU cores available on Augusta, several copies of each simulation could be run in parallel, each copy initialized with a different random seed and therefore each copy corresponding to an independent Markov chain. The natural binning given by treating expectation values of each chain as independent samples was used to avoid the problem of correlation altogether.
Once a certain number of uncorrelated samples is available, a common algorithm for error estimate if the jackknife [39]. Given N uncorrelated measurements $f_1, \ldots, f_N$, the jackknife algorithm requires the calculation of $N + 1$ expectation values. The first one is simply:

$$\langle f \rangle = \frac{1}{N} \sum_{i=1}^{N} f_i \tag{3.18}$$

and the remaining N are obtained by leaving out each time one of the measurements:

$$\langle f \rangle_j = \frac{f_1 + \ldots f_{j-1} + f_{j+1} + \ldots f_N}{N-1}. \tag{3.19}$$

The jackknife estimate of the error on $\langle f \rangle$ is then given by:

$$\sqrt{\sum_{i=1}^{N} (\langle f \rangle - \langle f \rangle_i)^2}. \tag{3.20}$$

Chapter 4

One-matrix models

4.1 Introduction

The simplest Dirac operators are the ones built from (1,0) and (0,1) Clifford modules. These Dirac operators give rise to random matrix models that involve a single Hermitian matrix. Many analytical techniques have been developed for random one-matrix models, as opposed to multi-matrix models which are considerably less understood. Indeed, the eigenvalue distribution of (1,0) and (0,1) Dirac operators with quadratic plus quartic potential can be viewed as the solution to a Riemann-Hilbert problem [17] and solved for exactly. This technique has first been applied with success in [16], but their results were compromised by small oversights. The use of Monte Carlo simulations in combination with the Riemann-Hilbert approach has allowed to improve on the findings of [16] to the extent where the analytical results are in excellent agreement with the numerics.

4.2 The matrix models

The (1,0) and (0,1) Dirac operators are:

$$D_{(1,0)} = \{H, \cdot\} \tag{4.1}$$
$$D_{(0,1)} = [H, \cdot] \tag{4.2}$$

where H is a Hermitian $n \times n$ matrix.
The action $S = g_2 \operatorname{Tr} D^2 + \operatorname{Tr} D^4$ in terms on the H matrix is:

$$S_{(1,0)} = 2n(g_2 \operatorname{Tr} H^2 + \operatorname{Tr} H^4) + 2g_2(\operatorname{Tr} H)^2 + 8 \operatorname{Tr} H \operatorname{Tr} H^3 + 6(\operatorname{Tr} H^2)^2 \tag{4.3}$$
$$S_{(0,1)} = 2n(g_2 \operatorname{Tr} H^2 + \operatorname{Tr} H^4) - 2g_2(\operatorname{Tr} H)^2 - 8 \operatorname{Tr} H \operatorname{Tr} H^3 + 6(\operatorname{Tr} H^2)^2. \tag{4.4}$$

As in standard random matrix theory one can integrate over unitary transformations, which amounts to the Vandermonde determinant:

$$\int e^{-S[H]}\, dH = \int e^{-S[\lambda]} \prod_{i<j} |\lambda_i - \lambda_j|^2\, d\lambda \tag{4.5}$$

where λ_i are the eigenvalues of H. The initial integral over $n \times n$ Hermitian matrices becomes an integral over n real variables with action:

$$S = 2n \sum_{i=1}^{n} \Big[g_2 \lambda_i^2 + \lambda_i^4 \Big] + 2 \sum_{i,j=1}^{n} \Big[\pm g_2 \lambda_i \lambda_j \pm 4 \lambda_i \lambda_j^3 + 3 \lambda_i^2 \lambda_j^2 \Big] - \sum_{1 \le i < j \le n} 2 \log |\lambda_i - \lambda_j| \tag{4.6}$$

where $\pm$ refers to the $(1,0)$ and $(0,1)$ respectively. Or, written in a way that optimizes calculations on a computer:

$$\begin{aligned} S_{(1,0)} = 2 \sum_{i=1}^{n} \Big[g_2 (n+1) \lambda_i^2 + (n+7) \lambda_i^4 \Big] \\ + 2 \sum_{1 \le i < j \le n} \Big[2 g_2 \lambda_i \lambda_j + 4 (\lambda_i \lambda_j^3 + \lambda_j \lambda_i^3) + 6 \lambda_i^2 \lambda_j^2 - \log |\lambda_i - \lambda_j| \Big] \end{aligned} \tag{4.7}$$

$$\begin{aligned} S_{(0,1)} = 2(n-1) \sum_{i=1}^{n} \Big[g_2 \lambda_i^2 + \lambda_i^4 \Big] \\ + 2 \sum_{1 \le i < j \le n} \Big[- 2 g_2 \lambda_i \lambda_j - 4 (\lambda_i \lambda_j^3 + \lambda_j \lambda_i^3) + 6 \lambda_i^2 \lambda_j^2 - \log |\lambda_i - \lambda_j| \Big]. \end{aligned} \tag{4.8}$$

From the n eigenvalues of H one can easily compute the n^2 eigenvalues of D:

$$\lambda_i + \lambda_j \quad \text{for } D_{(1,0)} \tag{4.9}$$

$$\lambda_i - \lambda_j \quad \text{for } D_{(0,1)}. \tag{4.10}$$

4.3 Density of states, existing results

In [16] the density of states for H and D is calculated analytically in the large n limit for both (1,0) and (0,1), for which the results turn out to be identical. The existence of a transition between a single-cut and a double-cut phase is proven, with the critical point being at $g_2 = -5\sqrt{2}/2$.
The results are as follows. The density of states for the H matrix in the single-cut phase supported on $[-2a, 2a]$ is:

$$\Psi(x) = \frac{1}{\pi} (-4a^2 + \frac{1}{2a^2} + 4x^2) \sqrt{4a^2 - x^2} \tag{4.11}$$

with a given as the solution to:

$$g_2 = -24a^6 - 9a^2 + \frac{1}{4a^2}$$

which, modulo a sign, has only one real root.
For the double-cut phase supported on $[-a, -b] \cup [b, a]$, the density of states for H is:

$$\Psi(x) = \frac{2}{\pi} |x| \sqrt{(x^2 - a^2)(b^2 - x^2)} \tag{4.12}$$

with:

$$a^2 = -\frac{1}{5}g_2 + \frac{\sqrt{2}}{2}$$

$$b^2 = -\frac{1}{5}g_2 - \frac{\sqrt{2}}{2}.$$

The density of states ρ for D is calculated as the convolution:

$$\rho(x) = \int \Psi(x \mp y)\Psi(y)\ dy \tag{4.13}$$

and, although not solvable analytically, it can be calculated numerically from (4.11) and (4.12). The first sign of a problem appears in (4.12), which is not properly normalized. The issue is more serious than it might seem, since the normalization condition is not imposed a posteriori on the density, but rather it comes from the theory of Riemann-Hilbert problems itself. Further issues will be uncovered by simulating the model non-perturbatively with Metropolis Monte Carlo.

4.4 Density of states, numerical results

Monte Carlo simulations give a different picture as the one described in the previous section.
In the one-cut phase the numerical results seem to resemble the analytical ones, but for a different value of the coupling constant as Figure 4.1 shows.
In the two-cut phase, the two models behave differently. The spectrum of a typical H matrix in the $(1, 0)$ ensemble is not symmetric around zero, nor is its support, breaking the assumptions made in [16]. This asymmetry doesn't seem to be a finite-size effect, since there is no appreciable scaling with the matrix size (Figure 4.2). The $(0, 1)$ model is on the other hand symmetric, but again the numerical and analytical results agree for different values of the coupling constant (Figure 4.3). Moreover, the transition appears to be between $g_2 = -3.2$ and $g_2 = -3.3$ for the $(1, 0)$, and somewhere between $g_2 = -5.5$ and $g_2 = -6$ for the $(0, 1)$ (Figure 4.4 and 4.5), instead of the predicted $g_2 \approx -3.5$ for both.

4.5 Asymmetry tests on the $(1, 0)$ model

The typical H matrix after the phase transition has an asymmetric spectrum that is very different from the one calculated analytically by [16]. In order to test whether the asymmetry is a simulation artifact (due, for example, to failed thermalization) or a real effect, simulations where performed with two types of constraint on the spectrum.

- Type 1
  An infinite potential wall was introduced so that the spectrum is forced to lie within $[-a, a]$ for some $a \in \mathbb{R}$, without necessarily being symmetric.

- Type 2
  The spectrum is forced to be symmetric around zero. After a certain time,

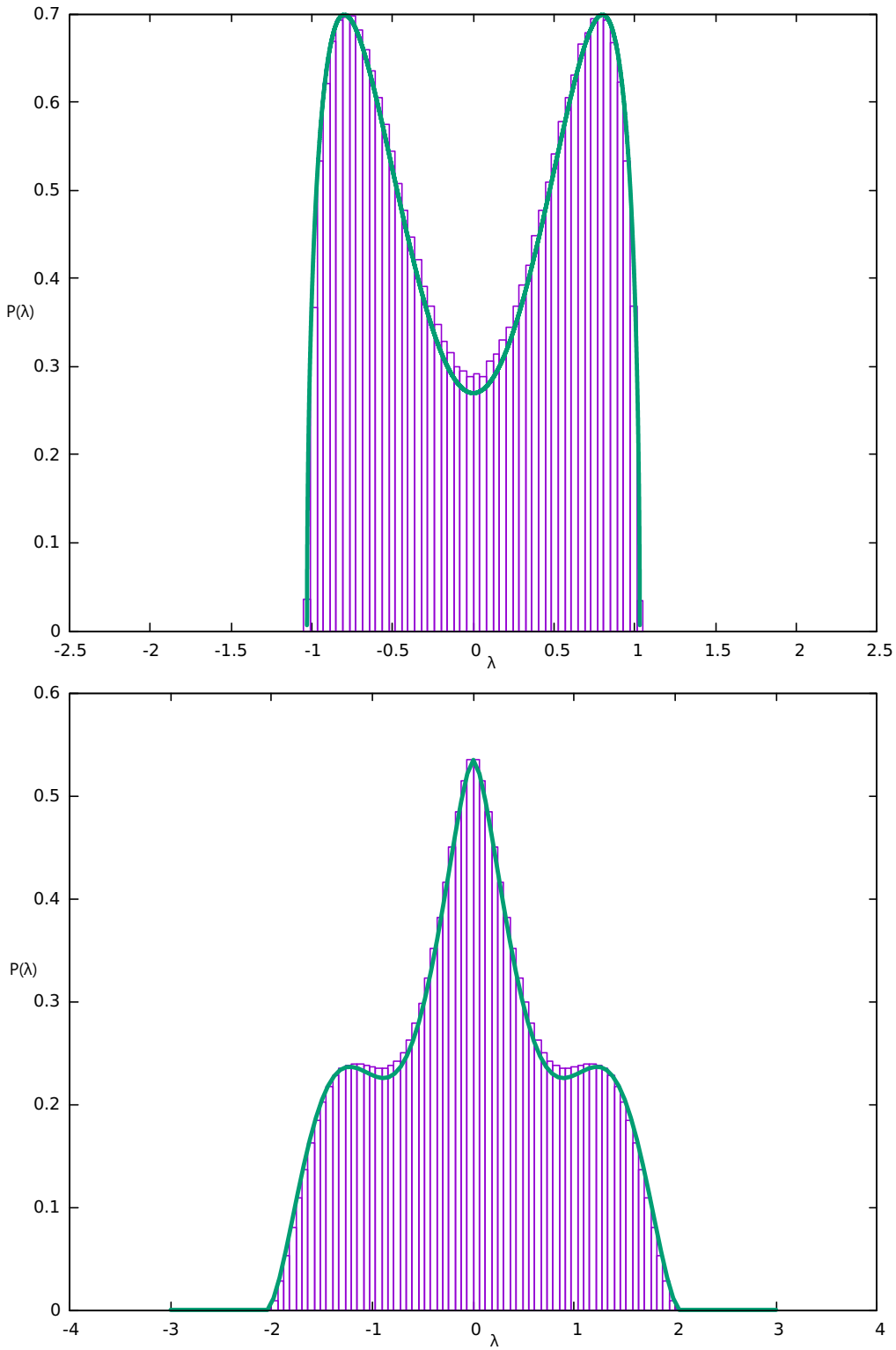

Figure 4.1: Density of states obtained numerically for H (top) and D (bottom) in the $(1,0)$ model, $n = 1024$, at $g_2 = -3$ (purple boxes). The results seem to agree with the one-cut analytical formula, but calculated at $g_2 = -1.89$ (green line).

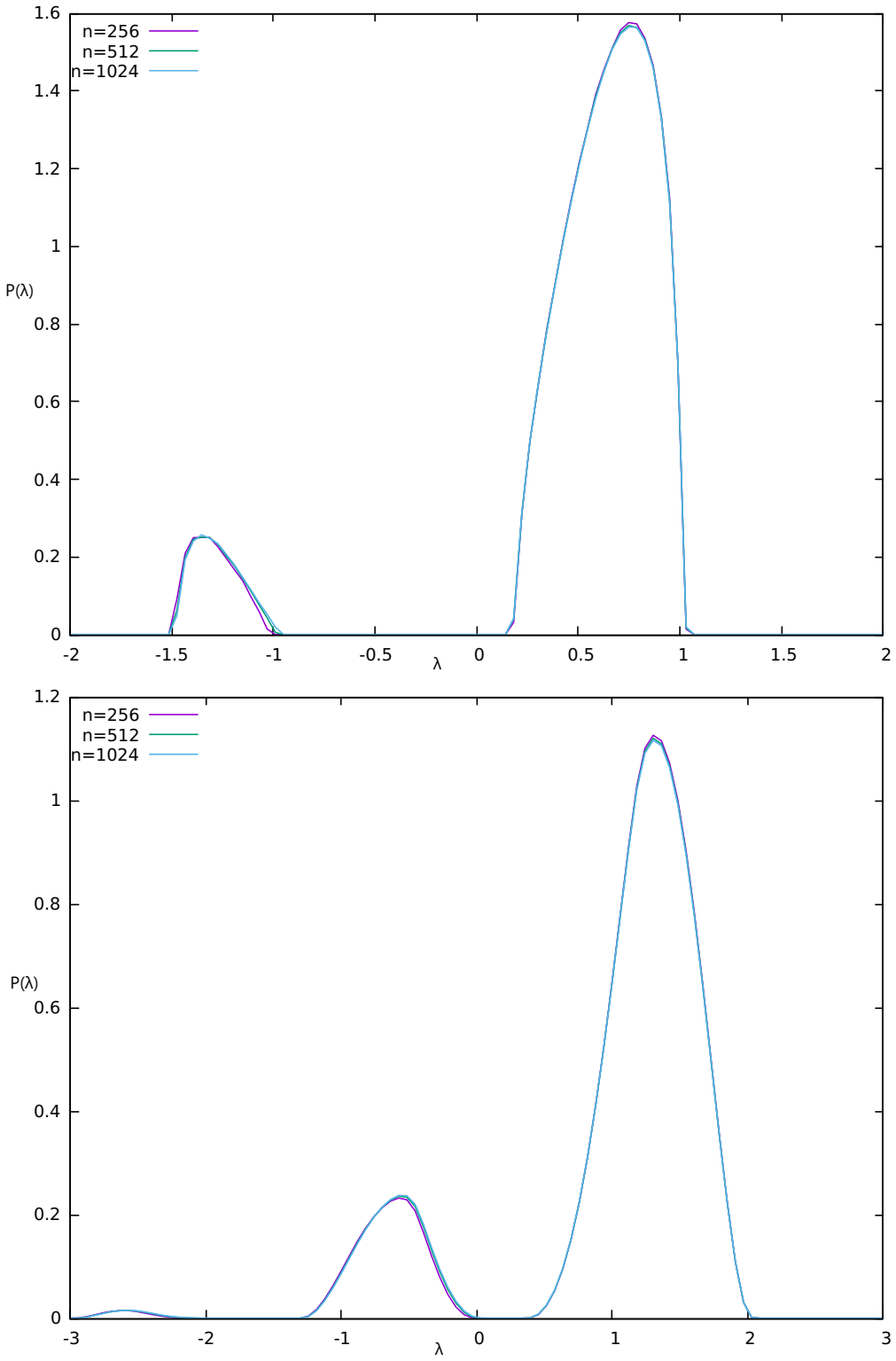

Figure 4.2: Spectrum of a typical H matrix (top) and Dirac operator D (bottom) in the $(1, 0)$ model for various matrix sizes at $g_2 = -4$.

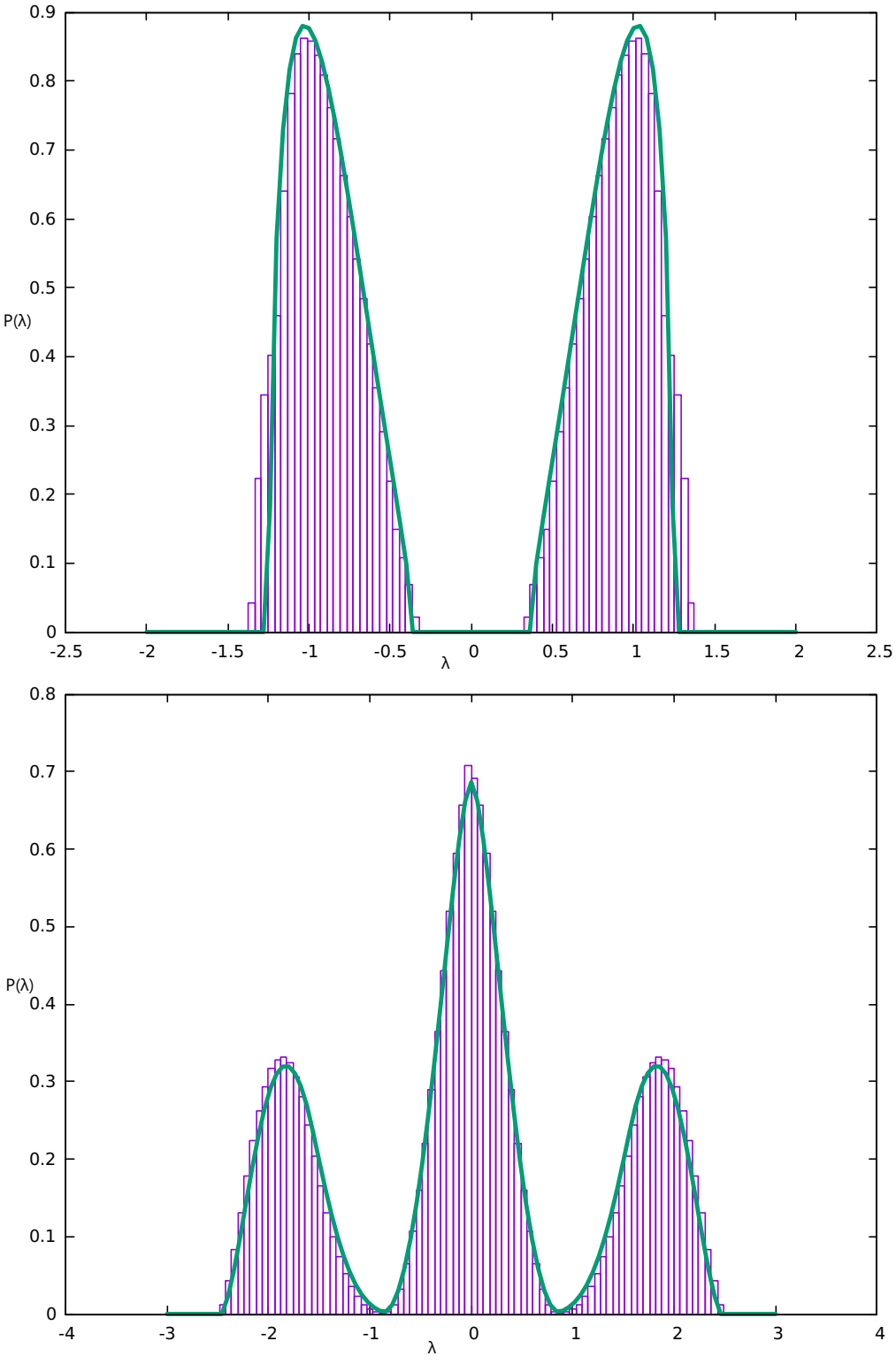

Figure 4.3: Density of states obtained numerically for H (top) and D (bottom) in the $(0,1)$ model, $n = 1024$, at $g_2 = -7$ (purple boxes). The results seem to agree with the two-cut analytical formula, but calculated at $g_2 = -4.2$ (green line).

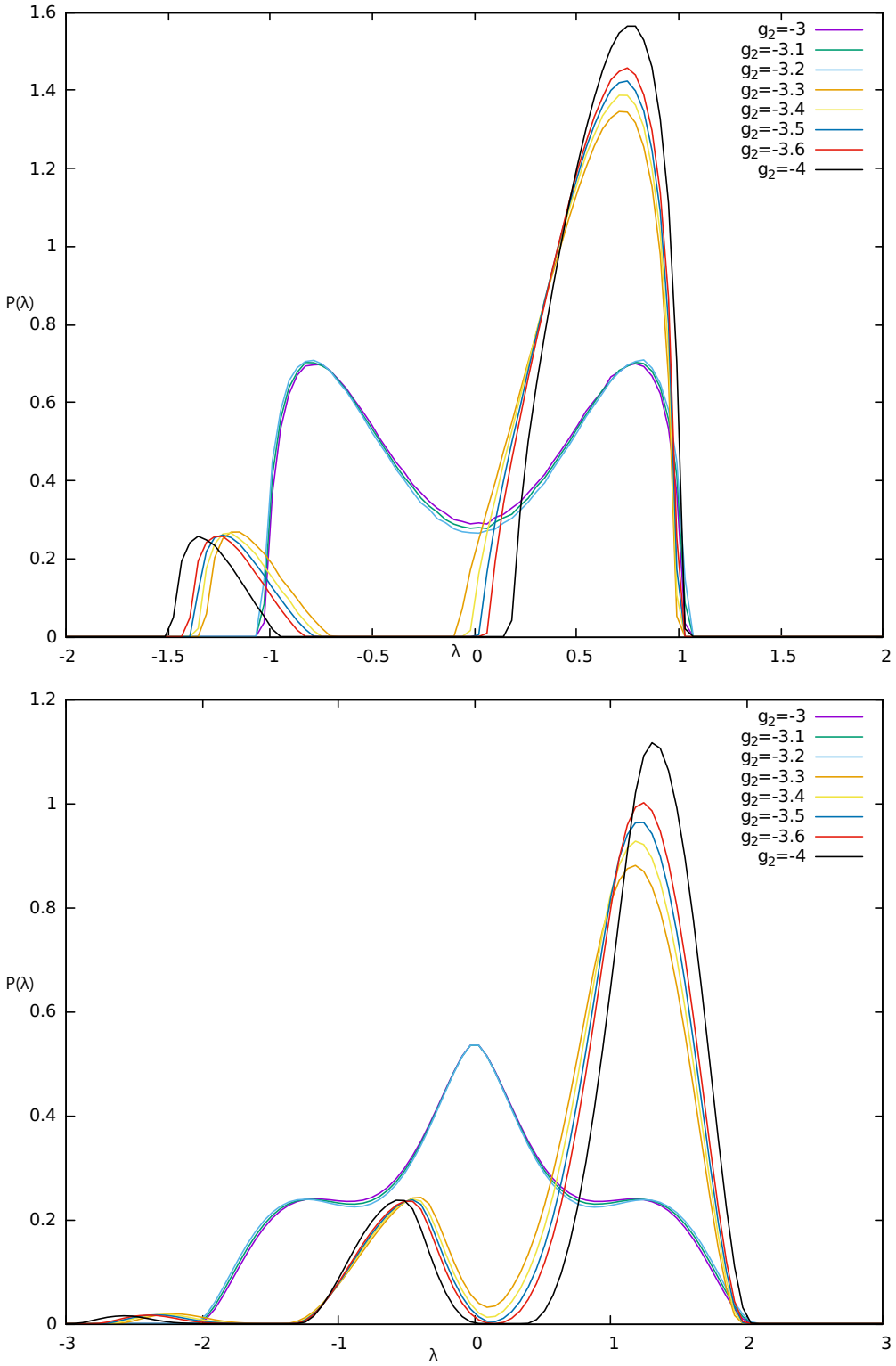

Figure 4.4: Density of states obtained numerically for H (top) and D (bottom) in the $(1,0)$ model, $n = 1024$, at various values of g_2. The one- to two-cut transition appears at $g_2 \in (-3.2, -3.3)$ instead of the predicted -3.5.

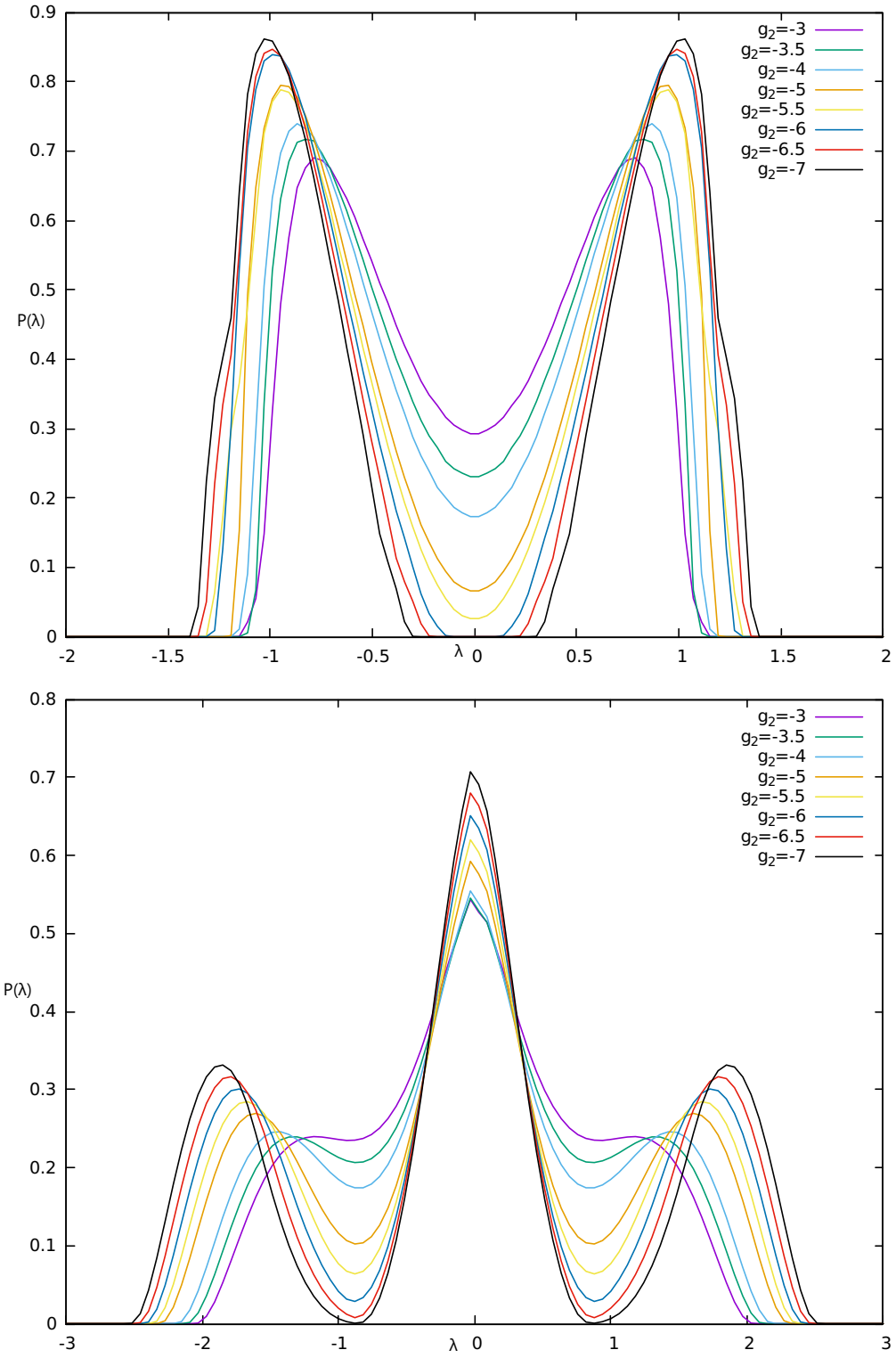

Figure 4.5: Density of states obtained numerically for H (top) and D (bottom) in the $(0, 1)$ model, $n = 1024$, at various values of g_2. The one- to two-cut transition appears at $g_2 \in (-5.5, -6)$ instead of the predicted -3.5.

the constraint is released to check whether the spectrum relaxes again towards the asymmetric shape.

The results are as follows. When the wall in the first type of constraint cuts part of the smaller peak, the eigenvalues that have been cut-off just accumulate against the wall (purple and green line in Figure 4.6). If instead the wall is placed so that is does not interfere with the smaller peak, no difference is observed with the unconstrained model (blue and orange line in Figure 4.6).
On the other hand, the second (and stronger) constraint gives a distribution identical to the $(0, 1)$, as shown in Figure 4.7. Suddenly releasing the constraint makes the distribution fall back to the asymmetric shape, confirming that that is indeed the stable vacuum configuration.
The key to understanding the inconsistencies between theory and numerics is to revisit the Riemann-Hilbert method.

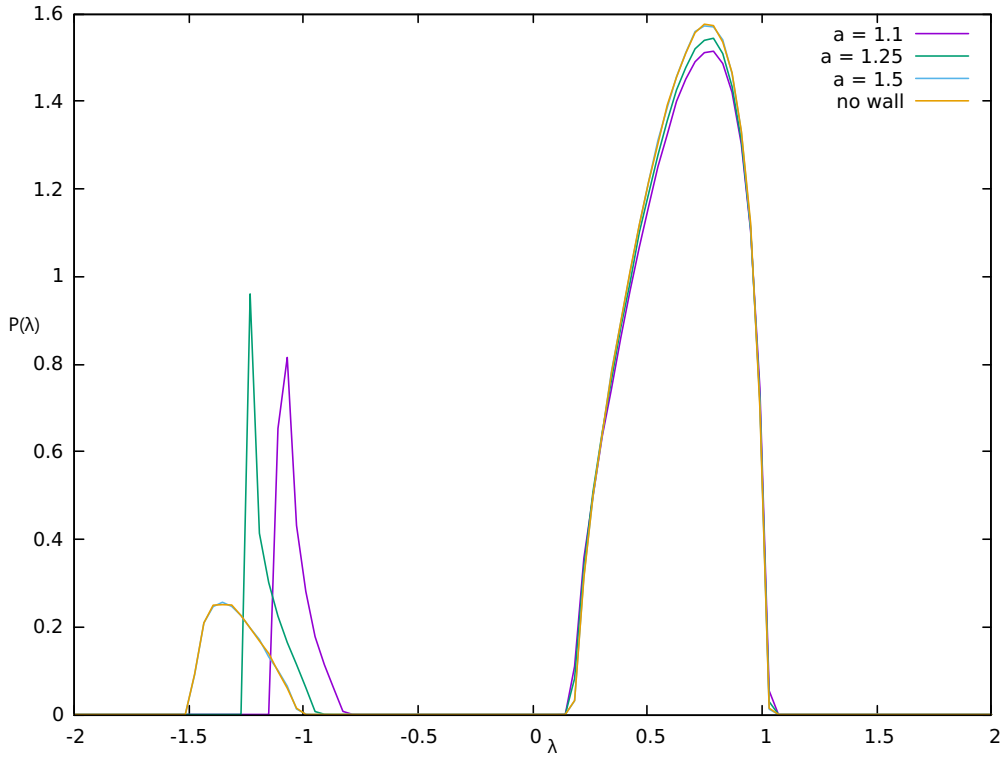

Figure 4.6: Density of states obtained numerically for H in the $(1, 0)$ model, with a potential wall in various positions. For comparison, the unconstrained spectrum is also included. $n = 256$, $g_2 = -4$.

4.6 Riemann-Hilbert approach to equilibrium measures

The authors of [16] rely on the method outlined in [17] for finding the equilibrium measure in the two-cut case, which amounts to solving a Riemann-Hilbert problem. The method is general enough to be applied to k cuts, although [17] deals with potentials with no interactions between eigenvalues, as opposed to the present

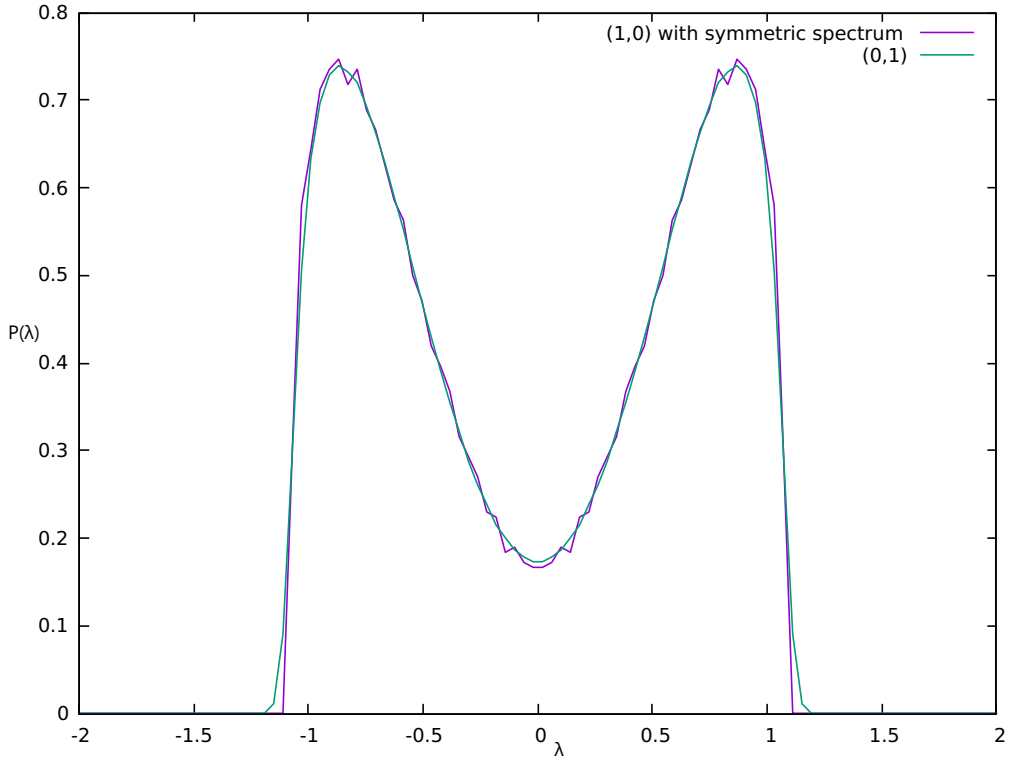

Figure 4.7: Density of states obtained numerically for H in the $(1,0)$ model, with spectrum forced to be symmetric around zero. For comparison, the spectrum of a $(0,1)$ matrix is also included. $n = 256$ for $(1,0)$, $n = 1024$ for $(0,1)$, $g_2 = -4$.

case.
Riemann-Hilbert problems are slightly more general than what is needed here, which is called a scalar R-H problem. The statement of the problem goes as follows. Let Σ be a finite union of disjoint open intervals on $\mathbb{R}$. Given a smooth function $v(z) : \Sigma \to \mathbb{C}$, find a complex-valued function m such that:

1. m is analytic in $\mathbb{C} \setminus \Sigma$;
2. $m_+(z) = m_-(z)v(z)$, $z \in \mathbb{R}$;
3. $m(z) \to 1$ as $z \to \infty$.

The notation $m_\pm$ indicates the limit of $m(z')$ for $z' \to \Sigma$ from above and below respectively. Notice that whenever a subscript $+$ or $-$ is added to a function, the argument of that function is automatically real as $\Sigma \subset \mathbb{R}$. Taking the logarithm in 2. gives:

$$\log m_+(z) - \log m_-(z) = \log v(z) \tag{4.14}$$

whose solution is given by the Plemelj formula:

$$\log m(z) = \frac{1}{2\pi i} \int_\Sigma \frac{\log v(s)}{s - z} ds, \quad \text{for } z \in \mathbb{C} \setminus \Sigma. \tag{4.15}$$

The way an equilibrium measure $\psi(x)$ can be found by solving a scalar R-H problem is to consider the Borel transform of ψ:

$$G(z) = \frac{1}{i\pi}\int_{\Sigma}\frac{\psi(y)}{y-z}dy \tag{4.16}$$

where Σ here indicates the support of ψ. To fix the notation, call a_i and b_i the extrema of the i-th cut:

$$\Sigma = \bigcup_{i=1}^{k}(a_i, b_i). \tag{4.17}$$

Consider

$$q(z) = \prod_{i=1}^{k}(z-a_i)(z-b_i) \tag{4.18}$$

and define $\sqrt{q(z)}$ such that $\sqrt{q(z)} \sim +z^k$ as $z \to \infty$. Notice that $\sqrt{q(z)}_+ = -\sqrt{q(z)}_-$. Consider now:

$$\tilde{G}(z) = \frac{G(z)}{\sqrt{q(z)}} \tag{4.19}$$

and write:

$$\tilde{G}_+(z) - \tilde{G}_-(z) = \frac{G_+(z) + G_-(z)}{\sqrt{q(z)}_+}. \tag{4.20}$$

By the real version of the Sokhotski-Plemelj theorem, $G_\pm(x)$ can be written as a principal value plus Dirac delta:

$$\begin{aligned} G_\pm(x) &= \lim_{\epsilon\to 0}\frac{1}{i\pi}\int\frac{\psi(y)}{y-(x\pm i\epsilon)}dy \\ &= \frac{1}{i\pi}\left(-P.V.\int\frac{\psi(y)}{y-x}dy \pm i\pi\int\delta(y-x)\psi(y)dy\right) \\ &= iH\psi(x) \pm \psi(x) \end{aligned} \tag{4.21}$$

where $H\psi(x)$ indicates the Hilbert transform of ψ:

$$H\psi(x) = \frac{1}{\pi}P.V.\int_{\Sigma}\frac{\psi(y)}{x-y}dy. \tag{4.22}$$

Therefore:

$$\tilde{G}_+(z) - \tilde{G}_-(z) = 2i\frac{H\psi(z)}{\sqrt{q(z)}_+} \tag{4.23}$$

defines a scalar R-H problem. Once $G(z)$ is found by solving (4.23) with the Plemelj formula, it is clear from (4.21) that the equilibrium measure is given by $\mathrm{Re}\, G(x)_+$.

The discussion so far holds under rather general assumptions and does not make reference to the specific model one is trying to solve. The last step is to find an expression for the Hilbert transform of ψ. This is found by setting up a minimization problem for the equilibrium measure $\psi(x)dx$, which will establish a relation between the Hilbert transform of ψ and the action of the random matrix model.

Consider the action for the $(1,0)$ and $(0,1)$ models written in terms of the eigen-

values:

$$S = n\sum_{i=1}^{n} V(\lambda_i) + \sum_{i,j=1}^{n} U(\lambda_i, \lambda_j) + \sum_{i\neq j} \log|\lambda_i - \lambda_j|^{-1}. \tag{4.24}$$

where

$$V(x) = 2g_2x^2 + 2x^4 \tag{4.25}$$

$$U(x,y) = \pm 2g_2xy \pm 8xy^3 + 6x^2y^2. \tag{4.26}$$

Define the counting measure:

$$d\mu_n(x) = \frac{1}{n}\sum_i \delta(\lambda_i - x)dx \tag{4.27}$$

so that the action can be rewritten in the continuum:

$$S = n^2\left[\int V(x)d\mu_n(x) + \int\int U(x,y)d\mu_n(x)d\mu_n(y) + \int\int \log|x-y|^{-1}d\mu_n(x)d\mu_n(y)\right]. \tag{4.28}$$

In the large n limit the assumption is that the equilibrium measure is the unique measure that minimizes the action, and therefore one is led to the minimization problem:

$$\inf_{\mu}\left[\int V(x)d\mu(x) + \int\int U(x,y)d\mu(x)d\mu(y) + \int\int \log|x-y|^{-1}d\mu(x)d\mu(y)\right]. \tag{4.29}$$

By repeating the proof of theorem 6.126 in [17] it follows that, if the equilibrium measure is assumed to be of the form $d\mu(x) = \psi(x)dx$ for a continuous function ψ with compact support, the minimization problem is equivalent to the existence of a real constant l such that:

$$2\int \log|x-y|^{-1}\psi(y)dy + 2\int U(x,y)\psi(y)dy + V(x) \geq l \quad \forall x \in \mathbb{R} \tag{4.30}$$

$$2\int \log|x-y|^{-1}\psi(y)dy + 2\int U(x,y)\psi(y)dy + V(x) = l \quad \{x : \psi(x) \geq 0\} \tag{4.31}$$

where, importantly, U is used in its symmetrized form:

$$U(x,y) = \pm 2g_2xy \pm 4xy^3 \pm 4x^3y + 6x^2y^2. \tag{4.32}$$

To eliminate the constant l from (4.31) one can take a derivative with respect to x. The U integral is a sum of terms of the form:

$$\int x^j y^k \psi(y)dy. \tag{4.33}$$

Recalling the definition of the k-th moment m_k of a measure:

$$m_k := \int y^k \psi(y)dy \tag{4.34}$$

it is clear that ultimately the U integral is a polynomial in x with coefficients depending on the moments of ψ:

$$\int U(x,y)\psi(y)dy = \pm 2g_2 m_1 x \pm 4m_3 x \pm 4m_1 x^3 + 6m_2 x^2 \tag{4.35}$$

and therefore its derivative with respect to x can be calculated in a straightforward way. The derivative of the logarithmic term, which is actually a weak derivative in the distributional sense, is proportional to the Hilbert transform of ψ [17]:

$$2\frac{\partial}{\partial x}\int \log|x-y|^{-1}\psi(y)dy = -2\pi H\psi(x) \tag{4.36}$$

and therefore (4.31) can be written:

$$2\pi H\psi(x) = 2\ P.V.\int_\Sigma \frac{\psi(y)}{x-y}dy = 8x^3 \pm 24m_1x^2 + (4g_2+24m_2)x \pm 4g_2m_1 \pm 8m_3 \tag{4.37}$$

where the RHS is the derivative:

$$\mathcal{V}'(x) := \frac{\partial}{\partial x}\left[2\int U(x,y)\psi(y)dy + V(x)\right] \tag{4.38}$$

The R-H problem (4.23) is then given in its final form:

$$\tilde{G}_+(z) - \tilde{G}_-(z) = \frac{\frac{i}{\pi}\mathcal{V}'(z)}{\sqrt{q(z)}_+}. \tag{4.39}$$

Compare $\mathcal{V}'(x)$ with the one given in [16]:

$$8x^3 + (4g_2+12m_2)x \pm 2g_2m_1 \pm 8m_3. \tag{4.40}$$

The quadratic term $24m_1x^2$ is missing because U is not properly symmetrized, and there is a missing factor of 2 in the terms coming from the double integral in U. The correct $\mathcal{V}'(x)$ given by (4.37) will fix the incompatibilities found between the numerical simulations and [16].

4.7 One-cut solution

In the one-cut phase, the numerical simulations show a symmetric eigenvalue density and no differences between the $(1,0)$ and $(0,1)$ models. The analysis in [16] is therefore valid insofar as the correct $\mathcal{V}'(x)$ is used. If the density function is supported on $[-2a, 2a]$, then:

$$\psi(x) = \frac{1}{\pi}\left(-4a^2 + \frac{1}{2a^2} + 4x^2\right)\sqrt{4a^2-x^2} \tag{4.41}$$

with a and the coupling constant g_2 related in the following way:

$$g_2 = \frac{1}{4a^2} - 12a^2 - 48a^6 \tag{4.42}$$

which has a unique real solution:

$$a^2 = \frac{1}{4\sqrt{3}} \left(\sqrt{F(g_2) - 2} + \sqrt{-\frac{\sqrt{3} g_2}{\sqrt{F(g_2) - 2}} - 4 - F(g_2)} \right) \tag{4.43}$$

with

$$F(g_2) := \frac{(32 + 3g_2^2)^{\frac{1}{3}}}{2^{\frac{2}{3}}}. \tag{4.44}$$

The relation between a and g_2 given here agrees very well with the numerics.

4.8 Two-cut solution

The authors in [16] perform the two-cut analysis assuming that the support is symmetric around zero. The numerical results show how this assumption is too restrictive, at least for the $(1, 0)$ model. The correct solution can be found by adapting the approach outlined in [17].
Set up the scalar Riemann-Hilbert problem (4.39), with solution:

$$G(z) = \frac{\sqrt{q(z)}}{2\pi i} \int_\Sigma \frac{\frac{i}{\pi}\mathcal{V}'(s)}{\sqrt{q(s)}_+} \frac{ds}{s - z} \tag{4.45}$$

and $\mathcal{V}'(z)$ given by (4.38). In order to rewrite (4.45), assume that the support is comprised of exactly two intervals $(a_1, b_1),\ (a_2, b_2)$ (as the numerics suggest) and consider the integral

$$\int_C \frac{\frac{i}{\pi}\mathcal{V}'(s)}{\sqrt{q(s)}} \frac{ds}{s - z} \tag{4.46}$$

where $C = c_1 + \ldots + c_{16}$ is shown in Figure 4.8. The branch cuts are indicated by dashed lines, and $c_2,\ c_4,\ c_6,\ c_8,\ c_{10},\ c_{12},\ c_{14},\ c_{16}$ lie on the axis even though they are drawn away from it.
The interior of the contour is simply connected and lies entirely in the domain of analyticity of $\mathcal{V}'/\sqrt{q}$, therefore Cauchy's integral formula can be applied and gives:

$$\int_C \frac{\frac{i}{\pi}\mathcal{V}'(s)}{\sqrt{q(s)}} \frac{ds}{s - z} = 2\pi i \frac{\frac{i}{\pi}\mathcal{V}'(z)}{\sqrt{q(z)}}. \tag{4.47}$$

On the other hand, since the contributions of c_2 and c_{16} cancel with the contributions of c_8 and c_{10}, when taking the limit for $R \to \infty$ and $\epsilon \to 0$ the integral evaluates to

$$\int_C \frac{\frac{i}{\pi}\mathcal{V}'(s)}{\sqrt{q(s)}} \frac{ds}{s - z} = 2 \int_\Sigma \frac{\frac{i}{\pi}\mathcal{V}'(s)}{\sqrt{q(s)}_+} \frac{ds}{s - z} + \int_c \frac{\frac{i}{\pi}\mathcal{V}'(s)}{\sqrt{q(s)}} \frac{ds}{s - z} \tag{4.48}$$

where the first term on the RHS comes from the two clockwise dumbbells ($c_3 + c_4 + c_5 + c_6 + c_7$ and $c_{11} + c_{12} + c_{13} + c_{14} + c_{15}$), while $c = c_1 + c_9$ is the large circle of radius R oriented counter-clockwise. Inverting the orientation of c and putting

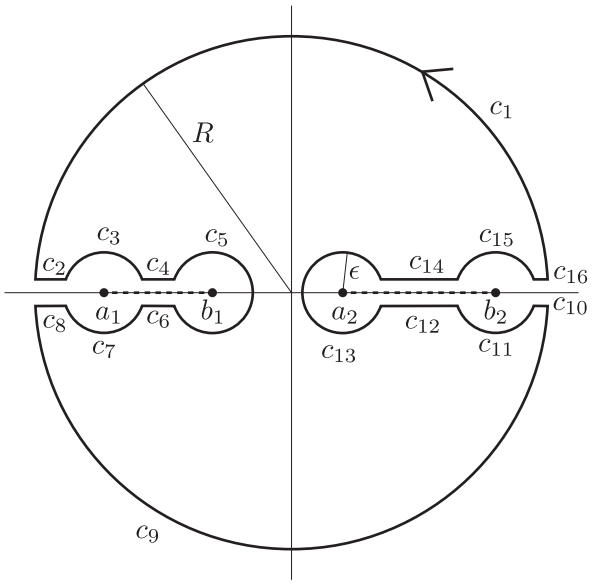

Figure 4.8: Integration contour

(4.47) and (4.48) together gives:

$$2\pi i \frac{\frac{i}{\pi}\mathcal{V}'(z)}{\sqrt{q(z)}} + \int_{-c} \frac{\frac{i}{\pi}\mathcal{V}'(s)}{\sqrt{q(s)}} \frac{ds}{s-z} = 2\int_{\Sigma} \frac{\frac{i}{\pi}\mathcal{V}'(s)}{\sqrt{q(s)}_+} \frac{ds}{s-z} \tag{4.49}$$

and finally, substituting (4.45) in (4.49):

$$G(z) = \frac{i}{2\pi}\mathcal{V}'(z) + \frac{\sqrt{q(z)}}{4\pi i} \int_{-c} \frac{\frac{i}{\pi}\mathcal{V}'(s)}{\sqrt{q(s)}} \frac{ds}{s-z} \tag{4.50}$$

which is equation (6.149) in [17].
The integral in (4.50) can be computed by calculating the residue at infinity:

$$\frac{1}{2\pi i}\int_{-c} \frac{\mathcal{V}'(s)}{\sqrt{q(s)}} \frac{ds}{s-z} = \mathrm{Res}_{s=\infty}\left(\frac{\mathcal{V}'(s)}{\sqrt{q(s)}}\frac{1}{s-z}\right) = -\,\mathrm{Res}_{t=0}\left(\frac{1}{t^2}\frac{\mathcal{V}'\left(\frac{1}{t}\right)}{\sqrt{q\left(\frac{1}{t}\right)}}\frac{1}{\frac{1}{t}-z}\right) \tag{4.51}$$

A Laurent expansion of the function yields:

$$\begin{aligned}
&\mathcal{V}'\left(\frac{1}{t}\right)\frac{1}{t^2}\left[\left(\frac{1}{t}-a_1\right)\left(\frac{1}{t}-a_2\right)\left(\frac{1}{t}-b_1\right)\left(\frac{1}{t}-b_2\right)\right]^{-\frac{1}{2}}\left(\frac{1}{t}-z\right)^{-1} \\
&= \mathcal{V}'\left(\frac{1}{t}\right)\frac{1}{t^2}\left[\frac{1}{t^4}\left(1-ta_1\right)\left(1-ta_2\right)\left(1-tb_1\right)\left(1-tb_2\right)\right]^{-\frac{1}{2}}\left(\frac{1}{t}(1-tz)\right)^{-1} \\
&= \sum_{k,i_1,i_2,j_1,j_2=0}^{\infty} z^k \binom{i_1-\frac{1}{2}}{i_1}\binom{i_2-\frac{1}{2}}{i_2}\binom{j_1-\frac{1}{2}}{j_1}\binom{j_2-\frac{1}{2}}{j_2} a_1^{i_1}a_2^{i_2}b_1^{j_1}b_2^{j_2}\ \mathcal{V}'\left(\frac{1}{t}\right)\ t^{1+k+i_1+i_2+j_1+j_2}
\end{aligned} \tag{4.52}$$

where convergency of the series is guaranteed by the fact that $|t| \ll 1$.
The potential $\mathcal{V}'\left(\frac{1}{t}\right)$ has the general form:

$$\mathcal{V}'\left(\frac{1}{t}\right) = \alpha\frac{1}{t^3} + \beta\frac{1}{t^2} + \gamma\frac{1}{t} + \delta. \tag{4.53}$$

By power counting, it follows that the only terms with a non-vanishing residue arise from the quadratic term in $\mathcal{V}'$ and all indices $k,\ i_1,\ i_2,\ j_1,\ j_2$ equal to zero, or from the cubic term and one index among $k,\ i_1,\ i_2,\ j_1,\ j_2$ equal to 1. Therefore:

$$\frac{1}{2\pi i}\int_{-c}\frac{\mathcal{V}'(s)}{\sqrt{q(s)}}\frac{ds}{s-z} = -\beta - \alpha\left(z + \frac{a_1+a_2+b_1+b_2}{2}\right) \tag{4.54}$$

and (4.50) evaluates to:

$$G(z) = \frac{i}{2\pi}\mathcal{V}'(z) + \frac{\sqrt{q(z)}}{2\pi i}\left[\beta + \alpha\left(z + \frac{a_1+a_2+b_1+b_2}{2}\right)\right]. \tag{4.55}$$

The distribution $\psi(x)$ is then found as:

$$\psi(x) = \operatorname{Re} G(x)_+ \tag{4.56}$$

which requires some caution when taking the limit of the square root. When approaching the (a_1, b_1) cut from above, the arguments of the factors in $\sqrt{q(z)}$ are:

$$\begin{aligned}
\arg(z-a_1) &= \epsilon \\
\arg(z-b_1) &= \pi - \epsilon \\
\arg(z-a_2) &= \pi - \epsilon \\
\arg(z-b_2) &= \pi - \epsilon
\end{aligned}$$

and the square root evaluates to:

$$\left(\rho_{a_1}\rho_{b_1}\rho_{a_2}\rho_{b_2}e^{i\epsilon}e^{i(\pi-\epsilon)}e^{i(\pi-\epsilon)}e^{i(\pi-\epsilon)}\right)^{\frac{1}{2}} \sim \rho e^{\frac{3}{2}i\pi} = -i\rho \tag{4.57}$$

while instead, when approaching the (a_2, b_2) cut from above, the arguments are:

$$\begin{aligned}
\arg(z-a_1) &= \epsilon \\
\arg(z-b_1) &= \epsilon \\
\arg(z-a_2) &= \epsilon \\
\arg(z-b_2) &= \pi - \epsilon
\end{aligned}$$

and the square root evaluates to:

$$\left(\rho_{a_1}\rho_{b_1}\rho_{a_2}\rho_{b_2}e^{i\epsilon}e^{i\epsilon}e^{i\epsilon}e^{i(\pi-\epsilon)}\right)^{\frac{1}{2}} \sim \rho e^{i\frac{\pi}{2}} = i\rho. \tag{4.58}$$

In other words, the square root is imaginary and it picks up a sign on the (a_1, b_1) cut. Ultimately one finds:

$$\begin{aligned}\psi(x) = \operatorname{Re} G(x)_+ &= \frac{1}{2\pi}\sqrt{-q(x)}\ \operatorname{cut}(x)\left[\beta + \alpha\left(x + \frac{a_1+a_2+b_1+b_2}{2}\right)\right] \\ &= \frac{1}{2\pi}\sqrt{-q(x)}\ \operatorname{cut}(x)\left[\pm 24 m_1 + 8\left(x + \frac{a_1+a_2+b_1+b_2}{2}\right)\right]\end{aligned} \tag{4.59}$$

where $\operatorname{cut}(x) = \pm 1$ is defined in the following way:

$$\operatorname{cut}(x) = \begin{cases} -1 & x \in (a_1, b_1) \\ +1 & x \in (a_2, b_2) \end{cases} \tag{4.60}$$

Notice how for a symmetric density (i.e. $a_1 = -b_2$, $b_1 = -a_2$ and vanishing odd moments), the formula agrees with [16] if not for a factor of 2. This goes back to the observation that the density found by [16] in the two-cut case is not properly normalized, which in turn is a consequence of an overall factor of 2 missing in the U integral of (4.31).
The two matrix models will now be discussed separately. The $(0, 1)$ model will be discussed first, as the assumption of a symmetric density simplifies the calculations. Afterwards, the full asymmetric case for the $(1, 0)$ model is presented.

4.8.1 Symmetric two-cut case: the $(0, 1)$ model

A symmetric density translates to two conditions:

1. the support is assumed to be $(-b, -a) \cup (a, b)$ for $0 < a < b$;
2. all the odd moments vanish.

The density (4.59) therefore reads:

$$\psi(x) = \frac{4}{\pi}|x|\sqrt{-(x^2 - a^2)(x^2 - b^2)}. \tag{4.61}$$

Following [17], the relations between g_2, a and b are found by imposing the correct asymptotics for the Borel transform $G(z)$ as $z \to \infty$. There are three equations to satisfy:

$$\int_\Sigma \frac{\mathcal{V}'(s)}{\sqrt{q(s)}_+} ds = 0 \tag{4.62}$$

$$\int_\Sigma \frac{\mathcal{V}'(s)}{\sqrt{q(s)}_+} s\ ds = 0 \tag{4.63}$$

$$\int_\Sigma \frac{\mathcal{V}'(s)}{\sqrt{q(s)}_+} s^2\ ds = -2\pi i. \tag{4.64}$$

By using the same contour of Figure 4.8 and noticing that this time no poles are included in the interior, the integrals reduce once again to calculating residues at

infinity:

$$\int_\Sigma \frac{\mathcal{V}'(s)}{\sqrt{q(s)}_+} s^k \, ds = \frac{1}{2}\int_{-c_1} \frac{\mathcal{V}'(z)}{\sqrt{q(z)}} z^k \, dz = -\pi i \, \mathrm{Res}_{t=0}\left(\frac{1}{t^{2+k}} \frac{\mathcal{V}'\left(\frac{1}{t}\right)}{\sqrt{q\left(\frac{1}{t}\right)}}\right). \quad (4.65)$$

A Laurent expansion gives:

$$\frac{1}{t^{2+k}} \frac{\mathcal{V}'\left(\frac{1}{t}\right)}{\sqrt{q\left(\frac{1}{t}\right)}} = \sum_{i,j=0}^{\infty} \binom{i-\frac{1}{2}}{i} \binom{j-\frac{1}{2}}{j} a^{2i} b^{2j} \; \mathcal{V}'\left(\frac{1}{t}\right) t^{2i+2j-k} \quad (4.66)$$

and therefore the three conditions (4.62), (4.63) and (4.64) read:

$$4(a^2+b^2) + 4g_2 + 24m_2 = 0 \quad (4.67)$$
$$4g_2 m_1 + 8m_3 + 12m_1(a^2+b^2) = 0 \quad (4.68)$$
$$2g_2(a^2+b^2) + 12m_2(a^2+b^2) + 2a^2b^2 + 3(a^4+b^4) = 2. \quad (4.69)$$

Notice that the second equation is automatically satisfied because of vanishing odd moments. The second moment m_2 is correctly computed in [16] as

$$m_2 = -\frac{\gamma}{\alpha} \quad (4.70)$$

with α and γ defined to be the coefficient of the cubic and linear term respectively in (4.53), which in this case gives[1]:

$$m_2 = -\frac{g_2}{8}. \quad (4.71)$$

One is then left with two equations:

$$a^2 + b^2 = -\frac{g_2}{4} \quad (4.72)$$
$$\frac{g_2}{4}(a^2+b^2) + \frac{3}{2}(a^2+b^2)^2 - 2a^2b^2 = 1. \quad (4.73)$$

The first one says that a and b can be written as:

$$a = r\cos\theta, \quad b = r\sin\theta \quad (4.74)$$

for $r^2 = -g_2/4$ and some angle θ. Solving the system for θ ultimately gives:

$$a^2 = -\frac{g_2}{8} - \frac{\sqrt{2}}{2} \quad (4.75)$$
$$b^2 = -\frac{g_2}{8} + \frac{\sqrt{2}}{2}. \quad (4.76)$$

[1]The moment m_2 is $\mathbb{E}[\mathrm{Tr}\, H^2]/n$, and it is a recurring feature of random matrix models coming from fuzzy spectral triples, even higher types like the $(2,0)$, that this quantity turns out to be $-g_2/8$ on the stationary solution.

As a final observation, notice that the extremal value of g_2 for which the expression for a^2 makes sense is:

$$g_2 = -4\sqrt{2} \tag{4.77}$$

which, as confirmed by the numerics, is the critical coupling separating one- and two-cut solution in the $(0,1)$ model.

4.8.2 Asymmetric two-cut case: the $(1,0)$ model

In the absence of symmetry the density (4.59) cannot be simplified further. It is reported here for convenience:

$$\psi(x) = \frac{1}{2\pi}\sqrt{-q(x)}\ \mathrm{cut}(x)\left[24m_1 + 8\left(x + \frac{a_1 + a_2 + b_1 + b_2}{2}\right)\right]. \tag{4.78}$$

A first test for the validity of (4.78) would be to find the unknown parameters a_1, a_2, b_1, b_2 and m_1 by fitting the function to the numerical data. For $n = 1024$ and $g_2 = -4$, the fit shown in Figure 4.9 gives:

$$\begin{aligned} a_1 &= -1.4770(5) \\ b_1 &= -0.949(4) \\ a_2 &= 0.1897(8) \\ b_2 &= 1.0130(3) \\ m_1 &= 0.5022(7) \end{aligned} \tag{4.79}$$

The agreement between the fitted function and the numerical data is excellent.

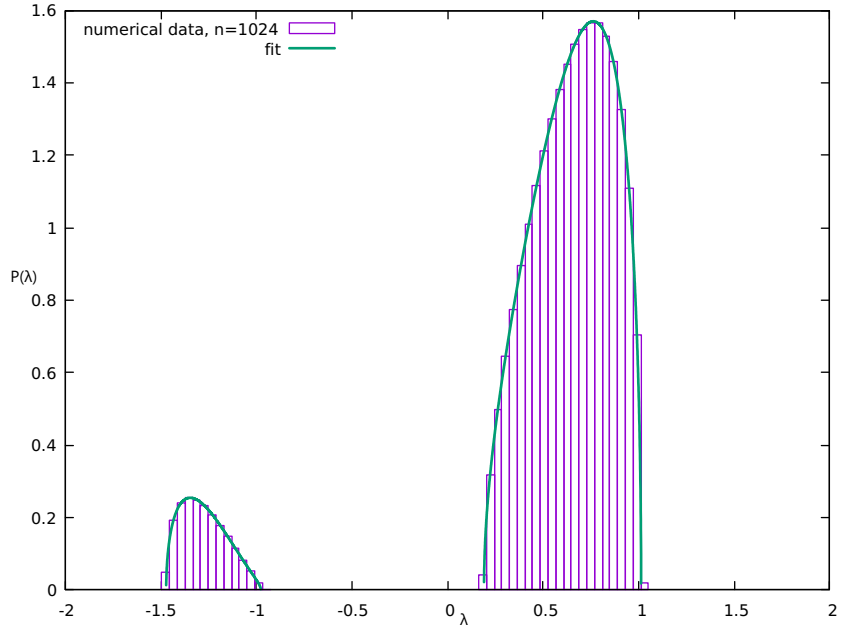

Figure 4.9: Fitting the numerical data of a simulation performed with $n = 1024$ and $g_2 = -4$ gives a good agreement with the density (4.78)

The asymptotics of the Borel transform give conditions relating the support end-points and the coupling constant, but they are not enough to fix all parameters.

The three equations are still (4.62), (4.63) and (4.64), but this time there are no relations a priori among the endpoints in $\sqrt{q(s)}$. The Laurent expansion in this case reads:

$$\frac{1}{t^{2+k}}\frac{\mathcal{V}'\left(\frac{1}{t}\right)}{\sqrt{q\left(\frac{1}{t}\right)}} = \sum_{i_1,i_2,j_1,j_2=0}^{\infty} \binom{i_1-\frac{1}{2}}{i_1}\binom{i_2-\frac{1}{2}}{i_2}\binom{j_1-\frac{1}{2}}{j_1}\binom{j_2-\frac{1}{2}}{j_2} a_1^{i_1} a_2^{i_2} b_1^{j_1} b_2^{j_2}\ \mathcal{V}'\left(\frac{1}{t}\right) \times t^{i_1+i_2+j_1+j_2-k}. \tag{4.80}$$

The higher k, the more contributions there are to the residue because more index combinations result in t^{-1}. The worst case arises from the cubic term in $\mathcal{V}'$ and $k=2$. In this case one needs to find all combinations of i_1, i_2, j_1, j_2 such that:

$$t^{i_1+i_2+j_1+j_2-5} = t^{-1}. \tag{4.81}$$

It is not hard to see that these correspond to all possible integer partitions of $5-1=4$ of length ≤ 4. They are reported in Appendix D, where partition y of integer x is denoted $C^{(x)}_{(y)}$. The three equations (4.62), (4.63) and (4.64) then read:

$$\alpha C^{(2)} + \beta C^{(1)} + \gamma = 0 \tag{4.82}$$

$$\alpha C^{(3)} + \beta C^{(2)} + \gamma C^{(1)} + \delta = 0 \tag{4.83}$$

$$\alpha C^{(4)} + \beta C^{(3)} + \gamma C^{(2)} + \delta C^{(1)} = 2 \tag{4.84}$$

where

$$C^{(x)} := \sum_y C^{(x)}_{(y)}. \tag{4.85}$$

Notice how these equations involve the moments m_1, m_2 and m_3 through the coefficients β, γ and δ, as well as the endpoints a_1, a_2, b_1 and b_2 through the coefficients $C^{(x)}_{(y)}$, for a total of 7 unknowns.
The moments can be calculated from their definition (4.34) with ψ as in (4.78). Using once again the same contour technique, the moments turn out to be:

$$m_k = (12m_1 + 2(a_1+a_2+b_1+b_2))\,\mathrm{Res}_{t=0}\left(\frac{1}{t^{k+2}}\sqrt{q\left(\frac{1}{t}\right)}\right) + 4\,\mathrm{Res}_{t=0}\left(\frac{1}{t^{k+3}}\sqrt{q\left(\frac{1}{t}\right)}\right) \tag{4.86}$$

and the corresponding Laurent expansion reads:

$$\frac{1}{t^p}\sqrt{q\left(\frac{1}{t}\right)} = \sum_{i_1,i_2,j_1,j_2} \binom{\frac{1}{2}}{i_1}\binom{\frac{1}{2}}{i_2}\binom{\frac{1}{2}}{j_1}\binom{\frac{1}{2}}{j_2}(-1)^{i_1+i_2+j_1+j_2}\ a_1^{i_1} a_2^{i_2} b_1^{j_1} b_2^{j_2}\ t^{i_1+i_2+j_1+j_2-p-2} \tag{4.87}$$

which shows how the expression becomes rather cumbersome even for low moments. For m_1, for example, $p = 3, 4$ in (4.87), and therefore the contributions to the residues come from integer partitions of 4 and 5 with length ≤ 4. As before, the coefficient are reported in Appendix D to avoid clutter and denoted $D^{(x)}_{(y)}$.
The moments then read:

$$m_1 = -(12m_1 + 2(a_1 + a_2 + b_1 + b_2))D^{(4)} - 4D^{(5)} \tag{4.88}$$
$$m_2 = -(12m_1 + 2(a_1 + a_2 + b_1 + b_2))D^{(5)} - 4D^{(6)} \tag{4.89}$$
$$m_3 = -(12m_1 + 2(a_1 + a_2 + b_1 + b_2))D^{(6)} - 4D^{(7)} \tag{4.90}$$

where

$$D^{(x)} := \sum_y D^{(x)}_{(y)}. \tag{4.91}$$

Equations (4.82), (4.83), (4.84), (4.88), (4.89), (4.90) are ultimately a system of six equations in seven unknowns. The solution is too hard to find even numerically, but what one can do to validate the method is to substitute the empirical values (4.79) and solve the remaining equations in m_2 and m_3 .
Equation (4.88) simplifies completely to

$$0 = 0.002 \pm 0.017. \tag{4.92}$$

Equations (4.82) and (4.89) give two independent estimates of m_2:

$$m_2 = 0.5661 \pm 0.0013 \tag{4.93}$$
$$m_2 = 0.564 \pm 0.019. \tag{4.94}$$

Equation (4.90) gives an estimate of m_3:

$$m_3 = 0.156 \pm 0.022. \tag{4.95}$$

And finally equations (4.83) and (4.84) can be solved together to give a simultaneous estimate of m_2 and m_3:

$$m_2 = 0.566 \pm 0.006 \tag{4.96}$$
$$m_3 = 0.153 \pm 0.014. \tag{4.97}$$

The values are all consistent with each other, which is a good sanity check. A direct estimate of the moments from the Monte Carlo gives:

$$m_2 = 0.56249 \pm 0.00001 \tag{4.98}$$
$$m_3 = 0.15490 \pm 0.00002 \tag{4.99}$$

which are very close to the ones given in (4.93), (4.94), (4.95), (4.96) and (4.97).

Chapter 5

Two-matrix models

5.1 Two-matrix models

5.1.1 Introduction

The following is a study concerning the classical solutions to the equations of motion for the two-matrix, two-trace random matrix models arising from Dirac operators with action $S = g_2 \operatorname{Tr} D^2 + \operatorname{Tr} D^4$. There are three distinct models, obtained starting from a (p, q) Clifford module where $p + q = 2$. For this reason the three models will be referred to as the (2,0), (1,1) and (0,2).
The Clifford gamma matrices are two-dimensional and can be taken to be a pair of Hermitian or anti-Hermitian Pauli matrices. The corresponding Dirac operator will contain all linearly independent products of these, but subject to the axioms of non-commutative geometry [8]. Taking products of gamma matrices will produce something proportional to either the third Pauli matrix or the identity matrix, but these are excluded in all three cases because the Dirac operator is required to anti-commute with the chirality operator, which is proportional to the third Pauli matrix.
The three Dirac operators ultimately are:

$$D_{(2,0)} = \sigma_1 \otimes \{m_1, \cdot\} + \sigma_2 \otimes \{m_2, \cdot\} \tag{5.1}$$
$$D_{(1,1)} = \sigma_1 \otimes [m_1, \cdot] + \sigma_2 \otimes \{m_2, \cdot\} \tag{5.2}$$
$$D_{(0,2)} = \sigma_1 \otimes [m_1, \cdot] + \sigma_2 \otimes [m_2, \cdot] \tag{5.3}$$

where m denotes an arbitrary Hermitian matrix.
Commutators and anti-commutators are represented as linear operators in $\mathbb{C}^n \otimes \mathbb{C}^n$:

$$\{m, \cdot\} = m \otimes \mathbb{1}_n + \mathbb{1}_n \otimes m^T \tag{5.4}$$
$$[m, \cdot] = m \otimes \mathbb{1}_n - \mathbb{1}_n \otimes m^T. \tag{5.5}$$

Since the only real difference in the three models from a computational perspective is a sign due to the presence of a commutator or anti-commutator, where possible they will be treated collectively by storing the sign in a factor ϵ:

$$D = \sum_a \sigma_a \otimes \left(m_a \otimes \mathbb{1}_n + \epsilon_a \mathbb{1}_n \otimes m_a^T \right) \tag{5.6}$$

where the sum is over the two terms appearing in the Dirac operator.
Finally, where convenient, the whole expression for a commutator or anti-commutator will be condensed in a single capital letter:

$$D = \sum_a \sigma_a \otimes M_a. \tag{5.7}$$

5.1.2 Computing the action

Using the properties of the Pauli matrices, the action is easily computed in all three models:

$$S = 2g_2 \operatorname{Tr}(M_1^2 + M_2^2) + 2 \operatorname{Tr}(M_1^4 + M_2^4 + 4M_1^2 M_2^2 - 2M_1 M_2 M_1 M_2). \tag{5.8}$$

At this level the three models are equivalent, the difference being hidden in the ϵ signs inside the M matrices. Expanding these gives:

$$\begin{aligned} S = {} & 4g_2 \Big[n \operatorname{Tr}(m_1^2 + m_2^2) + \epsilon_1 (\operatorname{Tr} m_1)^2 + \epsilon_2 (\operatorname{Tr} m_2)^2 \Big] \\ & + 4n \Big[\operatorname{Tr}(m_1^4 + m_2^4) + 4 \operatorname{Tr} m_1^2 m_2^2 - 2 \operatorname{Tr} m_1 m_2 m_1 m_2 \Big] \\ & + 4 \Big[4\epsilon_1 \operatorname{Tr} m_1^3 \operatorname{Tr} m_1 + 4\epsilon_2 \operatorname{Tr} m_2^3 \operatorname{Tr} m_2 + 3(\operatorname{Tr} m_1^2)^2 + 3(\operatorname{Tr} m_2^2)^2 \Big] \\ & + 16\epsilon_1 \operatorname{Tr} m_1 m_2^2 \operatorname{Tr} m_1 + 16\epsilon_2 \operatorname{Tr} m_2 m_1^2 \operatorname{Tr} m_2 \\ & + 8 \operatorname{Tr} m_1^2 \operatorname{Tr} m_2^2 + 16\epsilon_1\epsilon_2 (\operatorname{Tr} m_1 m_2)^2. \end{aligned} \tag{5.9}$$

It is clear from this expression that the models are two-matrix, double-trace random matrix models indexed by $(\epsilon_1, \epsilon_2) = (1,1),\ (1,-1),\ (-1,-1)$.
As it will become clear later, the whole dynamics of the model is driven by the interplay between trace and traceless part of m_1 and m_2. If $m_i = t_i \mathbb{1} + v_i$, with $\operatorname{Tr} v_i = 0$, then the action is:

$$\begin{aligned} S = {} & 4g_2 n \left[n(1+\epsilon_1) t_1^2 + n(1+\epsilon_2) t_2^2 + \operatorname{Tr} v_1^2 + \operatorname{Tr} v_2^2 \right] + 16n^2 \left[(1+\epsilon_1) t_1^4 + (1+\epsilon_2) t_2^4 \right] \\ & + 48n \left[(1+\epsilon_1) t_1^2 \operatorname{Tr} v_1^2 + (1+\epsilon_2) t_2^2 \operatorname{Tr} v_2^2 \right] + 16n \left[(1+\epsilon_1) t_1 \operatorname{Tr} v_1^3 + (1+\epsilon_2) t_2 \operatorname{Tr} v_2^3 \right] \\ & + 16n^2 (\epsilon_1 + \epsilon_2 + \epsilon_1\epsilon_2 + 1) t_1^2 t_2^2 + 32n(\epsilon_1 + \epsilon_2 + \epsilon_1\epsilon_2 + 1) t_1 t_2 \operatorname{Tr} v_1 v_2 \\ & + 16n(1+\epsilon_1) \left[t_1^2 \operatorname{Tr} v_2^2 + t_1 \operatorname{Tr} v_1 v_2^2 \right] + 16n(1+\epsilon_2) \left[t_2^2 \operatorname{Tr} v_1^2 + t_2 \operatorname{Tr} v_2 v_1^2 \right] \\ & + 4n(\operatorname{Tr} v_1^4 + \operatorname{Tr} v_2^4) + 16n \operatorname{Tr} v_1^2 v_2^2 - 8n \operatorname{Tr} v_1 v_2 v_1 v_2 \\ & + 12 \left[(\operatorname{Tr} v_1^2)^2 + (\operatorname{Tr} v_2^2)^2 \right] + 8 \operatorname{Tr} v_1^2 \operatorname{Tr} v_2^2 + 16\epsilon_1\epsilon_2 (\operatorname{Tr} v_1 v_2)^2. \end{aligned} \tag{5.10}$$

Note that when $\epsilon_i = -1$, all terms involving t_i automatically vanish. This is a consequence of the fact that $\epsilon_i = -1$ means that m_i appears inside a commutator. Therefore, as can be seen explicitly in (5.5), its trace decouples from the action. Without loss of generality, we can then put $t_i = 0$ when $\epsilon_i = -1$.

5.1.3 Stationary equations

The variation of the action induced by an arbitrary variation $t_i \to t_i + \delta t_i$ and $v_i \to v_i + \delta v_i$ reads:

$$\begin{aligned}
\delta S = \; & \Big[8n^2 g_2 (1+\epsilon_1) t_1 + 64 n^2 (1+\epsilon_1) t_1^3 + 96 n (1+\epsilon_1) t_1 \operatorname{Tr} v_1^2 + 16 n (1+\epsilon_1) \operatorname{Tr} v_1^3 \\
& + 32 n (\epsilon_1 + \epsilon_2 + \epsilon_1 \epsilon_2 + 1) \left[n t_1 t_2^2 + t_2 \operatorname{Tr} v_1 v_2 \right] \\
& + 16 n (1+\epsilon_1) \left[2 t_1 \operatorname{Tr} v_2^2 + \operatorname{Tr} v_1 v_2^2 \right] \Big] \delta t_1 \\
& + \operatorname{Tr} \Big[8 n g_2 v_1 + 96 n (1+\epsilon_1) t_1^2 v_1 + 48 n (1+\epsilon_1) t_1 v_1^2 + 16 n (1+\epsilon_1) t_1 v_2^2 \\
& + 32 n (\epsilon_1 + \epsilon_2 + \epsilon_1 \epsilon_2 + 1) t_1 t_2 v_2 + 16 n (1+\epsilon_2) \left[2 t_2^2 v_1 + t_2 \{ v_1, v_2 \} \right] \\
& + 16 n v_1^3 + 16 n \{ v_1, v_2^2 \} - 16 n v_2 v_1 v_2 + 48 \left(\operatorname{Tr} v_1^2 \right) v_1 + 16 \left(\operatorname{Tr} v_2^2 \right) v_1 \\
& + 32 \epsilon_1 \epsilon_2 \left(\operatorname{Tr} v_1 v_2 \right) v_2 \Big] \delta v_1 \\
& + \text{exchange labels } 1 \leftrightarrow 2
\end{aligned} \tag{5.11}$$

and imposing $\delta S = 0$ for arbitrary δt_i and δv_i gives the stationary equations. This means putting to zero the coefficients of δt_i, while the coefficients of δv_i can be in general proportional to the identity. The equations are written explicitly in the next paragraphs to appreciate the differences and similarities across the three models

Stationary equations for the $(2,0)$ model

$$\begin{aligned}
t_1) \quad & 16 n^2 g_2 t_1 + 128 n^2 t_1^3 + 192 n t_1 \operatorname{Tr} v_1^2 + 32 n \operatorname{Tr} v_1^3 + 128 n^2 t_1 t_2^2 \\
& + 128 n t_2 \operatorname{Tr} v_1 v_2 + 64 n t_1 \operatorname{Tr} v_2^2 + 32 n \operatorname{Tr} v_1 v_2^2 = 0
\end{aligned} \tag{5.12}$$

$$t_2) \quad \text{same as } t_1 \text{ upon exchanging } 1 \leftrightarrow 2 \tag{5.13}$$

$$\begin{aligned}
v_1) \quad & 8 n g_2 v_1 + 192 n t_1^2 v_1 + 96 n t_1 v_1^2 + 128 n t_1 t_2 v_2 + 32 n t_1 v_2^2 + 64 n t_2^2 v_1 \\
& + 32 n t_2 \{ v_1, v_2 \} + 16 n v_1^3 + 16 n \{ v_1, v_2^2 \} - 16 n v_2 v_1 v_2 + 48 \left(\operatorname{Tr} v_1^2 \right) v_1 \\
& + 16 \left(\operatorname{Tr} v_2^2 \right) v_1 + 32 \left(\operatorname{Tr} v_1 v_2 \right) v_2 \propto \mathbb{1}
\end{aligned} \tag{5.14}$$

$$v_2) \quad \text{same as } v_1 \text{ upon exchanging } 1 \leftrightarrow 2 \tag{5.15}$$

Stationary equations for the $(1,1)$ model

$$t_1) \quad 16n^2 g_2 t_1 + 128n^2 t_1^3 + 192nt_1 \operatorname{Tr} v_1^2 + 32n \operatorname{Tr} v_1^3 + 64nt_1 \operatorname{Tr} v_2^2 + 32n \operatorname{Tr} v_1 v_2^2 = 0 \tag{5.16}$$

$$\begin{aligned} v_1) \quad & 8ng_2 v_1 + 192nt_1^2 v_1 + 96nt_1 v_1^2 + 32nt_1 v_2^2 + 16nv_1^3 + 16n\{v_1, v_2^2\} - 16nv_2 v_1 v_2 \\ & + 48\left(\operatorname{Tr} v_1^2\right) v_1 + 16\left(\operatorname{Tr} v_2^2\right) v_1 - 32\left(\operatorname{Tr} v_1 v_2\right) v_2 \propto \mathbb{1} \end{aligned} \tag{5.17}$$

$$\begin{aligned} v_2) \quad & 8ng_2 v_2 + 64nt_1^2 v_2 + 32nt_1\{v_1, v_2\} + 16nv_2^3 + 16n\{v_2, v_1^2\} - 16nv_1 v_2 v_1 \\ & + 48\left(\operatorname{Tr} v_2^2\right) v_2 + 16\left(\operatorname{Tr} v_1^2\right) v_2 - 32\left(\operatorname{Tr} v_1 v_2\right) v_1 \propto \mathbb{1} \end{aligned} \tag{5.18}$$

Stationary equations for the $(0,2)$ model

$$\begin{aligned} v_1) \quad & 8ng_2 v_1 + 16nv_1^3 + 16n\{v_1, v_2^2\} - 16nv_2 v_1 v_2 \\ & + 48\left(\operatorname{Tr} v_1^2\right) v_1 + 16\left(\operatorname{Tr} v_2^2\right) v_1 + 32\left(\operatorname{Tr} v_1 v_2\right) v_2 \propto \mathbb{1} \end{aligned} \tag{5.19}$$

$$v_2) \quad \text{same as } v_1 \text{ upon exchanging } 1 \leftrightarrow 2 \tag{5.20}$$

Finding values for the scalars t_α and the matrices v_α that satisfy the stationary equations amounts to finding the preferred configurations of a purely classical theory, *i.e.* a theory where random fluctuations do not play a role. These classical solutions represent the leading contribution to the full random behaviour, and for very deep potentials where the fluctuations are suppressed they acquire more and more importance, but one should keep in mind that the full random model can differ drastically. In particular, a ubiquitous phenomenon observed in random matrix models is that of eigenvalue repulsion, which lifts the high degeneracy in the matrix spectra typically seen in classical solutions.
In what follows, a particular type of stationary solution is completely classified in all three models, and then the behaviour of the full random theory as probed by numerical simulations is compared with the classical results.

5.2 Involutory solutions for the (0,2) and (1,1) models

In this section, the general solution to the stationary equations involving involutory matrices v_1 and v_2 is worked out in the (0,2) and (1,1) models. The only assumption is then:

$$v_1^2 = x^2 \mathbb{1}, \quad v_2^2 = y^2 \mathbb{1}, \quad x, y \in \mathbb{R}. \tag{5.21}$$

These solutions are later shown to be enough to explain to a large extent the behaviour of the full random models. Although a similar analysis can be performed on the (2,0) model, it is found in that case to be more convenient to reorganize its degrees of freedom first, and for this reason the (2,0) model will be treated

separately.

5.2.1 Involutory solutions for the $(0, 2)$ model

The $(0, 2)$ model, being the simplest one, is worked out first.

Proposition 1. *All solutions of the stationary equations (5.19) and (5.20) with* $v_1^2 = x^2\mathbb{1}$ *and* $v_2^2 = y^2\mathbb{1}$, $x, y \in \mathbb{R}$ *obey one of*

1. $v_1 = v_2 = 0$
2. $[v_1, v_2] = 0, \quad \operatorname{Tr} v_1 v_2 = 0, \quad x^2 = y^2 = -\frac{g_2}{12}$
3. $v_1 = \pm x v, \quad v_2 = \pm y v, \quad v^2 = \mathbb{1}, \quad x^2 + y^2 = -\frac{g_2}{8}$
4. $\{v_1, v_2\} \propto \mathbb{1}, \quad [v_1, v_2] \neq 0, \quad x^2 + y^2 = -\frac{g_2}{8}$

Proof. Substituting (5.21) into (5.19) and (5.20) gives:

$$av_1 + bv_2 - v_2 v_1 v_2 \propto \mathbb{1} \tag{5.22}$$
$$cv_2 + bv_1 - v_1 v_2 v_1 \propto \mathbb{1} \tag{5.23}$$

with

$$a = \frac{g_2}{2} + 4x^2 + 3y^2, \quad b = \frac{2}{n} \operatorname{Tr} v_1 v_2, \quad c = \frac{g_2}{2} + 4y^2 + 3x^2. \tag{5.24}$$

Note that every term on the left hand side of (5.22) and (5.23) is traceless, so that the two equations actually are:

$$av_1 + bv_2 = v_2 v_1 v_2 \tag{5.25}$$
$$cv_2 + bv_1 = v_1 v_2 v_1. \tag{5.26}$$

The trivial solutions are:

$$\boxed{\begin{aligned} &v_1 = v_2 = 0 && (5.27)\\ &v_1 = 0, \quad y^2 = -\frac{g_2}{8} && (5.28)\\ &v_2 = 0, \quad x^2 = -\frac{g_2}{8}. && (5.29) \end{aligned}}$$

For non-vanishing v_1 and v_2, multiply (5.25) by v_2 on the left and right:

$$av_2 v_1 + by^2\mathbb{1} = y^2 v_1 v_2 \tag{5.30}$$
$$av_1 v_2 + by^2\mathbb{1} = y^2 v_2 v_1 \tag{5.31}$$

and similarly for (5.26):

$$cv_1 v_2 + bx^2\mathbb{1} = x^2 v_2 v_1 \tag{5.32}$$
$$cv_2 v_1 + bx^2\mathbb{1} = x^2 v_1 v_2. \tag{5.33}$$

Taking (5.30) $\pm$ (5.31) and (5.32) $\pm$ (5.33) gives a system of four equations equivalent to the original (5.25) and (5.26) where the trace and traceless parts are

decoupled:

$$(y^2 + a)[v_1, v_2] = 0 \tag{5.34}$$
$$(x^2 + c)[v_1, v_2] = 0 \tag{5.35}$$
$$(y^2 - a)\{v_1, v_2\} = 2by^2\mathbb{1} \tag{5.36}$$
$$(x^2 - c)\{v_1, v_2\} = 2bx^2\mathbb{1}. \tag{5.37}$$

Note that $y^2 + a = x^2 + c$, therefore (5.34) and (5.35) describe the same equation. If $b = 0$, there are four possibilities:

$$\{v_1, v_2\} = 0, \quad [v_1, v_2] = 0 \tag{5.38}$$
$$\{v_1, v_2\} = 0, \quad (y^2 + a) = 0 \tag{5.39}$$
$$[v_1, v_2] = 0, \quad (y^2 - a) = 0, \quad (x^2 - c) = 0 \tag{5.40}$$
$$(y^2 + a) = 0, \quad (y^2 - a) = 0, \quad (x^2 - c) = 0 \tag{5.41}$$

but the first is not possible for non-singular matrices, and the last has no solutions in x and y. The remaining two read:

$$\boxed{\{v_1, v_2\} = 0, \quad [v_1, v_2] \neq 0, \quad x^2 + y^2 = -\frac{g_2}{8}} \tag{5.42}$$

and

$$\boxed{[v_1, v_2] = 0, \quad \operatorname{Tr} v_1 v_2 = 0, \quad x^2 = y^2 = -\frac{g_2}{12}.} \tag{5.43}$$

If instead $b \neq 0$ (which is to say $\operatorname{Tr} v_1 v_2 \neq 0$), then split $\{v_1, v_2\}$ into trace and traceless part:

$$\{v_1, v_2\} = b\mathbb{1} + r \tag{5.44}$$

and substitute it into (5.36) and (5.37):

$$(y^2 - a)r = (y^2 + a)b\mathbb{1} \tag{5.45}$$
$$(x^2 - c)r = (x^2 + c)b\mathbb{1}. \tag{5.46}$$

Assuming $r \neq 0$ amounts to (5.41) again, therefore $r = 0$ and

$$0 \neq \{v_1, v_2\} = b\mathbb{1}. \tag{5.47}$$

Equations (5.34) to (5.37) reduce to:

$$(y^2 + a)[v_1, v_2] = 0 \tag{5.48}$$
$$(y^2 + a) = 0 \tag{5.49}$$

which describe two distinct solutions:

$$\{v_1, v_2\} = b\mathbb{1}, \quad x^2 + y^2 = -\frac{g_2}{8}, \quad [v_1, v_2] = 0 \tag{5.50}$$

and

$$\boxed{\{v_1, v_2\} = b\mathbb{1}, \quad x^2 + y^2 = -\frac{g_2}{8}, \quad [v_1, v_2] \neq 0.} \tag{5.51}$$

The commutative one, since $\{v_1, v_2\} = 2v_1v_2 = b\mathbb{1}$, requires v_1 and v_2 to be proportional to each other (just multiply this last relation by v_1 or v_2). Therefore it can be expressed by a single matrix v such that $v^2 = \mathbb{1}$ as:

$$\boxed{v_1 = \pm xv, \quad v_2 = \pm yv, \quad v^2 = \mathbb{1}, \quad x^2 + y^2 = -\frac{g_2}{8}.} \tag{5.52}$$

Therefore the only solutions for involutory v_1 and v_2 are (5.27), (5.28), (5.29), (5.42), (5.43), (5.51), (5.52). Notice how (5.28) and (5.29) can be regarded as a particular case of (5.52), while (5.42) and (5.51) can be put together in a more general solution where the anti-commutator is proportional to the identity with a coefficient that is allowed to vanish, thus completing the proof of Proposition 1. □

Solutions of type 3 and 4 in Proposition 1 determine a Clifford algebra generated by v_1 and v_2. In principle they could be put together in a more general solution

$$\{v_1, v_2\} \propto \mathbb{1}, \quad x^2 + y^2 = -\frac{g_2}{8}$$

but the separation was preferred here as it highlights the fact that the generators of type 3 span a one-dimensional subspace while the generators of type 4 span a two-dimensional one.

It is not immediately clear whether type 2 solutions can exist as matrices. To give a concrete realization, notice that v_1 and v_2 can be diagonalized simultaneously, therefore the solution can be rewritten as real vector identities representing the diagonal of the two matrices. Call the vectors w_1 and w_2. The involutory property requires w_1 and w_2 to contain only $\pm x$ and $\pm y$ respectively. Tracelessness of v_1 and v_2 requires the number of plus signs to be the same as the number of minus signs, and indirectly restricts the matrix dimension to be even. Lastly, $\operatorname{Tr} v_1v_2 = 0$ requires w_1 and w_2 to be orthogonal. Satisfying all these properties further restricts the dimensionality. Without loss of generality, write w_2 with all the plus signs first:

$$w_2^T = y\,(+1, \ldots, +1, -1, \ldots, -1)\,. \tag{5.53}$$

Orthogonality then reads:

$$0 = \sum_{i=1}^{n} w_1^i w_2^i = y\left(\sum_{i=1}^{\frac{n}{2}} w_1^i - \sum_{i=\frac{n}{2}+1}^{n} w_1^i\right) \tag{5.54}$$

while from tracelessness of v_1:

$$0 = \sum_{i=1}^{\frac{n}{2}} w_1^i + \sum_{i=\frac{n}{2}+1}^{n} w_1^i \tag{5.55}$$

therefore w_1 splits into two vectors with separately vanishing sum of components, requiring the total dimension to be a multiple of 4. An alternative construction in terms of Clifford modules is given in Appendix E.

5.2.2 Involutory solutions for the (1,1) model

Proposition 2. *All solutions of the stationary equations (5.16), (5.17) and (5.18) with $v_1^2 = x^2\mathbb{1}$ and $v_2^2 = y^2\mathbb{1}$, $x, y \in \mathbb{R}$ obey one of*

1. $t_1 = v_1 = v_2 = 0$
2. $t_1^2 = -\frac{g_2}{8}, \quad v_1 = v_2 = 0$
3. $x^2 = -\frac{g_2}{8}, \quad t_1 = v_2 = 0$
4. $y^2 = -\frac{g_2}{8}, \quad t_1 = v_1 = 0$
5. $t_1^2 = -\frac{g_2}{56}, \quad x^2 = -\frac{g_2}{14}, \quad v_2 = 0$
6. $[v_1, v_2] = 0, \quad \operatorname{Tr} v_1 v_2 = 0, \quad t_1 = 0, \quad x^2 = y^2 = -\frac{g_2}{12}$
7. $v_1 = \pm xv, \quad v_2 = \pm yv, \quad v^2 = \mathbb{1}, \quad t_1 = 0, \quad x^2 = y^2 = -\frac{g_2}{8}$
8. $v_1 = \pm xv, \quad v_2 = \pm yv, \quad v^2 = \mathbb{1}, \quad t_1^2 = -\frac{g_2}{32}, \quad x^2 = -\frac{g_2}{32}, \quad y^2 = -3\frac{g_2}{32}$
9. $\{v_1, v_2\} = 0, \quad [v_1, v_2] \neq 0, \quad t_1 = 0, \quad x^2 + y^2 = -\frac{g_2}{8}$

Proof. First split the anti-commutator $\{v_1, v_2\}$ into its trace and traceless part in the following way:

$$\{v_1, v_2\} = -b\mathbb{1} + r \tag{5.56}$$

and then substitute (5.21) into the stationary equations, obtaining:

$$dt_1 = 0 \tag{5.57}$$
$$av_1 + bv_2 = v_2 v_1 v_2 \tag{5.58}$$
$$cv_2 + bv_1 + 2t_1 r = v_1 v_2 v_1 \tag{5.59}$$

with

$$a = \frac{g_2}{2} + 12t_1^2 + 4x^2 + 3y^2, \quad b = -\frac{2}{n}\operatorname{Tr} v_1 v_2,$$
$$c = \frac{g_2}{2} + 4t_1^2 + 3x^2 + 4y^2, \quad d = \frac{g_2}{4} + 2t_1^2 + 3x^2 + y^2. \tag{5.60}$$

Note how the identity terms just cancel with the right hand side of (5.17) and (5.18), leaving behind only the traceless part. The proof is divided into three parts for clarity. First the simplest solutions are worked out, where at least one of the matrices is vanishing. The second part deals with the case $t_1 = 0$, and in the last one all variables are assumed to be non-vanishing.

i) Trivial solutions
The simplest solutions are:

$$\boxed{\begin{aligned} &t_1 = v_1 = v_2 = 0 && (5.61)\\ &t_1^2 = -\frac{g_2}{8}, \quad v_1 = v_2 = 0 && (5.62)\\ &x^2 = -\frac{g_2}{8}, \quad t_1 = v_2 = 0 && (5.63)\\ &y^2 = -\frac{g_2}{8}, \quad t_1 = v_1 = 0. && (5.64) \end{aligned}}$$

For vanishing v_2 and non-vanishing t_1 and v_1 one has:

$$\boxed{t_1^2 = -\frac{g_2}{56}, \quad x^2 = -\frac{g_2}{14}, \quad v_2 = 0} \tag{5.65}$$

while vanishing v_1 gives (5.62) again.

ii) Solutions with $t_1 = 0$ and $v_1, v_2 \neq 0$
In this case (5.57) is satisfied, while (5.58) and (5.59) are the same as the (0,2) model, and therefore equivalent to:

$$\begin{aligned} &(y^2 + a)[v_1, v_2] = 0 && (5.66)\\ &(x^2 + c)[v_1, v_2] = 0 && (5.67)\\ &(y^2 - a)\{v_1, v_2\} = 2by^2\mathbb{1} && (5.68)\\ &(x^2 - c)\{v_1, v_2\} = 2bx^2\mathbb{1} && (5.69) \end{aligned}$$

but with b defined with the opposite sign. The case $b = 0$ then gives the same two solutions:

$$\boxed{t_1 = 0, \quad \{v_1, v_2\} = 0, \quad [v_1, v_2] \neq 0, \quad x^2 + y^2 = -\frac{g_2}{8}} \tag{5.70}$$

and

$$\boxed{t_1 = 0, \quad [v_1, v_2] = 0, \quad \mathrm{Tr}\, v_1 v_2 = 0, \quad x^2 = y^2 = -\frac{g_2}{12}} \tag{5.71}$$

while, if $b \neq 0$, substituting $\{v_1, v_2\} = -b\mathbb{1} + r$ into (5.68) and (5.69) gives:

$$\begin{aligned} &(y^2 - a)r = (3y^2 - a)b\mathbb{1} && (5.72)\\ &(x^2 - c)r = (3x^2 - c)b\mathbb{1} && (5.73) \end{aligned}$$

that again has no solutions if $r \neq 0$. Relation (5.47) is then replaced by

$$0 \neq \{v_1, v_2\} = -b\mathbb{1} \tag{5.74}$$

and (5.66) to (5.69) become:

$$(y^2 + a)[v_1, v_2] = 0 \tag{5.75}$$
$$(x^2 + c)[v_1, v_2] = 0 \tag{5.76}$$
$$(3y^2 - a) = 0 \tag{5.77}$$
$$(3x^2 - c) = 0. \tag{5.78}$$

The last two require

$$x^2 = y^2 = -\frac{g_2}{8} \tag{5.79}$$

which is incompatible with $(y^2 + a) = 0$ (or $(x^2 + c) = 0$, which is the same since $t_1 = 0$ by assumption), and therefore the only solution reads

$$t_1 = 0, \quad \{v_1, v_2\} = -b\mathbb{1}, \quad x^2 = y^2 = -\frac{g_2}{8}, \quad [v_1, v_2] = 0. \tag{5.80}$$

As already argued for the (0,2) model, this solution is better written in terms a single matrix v as:

$$\boxed{t_1 = 0, \quad v_1 = \pm xv, \quad v_2 = \pm yv, \quad v^2 = \mathbb{1}, \quad x^2 = y^2 = -\frac{g_2}{8}} \tag{5.81}$$

but this time (5.63) and (5.64) are not a particular case of (5.81).

iii) Solutions with $t_1, v_1, v_2 \neq 0$
First notice that

$$[v_1, r] = [v_2, r] = 0 \tag{5.82}$$

therefore using the same method of multiplying (5.58) and (5.59) by v_2 and v_1 on the left and on the right gives the following system of equations:

$$d = 0 \tag{5.83}$$
$$(y^2 + a)[v_1, v_2] = 0 \tag{5.84}$$
$$(x^2 + c)[v_1, v_2] = 0 \tag{5.85}$$
$$(y^2 - a)\{v_1, v_2\} = 2by^2\mathbb{1} \tag{5.86}$$
$$(x^2 - c)\{v_1, v_2\} - 4t_1v_1r = 2bx^2\mathbb{1}. \tag{5.87}$$

Necessarily $[v_1, v_2] = 0$, because otherwise satisfying (5.83), (5.84) and (5.85), i.e.:

$$d = 0, \quad y^2 + a = 0, \quad x^2 + c = 0 \tag{5.88}$$

requires $t_1 = 0$, which contradicts the hypotheses of (iii).
Therefore the system of equations reduces to:

$$d = 0 \tag{5.89}$$
$$(y^2 - a)r = (3y^2 - a)b\mathbb{1} \tag{5.90}$$
$$(x^2 - c)r - 8t_1x^2v_2 - 4t_1bv_1 = (3x^2 - c)b\mathbb{1} \tag{5.91}$$

where $\{v_1, v_2\} = 2v_1v_2 = -b\mathbb{1} + r$ was used repeatedly until every term was

manifestly trace or traceless.
If $b = 0$, then $r = 2v_1v_2$ and (5.91) reads

$$(x^2 - c)v_1v_2 = 4t_1x^2v_2 \tag{5.92}$$

and multiplying by v_2 on the right brings to either a contradiction with the hypotheses of (iii) or to $v_1 \propto \mathbb{1}$.
If instead $b \neq 0$, then separating trace and traceless components of (5.89), (5.90) and (5.91) gives the following system:

$$d = 0 \tag{5.93}$$
$$3y^2 - a = 0 \tag{5.94}$$
$$3x^2 - c = 0 \tag{5.95}$$
$$(y^2 - a)r = 0 \tag{5.96}$$
$$(x^2 - c)r = 8t_1x^2v_2 + 4t_1bv_1. \tag{5.97}$$

The subsystem (5.93) to (5.96) however has no solution for $r \neq 0$, therefore necessarily $r = 0$. In turn this means that v_1 and v_2 are proportional to each other (from $2v_1v_2 = -b\mathbb{1}$) and can be written in terms of a single matrix $v^2 = \mathbb{1}$ as $v_1 = \pm xv$ and $v_2 = \pm yv$. The traceless equations (5.96) and (5.97) then cancel no matter the relative sign of x and y, and the remaining ones (5.93), (5.94) and (5.95) give the last solution

$$\boxed{v_1 = \pm xv, \quad v_2 = \pm yv, \quad v^2 = \mathbb{1}, \quad t_1^2 = -\frac{g_2}{32}, \quad x^2 = -\frac{g_2}{32}, \quad y^2 = -3\frac{g_2}{32}} \tag{5.98}$$

thus completing the proof of Proposition 2. □

5.3 The (2,0) model

5.3.1 Model redefinition

It is possible to perform a change of variables in the (2,0) model that eliminates redundant degrees of freedom in the following way:

$$\gamma_\pm := \frac{1}{2}\left(\sigma_1 \mp i\sigma_2\right), \quad W := m_1 + im_2 \tag{5.99}$$

so that the Dirac operator becomes:

$$D = \gamma_+ \otimes \{W, \cdot\} + \gamma_- \otimes \{W^\dagger, \cdot\} \tag{5.100}$$

and the quadratic and quartic pieces of the action are:

$$\operatorname{Tr} D^2 = 4(n \operatorname{Tr} WW^\dagger + \operatorname{Tr} W \operatorname{Tr} W^\dagger) \tag{5.101}$$
$$\begin{aligned}\operatorname{Tr} D^4 = 4[&n \operatorname{Tr} WW^\dagger WW^\dagger + \operatorname{Tr} W^2 \operatorname{Tr} {W^\dagger}^2 + 2 \operatorname{Tr}(WW^\dagger)^2 \\ &+ 2 \operatorname{Tr} W^2W^\dagger \operatorname{Tr} W^\dagger + 2 \operatorname{Tr} {W^\dagger}^2 W \operatorname{Tr} W].\end{aligned} \tag{5.102}$$

This is now a model for an arbitrary complex matrix W. It turns out to be convenient to split W in trace and traceless part in the following way:

$$W = e^{i\theta}(\rho \mathbb{1} + V) \tag{5.103}$$

so that $\frac{1}{n}\operatorname{Tr} W = \rho e^{i\theta}$ and $\operatorname{Tr} V = 0$. Furthermore, split V in its Hermitian and anti-Hermitian part:

$$V = A + iB \tag{5.104}$$

Since every term in the action contains the same number of W and $W^\dagger$, the global phase $e^{i\theta}$ drops out and the relevant degrees of freedom are the positive number ρ and the Hermitian traceless matrices A and B. The action reads:

$$\begin{aligned} S = {} & 8n^2\rho^2(g_2 + 4\rho^2) + 4n\Big[(g_2 + 24\rho^2)\operatorname{Tr} A^2 + (g_2 + 8\rho^2)\operatorname{Tr} B^2 \\ & + 8\rho(\operatorname{Tr} A^3 + \operatorname{Tr} AB^2) + \operatorname{Tr} A^4 + \operatorname{Tr} B^4 + 4\operatorname{Tr} A^2B^2 - 2\operatorname{Tr} ABAB\Big] \\ & + 4\Big[3(\operatorname{Tr} A^2)^2 + 3(\operatorname{Tr} B^2)^2 + 2\operatorname{Tr} A^2 \operatorname{Tr} B^2 + 4(\operatorname{Tr} AB)^2\Big]. \end{aligned} \tag{5.105}$$

The stationary equations written in these new variables read:

$$\rho) \quad 16n^2\rho(g_2 + 8\rho^2) + 192n\rho \operatorname{Tr} A^2 + 64n\rho \operatorname{Tr} B^2 + 32n \operatorname{Tr} A^3 + 32n \operatorname{Tr} AB^2 = 0 \tag{5.106}$$

$$\begin{aligned} A) \quad & 8n(g_2 + 24\rho^2)A + 96n\rho A^2 + 32n\rho B^2 + 16nA^3 + 16n\{B^2, A\} - 16nBAB \\ & + 48(\operatorname{Tr} A^2)A + 16(\operatorname{Tr} B^2)A + 32(\operatorname{Tr} AB)B \propto \mathbb{1} \end{aligned} \tag{5.107}$$

$$\begin{aligned} B) \quad & 8n(g_2 + 8\rho^2)B + 32n\rho\{A, B\} + 16nB^3 + 16n\{A^2, B\} - 16nABA + 48(\operatorname{Tr} B^2)B \\ & + 16(\operatorname{Tr} A^2)B + 32(\operatorname{Tr} AB)A \propto \mathbb{1} \end{aligned} \tag{5.108}$$

Notice the asymmetry in the equations for A and B, which highlights the fact that they are not just v_1 and v_2 in disguise, but rather some non-trivial combination of these. Even more strikingly, the equations are formally identical to the ones for the (1,1) model if one identifies $t_1 \leftrightarrow \rho$, $v_1 \leftrightarrow A$ and $v_2 \leftrightarrow B$, except for the fact that here ρ is non-negative and the $\operatorname{Tr} AB$ term has the opposite sign. The same identification when $\rho = 0$ makes instead the model indistinguishable from the (0,2).

5.3.2 Involutory solutions for the (2,0) model

Proposition 3. *All solutions of the stationary equations (5.106), (5.107) and (5.108) with $A^2 = x^2\mathbb{1}$ and $B^2 = y^2\mathbb{1}$, $x, y \in \mathbb{R}$ obey one of*

1. $\rho = A = B = 0$
2. $\rho = -\frac{g_2}{8}, \quad A = B = 0$
3. $\rho^2 = -\frac{g_2}{56}, \quad x^2 = -\frac{g_2}{14}, \quad B = 0$
4. $[A, B] = 0, \quad \operatorname{Tr} AB = 0, \quad \rho = 0, \quad x^2 = y^2 = -\frac{g_2}{12}$

5. $A = \pm xv, \quad B = \pm yv, \quad v^2 = \mathbb{1}, \quad \rho = 0, \quad x^2 + y^2 = -\frac{g_2}{8}$

6. $\{A, B\} \propto \mathbb{1}, \quad [A, B] \neq 0, \quad \rho = 0, \quad x^2 + y^2 = -\frac{g_2}{8}$

Proof. Upon substituting $A = x^2\mathbb{1}$, $B = y^2\mathbb{1}$ and $\{A, B\} = b\mathbb{1} + r$ into (5.106), (5.107) and (5.108), the equations read:

$$d\rho = 0 \tag{5.109}$$
$$aA + bB = BAB \tag{5.110}$$
$$cB + bA + 2\rho r = ABA \tag{5.111}$$

with

$$\begin{aligned} a &= \frac{g_2}{2} + 12\rho^2 + 4x^2 + 3y^2, \quad b = \frac{2}{n}\operatorname{Tr} AB, \\ c &= \frac{g_2}{2} + 4\rho^2 + 3x^2 + 4y^2, \quad d = \frac{g_2}{4} + 2\rho^2 + 3x^2 + y^2. \end{aligned} \tag{5.112}$$

The solutions where at least one matrix is vanishing are the same as part (i) of the proof of Proposition 2, while for $\rho = 0$ the proof is formally identical to the one of Proposition 1. These account for all solutions listed in Proposition 3. What is left to show is that no solution exists for $\rho, A, B \neq 0$ simultaneously.
In this case, the same argument used in part (iii) of the proof of Proposition 2 leads necessarily to $[A, B] = 0$ and $b \neq 0$, which nevertheless amounts to solving again the system

$$d = 0, \quad y^2 + a = 0, \quad x^2 + c = 0 \tag{5.113}$$

that has no solution for $\rho \neq 0$. □

5.4 Numerical simulations

The solutions presented so far belong to the classical regime. When the models are promoted to random matrix models, however, their behaviour can change quite drastically. It is known for instance that random matrix models display eigenvalue repulsion effects, while the classical minimum of the action $S = g_2 \operatorname{Tr} D^2 + \operatorname{Tr} D^4$ presents a high eigenvalue degeneracy.
The random models are probed via Monte Carlo simulations. Earlier works [7] [12] [13] have employed the Metropolis algorithm, while here the Hamiltonian Monte Carlo algorithm as implemented in the RFL library is used.
Monte Carlo samples are collected from Hamiltonian trajectories with a number of steps fixed to $N_t = 10$ and a time discretization dt tuned in such a way as to hit a target acceptance rate of 80%. Expectation values are calculated as an average over 10 independent Markov chains each composed of 10^4 samples, and errors are calculated using a jackknife routine as explained in Section 3.5.7.

5.4.1 The random vacuum

The preferred vacuum of the random models can be established numerically by computing the expectation value of the observables:

$$\frac{1}{n}\operatorname{Tr} v_1^2 \overset{\text{on-shell}}{=} x^2 \tag{5.114}$$

$$\frac{1}{n}\operatorname{Tr} v_2^2 \overset{\text{on-shell}}{=} y^2. \tag{5.115}$$

Classically, the preferred vacuum corresponds to the global minimum of the action. The solutions of Proposition 1 give the following value for the action of the (0,2) model:

$$\begin{aligned} &1.\quad v_1 = v_2 = 0 \\ &\to S = 0 \end{aligned} \tag{5.116}$$

$$\begin{aligned} &2.\quad [v_1, v_2] = 0, \quad \operatorname{Tr} v_1 v_2 = 0, \quad x^2 = y^2 = -\frac{g_2}{12} \\ &\to S = -n^2 \frac{g_2^2}{3} \end{aligned} \tag{5.117}$$

$$\begin{aligned} &3.\quad v_1 = \pm x v, \quad v_2 = \pm y v, \quad v^2 = \mathbb{1}, \quad x^2 + y^2 = -\frac{g_2}{8} \\ &\to S = -n^2 \frac{g_2^2}{4} \end{aligned} \tag{5.118}$$

$$\begin{aligned} &4.\quad \{v_1, v_2\} \propto \mathbb{1}, \quad [v_1, v_2] \neq 0, \quad x^2 + y^2 = -\frac{g_2}{8} \\ &\to S = -n^2 \frac{g_2^2}{4}. \end{aligned} \tag{5.119}$$

Therefore, at a pure classical level, solutions of type 2 are preferred. The numerical results, shown in Figure 5.1, confirm this picture especially for very negative values of g_2. Closer to the origin (Figure 5.2) the potential well is shallower and the fluctuations around the minimum acquire more importance, causing the expectation value of the observables to move away from the stationary value. This phenomenon will be important in the analysis of the $(2,0)$ model.
The solutions of Proposition 2 give the following value for the action of the (1,1) model:

$$\begin{aligned} &1.\quad t_1 = v_1 = v_2 = 0 \\ &\to S = 0 \end{aligned} \tag{5.120}$$

$$\begin{aligned} &2.\quad t_1^2 = -\frac{g_2}{8}, \quad v_1 = v_2 = 0 \\ &\to S = -n^2 \frac{g_2^2}{2} \end{aligned} \tag{5.121}$$

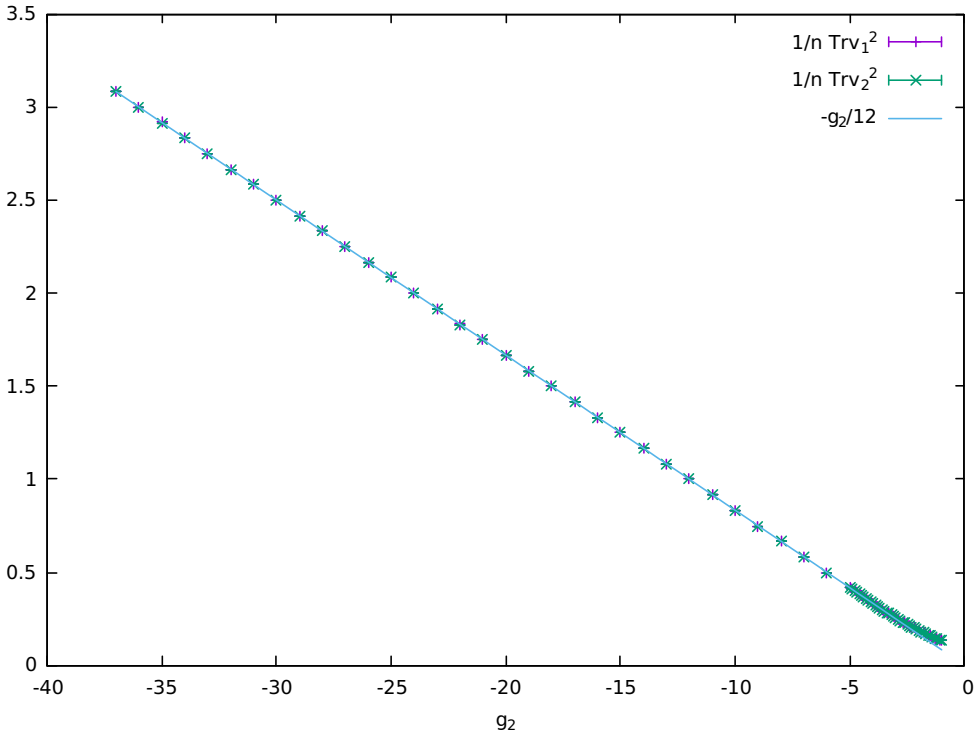

Figure 5.1: $1/n \operatorname{Tr} v_1^2$ (purple) and $1/n \operatorname{Tr} v_2^2$ (green) vs coupling constant g_2 for the $(0, 2)$ model and matrix dimension $n = 32$.

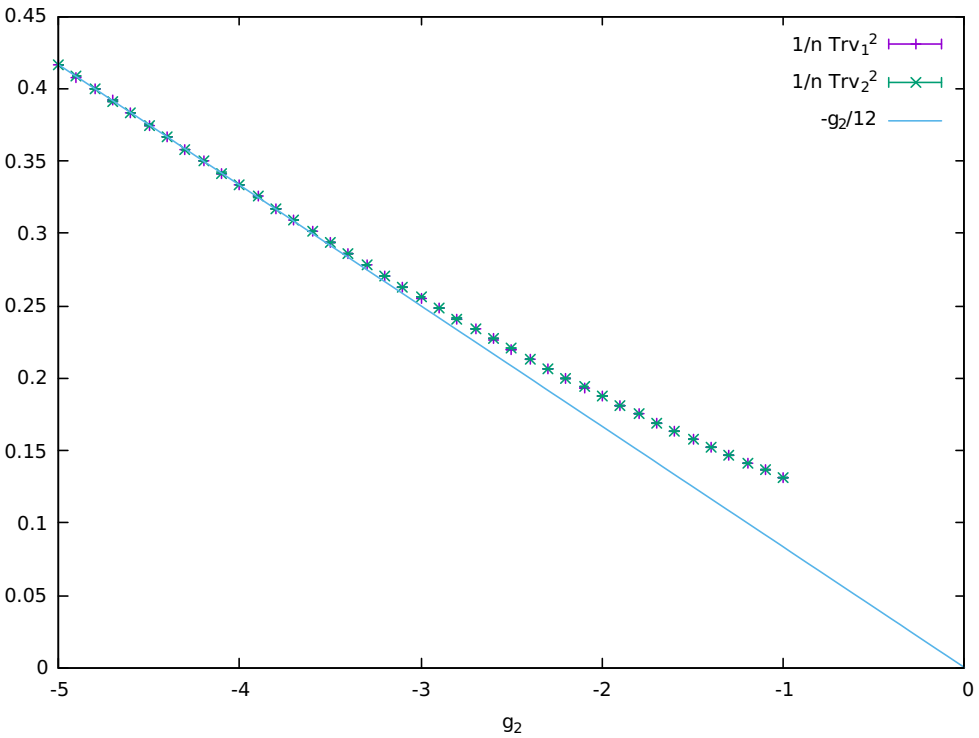

Figure 5.2: $1/n \operatorname{Tr} v_1^2$ (purple) and $1/n \operatorname{Tr} v_2^2$ (green) vs coupling constant g_2 for the $(0, 2)$ model and matrix dimension $n = 32$, close to the origin.

3. $x^2 = -\frac{g_2}{8}, \quad t_1 = v_2 = 0$

$$\rightarrow S = -n^2 \frac{g_2^2}{4} \tag{5.122}$$

4. $y^2 = -\frac{g_2}{8}, \quad t_1 = v_1 = 0$

$$\rightarrow S = -n^2 \frac{g_2^2}{4} \tag{5.123}$$

5. $t_1^2 = -\frac{g_2}{56}, \quad x^2 = -\frac{g_2}{14}, \quad v_2 = 0$

$$\rightarrow S = -3n^2 \frac{g_2^2}{14} \tag{5.124}$$

6. $[v_1, v_2] = 0, \quad \mathrm{Tr}\, v_1 v_2 = 0, \quad t_1 = 0, \quad x^2 = y^2 = -\frac{g_2}{12}$

$$\rightarrow S = -n^2 \frac{g_2^2}{3} \tag{5.125}$$

7. $v_1 = \pm x v, \quad v_2 = \pm y v, \quad v^2 = \mathbb{1}, \quad t_1 = 0, \quad x^2 = y^2 = -\frac{g_2}{8}$

$$\rightarrow S = -n^2 \frac{g_2^2}{2} \tag{5.126}$$

8. $v_1 = \pm x v, \quad v_2 = \pm y v, \quad v^2 = \mathbb{1}, \quad t_1^2 = -\frac{g_2}{32}, \quad x^2 = -\frac{g_2}{32}, \quad y^2 = -3\frac{g_2}{32}$

$$\rightarrow S = -3n^2 \frac{g_2^2}{8} \tag{5.127}$$

9. $\{v_1, v_2\} = 0, \quad [v_1, v_2] \neq 0, \quad t_1 = 0, \quad x^2 + y^2 = -\frac{g_2}{8}$

$$\rightarrow S = -n^2 \frac{g_2^2}{4}. \tag{5.128}$$

The minimum is achieved for type 2 and type 7. The results of the numerical simulations reported in Figure 5.3 clearly show that type 7 is preferred by the random model for a large range of g_2 values. It is worth noting that the oscillations of the data points in Figure 5.3 is larger than the error bars (the error bars are smaller than the point markers). Zooming in on t_1^2 for a typical Monte Carlo simulation uncovers a certain regularity, as can be seen in Figure 5.4. Most points are either close to zero, or very closely aligned with the line $-g_2/512$ or $-g_2/2048$. This suggests that the random model has a non-trivial landscape of local minima close to the true vacuum.
Finally, the solutions of Proposition 3 give the following value for the action of the

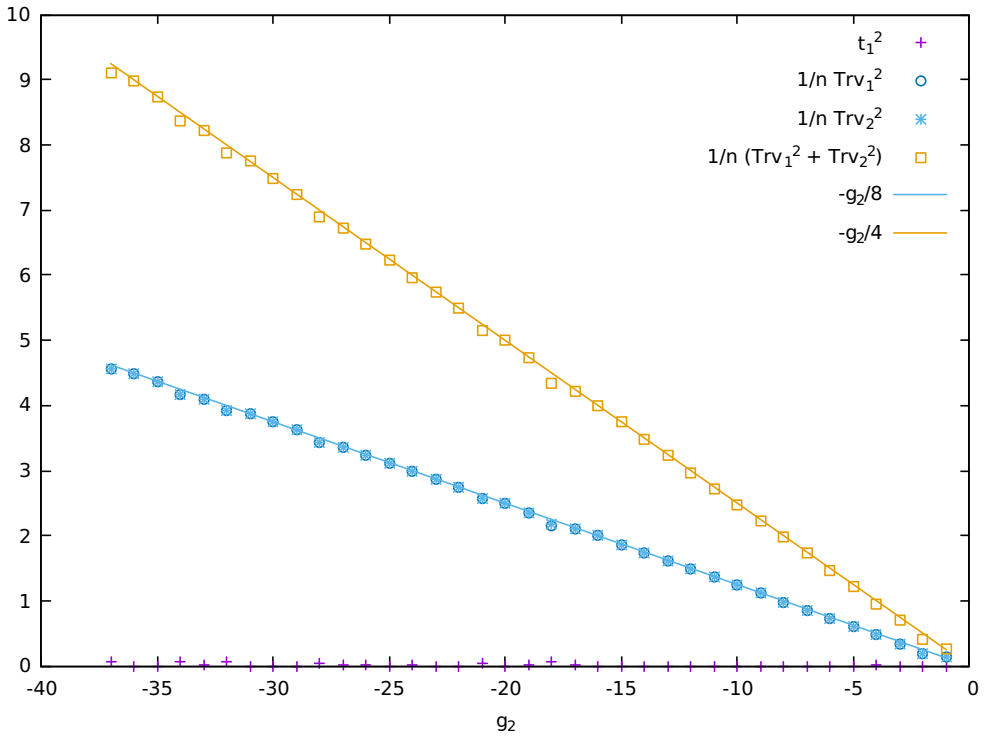

Figure 5.3: Expectation value of t_1^2 (purple), $1/n\,\mathrm{Tr}\,v_1^2$ (blue dots), $1/n\,\mathrm{Tr}\,v_2^2$ (blue crosses), $1/n(\mathrm{Tr}\,v_1^2 + \mathrm{Tr}\,v_2^2)$ (yellow squares) and the theoretical lines $-g_2/8$ (blue line) and $-g_2/4$ (yellow line) vs the coupling constant g_2 in the full random $(1,1)$ model for $n = 32$.

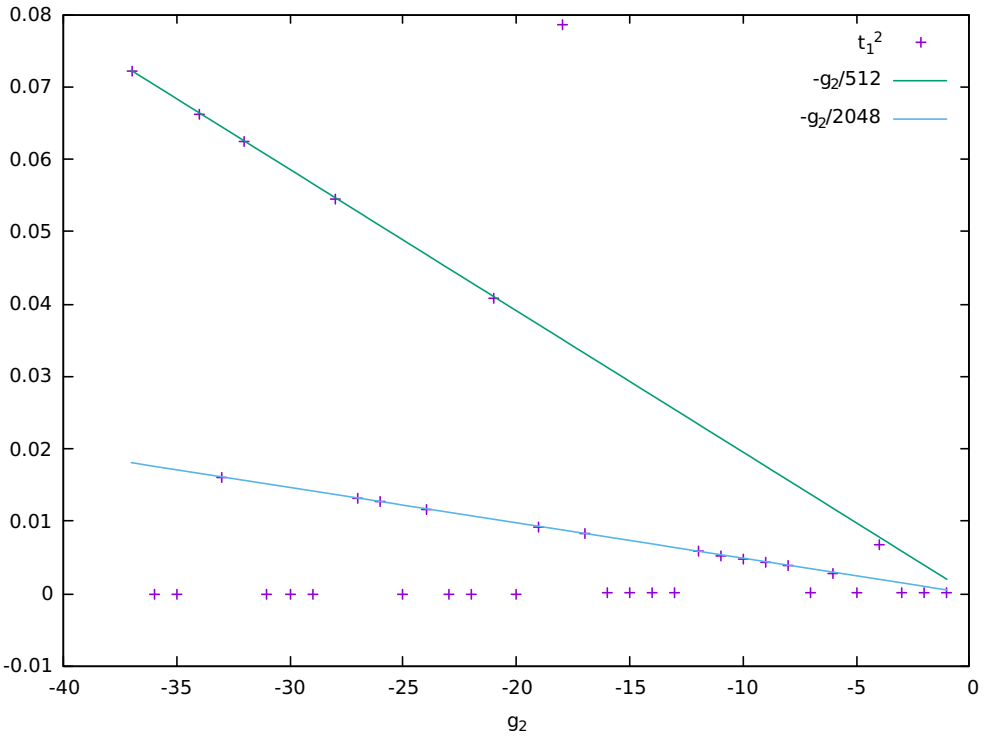

Figure 5.4: Expectation value of t_1^2 (purple), $-g_2/512$ (green line) and $-g_2/2048$ (blue line) vs the coupling constant g_2 in the full random $(1,1)$ model for $n = 32$.

(2,0) model:

$$1.\quad \rho = A = B = 0$$
$$\rightarrow S = 0 \tag{5.129}$$

$$2.\quad \rho = -\frac{g_2}{8},\quad A = B = 0$$
$$\rightarrow S = -n^2\frac{g_2^2}{2} \tag{5.130}$$

$$3.\quad \rho^2 = -\frac{g_2}{56},\quad x^2 = -\frac{g_2}{14},\quad B = 0$$
$$\rightarrow S = -3n^2\frac{g_2^2}{14} \tag{5.131}$$

$$4.\quad [A,B] = 0,\quad \mathrm{Tr}\, AB = 0,\quad \rho = 0,\quad x^2 = y^2 = -\frac{g_2}{12}$$
$$\rightarrow S = -n^2\frac{g_2^2}{3} \tag{5.132}$$

$$5.\quad A = \pm xv,\quad B = \pm yv,\quad v^2 = \mathbb{1},\quad \rho = 0,\quad x^2 + y^2 = -\frac{g_2}{8}$$
$$\rightarrow S = -n^2\frac{g_2^2}{4} \tag{5.133}$$

$$6.\quad \{A,B\} \propto \mathbb{1},\quad [A,B] \neq 0,\quad \rho = 0,\quad x^2 + y^2 = -\frac{g_2}{8}$$
$$\rightarrow S = -n^2\frac{g_2^2}{4}. \tag{5.134}$$

However, its behaviour can only be partially understood by stationary methods, and some features remain still obscure. The results of the random model are shown in Figure 5.5. For clarity, the g_2 axis will be divided into three regions and the results discussed separately.

Region I: $g_2 \in (-2.7, 0)$
In this region ρ^2 lies close to zero and a matrix solution dominates. Fitting $1/n\,\mathrm{Tr}\,(A^2 + B^2)$ to a linear function $mg_2 + q$ gives:

$$m = -0.124(1) \approx -\frac{1}{8}$$
$$q = 0.128(3). \tag{5.135}$$

The fact that the slope is compatible with $-1/8$ seems to indicate that a type 5 or 6 matrix solution is realized, albeit with a vertical displacement that is not accounted for at the level of the stationary analysis. It should be noticed, however, that the observable presents a perfect overlapping with the one of the $(0, 2)$ model

(Figure 5.6), which seems to suggest that the actual solution is a type 3 deformed by random fluctuations. Another argument can be made in support of a type 3 solution. A crucial difference between the two solutions is that type 3 implies the strong relation $x^2 = y^2$, while type 5 or 6 allows for every combination of x^2 and y^2, as long as their sum is $-g_2/8$. Plotting the Monte Carlo history of the two observables clearly shows how the strong constraint $x^2 = y^2$ is preferred (Figure 5.7).

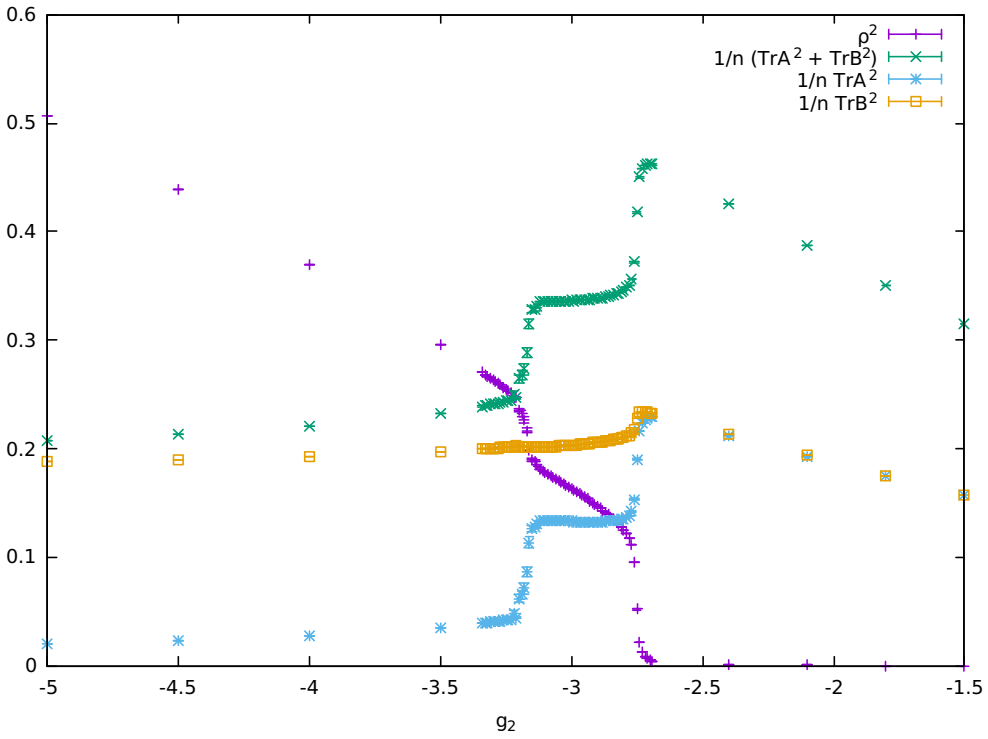

Figure 5.5: Expectation value of ρ^2 (purple), $1/n\,(\operatorname{Tr} A^2 + \operatorname{Tr} B^2)$ (green), $1/n \operatorname{Tr} A^2$ (blue) and $1/n \operatorname{Tr} B^2$ (yellow) vs the coupling constant g_2 in the full random $(2,0)$ model for $n = 32$.

Region II: $g_2 \in (-3.2, -2.7)$
Passing from region I to region II, the model undergoes a phase transition where ρ^2 acts as an order parameter. The growth of ρ^2 in this region is only roughly linear, with an estimated slope of $-0.151(1)$ that is perhaps not meaningful at a quantitative level. Interestingly, the matrix observable $1/n\,(\operatorname{Tr} A^2 + \operatorname{Tr} B^2)$ does not vanish, and instead it plateaus at a value of roughly 0.336.

Region III: $g_2 \in (-\infty, -3.2)$
The interface between region II and III is marked by a second jump in the order parameter, which is an interesting phenomenon in and on itself. Qualitatively the picture is unchanged in this region: ρ^2 grows linearly and $1/n\,(\operatorname{Tr} A^2 + \operatorname{Tr} B^2)$ plateaus. This time, however, the data can be taken for very large negative values of g_2, for which the stationary analysis should yield accurate predictions. Fitting

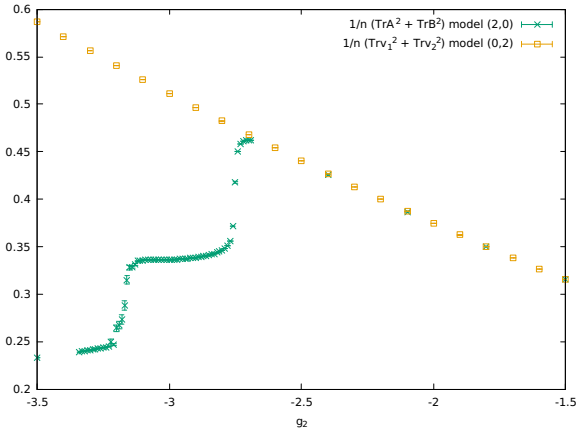

Figure 5.6: Expectation value of $1/n\,(\operatorname{Tr} A^2 + \operatorname{Tr} B^2)$ and $1/n\,(\operatorname{Tr} v_1^2 + \operatorname{Tr} v_2^2)$ vs the coupling constant g_2 in the full random $(0,2)$ (yellow) and $(2,0)$ (green) model for $n = 32$. The overlap for small $|g_2|$ suggests that the two models are indistinguishable in that region.

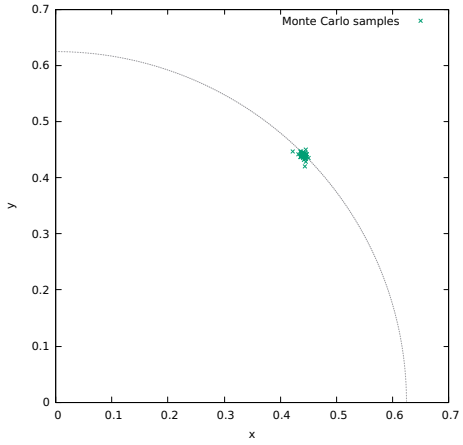

Figure 5.7: Monte Carlo samples (green) on the $x - y$ plane (only first quadrant shown) in the full random $(2,0)$ model for $n = 32$ and $g_2 = -2.1$. The grey dashed line is the expected distribution of samples if a solution of type 5 or 6 is realized. The random model shows a preference for the stronger constraint $x^2 = y^2$.

ρ^2 to a linear function $mg_2 + q$ gives:

$$\begin{aligned} m &= -0.125007(2) \approx -\frac{1}{8} \\ q &= -0.0919(4). \end{aligned} \tag{5.136}$$

The slope agrees with the expected $-1/8$ of the scalar solution, but the vertical displacement is not predicted by the stationary analysis. Nor is the non-vanishing plateau of the matrix observable $1/n\,(\operatorname{Tr} A^2 + \operatorname{Tr} B^2)$, estimated to be 0.1791(8). The data used for the linear fits was taken in a range $g_2 \in [-500, -30]$.

5.4.2 (2,0) phase diagram

The authors in [7] observed a phase transition in the model, which was further studied in [12], but the simulations were limited to matrix size $n \leq 10$. Simulations performed on larger matrices uncover an interesting phenomenon where a second criticality sprouts from the original one and moves away from it as the matrices are made larger. The critical points are identified with maxima of the variance of the action $\operatorname{Var}(S) = \langle S^2 \rangle - \langle S \rangle^2$, which is shown in Figure 5.8a and 5.8b. The splitting appears unequivocal at $n = 16$, but already $n = 14$ shows a faint trace of it. A natural order parameter for the phase transitions is the scalar observable ρ^2, whose variance leads to a similar picture (Figure 5.8c and 5.8d). Plotting the critical points as a function of g_2 and n results in the phase diagram of Figure 5.8e. No example could be found in the literature of a non-trivial phase diagram involving the matrix dimension.

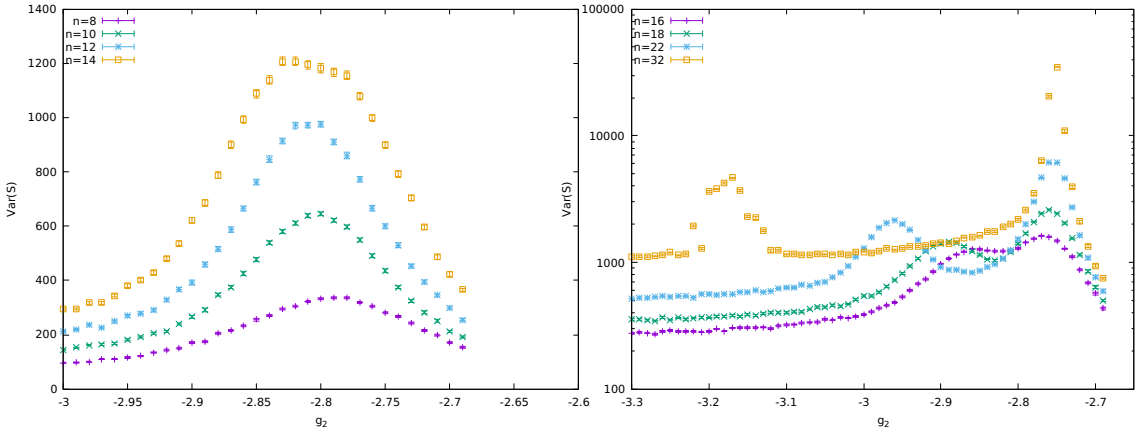

(a)

(b)

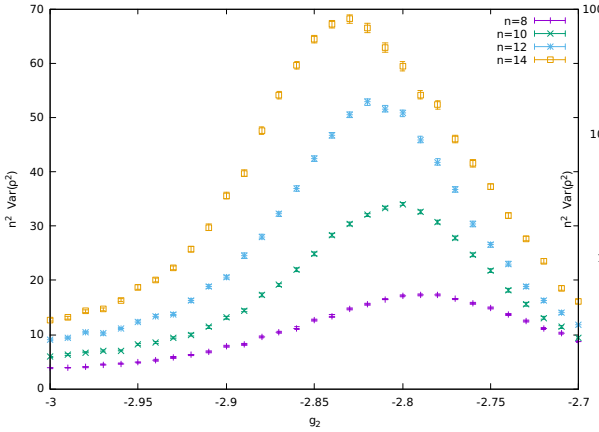

(c)

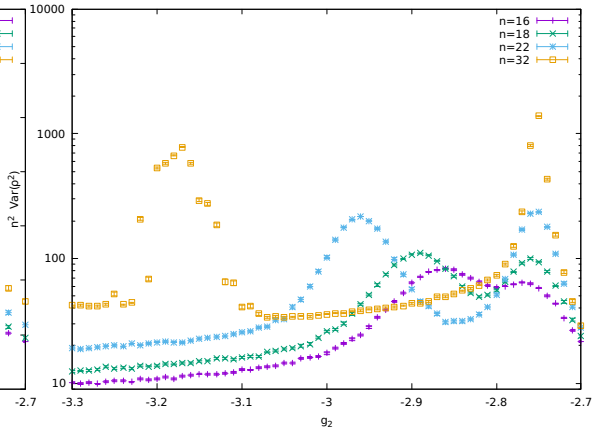

(d)

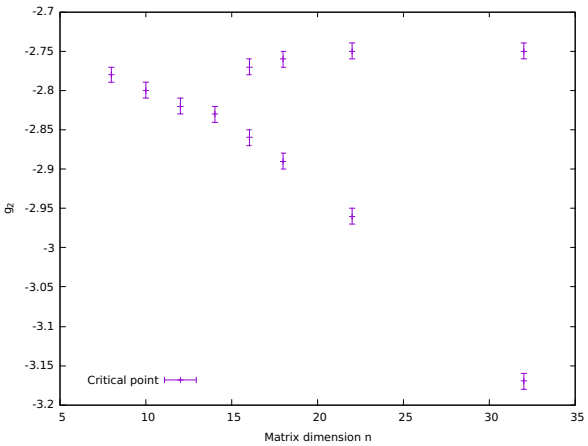

(e)

Figure 5.8: (a) $\mathrm{Var}(S)$ for $n \leq 14$. (b) $\mathrm{Var}(S)$ for $n \geq 16$. (c) $n^2\,\mathrm{Var}(\rho^2)$ for $n \leq 14$. (d) $n^2\,\mathrm{Var}(\rho^2)$ for $n \geq 16$. (e) Phase diagram of the full $(2,0)$ random model on the $n - g_2$ plane.

Analysis of the first phase transition

The first phase transition is identified with the rightmost peaks of Figure 5.8b and 5.8d. A finite-size scaling analysis is performed and an argument is given for the order of the transition.
Using standard notation, the critical exponents α, β, γ and ν are defined based on the behaviour of observables near criticality:

$$\xi \sim (g_2 - g_2^*)^{-\nu} \tag{5.137}$$
$$n^2\rho^2 \sim (g_2 - g_2^*)^{\beta} \tag{5.138}$$
$$\mathrm{Var}(n^2\rho^2) \sim (g_2 - g_2^*)^{-\gamma} \tag{5.139}$$
$$\mathrm{Var}(S) \sim (g_2 - g_2^*)^{-\alpha} \tag{5.140}$$

where g_2^* denotes the critical coupling and ξ is the correlation length. The standard theory of finite-size scaling [39] is usually developed on a lattice, where the correlation length is intuitively understood as the typical size of correlated clusters and therefore can never exceed the size of the lattice itself. In the context of random matrix theory the most natural cut-off scale is (some power of) the matrix size n. The simplest finite-size scaling ansatz is then found by proceeding in complete analogy with lattice systems and replacing the lattice size with n:

$$n^{\frac{\beta}{\nu}} n^2\rho^2 = f_1\left(n^{\frac{1}{\nu}} t\right) \tag{5.141}$$
$$n^{-\frac{\gamma}{\nu}} \mathrm{Var}(n^2\rho^2) = f_2\left(n^{\frac{1}{\nu}} t\right) \tag{5.142}$$
$$n^{-\frac{\alpha}{\nu}} \mathrm{Var}(S) = f_3\left(n^{\frac{1}{\nu}} t\right) \tag{5.143}$$

where t denotes the reduced coupling:

$$t := \frac{(g_2 - g_2^*)}{|g_2^*|} \tag{5.144}$$

and f_1, f_2 and f_3 are unknown functions that do not depend on the matrix size. The strategy is to find the correct values of the critical exponents and critical coupling that make the rescaled data points taken at different n collapse on the same curve. Notice how $n^2\rho^2$ was used as an order parameter instead of ρ^2. This was dictated by consistency since S is $O(n^2)$ while ρ^2 does not scale.
A good collapse is obtained with the following values:

$$\alpha = 1.81 \tag{5.145}$$
$$\beta = -0.87 \tag{5.146}$$
$$\gamma = 1.83 \tag{5.147}$$
$$\nu = 0.4 \tag{5.148}$$
$$g_2^* = -2.75 \tag{5.149}$$

and the universal functions are shown in Figure 5.9.
A few comments are given here.

1. Although rigorous error estimates on the exponents are not given, the col-

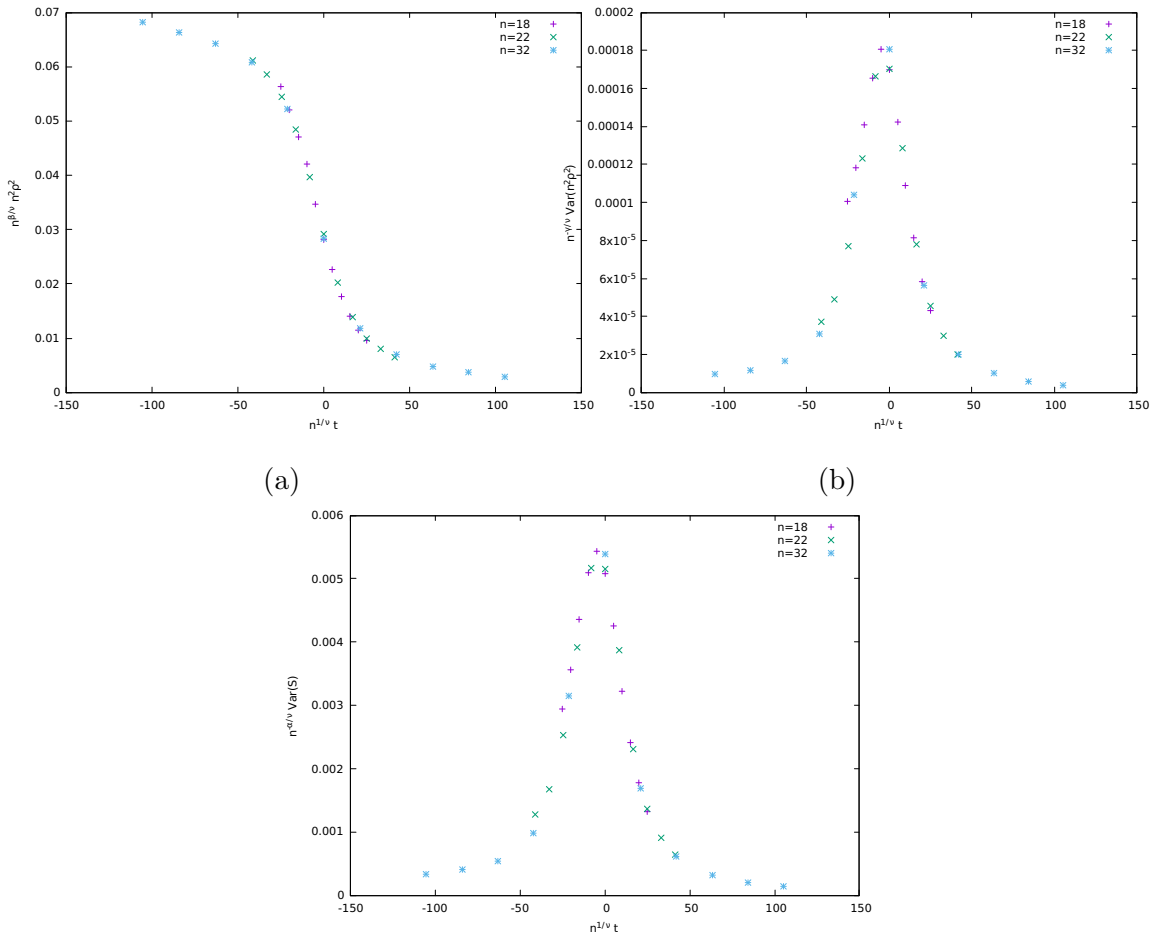

Figure 5.9: Universal finite-size scaling curves for (a) $n^2\rho^2$, (b) $\mathrm{Var}(n^2\rho^2)$ and (c) $\mathrm{Var}(S)$, first phase transition. The estimated critical exponents and critical coupling are $\alpha = 1.81$, $\beta = -0.87$, $\gamma = 1.83$, $\nu = 0.4$, and $g_2^* = -2.75$.

lapse is generally rather sensitive to a change is the first decimal digit.

2. The fact that the same value of ν allows to collapse all three observables is a good consistency check.

3. The negative value of β suggests that the order parameter diverges at criticality, which is rather unusual.

4. The critical exponents saturate to a good approximation Rushbrooke's inequality $\alpha + 2\beta + \gamma \geq 2$.

5. The set of critical exponents does not seem to belong to a known universality class.

A diverging correlation length at the critical point is an indication that the phase transition is second order. A second argument in support of this comes from analyzing the Monte Carlo history of the action and the order parameter around criticality. In a first order phase transition the two phases coexist at the critical point, therefore one would expect to see the observables tunnel back and forth between two distinct values throughout the simulation. If the transition is second order, however, the system interpolates smoothly across the critical point from one phase to the other, and Monte Carlo samples of the observables at criticality appear uniformly distributed along a range of values. The Monte Carlo history of S and ρ^2 around the phase transition is shown in Figure 5.10 and 5.11, while Figure 5.12 shows their distribution. The results seem to exclude the possibility of the transition being first order.

The second phase transition

A puzzling aspect of the second phase transition is that its location does not seem to converge around any finite value. This poses the question of whether it survives the large n limit or not. In addition, a finite-size scaling analysis is not possible since no critical value g_2^* can be found. However, there is good indication that the transition is first order. Plotting the distribution of S and ρ^2 at the critical point for some fixed n shows two clear maxima (Figure 5.14), indicating coexistence of two phases. The same phenomenon translates to back and forth tunneling in Monte Carlo time as already argued in the previous section (Figure 5.13).

5.4.3 Spectral data

Another important source of information comes from looking at the eigenvalue distribution of the matrices. The analysis will be presented separately for the three different phases.

Density of states in region I

The typical eigenvalue distribution of A and B for small g_2 is described very well by equation (4.5) in [47]:

$$P(\lambda) = \frac{8}{\pi} \frac{\lambda^2 + b}{c(c + 4b)} \sqrt{c - \lambda^2} \tag{5.150}$$

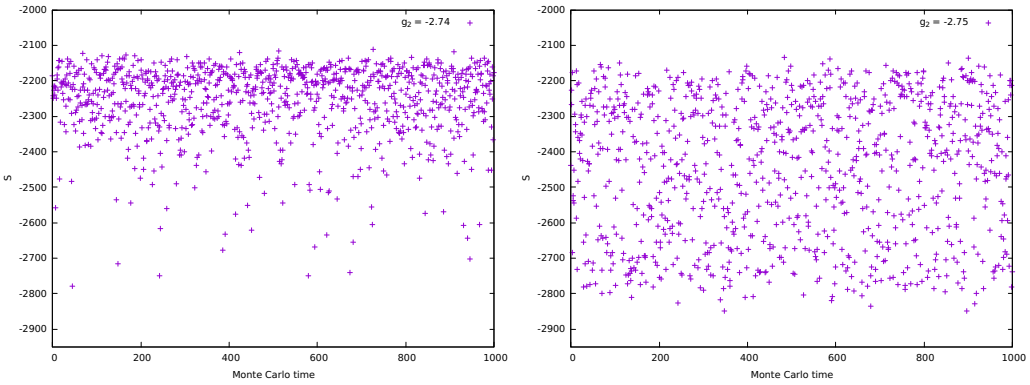

(a) $g_2 = -2.74$ (b) $g_2 = -2.75$

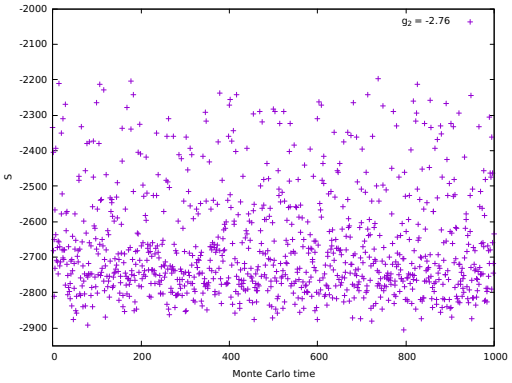

(c) $g_2 = -2.76$

Figure 5.10: Monte Carlo history of S for $n = 32$ before, during and after the phase transition.

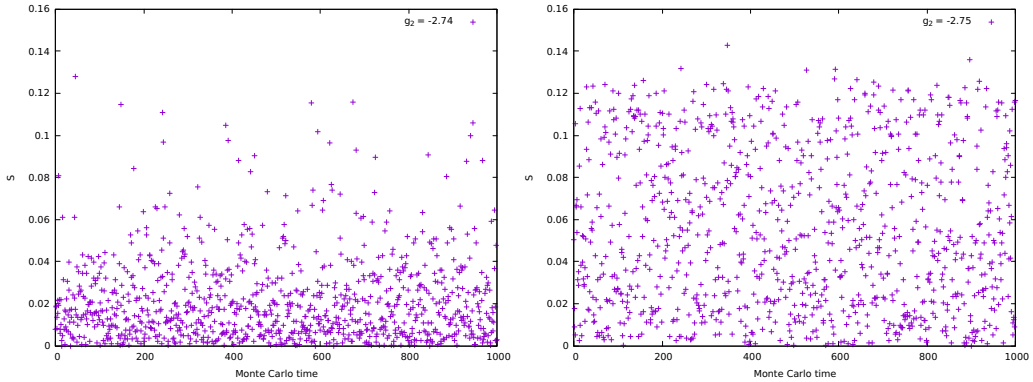

(a) $g_2 = -2.74$ (b) $g_2 = -2.75$

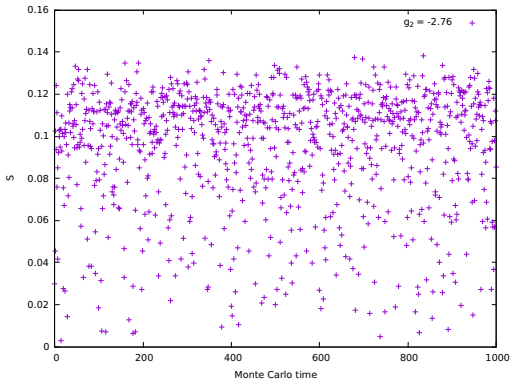

(c) $g_2 = -2.76$

Figure 5.11: Monte Carlo history of ρ^2 for $n = 32$ before, during and after the first phase transition.

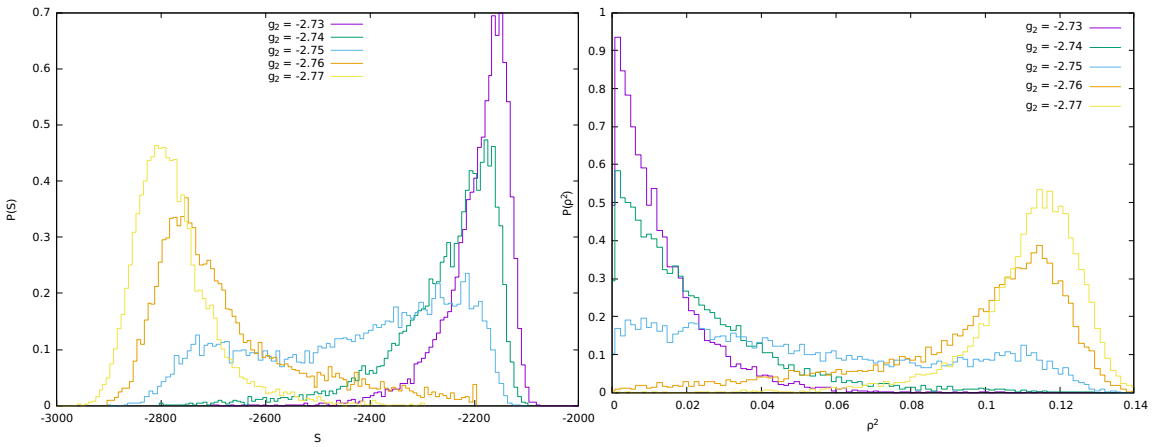

Figure 5.12: Distribution of S (left) and ρ^2 (right) across the first phase transition for $n = 32$.

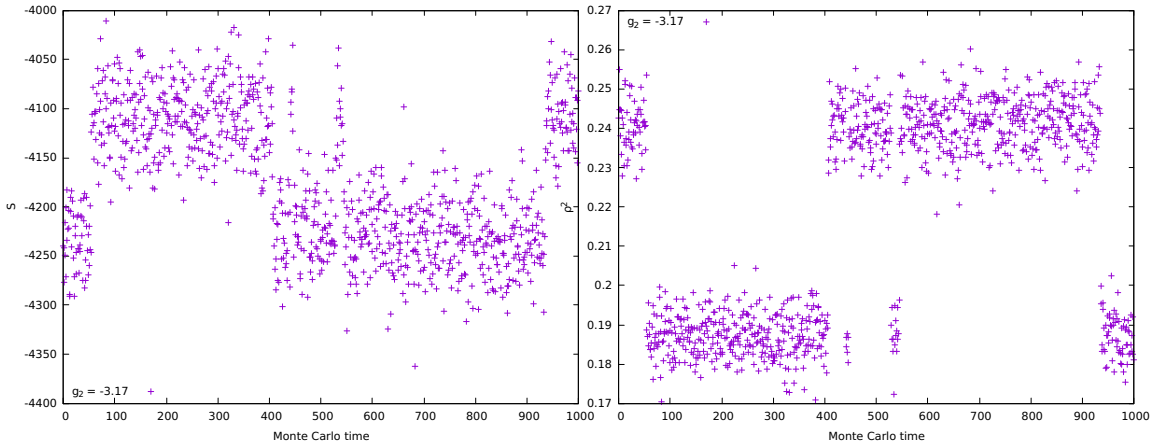

Figure 5.13: Monte Carlo history of S (left) and ρ^2 (right) at the second phase transition for $n = 32$. The critical point for this matrix size is estimated to be at $g_2 = -3.17$.

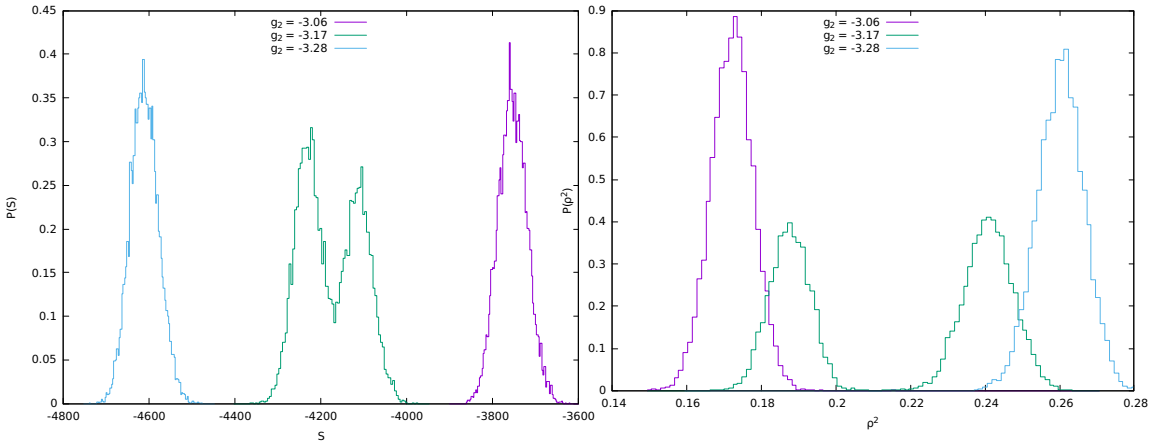

Figure 5.14: Distribution of S (left) and ρ^2 (right) across the second phase transition for $n = 32$. The critical point for this matrix size is estimated to be at $g_2 = -3.17$.

which is the one-cut solution for a matrix in a simple quartic potential. This suggests that in this region the two matrices decouple from each other and are subject to an effective potential of the form:

$$S_{\text{eff}} = (\alpha_2 \operatorname{Tr} A^2 + \alpha_4 \operatorname{Tr} A^4) + (\beta_2 \operatorname{Tr} B^2 + \beta_4 \operatorname{Tr} B^4). \tag{5.151}$$

If the distribution is supported on $[-a, a]$, the parameter c is related to a by $c = a^2$. Fitting (5.150) to A and B at $g_2 = -1.5$ for matrix size $n = 32$ gives:

$$A) \quad c = 0.523(2) \tag{5.152}$$
$$b = 0.54(2) \tag{5.153}$$

$$B) \quad c = 0.523(1) \tag{5.154}$$
$$b = 0.53(2) \tag{5.155}$$

and it is shown in Figure 5.15.

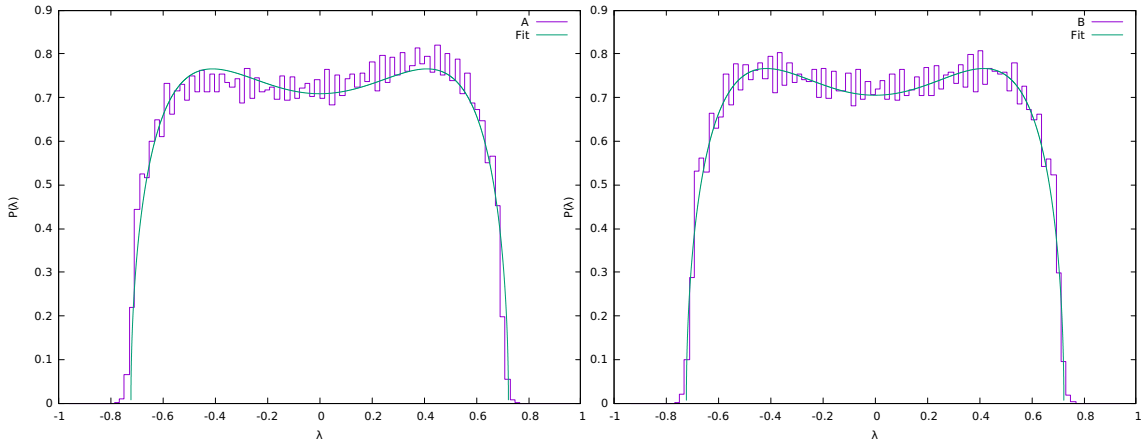

Figure 5.15: Density of states of A (left) and B (right) at $g_2 = -1.5$ for $n = 32$, and theoretical curve (5.150).

Notice how A appears skewed towards the positive peak. In fact, approaching the first phase transition the asymmetry becomes more and more pronounced, casting doubts on the validity of (5.150). However, the effect is due to the choice of variables. The true decoupled matrices are v_1 and v_2, which preserve the same shape up until the phase transition. Figure 5.16 shows the fit at $g_2 = -2.1$ for v_1 and v_2.

Density of states in region II

Crossing the first phase transition, A and B display drastically different behaviours. The asymmetry in A develops in a non-trivial two-cut solution with asymmetric support, while B goes from behaving like a matrix in a quartic potential to an even simpler free semicircle distribution. The description in terms of v_1 and v_2 is not so clear anymore, suggesting that A and B better represent the decoupled degrees of freedom of the model in this region. The crossing is shown in Figure 5.17.

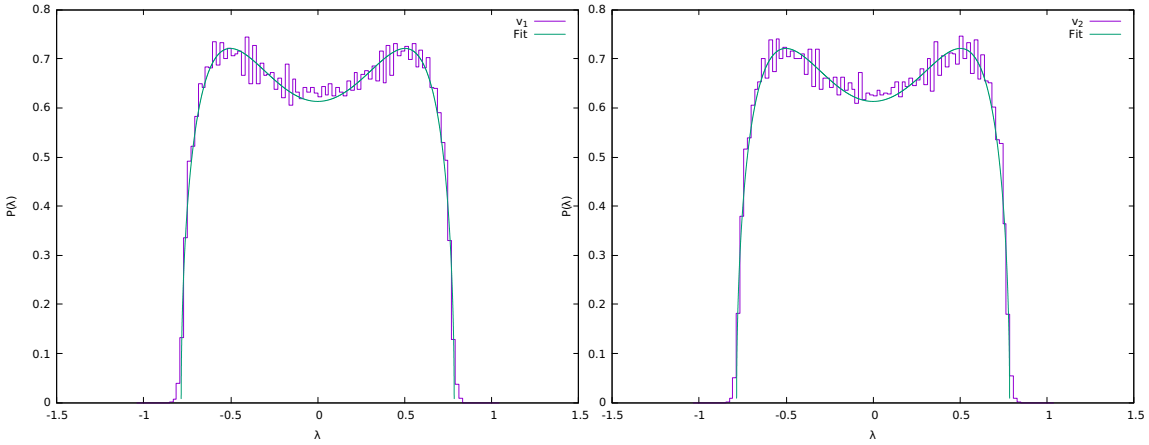

Figure 5.16: Density of states of v_1 (left) and v_2 (right) at $g_2 = -2.1$ for $n = 32$, and theoretical curve (5.150).

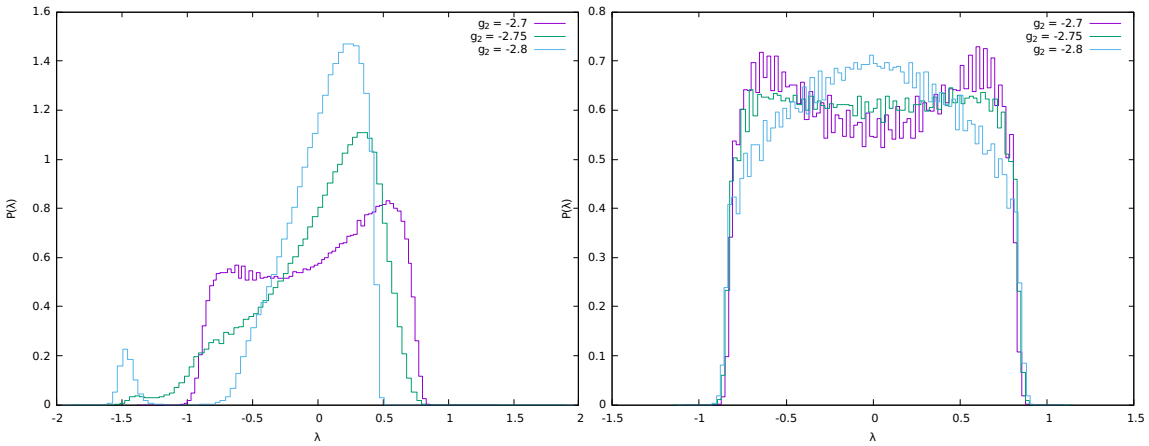

Figure 5.17: Density of states of A (left) and B (right) at $g_2 = -2.7, -2.75, -2.8$ for $n = 32$.

The asymmetric density of A resembles the one found for the $(1,0)$ Dirac operator. Indeed, the density (4.59) can be fitted to A at $g_2 = -2.8$ with reasonably good results, as shown in Figure 5.18. The fitted parameters are:

$a_1 = -1.560(5)$
$b_1 = -1.32(1)$
$a_2 = -0.78(5)$
$b_2 = 0.466(1)$
$\alpha = 11.0(2)$
$\beta = 26.3(3)$

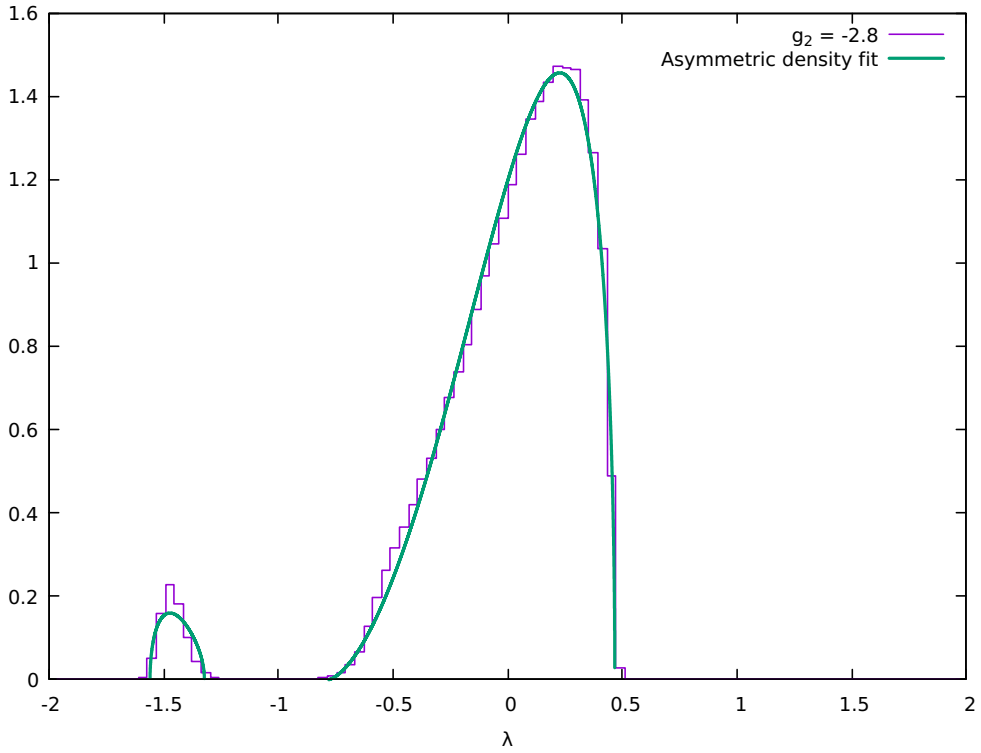

Figure 5.18: Fit of the (1,0) asymmetric density (4.59) to the density of states of A at $g_2 = -2.8$ in the full random $(2,0)$ model for $n = 32$.

Density of states in region III

The second phase transition is understood in terms of spectral data as A losing the smaller peak and going back to a one-cut distribution, albeit an asymmetric one (Figure 5.19a), while B does not play any role as it remains a free Gaussian throughout. In this phase A becomes itself a free Gaussian asymptotically, as Figure 5.19b, taken at $g_2 = -36$, indicates.

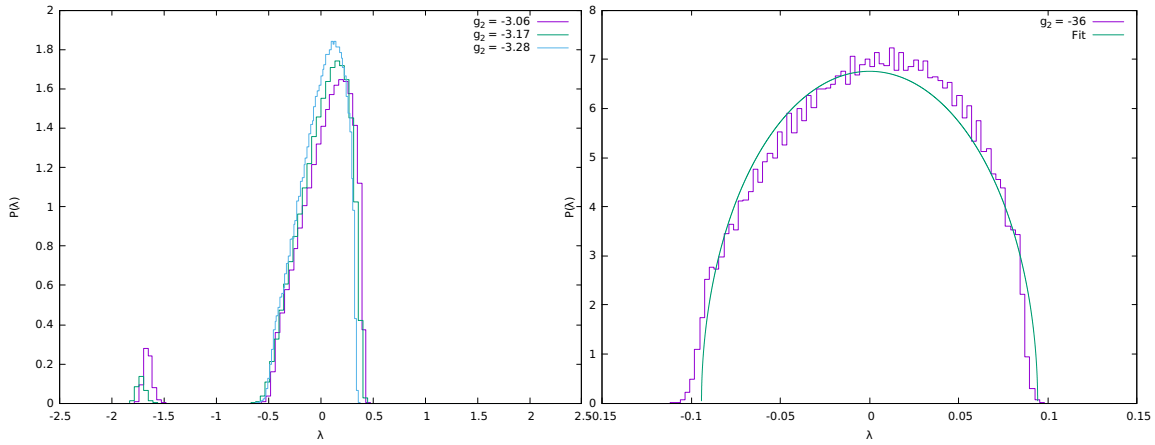

(a) (b)

Figure 5.19: (a) Density of states of A at $g_2 = -3.06, -3.17, -2.28$ for $n = 32$. (b) Density of states of A at $g_2 = -36$ and fit to Wigner's semicircle for $n = 32$.

Chapter 6

Four-matrix models

6.1 Four-matrix models

6.1.1 Introduction

The following is a study concerning the classical solutions to the equations of motion for the four-matrix, two-trace random Dirac operators with action $S = g_2 \operatorname{Tr} D^2 + \operatorname{Tr} D^4$. There are four distinct models, obtained starting from a (p, q) Clifford module where $p + q = 3$. For this reason the four models will be referred to as the (3,0), (2,1), (1,2) and (0,3).
The Clifford gamma matrices are two-dimensional and can be taken to be the Hermitian or anti-Hermitian Pauli matrices. The corresponding Dirac operator will contain all linearly independent products of these, which means including the identity.
The Dirac operators ultimately can be written:

$$D = \sum_{\alpha=0}^{3} \sigma_\alpha \otimes \left(m_\alpha \otimes \mathbb{1}_n + e_\alpha \mathbb{1}_n \otimes m_\alpha^T \right) \tag{6.1}$$

where the m are arbitrary Hermitian matrices, σ_0 is the identity 2×2 matrix, $\sigma_{1,2,3}$ are the Hermitian Pauli matrices, and the four models are determined by the values of $e_\alpha = (e_0, e_1, e_2, e_3)$, which are:

$$(-1, +1, +1, +1) \quad \text{for} \quad (p, q) = (3, 0) \tag{6.2}$$
$$(+1, +1, -1, +1) \quad \text{for} \quad (p, q) = (2, 1) \tag{6.3}$$
$$(-1, +1, -1, -1) \quad \text{for} \quad (p, q) = (1, 2) \tag{6.4}$$
$$(+1, -1, -1, -1) \quad \text{for} \quad (p, q) = (0, 3) \tag{6.5}$$

Finally, where convenient, the whole expression for a commutator or anti-commutator will be condensed in a single capital letter:

$$D = \sum_{\alpha=0}^{3} \sigma_\alpha \otimes M_\alpha. \tag{6.6}$$

In the following, Greek indices will run from 0 to 3, while Latin indices from 1 to 3.

6.1.2 Computing the action

Using the results of Appendix F, the action reads:

$$S = 2g_2 \operatorname{Tr} M_\alpha^2 + 2 \operatorname{Tr} \big[M_0^4 + 2M_0 M_a M_0 M_a + 4M_0^2 M_a^2 + 4i\epsilon_{abc}\, M_0 M_a M_b M_c + 2M_a^2 M_b^2 - M_a M_b M_a M_b\big] \quad (6.7)$$

where summation over repeated indices is assumed, and M_a^2 is used as a shorthand for $\sum_a M_a M_a$, not $\sum_{a,b} M_a M_b$.
At this level the four models are equivalent, the difference being hidden in the e signs inside the M matrices. Expanding these gives:

$$\begin{aligned} S = {} & 4g_2\Big[n \operatorname{Tr} m_\alpha^2 + e_\alpha (\operatorname{Tr} m_\alpha)^2\Big] \\ & + 4\Bigg[n \operatorname{Tr} m_0^4 + 4e_0 \operatorname{Tr} m_0 \operatorname{Tr} m_0^3 + 3\left(\operatorname{Tr} m_0^2\right)^2 + 2n \operatorname{Tr} m_0 m_a m_0 m_a \\ & \quad + 4n \operatorname{Tr} m_0^2 m_a^2 + 12 e_a \operatorname{Tr} m_a \operatorname{Tr} m_0^2 m_a + 12 e_0 \operatorname{Tr} m_0 \operatorname{Tr} m_a^2 m_0 \\ & \quad + 6 \operatorname{Tr} m_0^2 \operatorname{Tr} m_a^2 + 12 e_0 e_a \left(\operatorname{Tr} m_0 m_a\right)^2 + 2n \operatorname{Tr} m_a^2 m_b^2 \\ & \quad - n \operatorname{Tr} m_a m_b m_a m_b + 4 e_a \operatorname{Tr} m_a \operatorname{Tr} m_b^2 m_a + \operatorname{Tr} m_a^2 \operatorname{Tr} m_b^2 + 2 e_a e_b \left(\operatorname{Tr} m_a m_b\right)^2 \\ & \quad + 2i\epsilon_{abc}\Big[2n \operatorname{Tr} m_0 m_a m_b m_c + 2 e_a \operatorname{Tr} m_a \operatorname{Tr} m_0 m_b m_c + 2 e_0 \operatorname{Tr} m_0 \operatorname{Tr} m_a m_b m_c\Big]\Bigg]. \end{aligned} \quad (6.8)$$

As in the two-matrix models studied in the previous chapter, it is convenient to split $m_\alpha = t_\alpha \mathbb{1} + v_\alpha$, with $\operatorname{Tr} v_\alpha = 0$. Then the action reads:

$$\begin{aligned} S = {} & 4g_2 \sum_\alpha \Big[n^2 (1+e_\alpha) t_\alpha^2 + n \operatorname{Tr} v_\alpha^2\Big] \\ & + 4\Bigg[4n(1+e_0)\left(n t_0^4 + 3 t_0^2 \operatorname{Tr} v_0^2 + t_0 \operatorname{Tr} v_0^3\right) + n \operatorname{Tr} v_0^4 + 3\left(\operatorname{Tr} v_0^2\right)^2 \\ & \quad + \sum_a \Big[12n(1 + e_0 + e_a + e_0 e_a)\left(n t_0^2 t_a^2 + 2 t_0 t_a \operatorname{Tr} v_0 v_a\right) \\ & \quad + 12n(1+e_0)\left(t_0^2 \operatorname{Tr} v_a^2 + t_0 \operatorname{Tr} v_a^2 v_0\right) + 12n(1+e_a)\left(t_a^2 \operatorname{Tr} v_0^2 + t_a \operatorname{Tr} v_0^2 v_a\right) \\ & \quad + 2n \operatorname{Tr} v_0 v_a v_0 v_a + 4n \operatorname{Tr} v_0^2 v_a^2 + 6 \operatorname{Tr} v_0^2 \operatorname{Tr} v_a^2 + 12 e_0 e_a \left(\operatorname{Tr} v_0 v_a\right)^2 \Big] \\ & \quad + \sum_{a,b} \Big[2n(1 + e_a + e_b + e_a e_b)\left(n t_a^2 t_b^2 + 2 t_a t_b \operatorname{Tr} v_a v_b\right) \\ & \quad + 4n(1+e_a)\left(t_a^2 \operatorname{Tr} v_b^2 + t_a \operatorname{Tr} v_b^2 v_a\right) - n \operatorname{Tr} v_a v_b v_a v_b + 2n \operatorname{Tr} v_a^2 v_b^2 \\ & \quad + \operatorname{Tr} v_a^2 \operatorname{Tr} v_b^2 + 2 e_a e_b \left(\operatorname{Tr} v_a v_b\right)^2 \Big] \\ & \quad + 4ni \sum_{a,b,c} \epsilon_{abc}\Big[\operatorname{Tr} v_0 v_a v_b v_c + (1+e_0) t_0 \operatorname{Tr} v_a v_b v_c + (1+e_a) t_a \operatorname{Tr} v_0 v_b v_c\Big]\Bigg]. \end{aligned} \quad (6.9)$$

6.1.3 Stationary equations

From the action, the stationary equations are easily found:

$$
\begin{aligned}
t_0) \quad & (1+e_0)(g_2 n t_0 + 8 n t_0^3 + 12 t_0 \operatorname{Tr} v_0^2 + 2 \operatorname{Tr} v_0^3) \\
& + \sum_a (1+e_0)(12 t_0 \operatorname{Tr} v_a^2 + 6 \operatorname{Tr} v_a^2 v_0) \\
& + \sum_a (1+e_0+e_a+e_0 e_a)(12 n t_0 t_a^2 + 12 t_a \operatorname{Tr} v_0 v_a) \\
& + 2i(1+e_0) \sum_{a,b,c} \epsilon_{abc} \operatorname{Tr} v_a v_b v_c = 0
\end{aligned} \tag{6.10}
$$

$$
\begin{aligned}
t_c) \quad & (1+e_c)(g_2 n t_c + 12 t_c \operatorname{Tr} v_0^2 + 6 \operatorname{Tr} v_0^2 v_c) \\
& + (1+e_0+e_c+e_0 e_c)(12 n t_0^2 t_c + 12 t_0 \operatorname{Tr} v_0 v_c) \\
& + \sum_a (1+e_c)(4 t_c \operatorname{Tr} v_a^2 + 2 \operatorname{Tr} v_a^2 v_c) \\
& + \sum_a (1+e_a+e_c+e_a e_c)(4 n t_a^2 t_c + 4 t_a \operatorname{Tr} v_a v_c) \\
& + 2i(1+e_c) \sum_{a,b} \epsilon_{abc} \operatorname{Tr} v_0 v_a v_b = 0
\end{aligned} \tag{6.11}
$$

$$
\begin{aligned}
v_0) \quad & g_2 v_0 + 2 v_0^3 + \frac{6}{n} (\operatorname{Tr} v_0^2) v_0 + (1+e_0)(12 t_0^2 v_0 + 6 t_0 v_0^2) \\
& + \sum_a \Big[2 v_a v_0 v_a + 2\{v_a^2, v_0\} + \frac{6}{n} (\operatorname{Tr} v_a^2) v_0 + \frac{12}{n} e_0 e_a (\operatorname{Tr} v_0 v_a) v_a \\
& + 6(1+e_0) t_0 v_a^2 + (1+e_a)(12 t_a^2 v_0 + 6 t_a \{v_0, v_a\}) \Big] \\
& + 2i \sum_{a,b,c} \epsilon_{abc} \Big[(1+e_a) t_a v_b v_c + v_a v_b v_c \Big] \propto \mathbb{1}
\end{aligned} \tag{6.12}
$$

$$
\begin{aligned}
v_c) \quad & g_2 v_c + 2 v_0 v_c v_0 + 2\{v_0^2, v_c\} + \frac{6}{n} (\operatorname{Tr} v_0^2) v_c \\
& + \frac{12}{n} e_0 e_c (\operatorname{Tr} v_0 v_c) v_0 + (1+e_0)(12 t_0^2 v_c + 6 t_0 \{v_0, v_c\}) \\
& + \sum_a \Big[-2 v_a v_c v_a + 2\{v_a^2, v_c\} + \frac{2}{n} (\operatorname{Tr} v_a^2) v_c + \frac{4}{n} e_a e_c (\operatorname{Tr} v_a v_c) v_a \\
& + (1+e_a)(4 t_a^2 v_c + 2 t_a \{v_a, v_c\}) + 2(1+e_c) t_c v_a^2 + 4(1+e_a+e_c+e_a e_c) t_a t_c v_a \Big] \\
& + 2i \sum_{a,b} \epsilon_{abc} \Big[v_0 v_a v_b + v_a v_0 v_b + v_a v_b v_0 + 3(1+e_0) t_0 v_a v_b + (1+e_a) t_a [v_0, v_b] \Big] \propto \mathbb{1}
\end{aligned} \tag{6.13}
$$

Finding all possible solutions is hard for matrix equations in general. Some special solutions will be worked out by making simplifying assumptions in line with what already worked for the two-matrix models. The richness of these higher types,

however, will also allow for a new ansatz based on $su(2)$ algebra generators, raising the question of whether fuzzy sphere-like stationary solutions are realized in the model.

6.2 Solutions involving mainly scalar variables

6.2.1 All-scalar solutions

Solutions involving only the scalar variables are the easiest to work out. When $v_\alpha = 0$ for all α, the equations reduce to:

$$t_0) \quad (1+e_0)(g_2 n t_0 + 8 n t_0^3) + \sum_a (1 + e_0 + e_a + e_0 e_a) 12 n t_0 t_a^2 = 0 \tag{6.14}$$

$$\begin{aligned} t_c) \quad & (1+e_c) g_2 n t_c + (1 + e_0 + e_c + e_0 e_c) 12 n t_0^2 t_c \\ & + \sum_a (1 + e_a + e_c + e_a e_c) 4 n t_a^2 t_c = 0 \end{aligned} \tag{6.15}$$

The (3,0), (1,2) and (0,3) only have one type of scalar variable (either t_0 or t_c), and for this reason there is only one equation with a unique solution which is formally identical in all three models:

$$y^2 = -\frac{g_2}{8} \tag{6.16}$$

where

$$y^2 := \sum_{a=1}^{3} t_a^2 \qquad \text{(3,0) model} \tag{6.17}$$

$$y^2 := t_1^2 \qquad \text{(1,2) model} \tag{6.18}$$

$$y^2 := t_0^2 \qquad \text{(0,3) model.} \tag{6.19}$$

The (2,1) is the richer one, being the only model where both t_0 and t_c may be non-vanishing. In this case there are three distinct solutions:

$$1) \quad t_0 = 0, \quad t_1^2 + t_2^2 = -\frac{g_2}{8} \tag{6.20}$$

$$2) \quad t_0^2 = -\frac{g_2}{8}, \quad t_1 = t_2 = 0 \tag{6.21}$$

$$3) \quad t_0^2 = -\frac{g_2}{32}, \quad t_1^2 + t_2^2 = -\frac{g_2}{32}. \tag{6.22}$$

6.2.2 Scalar and $v_0^2 \propto \mathbb{1}$ solutions

Next are worked out solutions for scalars and v_0, in the special case where $v_0^2 = x^2 \mathbb{1}$ with $0 \neq x \in \mathbb{R}$. This involutory property on v_0 is restrictive, but the same strategy in the two-matrix models led to non-trivial results reproduced by the numerical simulations.

The equations in this case reduce to:

$$t_0) \quad (1+e_0)(g_2+8t_0^2+12x^2)t_0+\sum_a(1+e_0+e_a+e_0e_a)12t_0t_a^2=0 \tag{6.23}$$

$$\begin{aligned} t_c) \quad & (1+e_c)(g_2+12x^2)t_c+(1+e_0+e_c+e_0e_c)12t_ct_0^2 \\ & +\sum_a(1+e_a+e_c+e_ae_c)4t_ct_a^2=0 \end{aligned} \tag{6.24}$$

$$v_0) \quad g_2+8x^2+\sum_{\alpha=0}^{3}(1+e_\alpha)12t_\alpha^2=0. \tag{6.25}$$

Again the (3,0), (1,2) and (0,3) models all reduce to the same formal equations:

$$y) \quad (g_2+12x^2+8y^2)y=0 \tag{6.26}$$

$$v_0) \quad g_2+8x^2+24y^2=0. \tag{6.27}$$

with solution

$$x^2=-\frac{g_2}{8},\ y=0 \qquad \text{or} \qquad x^2=-\frac{g_2}{14},\ y^2=-\frac{g_2}{56}. \tag{6.28}$$

The remaining (2,1) model reduces to (6.26) and (6.27) again if either $t_0=0$ or $\sum t_a^2=0$. The extra solution arising here when all variables are non-vanishing is:

$$x^2=-\frac{g_2}{20}, \quad t_0^2=-\frac{g_2}{80}, \quad \sum_{a\neq 2}t_a^2=-\frac{g_2}{80}. \tag{6.29}$$

6.3 Commuting involutory matrix solutions

One step further in complexity is to assume non-vanishing commuting matrices. Again imposing the involutory property seems to be the best chance at getting a non-trivial solution.
The assumptions are as follows:

$$t_\alpha=0 \tag{6.30}$$

$$v_\alpha^2=x_\alpha^2\mathbb{1}, \quad x_\alpha\in\mathbb{R} \tag{6.31}$$

$$[v_\alpha,v_\beta]=0 \tag{6.32}$$

where $\alpha = 0, 1, 2, 3$. The equations for t_0 and t_c are automatically satisfied, and the remaining ones read:

$$v_0) \quad g_2 v_0 + 8x_0^2 v_0 + \sum_a \left[12 x_a^2 v_0 + \frac{12}{n} e_0 e_a (\mathrm{Tr}\, v_0 v_a) v_a \right] \propto \mathbb{1} \tag{6.33}$$

$$v_c) \quad g_2 v_c + 12 x_0^2 v_c + \frac{12}{n} e_0 e_c (\mathrm{Tr}\, v_0 v_c) v_0 + \sum_a \left[4 x_a^2 v_c + \frac{4}{n} e_a e_c (\mathrm{Tr}\, v_a v_c) v_a \right] \propto \mathbb{1}. \tag{6.34}$$

Notice how all terms are traceless, making the RHS =0. Now multiply the first equation by v_0 and the second by v_c. They become:

$$v_0) \quad \left(g_2 x_0^2 + 8x_0^4 + 12 x_0^2 \sum_a x_a^2 \right) \mathbb{1} + \frac{12}{n} \sum_a e_0 e_a (\mathrm{Tr}\, v_0 v_a) v_0 v_a = 0 \tag{6.35}$$

$$\begin{aligned} v_c) \quad & \Big(g_2 x_c^2 + 12 x_0^2 x_c^2 + 4 \sum_a x_a^2 x_c^2 \Big) \mathbb{1} + \frac{12}{n} e_0 e_c (\mathrm{Tr}\, v_0 v_c) v_0 v_c \\ & + \frac{4}{n} \sum_a e_a e_c (\mathrm{Tr}\, v_a v_c) v_a v_c = 0. \end{aligned} \tag{6.36}$$

Focus on the first one. Since the term proportional to $v_0 v_a$ is the only one that can have a traceless component, the equation can only be satisfied if either:

$$\mathrm{Tr}\, v_0 v_a = 0 \qquad \text{or} \qquad v_0 v_a = \frac{\mathrm{Tr}\, v_0 v_a}{n} \mathbb{1}.$$

Once one alternative is chosen, the same argument applies to the $v_a v_c$ term in the second equation. Therefore the solutions can be classified by a choice:

$$\mathrm{Tr}\, v_\alpha v_\beta = 0 \qquad \text{or} \qquad v_\alpha v_\beta = \frac{\mathrm{Tr}\, v_\alpha v_\beta}{n} \mathbb{1} \qquad \alpha \neq \beta = 0, \ldots, 3. \tag{6.37}$$

The first is an orthogonality condition on the matrices, while the second expresses the fact that the two matrices are proportional to each other (multiply by v_α and use commutation and involution). Realizing the orthogonality condition between more than two matrices can be done in the following way. As noted in the previous chapter, two $4k \times 4k$ traceless, involutory, commuting and mutually orthogonal matrices A and B can be written in the diagonalizing basis as:

$$A \propto \begin{pmatrix} \mathbb{1}_{2k} & \\ & -\mathbb{1}_{2k} \end{pmatrix}, \quad B \propto \begin{pmatrix} \mathbb{1}_k & & & \\ & -\mathbb{1}_k & & \\ & & \mathbb{1}_k & \\ & & & -\mathbb{1}_k \end{pmatrix} \tag{6.38}$$

This restricts the dimension of the matrices to be a multiple of 4. If one is interested in N matrices satisfying the same properties, then the same argument can be applied recursively to each block and one finds that the dimension must be a

multiple of 2^N. So for example for three matrices A, B and C, one finds:

$$A \propto \begin{pmatrix} \mathbb{1}_{4k} & \\ & -\mathbb{1}_{4k} \end{pmatrix}, \quad B \propto \begin{pmatrix} \mathbb{1}_{2k} & & & \\ & -\mathbb{1}_{2k} & & \\ & & \mathbb{1}_{2k} & \\ & & & -\mathbb{1}_{2k} \end{pmatrix}$$

$$C \propto \begin{pmatrix} \mathbb{1}_k & & & & & & & \\ & -\mathbb{1}_k & & & & & & \\ & & \mathbb{1}_k & & & & & \\ & & & -\mathbb{1}_k & & & & \\ & & & & \mathbb{1}_k & & & \\ & & & & & -\mathbb{1}_k & & \\ & & & & & & \mathbb{1}_k & \\ & & & & & & & -\mathbb{1}_k \end{pmatrix}. \tag{6.39}$$

Imposing one of the two conditions brings to several different combinations in the various models based on the relative sign $e_\alpha e_\beta$. As an intermediate step towards finding solutions, a generalized model will be written down first. Consider the following signature:

$$(+1, -1, \ldots, -1, +1, \ldots, +1) \tag{6.40}$$

where the first sign is associated with the index 0, the negative signs with a dotted index $\dot{c} \in J$, and the last group of positive signs with an undecorated index $c \in I$. The number of dotted and normal indices need not be specified. Consider a generalized version of (6.35) and (6.36):

$$\begin{aligned} v_0) \quad & \left(g_2 x_0^2 + 8x_0^4 + 12x_0^2 \sum_{a\in I} x_a^2 + 12x_0^2 \sum_{\dot{a}\in J} x_{\dot{a}}^2 \right) \mathbb{1} \\ & + \frac{12}{n} \sum_{a\in I} (\operatorname{Tr} v_0 v_a) v_0 v_a - \frac{12}{n} \sum_{\dot{a}\in J} (\operatorname{Tr} v_0 v_{\dot{a}}) v_0 v_{\dot{a}} = 0 \end{aligned} \tag{6.41}$$

$$\begin{aligned} v_c) \quad & \Big(g_2 x_c^2 + 12x_0^2 x_c^2 + 4 \sum_{a\in I} x_a^2 x_c^2 + 4 \sum_{\dot{a}\in J} x_{\dot{a}}^2 x_c^2 \Big) \mathbb{1} \\ & + \frac{12}{n} (\operatorname{Tr} v_0 v_c) v_0 v_c + \frac{4}{n} \sum_{a\in I} (\operatorname{Tr} v_a v_c) v_a v_c - \frac{4}{n} \sum_{\dot{a}\in J} (\operatorname{Tr} v_{\dot{a}} v_c) v_{\dot{a}} v_c = 0 \end{aligned} \tag{6.42}$$

$$\begin{aligned} v_{\dot{c}}) \quad & \Big(g_2 x_{\dot{c}}^2 + 12x_0^2 x_{\dot{c}}^2 + 4 \sum_{a\in I} x_a^2 x_{\dot{c}}^2 + 4 \sum_{\dot{a}\in J} x_{\dot{a}}^2 x_{\dot{c}}^2 \Big) \mathbb{1} \\ & - \frac{12}{n} (\operatorname{Tr} v_0 v_{\dot{c}}) v_0 v_{\dot{c}} - \frac{4}{n} \sum_{a\in I} (\operatorname{Tr} v_a v_{\dot{c}}) v_a v_{\dot{c}} + \frac{4}{n} \sum_{\dot{a}\in J} (\operatorname{Tr} v_{\dot{a}} v_{\dot{c}}) v_{\dot{a}} v_{\dot{c}} = 0. \end{aligned} \tag{6.43}$$

A choice of (6.37) amounts then to defining the following index sets:

$$I_\bullet = \{a \in I : \ v_\bullet v_a \propto \mathbb{1}\}$$
$$J_\bullet = \{\dot{a} \in J : \ v_\bullet v_{\dot{a}} \propto \mathbb{1}\}$$

where $\bullet = 0, c, \dot{c}$. Notice that not all possible combinations are equally valid, since for example if $a_1 \in I_{a_2}$, then necessarily $a_2 \in I_{a_1}$. The equations read:

$$v_0) \quad x_0^2 \left(2x_0^2 + 3 \sum_{a \in I - I_0} x_a^2 + 6 \sum_{a \in I_0} x_a^2 + 3 \sum_{\dot{a} \in J - J_0} x_{\dot{a}}^2 + \frac{g_2}{4} \right) = 0 \tag{6.44}$$

$$v_c) \quad x_c^2 \left(6x_0^2 + \sum_{a \in I - I_c} x_a^2 + 2 \sum_{a \in I_c} x_a^2 + \sum_{\dot{a} \in J - J_c} x_{\dot{a}}^2 + \frac{g_2}{4} \right) = 0, \quad \text{if } c \in I_0 \tag{6.45}$$

$$v_c) \quad x_c^2 \left(3x_0^2 + \sum_{a \in I - I_c} x_a^2 + 2 \sum_{a \in I_c} x_a^2 + \sum_{\dot{a} \in J - J_c} x_{\dot{a}}^2 + \frac{g_2}{4} \right) = 0, \quad \text{if } c \notin I_0 \tag{6.46}$$

$$v_{\dot{c}}) \quad x_{\dot{c}}^2 \left(\sum_{a \in I - I_{\dot{c}}} x_a^2 + \sum_{\dot{a} \in J - J_{\dot{c}}} x_{\dot{a}}^2 + 2 \sum_{\dot{a} \in J_{\dot{c}}} x_{\dot{a}}^2 + \frac{g_2}{4} \right) = 0, \quad \text{if } \dot{c} \in J_0 \tag{6.47}$$

$$v_{\dot{c}}) \quad x_{\dot{c}}^2 \left(3x_0^2 + \sum_{a \in I - I_{\dot{c}}} x_a^2 + \sum_{\dot{a} \in J - J_{\dot{c}}} x_{\dot{a}}^2 + 2 \sum_{\dot{a} \in J_{\dot{c}}} x_{\dot{a}}^2 + \frac{g_2}{4} \right) = 0, \quad \text{if } \dot{c} \notin J_0. \tag{6.48}$$

The four original models can be divided in two classes. The $(3,0)$ and $(0,3)$ model have index sets with cardinality $|I| = 0$ and $|J| = 3$, while the $(2,1)$ and $(1,2)$ model have $|I| = 2$ and $|J| = 1$. Explicit solutions for these two classes are listed in Appendix G. The trivial case where all variables vanish is omitted as it is always a solution.

6.4 $su(2)$ solutions

All the solutions presented so far are of limited physical interest. Even involutory commuting matrices are, in a sense, not much more than scalars. These four-matrix models, however, are rich enough to host an interesting class of solutions involving $su(2)$ commutation relations. Such solutions are related to the geometry of fuzzy spheres [35], and having them emerge as stationary configurations opens up the possibility of disordered-to-geometric transitions in the phase diagram of the matrix models. In the simplest case, these solutions arise when $v_0 = 0$ and $t_c = 0$ for $c = 1, 2, 3$. This leads to the following equations.

(3,0) stationary equations when $v_0 = 0$ and $t_c = 0$ for $c = 1, 2, 3$

$$t_c) \quad 4\sum_a \operatorname{Tr} v_a^2 v_c = 0 \tag{6.49}$$

$$v_0) \quad 2i\sum_{a,b,c} \epsilon_{abc} v_a v_b v_c \propto \mathbb{1} \tag{6.50}$$

$$\begin{aligned} v_c) \quad & g_2 v_c + \sum_a \Big[-2v_a v_c v_a + 2\{v_a^2, v_c\} + \frac{2}{n}(\operatorname{Tr} v_a^2) v_c \Big] \\ & + \sum_{a \neq c} \frac{4}{n}(\operatorname{Tr} v_a v_c) v_a + \frac{4}{n}(\operatorname{Tr} v_c^2) v_c \propto \mathbb{1} \end{aligned} \tag{6.51}$$

(2,1) stationary equations when $v_0 = 0$ and $t_c = 0$ for $c = 1, 2, 3$

$$t_0) \quad g_2 n t_0 + 8n t_0^3 + 12 t_0 \sum_a \operatorname{Tr} v_a^2 + 2i \sum_{a,b,c} \epsilon_{abc} \operatorname{Tr} v_a v_b v_c = 0 \tag{6.52}$$

$$t_{c\neq 2}) \quad 4\sum_a \operatorname{Tr} v_a^2 v_c = 0 \tag{6.53}$$

$$v_0) \quad 12 t_0 \sum_a v_a^2 + 2i \sum_{a,b,c} \epsilon_{abc} v_a v_b v_c \propto \mathbb{1} \tag{6.54}$$

$$\begin{aligned} v_c) \quad & g_2 v_c + 24 t_0^2 v_c + \sum_a \Big[-2v_a v_c v_a + 2\{v_a^2, v_c\} + \frac{2}{n}(\operatorname{Tr} v_a^2) v_c \Big] \\ & + \sum_{a \neq c} e_a e_c \frac{4}{n}(\operatorname{Tr} v_a v_c) v_a + \frac{4}{n}(\operatorname{Tr} v_c^2) v_c + 12 i t_0 \sum_{a,b} \epsilon_{abc} v_a v_b \propto \mathbb{1} \end{aligned} \tag{6.55}$$

(1,2) stationary equations when $v_0 = 0$ and $t_c = 0$ for $c = 1, 2, 3$

$$t_1) \quad 4\sum_a \operatorname{Tr} v_a^2 v_1 = 0 \tag{6.56}$$

$$v_0) \quad 2i\sum_{a,b,c} \epsilon_{abc} v_a v_b v_c \propto \mathbb{1} \tag{6.57}$$

$$\begin{aligned} v_c) \quad & g_2 v_c + \sum_a \Big[-2v_a v_c v_a + 2\{v_a^2, v_c\} + \frac{2}{n}(\operatorname{Tr} v_a^2) v_c \Big] \\ & + \sum_{a \neq c} e_a e_c \frac{4}{n}(\operatorname{Tr} v_a v_c) v_a + \frac{4}{n}(\operatorname{Tr} v_c^2) v_c \propto \mathbb{1} \end{aligned} \tag{6.58}$$

(0,3) stationary equations when $v_0 = 0$ and $t_c = 0$ for $c = 1, 2, 3$

$$t_0) \quad g_2 n t_0 + 8 n t_0^3 + 12 t_0 \sum_a \operatorname{Tr} v_a^2 + 2i \sum_{a,b,c} \epsilon_{abc} \operatorname{Tr} v_a v_b v_c = 0 \tag{6.59}$$

$$v_0) \quad 12 t_0 \sum_a v_a^2 + 2i \sum_{a,b,c} \epsilon_{abc} v_a v_b v_c \propto \mathbb{1} \tag{6.60}$$

$$\begin{aligned} v_c) \quad & g_2 v_c + 24 t_0^2 v_c + \sum_a \Big[-2 v_a v_c v_a + 2\{v_a^2, v_c\} + \frac{2}{n} (\operatorname{Tr} v_a^2) v_c \Big] \\ & + \sum_{a \neq c} \frac{4}{n} (\operatorname{Tr} v_a v_c) v_a + \frac{4}{n} (\operatorname{Tr} v_c^2) v_c + 12 i t_0 \sum_{a,b} \epsilon_{abc} v_a v_b \propto \mathbb{1} \end{aligned} \tag{6.61}$$

It is easy to see that upon imposing $su(2)$ commutation relations on the matrices, and assuming the representation is irreducible, the equations for t_c and v_0 are automatically satisfied in all models. This assumption also takes care, by orthogonality of the generators, of the only terms where the e signs still appear. The ansatz for a $su(2)$ solution therefore is:

$$v_a = R\, l_a, \quad R \in \mathbb{R} \tag{6.62}$$

$$[l_a, l_b] = i \sum_c \epsilon_{abc} l_c \tag{6.63}$$

$$\sum_a l_a^2 = C \mathbb{1}. \tag{6.64}$$

Equation (6.63) corresponds to the $su(2)$ condition, while (6.64) requires the representation to be irreducible. That means that C is really a known function of n, corresponding to the value of the quadratic Casimir:

$$C = \frac{n^2 - 1}{4}. \tag{6.65}$$

Upon substituting these relations, the (3,0) model becomes indistinguishable from the (1,2), while the (0,3) becomes indistinguishable from the (2,1). The two inequivalent systems of equations are:

$$g_2 + 2R^2 + \frac{16}{3} R^2 C = 0 \qquad \text{for (3,0) and (1,2)} \tag{6.66}$$

$$\begin{cases} g_2 t_0 + 8 t_0^3 + 12 t_0 R^2 C - 2 R^3 C = 0 \\ \\ g_2 + 24 t_0^2 + 2R^2 - 12 t_0 R + \frac{16}{3} R^2 C = 0 \end{cases} \qquad \text{for (0,3) and (2,1)} \tag{6.67}$$

The solution to (6.66) is easily found as:

$$R^2 = -\frac{g_2}{2 + \frac{16}{3}C} = -\frac{g_2}{2}\frac{3}{2n^2+1} \tag{6.68}$$

The presence of t_0 makes (6.67) hard to solve, and in general there is no common solution to all four models. However, (6.67) can be solved for fixed n, and the solutions compared with (6.68).
There are three distinct real solutions to (6.67) for R^2 and t_0^2, shown for $n = 8$ in Figure 6.1 and 6.2 and denoted $R^2_{(i)}$ and $t^2_{0(i)}$, $i = 1, 2, 3$. The unique solution to (6.66) is also shown as a solid red line in Figure 6.1 and quite remarkably it lies very close to $R^2_{(1)}$. Since the discrepancy is suppressed in n, (6.68) will be taken as an approximation to $R^2_{(1)}$.

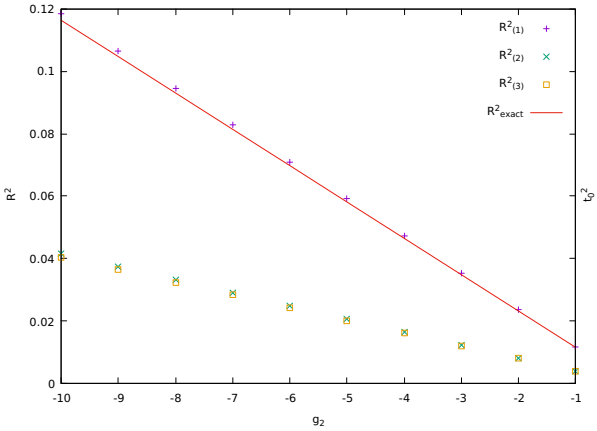

Figure 6.1: The three distinct numerical solutions to (6.67) for R^2 (purple, green and orange markers), and the unique solution to (6.66) (red line). The matrix dimension is fixed to $n = 8$.

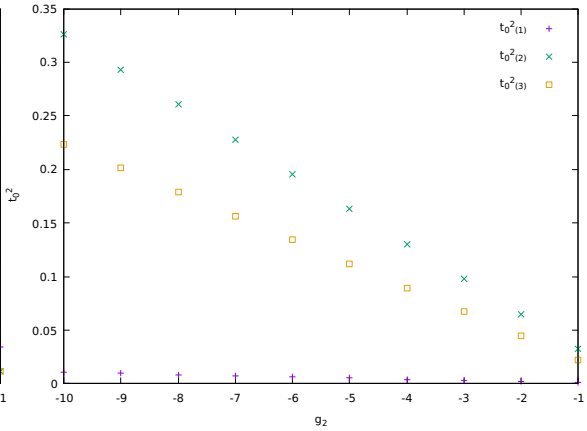

Figure 6.2: The three distinct numerical solutions to (6.67) for t_0^2. The matrix dimension is fixed to $n = 8$.

The explicit dependence on n of (6.68) makes R^2 an informative observable. On-shell, it is defined by:

$$R^2 = \frac{1}{nC}\,\mathrm{Tr}\sum_a v_a^2 \tag{6.69}$$

or, because of rotational invariance in v_1, v_2 and v_3:

$$R^2 = \frac{3}{nC}\,\mathrm{Tr}\,v_c^2, \quad c = 1, 2, 3. \tag{6.70}$$

Together with (6.68), it leads to the prediction:

$$\frac{1}{n}\,\mathrm{Tr}\,v_c^2 = -\frac{g_2}{8}\frac{n^2-1}{2n^2-1} \approx -\frac{g_2}{16}, \quad c = 1, 2, 3 \tag{6.71}$$

for large n. Should (6.71) be the preferred vacuum in any of the models, its characteristic scaling in n makes it in principle discernible in numerical simulations from the otherwise similar (G.33).

6.5 Numerical results

As a first general overview of the numerical results in the full random setting, the eight variables t_α, v_α are shown in Figure 6.3 for $n = 8$. The computational setup is identical to the one used for the two-matrix models (see Section 5.4).
The most noticeable feature is a change of behaviour happening at around $g_2 \approx -3.4$. For clarity, the region $g_2 \gtrsim -3.4$ will be referred to as region I, while $g_2 \lesssim -3.4$ as region II.
In region I the four models are basically indistinguishable, exhibiting what appears to be a rotational invariance in the v_c matrices for $c = 1, 2, 3$, while the corresponding scalars stay around zero. After the critical coupling, in region II, scalars acquire more importance and matrix variables start to split. This is not true for the (0,3) model however, where there seems to be no change at all throughout the whole g_2 range. Something similar happened in the two-matrix models, where (2,0) and (0,2) presented the same behaviour until the scalars of the (2,0) induced a phase transition that was absent in the (0,2).
These observations come in handy in interpreting the data in region I. In general any comparison between numerics and stationary solutions is only meaningful for very large negative values of g_2. There, the potential well is deep and oscillations around it are small. This means that data limited to region I is hardly understandable in terms of stationary solutions. The observations made before, however, allow one to speculate that, if the (0,3) model realizes any of the stationary solutions in region II, that would also be the solution around which *all models* fluctuate in region I.
Before moving on to analyze each model in more detail, note that the large fluctuations occurring in region II of Figure 6.3 are not necessarily due to numerical errors, but rather to a poor choice of variables. For instance the meaningful scalar quantity to monitor in the (3,0) model is the sum $t_1^2 + t_2^2 + t_3^2$, rather than each variable alone. Identifying the relevant variables for each model results in much more stable plots, as Figure 6.4 shows.

6.5.1 The (0,3) model

As argued in the previous paragraph, understanding the asymptotic behaviour of the (0,3) model might shed light on the small g_2 behaviour of all four models.
The most informative observables for the model are:

$$\frac{1}{n} \operatorname{Tr} v_c^2, \quad c = 1, 2, 3. \tag{6.72}$$

In region II they dominate over t_0 and v_0, they present rotational invariance and to a very good approximation they go as $-g_2/16$.
Good stationary solution candidates are either the $su(2)$ solution (6.71) or the all-orthogonal commuting involutory solution (G.33). If the commuting solution is realized then the asymptotics should be $-g_2/16$ regardless of n, while the $su(2)$ solution has a dimension-dependent correction. Moreover, the $su(2)$ solution gives a non-vanishing (albeit small) value for t_0. Precise enough numerical simulations at large negative g_2 values can establish which vacuum is the preferred one.
Numerical simulations are somewhat difficult in the (0,3) model. There is no

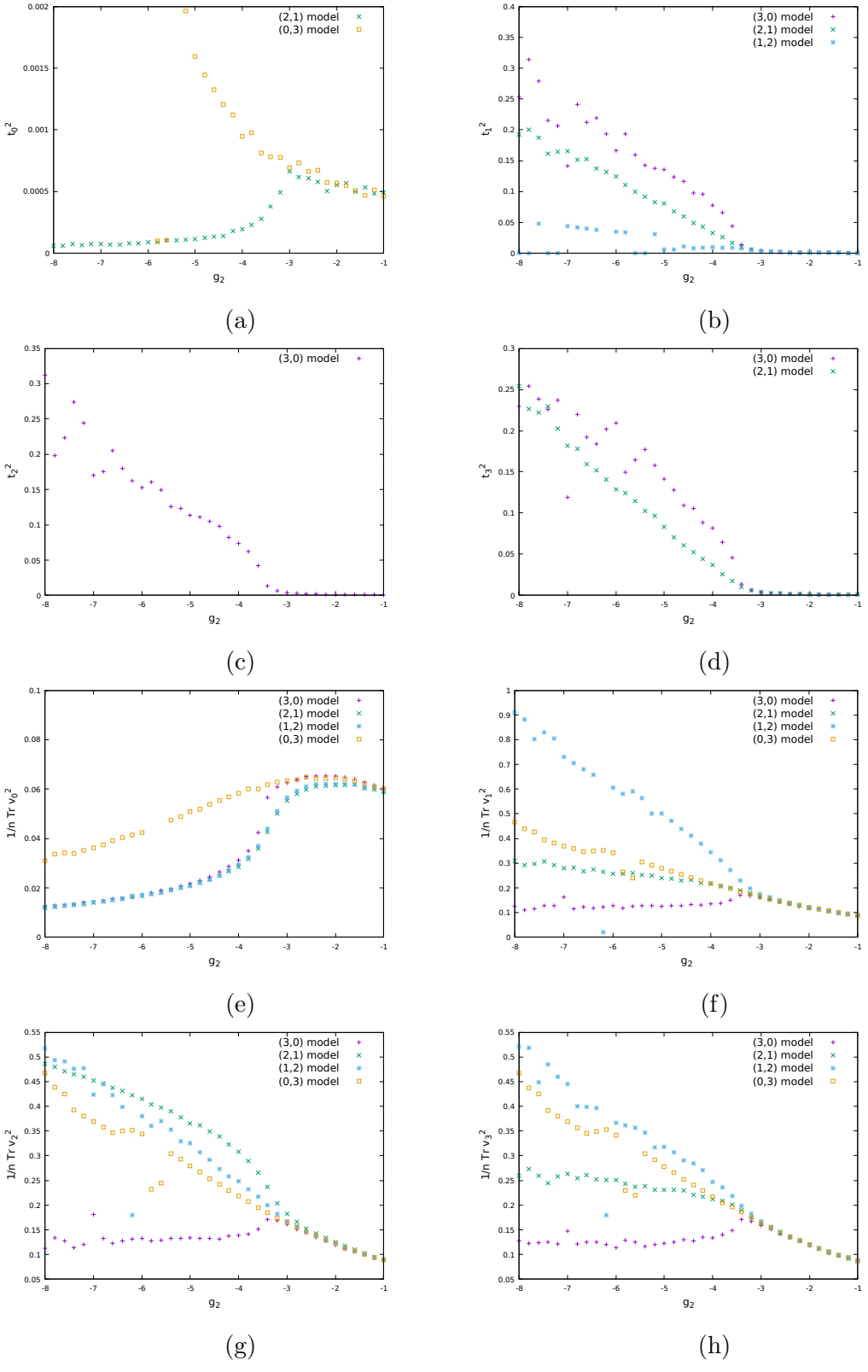

Figure 6.3: Plots (a) to (d) represent the four scalar variables t_0, t_1, t_2, t_3, while (e) to (h) the four matrix variables $n^{-1}\,\mathrm{Tr}\,v_0^2$, $n^{-1}\,\mathrm{Tr}\,v_1^2$, $n^{-1}\,\mathrm{Tr}\,v_2^2$, $n^{-1}\,\mathrm{Tr}\,v_3^2$, vs the coupling constant g_2 in the four models for $n = 8$. A critical change of behaviour happens at $g_2 \approx -3.4$. Less negative values of g_2 will be referred to as region I, while more negative values as region II.

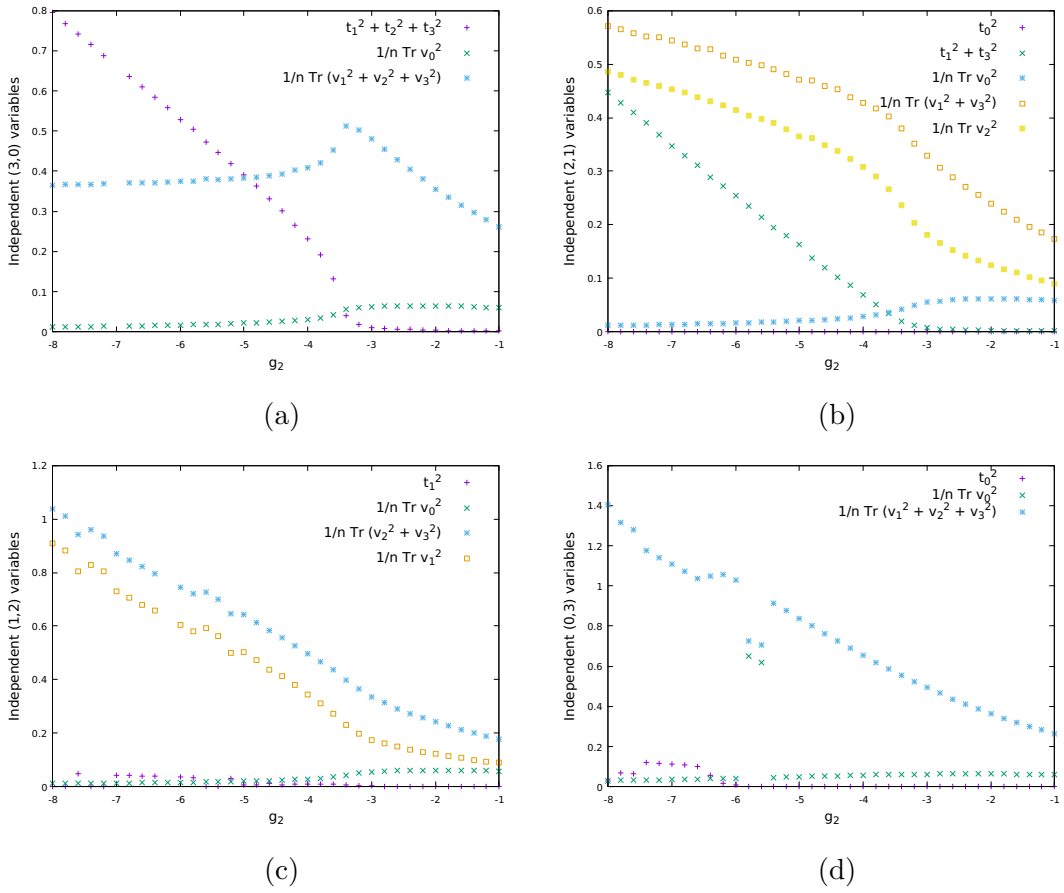

Figure 6.4: Looking at each of the eight variables t_α, v_α separately is not necessarily the best way to interpret the data in region II. In some cases the interesting observable is actually a combination of them. The best setup can be found by grouping together the spatial indices (1, 2 and 3) according to the model's signature. (a) The (3,0) model shows signs of a phase transition where the scalar variables acquire spherical symmetry while the matrix variables plateau. (b) In the (2,1) model both scalar and matrix variables maintain a linear dependence on g_2 after the critical coupling. (c) The (1,2) model is always dominated by the matrix variables, even though there is a change of slope at the transition. (d) The (0,3) model does not show signs of a transition. The data shown is for $n = 8$.

guarantee, as there is in models with even KO-dimension for example, that the the Dirac operator has a symmetric spectrum around zero. This means that two inequivalent local minima might be separated by a potential barrier represented by one (or a few) of the eigenvalues jumping to the opposite well as depicted schematically in Figure 6.5. If the simulation finds itself in one of the two configurations, tunneling to the other might be difficult, but nonetheless necessary, in order to thermalize correctly.

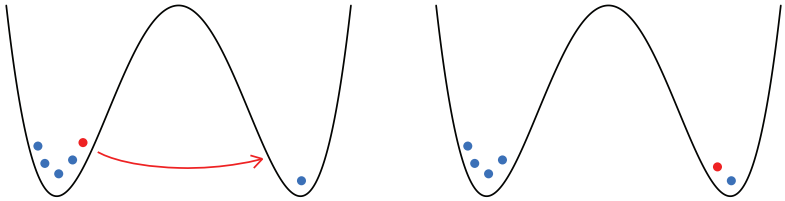

Figure 6.5: Schematic representation of an eigenvalue overcoming the potential barrier and jumping to the opposite well in an asymmetric spectrum.

Keeping in mind this difficulty, numerical simulations performed for matrices of dimension $n = 10$ and 12 in the asymptotic regime of region II fall predominantly onto the $su(2)$ solution (6.71), with some minor deviations in the form of (G.33) or other unknown ones. The expectation values reported in Table 6.1 and 6.2 are the result of four independent Markov chains evolved for each matrix dimension and each value of the coupling constant.

g_2	Chain 1	Chain 2	Chain 3	Chain 4	$su(2)$	$-g_2/16$
-300	**18.6703(4)**	**18.6704(2)**	**18.6704(3)**	**18.6704(3)**	18.6709	18.75
-150	**9.3474(2)**	9.3738(2)	**9.3344(2)**	**9.3342(4)**	9.3354	9.375
-100	**6.2221(3)**	6.1415(1)	**6.2221(3)**	**6.2220(2)**	6.2236	6.25

Table 6.1: The table shows the expectation value of $\frac{1}{n}\operatorname{Tr} v_c^2$ in a (0,3) model with matrix dimension $n = 10$ at $g_2 = -300, -150$ and -100. The first four columns show the result of four independent Monte Carlo simulations. The last two columns show the values predicted for the same observable by the $su(2)$ solution and the all-orthogonal commutative involutory matrix solution. In bold the values compatible with the $su(2)$ solution.

g_2	Chain 1	Chain 2	Chain 3	Chain 4	$su(2)$	$-g_2/16$
-300	**18.6946(3)**	**18.6946(2)**	**18.6945(2)**	**18.6946(2)**	18.6951	18.75
-150	**9.3465(3)**	9.3740(3)	**9.3465(2)**	9.3739(2)	9.3476	9.375
-100	**6.2301(2)**	**6.2301(3)**	**6.2301(2)**	**6.2301(3)**	6.2317	6.25

Table 6.2: Same data as Table 6.1, but for matrix dimension $n = 12$.

An even stronger sign of the emergence of a $su(2)$ solution comes from the spectra of the v_c matrices. The generators of an n-dimensional irreducible representation of $su(2)$ have equally spaced eigenvalues:

$$\lambda = j, j-1, \ldots, -j \quad \text{with } j = \frac{n-1}{2}. \tag{6.73}$$

In particular, for $n = 12$:

$$\lambda = 5.5, 4.5, \ldots, -4.5, -5.5. \tag{6.74}$$

A direct comparison can be made with the spectrum of any of the v_c matrices, normalized by a factor of R. Figure 6.6 shows the eigenvalue density of v_1/R at $g_2 = -300$ as an example, where this behaviour is clearly observed. As suggested in [47], the same plot also shows the spectrum of the commutator:

$$i[v_2, v_3] \propto v_1 \tag{6.75}$$

normalized by R^2. Different eigenvalues appear to have different multiplicities. This artifact is due to the fact that larger eigenvalues are more peaked around their mean, while eigenvalues closer to zero have a broader distribution. The area of the histogram, however, is the same at each half-integer position.

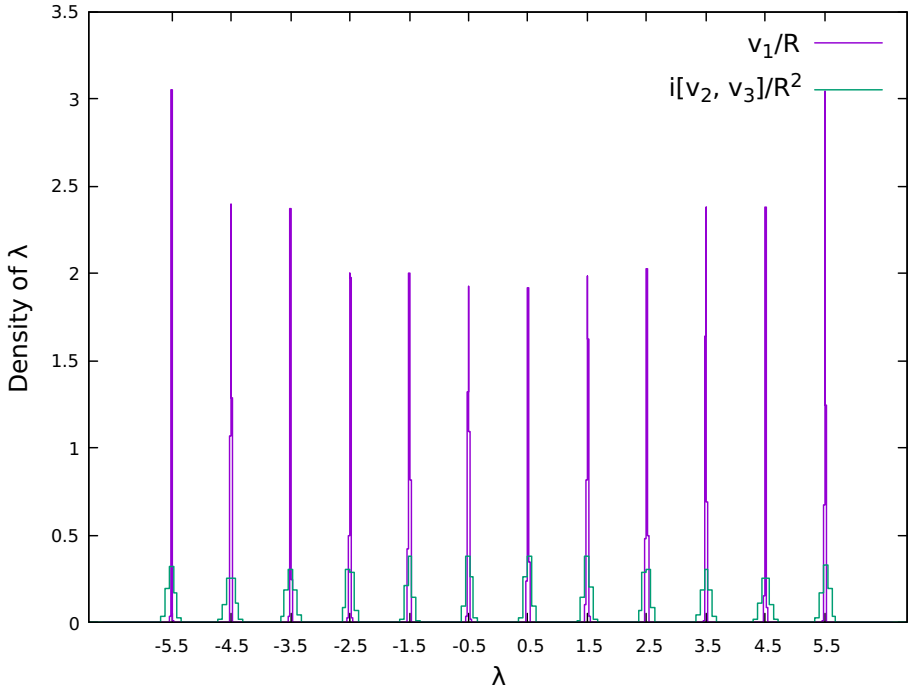

Figure 6.6: Model (0,3), eigenvalue density of v_1/R (purple) and $i[v_2, v_3]/R^2$ (green) for $n = 12$, $g_2 = -300$. The spectrum is compatible with an $su(2)$ solution.

The same analysis can be performed on the Dirac operator as a whole. When rescaling v_1, v_2 and v_3 by a factor of R^{-1} and m_0 by a factor of t_0^{-1}, one expects the spectrum of a Grosse-Presnajder operator [36], [8]:

$$\lambda = \pm 1,\ \pm 2,\ \ldots,\ \pm(n-1),\ +n. \tag{6.76}$$

Notice that the last eigenvalue appears only with the positive sign, thus making the spectrum asymmetric. The measured spectrum of the rescaled Dirac operator for $n = 12$ at $g_2 = -300$ is shown in Figure 6.7. It agrees with the Grosse-Presnajder spectrum, if not for an overall shift of 3 towards the negative numbers.

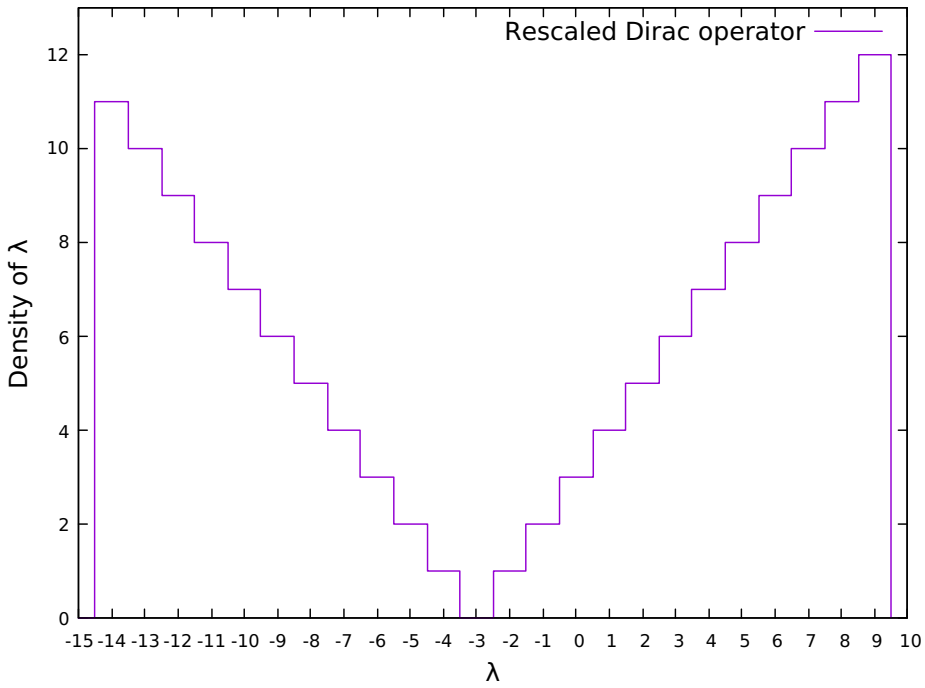

Figure 6.7: Eigenvalue density of the rescaled (0,3) Dirac operator for $n = 12$ and $g_2 = -300$. The matrices $m_1,\ m_2,\ m_3$ were rescaled by a factor of R^{-1}, while m_0 by a factor of t_0^{-1}. The histogram was normalized so that the smaller eigenvalues would appear with multiplicity 1. It resembles the Grosse-Presnajder spectrum, but shifted by 3 towards the negative side.

6.5.2 The (3,0) model

At the other end of the signature spectrum lies the (3,0) model. In region I the (3,0) and the (0,3) behave essentially in the same manner, but for a critical value of the coupling g_2 the (3,0) undergoes a phase transition with order parameter:

$$\rho^2 := t_1^2 + t_2^2 + t_3^2. \tag{6.77}$$

Plotting their Monte Carlo history shows how in region II the three traces act as coordinates on a two-sphere, ρ being the radius (Figure 6.8).
The transition appears to be second order, as plotting the histogram of ρ^2 before, during and after the phase transition shows how the order parameter does not jump from one value to the other, but rather it smoothly interpolates between them (Figure 6.9).
As for the (2,0) phase transition, a finite-size scaling analysis is attempted. Denoting g_2^* the critical coupling, the ansatz is the following:

$$n^{\frac{\beta}{\nu}}\rho^2 = f_1\left(n^{\frac{1}{\nu}}t\right) \tag{6.78}$$

$$n^{-\frac{\gamma}{\nu}}n^3\,\mathrm{Var}(\rho^2) = f_2\left(n^{\frac{1}{\nu}}t\right) \tag{6.79}$$

$$n^{-\frac{\alpha}{\nu}}n^{-3}\,\mathrm{Var}(S) = f_3\left(n^{\frac{1}{\nu}}t\right) \tag{6.80}$$

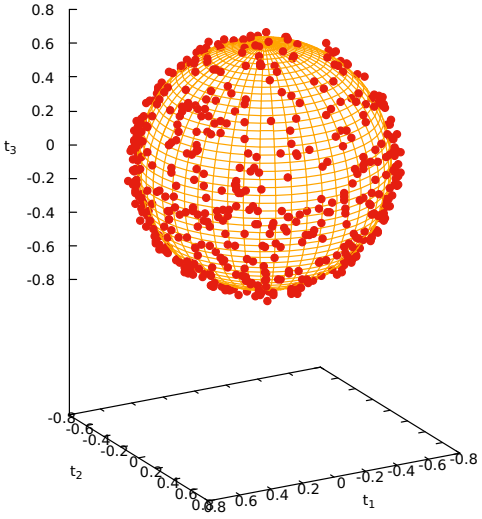

Figure 6.8: Monte Carlo history of t_1, t_2 and t_3 in region II of the (3,0) model at $g_2 = -6$, $n = 8$. The solid orange sphere is a guide for the eyes.

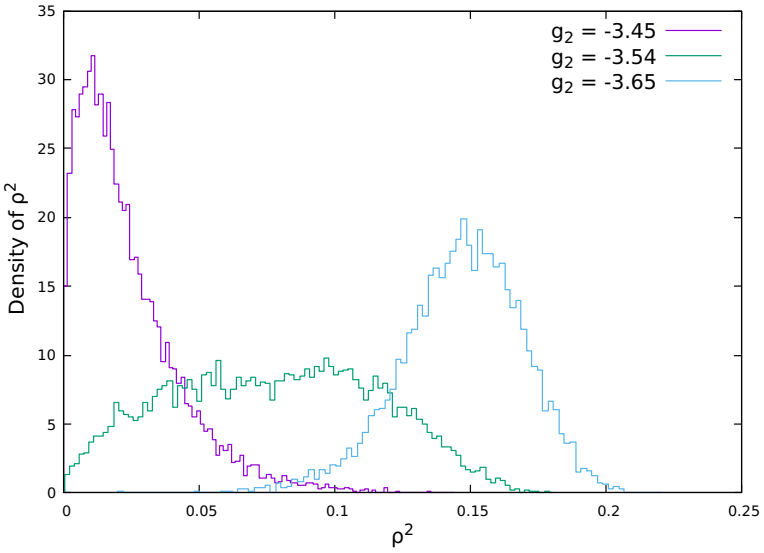

Figure 6.9: Model (3,0), distribution of ρ^2 across the phase transition for $n = 14$. The flat density for $g_2 = -3.54$ indicates that the phase transition is second order.

where t denotes the reduced coupling:

$$t := \frac{(g_2 - g_2^*)}{|g_2^*|}. \tag{6.81}$$

Interestingly, the best numerical values [48] for the critical exponents of the 3D Ising universality class allow to collapse the data fairly well, as shown in Figure 6.10. The estimated critical coupling is $g_2^* = -3.54$.

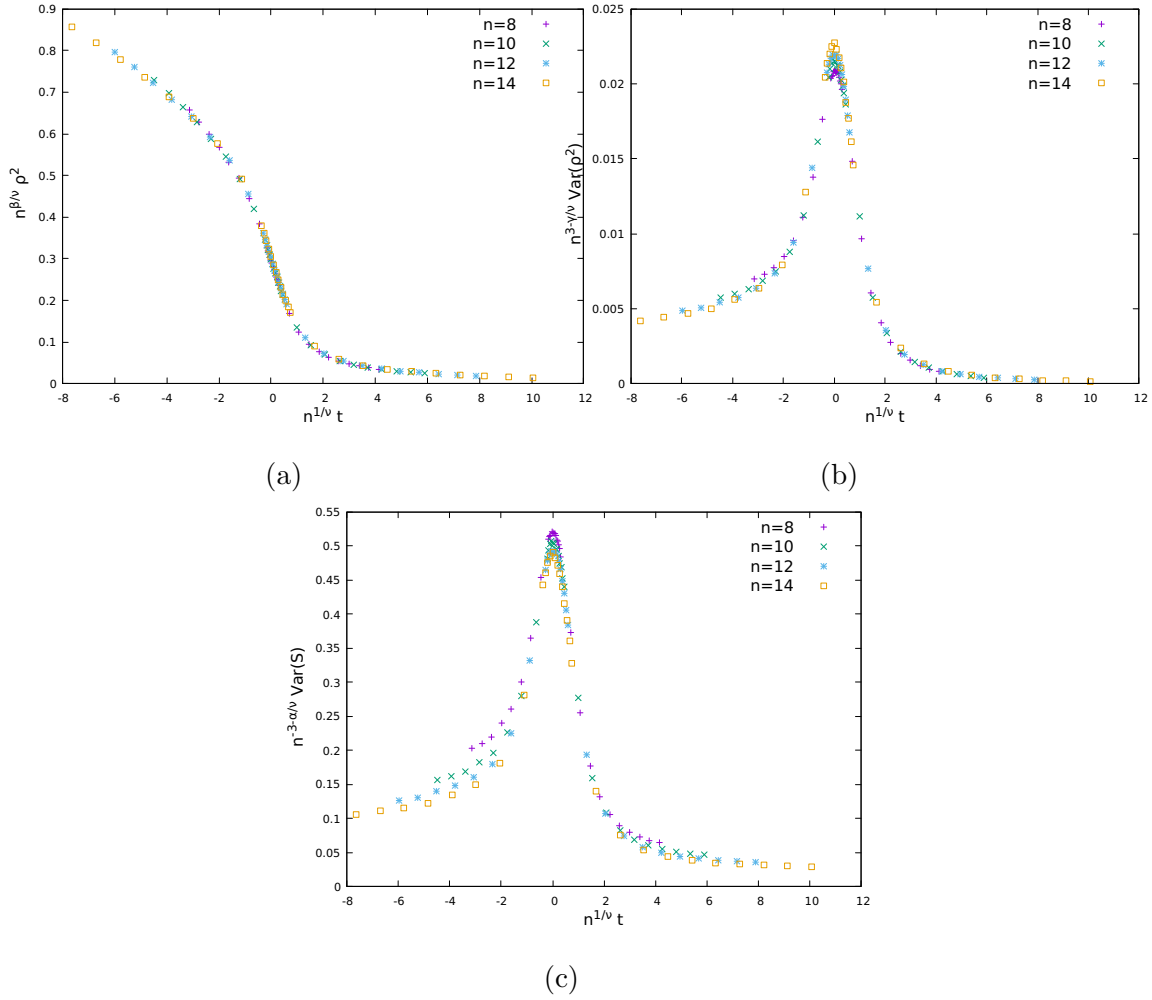

(a) (b)

(c)

Figure 6.10: Model (3,0), universal finite-size scaling curves for (a) ρ^2, (b) $n^3\,\mathrm{Var}(\rho^2)$ and (c) $n^{-3}\,\mathrm{Var}(S)$. The data is collapsed with the 3D Ising critical exponents. The estimated critical coupling is $g_2^* = -3.54$.

Chapter 7

Miscellaneous topics

7.1 Dirac Operators and Yang-Mills matrix models

Arguably, the observed dynamical emergence of $su(2)$ Dirac operators is one of the main outcomes of this work. Other random matrix models have been proposed in the past that have similar solutions, and they all fall under the general class of Yang-Mills matrix models [49]. A notable example is the IKKT matrix model [50].
Surprisingly, fuzzy Dirac operators and Yang-Mills matrix models have more in common than what might appear at first sight. To highlight the link between the two, consider a simple bosonic action for a Yang-Mills matrix model:

$$S_{YM} = -\alpha \sum_{a,b} \mathrm{Tr}[X_a, X_b]^2 + \beta \sum_a \mathrm{Tr}\, X_a^2, \quad a = 1, 2, 3 \tag{7.1}$$

where X_a are traceless Hermitian matrices and $\alpha, \beta > 0$ are coupling constants. If β was not assumed to be positive, the action for commuting matrices would be unbounded from below. Moreover, for non-commuting matrices, $[X_a, X_b] = iH$ for some Hermitian matrix H, therefore the quartic term picks up a sign when squared, leading to a converging integral. One could include a cubic Chern-Simons-like term in the action as in [51]. The argument would follow through without substantial changes, and therefore for the purposes of this discussion the cubic term will be omitted.
Now consider the following matrix:

$$D = \sum_a \sigma_a \otimes M_a, \quad a = 1, 2, 3 \tag{7.2}$$

where σ_a are the Pauli matrices and M_a are Hermitian matrices. D has the form of a (0,3) or (3,0) Dirac operator where the zeroth component is dropped and the dynamical matrices appear naked instead of inside (anti-)commutators. Take the usual Dirac operator action

$$S_D = \alpha\, \mathrm{Tr}\, D^4 + \beta\, \mathrm{Tr}\, D^2 \tag{7.3}$$

and expand it in terms of the M_a components. A calculation similar to (6.7) leads to:

$$S_D = -\alpha \sum_{a,b} \mathrm{Tr}[M_a, M_b]^2 + 2\alpha \sum_{a,b} \mathrm{Tr}\, M_a^2 M_b^2 + 2\beta \sum_a \mathrm{Tr}\, M_a^2. \tag{7.4}$$

The similarity between (7.1) and (7.4) is evident, the only difference being an extra $\mathrm{Tr}\, M_a^2 M_b^2$ term in the Dirac-like action. The effect of this extra piece is to add a $\sum_a M_a^2 M_b$ term to the equations of motion, which quite conveniently forces the $su(2)$ representation to be irreducible.

This simple calculation shows how the emergence of $su(2)$ solutions in Dirac operators is perhaps not surprising at all, since they can be related so directly to Yang-Mills matrix models. In a sense, Yang-Mills matrix models describe Dirac operators without the bimodule structure that gives rise to a left and right action. It should be noted that the possibility of obtaining a Yang-Mills matrix model from the action of a single matrix was first pointed out in [52]. The theory of fuzzy spectral triples had not been worked out at the time, and the proposal remained just an unexplored observation.

It is remarkable how two matrix models with such a drastically different origin can end up sharing crucial features. Fuzzy Dirac operators stand on the axiomatic grounds of non-commutative geometry and spectral triples, while Yang-Mills matrix models can be formally obtained by dimensional reduction of Yang-Mills theory to zero dimensions. One could hope that the fortuitous convergence of such different paths is a sign that the direction is the right one.

7.2 Dual pairs and non-commutative to commutative transition

Looking at the numerical results collected for the $p+q=2$ and $p+q=3$ types, an interesting duality starts taking shape.

Consider the $p+q=2$ types first, and in particular the $(2,0)$ and $(0,2)$ models. It was shown in Chapter 5 that the random vacuum of the two models for small values of the coupling constant appears to be the same, and it is dominated by the two matrix variables v_1 and v_2. At some critical coupling, however, the $(2,0)$ undergoes a phase transition and it settles around a different vacuum which is instead dominated by the trace degrees of freedom.

Something completely analogous happens between the $(0,3)$ and $(3,0)$ models. Accurate Monte Carlo simulations have confirmed that in the large negative g_2 regime, where fluctuations of the random model are suppressed, the $(0,3)$ Dirac operator chooses a $su(2)$ vacuum. The numerical data can be traced back up to small g_2 values with no clear deviations in the form of phase transitions (Figure 6.4d), which suggests that the model preserves the $su(2)$ behaviour throughout the whole range, albeit a very fluctuating one close to the origin where the potential well is shallow. Also in this case the matrix variables of the $(3,0)$ and $(0,3)$ behave similarly up until the $(3,0)$ phase transition (Figure 6.3f, 6.3g, 6.3h), suggesting that the $(3,0)$ might be a $su(2)$ Dirac operator hidden by large fluctuations for small g_2. This is further supported by looking at the spectrum of the v_i matrices for small g_2 in both models. As shown in Figure 7.1, the characteristic peaks of $su(2)$ generators are clearly visible in both models at $g_2 = -3$, but they are con-

siderably broader and somewhat displaced from their exact half-integer values.

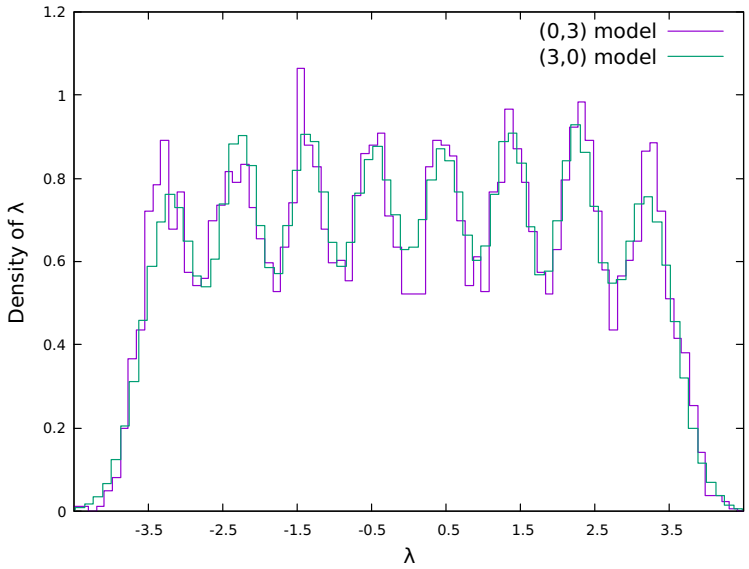

Figure 7.1: Eigenvalue density of v_1/R in the $(0,3)$ (purple) and $(3,0)$ (green) models for $n = 8$, $g_2 = -3$. The peaks are broadened and shifted by random fluctuations, but they are still clearly visible.

Then the phase transition in the model can be seen as a transition from non-commutative to commutative spherical variables. That is, the $(3,0)$ model is characterized by two phases: one where three non-commutative variables (the v_a matrices) arrange themselves in a (highly fluctuating) $su(2)$ configuration, and a second phase where the commutative variables (the t_a scalars) act as coordinates on a sphere.

This motivates the following conjecture on the existence of "dual" pairs among models with the same $p + q$, which will be denoted (T, M), with the following characteristics:

1. T is the element of a dual pair with a majority of anti-commutators in the Dirac operator (hence trace varaibles), while M is the element with a majority of commutators.

2. T is dominated in the asymptotic regime by a solution where the traces act as coordinates on a manifold. The manifold was S^1 for the $(2,0)$ model, and S^2 for the $(3,0)$ model.

3. The asymptotic manifold can be obtained by solving the equations of motion of a simplified version of T where the matrix variables are deleted and only the traces survive.

4. The asymptotic regime of M is dominated by some fuzzy version of the asymptotic manifold of T.

5. T undergoes a phase transition from the manifold to its fuzzy version.

7.3 Higher types

Moving up in the ladder of Clifford modules, the next dual pair is given by the $(3,1)$ and $(1,3)$ models. These are random matrix models with eight Hermitian matrices: two commutators and six anti-commutators for the $(3,1)$, and vice versa for the $(1,3)$. In a compact notation, the Dirac operator reads:

$$D = \sum_{\alpha=0}^{3} \begin{pmatrix} 0 & \sigma_\alpha \otimes N_\alpha^\dagger \\ \sigma_\alpha \otimes N_\alpha & 0 \end{pmatrix} \tag{7.5}$$

where:

$$\begin{aligned} N_0 &= M_0^{(1)} + iM_0^{(2)} \\ N_1 &= M_1^{(1)} + iM_1^{(2)} \\ N_2 &= M_2^{(1)} + iM_2^{(2)} \\ N_3 &= M_3^{(1)} + iM_3^{(2)} \end{aligned}$$

and

$$\begin{aligned} (3,1): &\quad \begin{cases} M_0^{(i)} = [m_0^{(i)}, \cdot] & \text{for } i = 1,2 \\ M_a^{(i)} = \{m_a^{(i)}, \cdot\} & \text{for } a = 1,2,3 \text{ and } i = 1,2 \end{cases} \\ (1,3): &\quad \begin{cases} M_0^{(i)} = \{m_0^{(i)}, \cdot\} & \text{for } i = 1,2 \\ M_a^{(i)} = [m_a^{(i)}, \cdot] & \text{for } a = 1,2,3 \text{ and } i = 1,2 \end{cases} \end{aligned}$$

The degrees of freedom are the eight Hermitian matrices $m_\alpha^{(i)}$, with $\alpha = 0, \ldots, 3$ and $i = 1, 2$.
Numerical simulations as well as analytical calculations start to be rather cumbersome because of the large number of free matrices, therefore this is an optimal candidate to test whether the assumptions of the dual pair conjecture can help ease the treatment.
The first thing to do is to calculate the asymptotic manifold of the $(3,1)$ model. Simplify the model by putting $m_0^{(1)} = m_0^{(2)} = 0$ and $m_a^{(i)} = t_a^{(i)} \mathbb{1}$ for some real scalars $t_a^{(i)}$, and then define $z_a := t_a^{(1)} + it_a^{(2)} \in \mathbb{C}$. The action of the simplified model reads:

$$S = 16n^2 \left[g_2 \sum_{a=1}^{3} |z_a|^2 + 2 \sum_{a,b=1}^{3} \left(2|z_a|^2 |z_b|^2 - \bar{z}_a^2 z_b^2 \right) \right] \tag{7.6}$$

And the variation to first order is:

$$\begin{aligned} \delta S = 16n^2 \sum_b \Bigg[& \left(g_2 z_b + 4 \sum_a \left(2|z_a|^2 z_b - \bar{z}_b z_a^2 \right) \right) \delta \bar{z}_b \\ & + \left(g_2 \bar{z}_b + 4 \sum_a \left(2|z_a|^2 \bar{z}_b - z_b \bar{z}_a^2 \right) \right) \delta z_b \Bigg]. \end{aligned} \tag{7.7}$$

The two equations of motion, coming from putting to zero the coefficient of δz and $\delta\bar{z}$, are one the complex conjugate of the other. Take the first one:

$$g_2 z_b + 4\sum_a \left(2|z_a|^2 z_b - \bar{z}_b z_a^2\right) = 0 \tag{7.8}$$

multiply by $\bar{z}_b$:

$$g_2|z_b|^2 + 4\sum_a \left(2|z_a|^2|z_b|^2 - \bar{z}_b^2 z_a^2\right) = 0 \tag{7.9}$$

and divide by $4|z_b|^2$:

$$\sum_a \left(2|z_a|^2 - \frac{\bar{z}_b^2 z_a^2}{|z_b|^2}\right) = -\frac{g_2}{4}. \tag{7.10}$$

Now switch to polar form $z_a = r_a e^{i\theta_a}$:

$$\sum_a \left(2 - e^{2i(\theta_a - \theta_b)}\right) r_a^2 = -\frac{g_2}{4} \tag{7.11}$$

and remember that the equation is for fixed b and $a = 1, 2, 3$. Call b_1 and b_2 the two indices different from b, and expand the sum:

$$\left(2 - e^{2i(\theta_{b_1} - \theta_b)}\right) r_{b_1}^2 + \left(2 - e^{2i(\theta_{b_2} - \theta_b)}\right) r_{b_2}^2 + r_b^2 = -\frac{g_2}{4}. \tag{7.12}$$

Notice that the equation constrains the left-hand side to be real, therefore a set of solutions is given by:

$$\begin{aligned} \theta_{b_1} - \theta_b &= k_1\pi, \quad k_1 \in \mathbb{Z} \\ \theta_{b_2} - \theta_b &= k_2\pi, \quad k_2 \in \mathbb{Z} \end{aligned} \tag{7.13}$$

and in terms of the complex numbers z_1, z_2 and z_3 this means that either all three are aligned, or two of them are aligned and the third one is π apart, while the sum of their radii squared amounts to a constant.
Take the first case, where all three are aligned. The stationary manifold is then given by the map

$$\psi : S^1 \times S^2 \to S^5 \subset \mathbb{R}^6$$

defined as:

$$\begin{aligned} \psi(\theta, \rho, \sigma) = (x, y, z, t, u, v) = \big(&\cos(\theta)\cos(\rho)\sin(\sigma),\ \sin(\theta)\cos(\rho)\sin(\sigma), \\ &\cos(\theta)\sin(\rho)\sin(\sigma),\ \sin(\theta)\sin(\rho)\sin(\sigma), \\ &\cos(\theta)\cos(\sigma),\ \sin(\theta)\cos(\sigma)\big). \end{aligned} \tag{7.14}$$

The S^1 part corresponds to the freedom in orienting the z_a numbers, i.e. the θ angle in $z_a = r_a e^{i\theta}$, while the S^2 part corresponds to their absolute values r_a acting as coordinates on a sphere. Numerical evidence suggests that this is indeed the correct manifold. Figure 7.2 and 7.3 show a comparison of the two inequivalent projections onto 2D subspaces for uniformly random samples of the map ψ and for Monte Carlo samples of the trace variables $t_a^{(i)}$ of the $(3, 1)$ model at $g_2 = -4$ and $n = 8$. Figure 7.4 shows the surface defined by (x, y, t) with $\sigma = \pi/2$, and how the corresponding Monte Carlo samples are bounded by it.

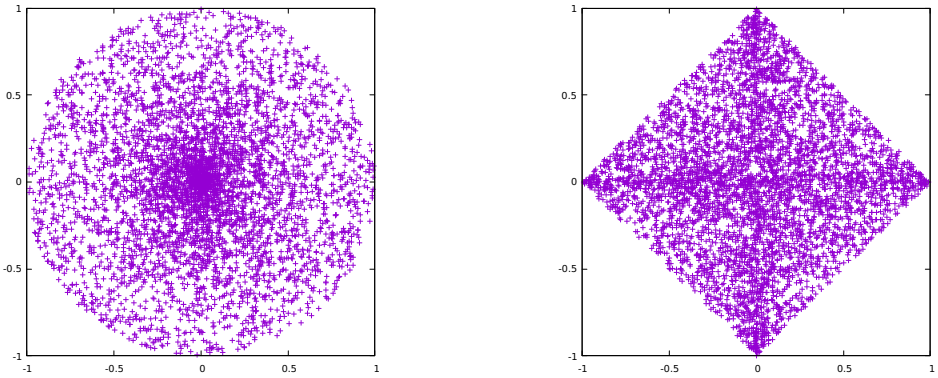

Figure 7.2: Inequivalent 2D projections of uniformly random samples of the map ψ.

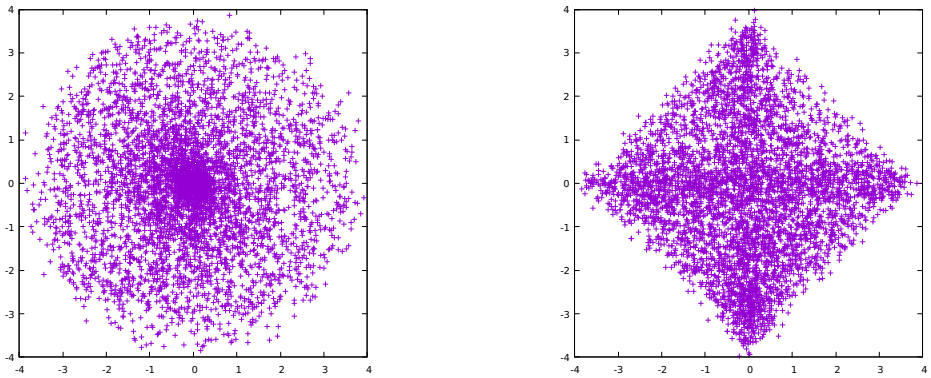

Figure 7.3: Inequivalent 2D projections of Monte Carlo samples of the trace variables $t_a^{(i)}$ of the $(3,1)$ model at $g_2 = -4$ and $n = 8$.

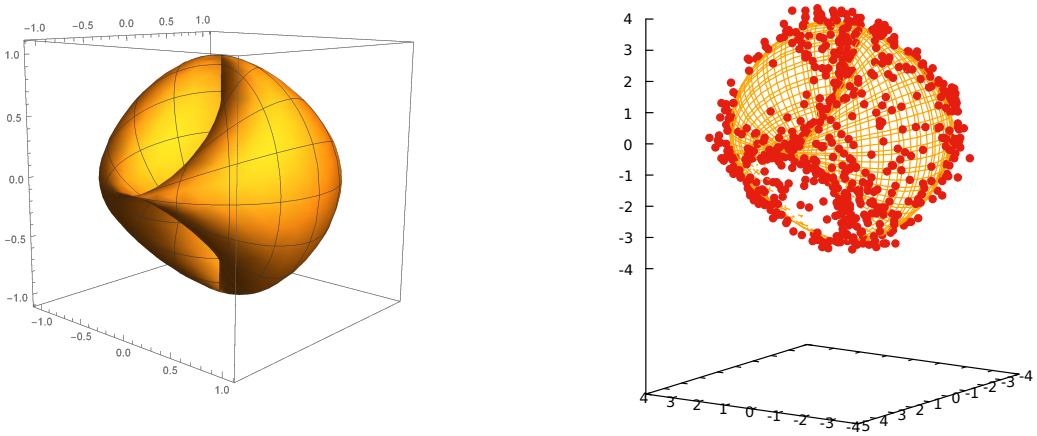

Figure 7.4: (left) Parametric plot of the surface defined by (x, y, t) in (7.14) with $\sigma = \pi/2$. (right) Projection onto $t_1^{(1)}, t_1^{(2)}, t_2^{(2)}$ of Monte Carlo samples of the $t_a^{(i)}$ traces of the $(3,1)$ model at $g_2 = -4$, $n = 8$. Modulo fluctuations, the samples remain bounded by the surface.

Now consider the $(1,3)$ model. The fourth point of the dual pair ansatz claims that the asymptotics of the $(1,3)$ are described by a fuzzy version of ψ. As it turns out, it is possible to show that there are stationary $su(2)$ solutions to the $(1,3)$ model with an extra S^1 degree of freedom, hence at least a partial fuzzification of ψ.
To see that, write the action of the $(1,3)$ Dirac operator (7.5) using the results of Appendix F:

$$\operatorname{Tr} D^2 = 4\sum_{\alpha=0}^{3} \operatorname{Tr} N_\alpha N_\alpha^\dagger \tag{7.15}$$

$$\begin{aligned}\operatorname{Tr} D^4 = 4\operatorname{Tr}\Big[& N_0^\dagger N_0 N_0^\dagger N_0 \\ & + N_0^\dagger N_a N_0^\dagger N_a + N_0 N_a^\dagger N_0 N_a^\dagger \\ & + 2N_0^\dagger N_0 N_a^\dagger N_a + 2N_0 N_0^\dagger N_a N_a^\dagger \\ & + 2i\epsilon_{abc}\left(N_0^\dagger N_a N_b^\dagger N_c + N_0 N_a^\dagger N_b N_c^\dagger\right) \\ & + N_a N_a^\dagger N_b N_b^\dagger + N_a^\dagger N_a N_b^\dagger N_b - N_a^\dagger N_b N_a^\dagger N_b\Big].\end{aligned} \tag{7.16}$$

Taking inspiration from the way the variables are arranged in the $(3,1)$ case, observe that if:

$$\begin{aligned} M_\alpha^{(1)} &= \cos(\theta) M_\alpha \\ M_\alpha^{(2)} &= \sin(\theta) M_\alpha \end{aligned}$$

for some angle θ, then:

$$N_\alpha = e^{i\theta} M_\alpha.$$

The dependence on the angle drops out of the action, which then becomes identical to (6.7), i.e. the action of the $(0,3)$ Dirac operator that was worked out in Chapter 6, and that was shown to have $su(2)$ solutions. However, in this case the $su(2)$ generators have an extra global S^1 degree of freedom parametrized by θ.

Conclusions

Non-commutative fuzzy spaces have emerged as an interesting concept in quantum gravity proposals thanks to the way they naturally incorporate a fundamental length scale. The axiomatization of fuzzy spaces in the formalism of Alain Connes' spectral triples allows the construction of a path integral over fuzzy geometries that takes the form of a random matrix theory for Dirac operators. The purpose of this thesis was to study the path integral numerically using Markov chain Monte Carlo methods, and when possible to complement the study with analytical results.

The interesting regime for random matrix theories is in the large n limit, and for this reason it is crucial for the numerical code to be able to handle in a reasonable amount of time as large a matrix size as possible. The first practical outcome of this work was the writing of RFL, a C++ numerical library for Monte Carlo simulation of fuzzy spaces where much emphasis was put into performing the calculations as efficiently as possible. Researchers interested in writing their own code might nonetheless find it useful to look at the second half of Chapter 2, where the formulas are worked out.

For the simplest Dirac operators, the ones with a single free Hermitian matrix, the theory of Riemann-Hilbert problems has proven to be a powerful tool for solving the random matrix model exactly. A symmetric one-cut solution for the density of states was found analytically, as well as a non-necessarily symmetric two-cut solution. The two-cut solution was written parametrically in terms of its first moment and the extrema of the support. The system of equations fixing the value of these parameters could be solved in the symmetrized case, but turned out to be too hard to solve in general. Self-consistency was checked by plugging in numerical values obtained by Monte Carlo simulations, confirming the validity of the equations.

Higher types are less amenable to exact methods. Random matrix models involving more than one matrix are considerably less studied in the literature. Good analytical results for Dirac operators with $p+q > 1$ could be obtained via a stationary analysis aimed at finding classical solutions for the models. These are solutions of the matrix model where the random fluctuations are suppressed, and typically they are good approximations to the full random vacuum when the potential well is very deep, which in this case means large negative g_2. There is an argument to disregard classical solutions as completely uninteresting, because they are easily written in terms of the Dirac operator:

$$\delta S = \mathrm{Tr}\left[2g_2 D + 4D^3\right]\delta D = 0 \implies 2g_2 D + 4D^3 = 0$$

and they are given by a Dirac operator with a highly degenerate spectrum

$$\sigma(D) = \left\{ \sqrt{-\frac{g_2}{2}}, 0, -\sqrt{-\frac{g_2}{2}} \right\}.$$

However, triviality in the spectrum of D does not necessarily reflect a triviality in the subcomponents of D. Some of these classical solutions can be for example $su(2)$ Dirac operators, as shown in Chapter 6, where the submatrices form irreducible representations of $su(2)$. In these cases the interplay between analytics and numerics is a valuable tool to shed light on the behavior of the models. A stationary analysis informs the choice of observables, and their numerical expectation values help discriminate between the potential classical solutions.

A complete classification of the stationary solutions for the $(0,2), (1,1)$ and $(2,0)$ models involving involutory matrices was achieved, and they were shown to account, up to fluctuations, for the behavior of the $(0,2)$ and $(1,1)$. Some exact results making use of character expansion methods [53] might be of interest for these models, but they were not pursued. A new phenomenon was observed in the $(2,0)$ model, where a single phase transition splits into two separate ones, one second-order and the other first-order, when the matrix size is large enough. No mention of such phenomenon could be found in the literature, and it remains unexplained. A finite-size scaling analysis was performed on the second-order phase transition, and despite the critical exponents not belonging to a known universality class, they were shown to saturate Rushbrooke's inequality.

A stationary analysis was also performed on the $(0,3), (1,2), (2,1)$ and $(3,0)$ models, which are random matrix models involving four Hermitian matrices. Some scalar and involutory solution with commuting matrices were found but, most importantly, $su(2)$ solutions were shown to exist in all four models. These solutions have very distinctive fingerprints: they follow a precise scaling with the matrix dimension n, and the spectrum concentrates around half-integer values. Such fingerprints were found in the Monte Carlo data of the $(0,3)$ model, whose Dirac operator was shown to resemble asymptotically the Grosse-Presnajder Dirac operator on the fuzzy sphere, pointing towards the dynamical emergence of structured fuzzy spaces as a concrete possibility. The $(3,0)$ model, on the other hand, undergoes a phase transition that marks the separation between two regimes: one where matrix (hence non-commutative) variables dominate, and one where scalar (hence commutative) variables dominate. Large negative values of g_2 correspond to the scalar regime, and therefore the asymptotic presence of $su(2)$ matrices could not be verified. However, $su(2)$ fingerprints in the spectrum of the matrices were observed far from the asymptotic regime as well. Finally, a finite-size scaling analysis was performed on the $(3,0)$ phase transition, giving indication that it might belong to the 3D Ising universality class.

Building on the way the models interact with each other at each $p+q$ level, a conjecture was put forward about the existence of pairs of models whose behaviour is in some sense dual to each other. The idea is related to what happens between the $(3,0)$ and the $(0,3)$, with the former transitioning between a commutative and non-commutative regime, and the latter exhibiting the non-commutative regime

asymptotically. Far from being a rigorous framework, the concept of dual pair should be seen as a heuristic to facilitate the study of higher models. To this end, the idea was tested on the $(1,3)$ and $(3,1)$ models. The commutative regime of the $(3,1)$ was shown to be a certain submanifold of S^5, that becomes partially fuzzified in the non-commutative regime in terms of $su(2)$ generators with a global S^1 degree of freedom.

Random matrix models with $su(2)$ solutions are generally associated to the widely-studied class of Yang-Mills matrix models. A clear connection between fuzzy Dirac operators and Yang-Mills matrix models was uncovered, showing how the two are not so dissimilar. The random matrix theory arising from fuzzy Dirac operators appears to be to some extent a Yang-Mills matrix model augmented with a right action of the matrix algebra.

Bibliography

[1] Alain Connes. *Noncommutative Geometry*. Academic Press, 1995.

[2] E. Brézin et al. "Planar diagrams". In: *Communications in Mathematical Physics* 59.1 (Feb. 1978), pp. 35–51. ISSN: 1432-0916. DOI: 10.1007/BF01614153. URL: https://doi.org/10.1007/BF01614153.

[3] J. Ambjørn et al. "Nonperturbative quantum gravity". In: *Physics Reports* 519.4 (2012). Nonperturbative Quantum Gravity, pp. 127–210. ISSN: 0370-1573. DOI: https://doi.org/10.1016/j.physrep.2012.03.007. URL: https://www.sciencedirect.com/science/article/pii/S0370157312001482.

[4] Jan Ambjørn et al. "Second-Order Phase Transition in Causal Dynamical Triangulations". In: *Phys. Rev. Lett.* 107 (21 Nov. 2011), p. 211303. DOI: 10.1103/PhysRevLett.107.211303. URL: https://link.aps.org/doi/10.1103/PhysRevLett.107.211303.

[5] Sumati Surya. "Evidence for the continuum in 2D causal set quantum gravity". In: *Classical and Quantum Gravity* 29.13 (June 2012), p. 132001. DOI: 10.1088/0264-9381/29/13/132001. URL: https://doi.org/10.1088/0264-9381/29/13/132001.

[6] Lisa Glaser, Denjoe O'Connor, and Sumati Surya. "Finite size scaling in 2d causal set quantum gravity". In: *Classical and Quantum Gravity* 35.4 (Jan. 2018), p. 045006. DOI: 10.1088/1361-6382/aa9540. URL: https://doi.org/10.1088/1361-6382/aa9540.

[7] John W Barrett and Lisa Glaser. "Monte Carlo simulations of random noncommutative geometries". In: *Journal of Physics A: Mathematical and Theoretical* 49.24 (May 2016), p. 245001. DOI: 10.1088/1751-8113/49/24/245001. URL: https://doi.org/10.1088%2F1751-8113%2F49%2F24%2F245001.

[8] John W. Barrett. "Matrix geometries and fuzzy spaces as finite spectral triples". In: *Journal of Mathematical Physics* 56.8 (2015), p. 082301. DOI: 10.1063/1.4927224. eprint: https://doi.org/10.1063/1.4927224. URL: https://doi.org/10.1063/1.4927224.

[9] Eugene P. Wigner. "On the Distribution of the Roots of Certain Symmetric Matrices". In: *Annals of Mathematics* 67.2 (1958), pp. 325–327. ISSN: 0003486X. URL: http://www.jstor.org/stable/1970008.

[10] Allen Knutson and Terence Tao. *Honeycombs and sums of Hermitian matrices*. 2000. DOI: 10.48550/ARXIV.MATH/0009048. URL: https://arxiv.org/abs/math/0009048.

[11] "Elliptic operators, topology and asymptotic methods". In: *Acta Applicandae Mathematica* 20.1 (July 1990), pp. 193–194. ISSN: 1572-9036. DOI: 10.1007/BF00046916. URL: https://doi.org/10.1007/BF00046916.

[12] Lisa Glaser. "Scaling behaviour in random non-commutative geometries". In: *Journal of Physics A: Mathematical and Theoretical* 50.27 (June 2017), p. 275201. DOI: 10.1088/1751-8121/aa7424. URL: https://doi.org/10.1088%2F1751-8121%2Faa7424.

[13] John W Barrett, Paul Druce, and Lisa Glaser. "Spectral estimators for finite non-commutative geometries". In: *Journal of Physics A: Mathematical and Theoretical* 52.27 (June 2019), p. 275203. DOI: 10.1088/1751-8121/ab22f8. URL: https://doi.org/10.1088%2F1751-8121%2Fab22f8.

[14] J. Ambjørn, J. Jurkiewicz, and R. Loll. "The Spectral Dimension of the Universe is Scale Dependent". In: *Phys. Rev. Lett.* 95 (17 Oct. 2005), p. 171301. DOI: 10.1103/PhysRevLett.95.171301. URL: https://link.aps.org/doi/10.1103/PhysRevLett.95.171301.

[15] John W. Barrett and James Gaunt. *Finite spectral triples for the fuzzy torus*. 2019. arXiv: 1908.06796 [math.QA].

[16] Masoud Khalkhali and Nathan Pagliaroli. "Phase transition in random non-commutative geometries". In: *Journal of Physics A: Mathematical and Theoretical* 54.3 (Dec. 2020), p. 035202. DOI: 10.1088/1751-8121/abd190. URL: https://doi.org/10.1088/1751-8121/abd190.

[17] Percy Deift. *Orthogonal polynomials and random matrices: A Riemann-Hilbert approach*. New York University, 1999.

[18] Walter D. van Suijlekom. *Noncommutative Geometry and Particle Physics*. Springer, 2014.

[19] A. H. Chamseddine and A. Connes. "The Spectral Action Principle". In: *Communications in Mathematical Physics* 186.3 (July 1997), pp. 731–750. ISSN: 1432-0916. DOI: 10.1007/s002200050126. URL: https://doi.org/10.1007/s002200050126.

[20] Daniel Kastler. "Noncommutative geometry and fundamental physical interactions: The Lagrangian level—Historical sketch and description of the present situation". In: *Journal of Mathematical Physics* 41.6 (2000), pp. 3867–3891. DOI: 10.1063/1.533330. eprint: https://doi.org/10.1063/1.533330. URL: https://doi.org/10.1063/1.533330.

[21] Alain Connes. "Gravity coupled with matter and the foundation of non-commutative geometry". In: *Communications in Mathematical Physics* 182.1 (Dec. 1996), pp. 155–176. ISSN: 1432-0916. DOI: 10.1007/BF02506388. URL: https://doi.org/10.1007/BF02506388.

[22] Alain Connes. "Noncommutative geometry and the standard model with neutrino mixing". In: *Journal of High Energy Physics* 2006.11 (Nov. 2006), pp. 081–081. DOI: 10.1088/1126-6708/2006/11/081. URL: https://doi.org/10.1088/1126-6708/2006/11/081.

[23] Gerhard Grensing. *Structural Aspects of Quantum Field Theory and Noncommutative Geometry*. WORLD SCIENTIFIC, 2013. DOI: 10.1142/8771. eprint: https://www.worldscientific.com/doi/pdf/10.1142/8771. URL: https://www.worldscientific.com/doi/abs/10.1142/8771.

[24] Istvan Montvay and Gernot Münster. *Quantum Fields on a Lattice*. Cambridge Monographs on Mathematical Physics. Cambridge University Press, 1994. DOI: 10.1017/CBO9780511470783.

[25] Madan Lal Mehta. *Random Matrices*. Academic Press, 2004.

[26] William Feller. *An Introduction to Probability Theory and Its Applications, Volume 1, 3rd Edition*. Wiley, 1991.

[27] Nicholas Metropolis et al. "Equation of State Calculations by Fast Computing Machines". In: *The Journal of Chemical Physics* 21.6 (1953), pp. 1087–1092. DOI: 10.1063/1.1699114. eprint: https://doi.org/10.1063/1.1699114. URL: https://doi.org/10.1063/1.1699114.

[28] W. K. Hastings. "Monte Carlo sampling methods using Markov chains and their applications". In: *Biometrika* 57.1 (Apr. 1970), pp. 97–109. ISSN: 0006-3444. DOI: 10.1093/biomet/57.1.97. eprint: https://academic.oup.com/biomet/article-pdf/57/1/97/23940249/57-1-97.pdf. URL: https://doi.org/10.1093/biomet/57.1.97.

[29] Simon Duane et al. "Hybrid Monte Carlo". In: *Physics Letters B* 195.2 (1987), pp. 216–222. ISSN: 0370-2693. DOI: https://doi.org/10.1016/0370-2693(87)91197-X. URL: http://www.sciencedirect.com/science/article/pii/037026938791197X.

[30] Alain Connes. "On the spectral characterization of manifolds". In: *J. Noncommut. Geom.* 7 (2013), pp. 1–82. DOI: 10.4171/JNCG/108. arXiv: 0810.2088 [math.OA].

[31] Alain Connes and John Lott. "Particle models and noncommutative geometry". In: *Nuclear Physics B - Proceedings Supplements* 18.2 (1991), pp. 29–47. ISSN: 0920-5632. DOI: https://doi.org/10.1016/0920-5632(91)90120-4. URL: https://www.sciencedirect.com/science/article/pii/0920563291901204.

[32] Peter B. Gilkey. *Invariance Theory, the Heat Equation and the Atiyah-Singer Index Theorem*. CRC Press, 1994.

[33] John W. Barrett. "Lorentzian version of the noncommutative geometry of the standard model of particle physics". In: *Journal of Mathematical Physics* 48.1 (2007), p. 012303. DOI: 10.1063/1.2408400. eprint: https://doi.org/10.1063/1.2408400. URL: https://doi.org/10.1063/1.2408400.

[34] Ali H. Chamseddine, Alain Connes, and Matilde Marcolli. "Gravity and the standard model with neutrino mixing". In: *Advances in Theoretical and Mathematical Physics* 11.6 (2007), pp. 991–1089. ISSN: 1095-0753. DOI: 10.4310/atmp.2007.v11.n6.a3. URL: http://dx.doi.org/10.4310/ATMP.2007.v11.n6.a3.

[35] J Madore. "The fuzzy sphere". In: *Classical and Quantum Gravity* 9.1 (Jan. 1992), pp. 69–87. DOI: 10.1088/0264-9381/9/1/008. URL: https://doi.org/10.1088/0264-9381/9/1/008.

[36] H. Grosse and P. Prešnajder. "The dirac operator on the fuzzy sphere". In: *Letters in Mathematical Physics* 33.2 (Feb. 1995), pp. 171–181. ISSN: 1573-0530. DOI: 10.1007/BF00739805. URL: https://doi.org/10.1007/BF00739805.

[37] Steve Brooks et al. *Handbook of Markov Chain Monte Carlo*. CRC Press, 2011. DOI: 10.1201/b10905.

[38] David A. Levin, Yuval Peres, and Elizabeth L. Wilmer. *Markov Chains and Mixing Times*. American Mathematical Society, 2008.

[39] M. E. J. Newman and G. T. Barkema. *Monte Carlo Methods in Statistical Physics*. Clarendon Press, 1999.

[40] A. Gelman, W. R. Gilks, and G. O. Roberts. "Weak convergence and optimal scaling of random walk Metropolis algorithms". In: *The Annals of Applied Probability* 7.1 (1997), pp. 110–120. DOI: 10.1214/aoap/1034625254. URL: https://doi.org/10.1214/aoap/1034625254.

[41] Matthew D. Homan and Andrew Gelman. "The No-U-Turn Sampler: Adaptively Setting Path Lengths in Hamiltonian Monte Carlo". In: *J. Mach. Learn. Res.* 15.1 (Jan. 2014), pp. 1593–1623. ISSN: 1532-4435.

[42] Christophe Andrieu and Johannes Thoms. "A tutorial on adaptive MCMC". In: *Statistics and Computing* 18.4 (Dec. 2008), pp. 343–373. ISSN: 1573-1375. DOI: 10.1007/s11222-008-9110-y. URL: https://doi.org/10.1007/s11222-008-9110-y.

[43] Yurii Nesterov. "Primal-dual subgradient methods for convex problems". In: *Mathematical Programming* 120.1 (Aug. 2009), pp. 221–259. ISSN: 1436-4646. DOI: 10.1007/s10107-007-0149-x. URL: https://doi.org/10.1007/s10107-007-0149-x.

[44] Conrad Sanderson and Ryan Curtin. "Armadillo: a template-based C++ library for linear algebra". In: *Journal of Open Source Software* 1.2 (2016), p. 26. DOI: 10.21105/joss.00026. URL: https://doi.org/10.21105/joss.00026.

[45] Mark Galassi et al. *GNU Scientific Library Reference Manual*. 2018. URL: https://www.gnu.org/software/gsl/.

[46] Benedict Leimkuhler and Sebastian Reich. *Simulating Hamiltonian Dynamics*. Cambridge Monographs on Applied and Computational Mathematics. Cambridge University Press, 2005. DOI: 10.1017/CBO9780511614118.

[47] Rodrigo Delgadillo-Blando, Denjoe O'Connor, and Badis Ydri. "Matrix models, gauge theory and emergent geometry". In: *Journal of High Energy Physics* 2009.05 (May 2009), pp. 049–049. DOI: 10.1088/1126-6708/2009/05/049. URL: https://doi.org/10.1088/1126-6708/2009/05/049.

[48] Sheer El-Showk et al. "Solving the 3d Ising Model with the Conformal Bootstrap II. c-Minimization and Precise Critical Exponents". In: *Journal of Statistical Physics* 157.4 (Dec. 2014), pp. 869–914. ISSN: 1572-9613. DOI: 10.1007/s10955-014-1042-7. URL: https://doi.org/10.1007/s10955-014-1042-7.

[49] Harold Steinacker. "Emergent geometry and gravity from matrix models: an introduction". In: *Classical and Quantum Gravity* 27.13 (May 2010), p. 133001. DOI: 10.1088/0264-9381/27/13/133001. URL: https://doi.org/10.1088/0264-9381/27/13/133001.

[50] Nobuyuki Ishibashi et al. "A large-N reduced model as superstring". In: *Nuclear Physics B* 498.1 (1997), pp. 467–491. ISSN: 0550-3213. DOI: https://doi.org/10.1016/S0550-3213(97)00290-3. URL: https://www.sciencedirect.com/science/article/pii/S0550321397002903.

[51] Takehiro Azuma et al. "Nonperturbative studies of fuzzy spheres in a matrix model with the Chern-Simons term". In: *Journal of High Energy Physics* 2004.05 (May 2004), pp. 005–005. DOI: 10.1088/1126-6708/2004/05/005. URL: https://doi.org/10.1088/1126-6708/2004/05/005.

[52] Harold Steinacker. "Quantized gauge theory on the fuzzy sphere as random matrix model". In: *Nuclear Physics B* 679.1 (2004), pp. 66–98. ISSN: 0550-3213. DOI: https://doi.org/10.1016/j.nuclphysb.2003.12.005. URL: https://www.sciencedirect.com/science/article/pii/S0550321303010526.

[53] Vladimir A. Kazakov and Paul Zinn-Justin. "Two-matrix model with ABAB interaction". In: *Nuclear Physics B* 546.3 (1999), pp. 647–668. ISSN: 0550-3213. DOI: https://doi.org/10.1016/S0550-3213(99)00015-2. URL: https://www.sciencedirect.com/science/article/pii/S0550321399000152.

Appendix A

Metropolis formulas

A.1 Formula for generic p

Using the following notation:

$$D = \sum_{i \in I} \omega_i \otimes [M_i, \cdot]_{\epsilon_i} \tag{A.1}$$

$$\delta D = \omega_x \otimes [m_x, \cdot]_{\epsilon_x} \tag{A.2}$$

$$[M, \cdot]_\epsilon = \sum_{q=0}^{1} \epsilon^{1-q} M^q \otimes (M^T)^{1-q} \tag{A.3}$$

where $x \in I$ is a fixed index and m_x is a random Hermitian matrix, Eq.(2.24) becomes:

$$(D')^p - D^p = \sum_{s=1}^{p} \sum_{i_1,..,i_{p-s} \in I} \sum_{\substack{k_1,...,k_{p-s}=0 \\ \sum k_j \leq s}}^{s} \sum_{\substack{l_1,..,l_{p-s}=0 \\ l_j \leq k_j}}^{s} \sum_{l'=0}^{s-\sum k_j} \sum_{q_1,..,q_{p-s}=0}^{1} \cdot \Bigg[$$

$$\cdot \Bigg[\binom{k_1}{l_1} \dots \binom{k_{p-s}}{l_{p-s}} \binom{s - \sum k_j}{l'} (\epsilon_x)^{s-\sum l_j - l'} (\epsilon_{i_1})^{1-q_1} \dots (\epsilon_{i_{p-s}})^{1-q_{p-s}} \cdot$$

$$\cdot \quad (\omega_x)^{k_1} \omega_{i_1} \dots (\omega_x)^{k_{p-s}} \omega_{i_{p-s}} (\omega_x)^{s-\sum k_j} \quad \otimes$$

$$(m_x)^{l_1} (M_{i_1})^{q_1} \dots (m_x)^{l_{p-s}} (M_{i_{p-s}})^{q_{p-s}} (m_x)^{l'} \quad \otimes$$

$$(m_x^T)^{k_1 - l_1} (M_{i_1}^T)^{1-q_1} \dots (m_x^T)^{k_{p-s} - l_{p-s}} (M_{i_{p-s}}^T)^{1-q_{p-s}} (m_x^T)^{s-\sum k_j - l'} \Bigg] \Bigg]. \tag{A.4}$$

A.2 Formulas for $p = 2, 4$

Suppose m_x has the following form:

$$(m_x)_{ij} = z \delta_{iI} \delta_{jJ} + z^* \delta_{iJ} \delta_{jI} \tag{A.5}$$

where z is a complex number, δ_{ij} is the Kronecker delta, and I, J are the indices of the only non-vanishing entries: $(m_x)_{IJ} = (m_x)^*_{JI} = z \neq 0$.
If n is the dimension of the matrix algebra and C is the dimension of the Clifford module, then for $p = 2$:

1. if $I \neq J$:
$$\mathrm{Tr}[(D')^2 - D^2] = 4\ C\ n\ [\ 2\,\mathrm{Re}(z(M_x)_{JI}) + |z|^2\ ] \tag{A.6}$$

2. if $I = J$:
$$\mathrm{Tr}[(D')^2 - D^2] = 8\ C\ \ \mathrm{Re}(z)\ [\ n\ (\ \mathrm{Re}(M_x)_{II} + \mathrm{Re}(z)\ )\ +\ \epsilon_x(\mathrm{Tr}\, M_x + \mathrm{Re}(z))] \tag{A.7}$$

While for $p = 4$:

1. if $I \neq J$:
$$\mathrm{Tr}\, D^3\delta D = \sum_{\substack{i_1<i_3\\ i_2}} 2\,\mathrm{Re}\,\mathrm{Tr}(A[i_1, i_2, i_3, x]) + \sum_i \mathrm{Re}\,\mathrm{Tr}(A[i, x, i, x])$$
$$\begin{aligned} A[i_1, i_2, i_3, x] = \mathrm{Tr}(\omega_{i_1}\omega_{i_2}\omega_{i_3}\omega_x)\Big[& \\ & n[1 + \epsilon_{i_1}\epsilon_{i_2}\epsilon_{i_3}\epsilon_x *][(M_{i_1}M_{i_2}M_{i_3})_{JI}z + (M_{i_1}M_{i_2}M_{i_3})_{IJ}z^*]+ \\ & \sum_{\{\alpha,\beta,\gamma\}} [\epsilon_\gamma + \epsilon_\alpha\epsilon_\beta\epsilon_x *][(M_\alpha M_\beta)_{JI}z + (M_\alpha M_\beta)_{IJ}z^*]+ \\ & [\epsilon_\alpha\epsilon_\beta + \epsilon_\gamma\epsilon_x]2\,\mathrm{Re}((M_\gamma)_{JI}z)\,\mathrm{Tr}\, M_\alpha M_\beta)\Big] \\ \text{with} \quad & \{\alpha, \beta, \gamma\} = \{i_1, i_2, i_3\}, \{i_1, i_3, i_2\}, \{i_2, i_3, i_1\} \end{aligned} \tag{A.8}$$

$$\begin{aligned} \mathrm{Tr}\, D^2(\delta D)^2 = \sum_i C\Big[& |z|^2[2n((M_i^2)_{II} + (M_i^2)_{JJ})+ \\ & 4\epsilon_i\,\mathrm{Tr}\, M_i((M_i)_{II} + (M_i)_{JJ})+ \\ & 4\,\mathrm{Tr}\, M_i^2] + 16\epsilon_i\epsilon_x\,\mathrm{Re}((M_i)_{JI}z)^2\Big] \end{aligned} \tag{A.9}$$

$$\begin{aligned} \mathrm{Tr}\, D\delta D D\delta D = \sum_i \mathrm{Tr}(\omega_i\omega_x\omega_i\omega_x)\Big[& 4n(\mathrm{Re}((M_i)^2_{JI}z^2)+ \\ & |z|^2\,\mathrm{Re}((M_i)_{II}(M_i)_{JJ})+ \\ & |z|^2[4\epsilon_i\,\mathrm{Tr}\, M_i((M_i)_{II} + (M_i)_{JJ}) + 4\,\mathrm{Tr}\, M_i^2]+ \\ & 16\epsilon_i\epsilon_x\,\mathrm{Re}((M_i)_{JI}z)^2\Big] \end{aligned} \tag{A.10}$$

$$\mathrm{Tr}\, D(\delta D)^3 = 4C(n+6)|z|^2\,\mathrm{Re}((M_x)_{JI}z) \tag{A.11}$$

$$\mathrm{Tr}(\delta D)^4 = 4C(n+6)|z|^4 \tag{A.12}$$

2. if $I = J$:

$$\operatorname{Tr} D^3\delta D = \sum_{\substack{i_1<i_3\\ i_2}} 2\operatorname{Re}\operatorname{Tr}(A[i_1,i_2,i_3,x]) + \sum_i \operatorname{Re}\operatorname{Tr}(A[i,x,i,x])$$

$$\begin{aligned} A[i_1,i_2,i_3,x] = \operatorname{Tr}(\omega_{i_1}\omega_{i_2}\omega_{i_3}\omega_x) 2\operatorname{Re} z\Big[& \\ & n[1+\epsilon_{i_1}\epsilon_{i_2}\epsilon_{i_3}\epsilon_x *](M_{i_1}M_{i_2}M_{i_3})_{II} + \\ & [\epsilon_x + \epsilon_{i_1}\epsilon_{i_2}\epsilon_{i_3}*]\operatorname{Tr} M_{i_1}M_{i_2}M_{i_3} + \\ & \sum_{\{\alpha,\beta,\gamma\}} [\epsilon_\gamma + \epsilon_\alpha\epsilon_\beta\epsilon_x *](M_\alpha M_\beta)_{II}\operatorname{Tr} M_\gamma + \\ & [\epsilon_\alpha\epsilon_\beta + \epsilon_\gamma\epsilon_x](M_\gamma)_{II}\operatorname{Tr} M_\alpha M_\beta)\Big] \\ \text{with} \quad \{\alpha,\beta,\gamma\} = \{i_1,i_2,i_3\},\{i_1,i_3,i_2\},\{i_2,i_3,i_1\} & \end{aligned} \tag{A.13}$$

$$\begin{aligned} \operatorname{Tr} D^2(\delta D)^2 = \sum_i C(\operatorname{Re} z)^2\Big[& 2n(M_i)_{II} + 4\epsilon_x(M_i^2)_{II} + \\ & 4\epsilon_i(M_i)_{II}\operatorname{Tr} M_i + 4\epsilon_i\epsilon_x(M_i)_{II}^2 + 2\operatorname{Tr} M_i^2\Big] \end{aligned} \tag{A.14}$$

$$\begin{aligned} \operatorname{Tr} D\delta D D\delta D = \sum_i \operatorname{Tr}(\omega_i\omega_x\omega_i\omega_x)(\operatorname{Re} z)^2\Big[& 2n(M_i)_{II} + 4\epsilon_x(M_i^2)_{II} + \\ & 4\epsilon_i(M_i)_{II}\operatorname{Tr} M_i + 4\epsilon_i\epsilon_x(M_i)_{II}^2 + 2\operatorname{Tr} M_i^2\Big] \end{aligned} \tag{A.15}$$

$$\operatorname{Tr} D(\delta D)^3 = 16C(\operatorname{Re} z)^3((n+3\epsilon_x+3)(M_x)_{II} + \epsilon_x\operatorname{Tr} M_x) \tag{A.16}$$

$$\operatorname{Tr}(\delta D)^4 = 32C(n+4\epsilon_x+3)(\operatorname{Re} z)^4 \tag{A.17}$$

Appendix B

The coefficients $\mathcal{A}_k$

The explicit form of $\mathcal{A}_k(i,i,k)$, $\mathcal{A}_k(i,k,i)$ and $\mathcal{A}_k(k,k,k)$ is given.

$$\begin{aligned}
\mathcal{A}_k(i,i,k) &= \mathrm{Tr}(\omega_k\omega_i\omega_i\omega_k)A(k,i,i,k) = CA(k,i,i,k) \\
\mathcal{A}_k(i,k,i) &= \mathrm{Tr}(\omega_k\omega_i\omega_k\omega_i)A(k,i,k,i) = \pm CA(k,i,k,i) \\
\mathcal{A}_k(k,k,k) &= \mathrm{Tr}(\omega_k\omega_k\omega_k\omega_k)A(k,k,k,k) = CA(k,k,k,k)
\end{aligned} \tag{B.1}$$

where C is the dimension of the Clifford module and the A matrices are:

$$\begin{aligned}
A(k,i,i,k) = {} & n[1+\epsilon\ \dagger]M_i^2M_k + \\
& \epsilon_k I[1+\epsilon]\,\mathrm{Tr}\,M_i^2M_k + \\
& 2\epsilon_i\,\mathrm{Tr}\,M_i[1+\epsilon\ \dagger]M_iM_k + \\
& 2\epsilon_k\epsilon_i M_i[1+\epsilon]\,\mathrm{Tr}\,M_iM_k + \\
& \epsilon_k\,\mathrm{Tr}\,M_k[1+\epsilon]M_i^2 + \\
& M_k[1+\epsilon]\,\mathrm{Tr}\,M_i^2
\end{aligned} \tag{B.2}$$

$$\begin{aligned}
A(k,i,k,i) = {} & n[1+\epsilon]M_iM_kM_i + \\
& \epsilon_k I[1+\epsilon]\,\mathrm{Tr}\,M_i^2M_k + \\
& \epsilon_i\,\mathrm{Tr}\,M_i[1+\epsilon][1+\dagger]M_iM_k + \\
& 2\epsilon_k\epsilon_i M_i[1+\epsilon]\,\mathrm{Tr}\,M_iM_k + \\
& \epsilon_k\,\mathrm{Tr}\,M_k[1+\epsilon]M_i^2 + \\
& M_k[1+\epsilon]\,\mathrm{Tr}\,M_i^2
\end{aligned} \tag{B.3}$$

$$\begin{aligned}
A(k,k,k,k) = {} & 2nM_k^3 + 2\epsilon_k I\,\mathrm{Tr}\,M_k^3 + \\
& 6M_k\,\mathrm{Tr}\,M_k^2 + 6\epsilon_k M_k^2\,\mathrm{Tr}\,M_k.
\end{aligned} \tag{B.4}$$

Appendix C

Matrix identity

Suppose D is a matrix in which m entries are linearly independent. An arbitrary entry can then be written as:

$$D_{ab} = \sum_{ij} c_{ab}^{ij} D_{ij} \tag{C.1}$$

where c_{ab}^{ij} are coefficients and the sum runs over the independent components. This is the case for fuzzy Dirac operators.
The following identity will be proven:

$$\sum_{ij} D_{ij} \frac{\partial}{\partial D_{ij}} \operatorname{Tr} D^p = p \operatorname{Tr} D^p. \tag{C.2}$$

An explicit calculation gives:

$$\begin{aligned}
&\sum_{ij} D_{ij} \frac{\partial}{\partial D_{ij}} \operatorname{Tr} D^p = \sum_{ij} D_{ij} \frac{\partial}{\partial D_{ij}} \sum_{a_1 \cdots a_p} D_{a_1 a_2} \cdots D_{a_p a_1} = \\
&= \sum_{ij} D_{ij} \sum_{a_1 \cdots a_p} \left(c_{a_1 a_2}^{ij} D_{a_2 a_3} \cdots D_{a_p a_1} + \cdots + D_{a_1 a_2} \cdots D_{a_{p-1} a_p} c_{a_p a_1}^{ij} \right) = \\
&= \sum_{a_1 \cdots a_p} \left(\left(\sum_{ij} c_{a_1 a_2}^{ij} D_{ij} \right) D_{a_2 a_3} \cdots D_{a_p a_1} + \cdots + D_{a_1 a_2} \cdots D_{a_{p-1} a_p} \left(\sum_{ij} c_{a_p a_1}^{ij} D_{ij} \right) \right) = \\
&= p \sum_{a_1 \cdots a_p} D_{a_1 a_2} \cdots D_{a_p a_1} = p \operatorname{Tr} D^p
\end{aligned} \tag{C.3}$$

Appendix D

Residues

In what follows, the residues of (4.80) and (4.87) are worked out and denoted C and D respectively. They correspond to certain integer partitions of length ≤ 4. For example, the coefficient denoted $C^{(3)}_{(2,1)}$ corresponds to the partition $3 = 2 + 1$.

$$
\begin{aligned}
C^{(4)}_{(4)} &= \frac{35}{128}\big(a_1^4 + a_2^4 + b_1^4 + b_2^4\big) \\
C^{(4)}_{(3,1)} &= \frac{5}{32}\big(a_1^3(a_2 + b_1 + b_2) + a_2^3(a_1 + b_1 + b_2) + b_1^3(a_1 + a_2 + b_2) + b_2^3(a_1 + a_2 + b_1)\big) \\
C^{(4)}_{(2,2)} &= \frac{9}{64}\big(a_1^2a_2^2 + a_1^2b_1^2 + a_1^2b_2^2 + a_2^2b_1^2 + a_2^2b_2^2 + b_1^2b_2^2\big) \\
C^{(4)}_{(2,1,1)} &= \frac{3}{32}\big(a_1^2(a_2b_1 + a_2b_2 + b_1b_2) + a_2^2(a_1b_1 + a_1b_2 + b_1b_2) \\
&\quad + b_1^2(a_1a_2 + a_1b_2 + a_2b_2) + b_2^2(a_1a_2 + a_1b_1 + a_2b_1)\big) \\
C^{(4)}_{(1,1,1,1)} &= \frac{1}{16}a_1a_2b_1b_2
\end{aligned}
$$

$$
\begin{aligned}
C^{(3)}_{(3)} &= \frac{5}{16}\big(a_1^3 + a_2^3 + b_1^3 + b_2^3\big) \\
C^{(3)}_{(2,1)} &= \frac{3}{16}\big(a_1^2(a_2 + b_1 + b_2) + a_2^2(a_1 + b_1 + b_2) + b_1^2(a_1 + a_2 + b_2) + b_2^2(a_1 + a_2 + b_1)\big) \\
C^{(3)}_{(1,1,1)} &= \frac{1}{8}\big(a_1a_2b_1 + a_1a_2b_2 + a_1b_1b_2 + a_2b_1b_2\big)
\end{aligned}
$$

$$
\begin{aligned}
C^{(2)}_{(2)} &= \frac{3}{8}\big(a_1^2 + a_2^2 + b_1^2 + b_2^2\big) \\
C^{(2)}_{(1,1)} &= \frac{1}{4}\big(a_1a_2 + a_1b_1 + a_1b_2 + a_2b_1 + a_2b_2 + b_1b_2\big)
\end{aligned}
$$

$$
C^{(1)}_{(1)} = \frac{1}{2}\big(a_1 + a_2 + b_1 + b_2\big)
$$

$$
C^{(0)}_{(0)} = 1
$$

$$
\begin{aligned}
D^{(7)}_{(7)} &= -\frac{33}{2048}\big(a_1^7 + a_2^7 + b_1^7 + b_2^7\big)\\
D^{(7)}_{(6,1)} &= \frac{21}{2048}\big(a_1^6(a_2+b_1+b_2) + a_2^6(a_1+b_1+b_2) + b_1^6(a_1+a_2+b_2) + b_2^6(a_1+a_2+b_1)\big)\\
D^{(7)}_{(5,2)} &= \frac{7}{2048}\big(a_1^5(a_2^2+b_1^2+b_2^2) + a_2^5(a_1^2+b_1^2+b_2^2) + b_1^5(a_1^2+a_2^2+b_2^2) + b_2^5(a_1^2+a_2^2+b_1^2)\big)\\
D^{(7)}_{(5,1,1)} &= -\frac{7}{1024}\big(a_1^5(a_2b_1+a_2b_2+b_1b_2) + a_2^5(a_1b_1+a_1b_2+b_1b_2)\\
&\quad + b_1^5(a_1a_2+a_1b_2+a_2b_2) + b_2^5(a_1a_2+a_1b_1+a_2b_1)\big)\\
D^{(7)}_{(4,3)} &= \frac{5}{2048}\big(a_1^4(a_2^3+b_1^3+b_2^3) + a_2^4(a_1^3+b_1^3+b_2^3) + b_1^4(a_1^3+a_2^3+b_2^3) + b_2^4(a_1^3+a_2^3+b_1^3)\big)\\
D^{(7)}_{(4,2,1)} &= -\frac{5}{2048}\Big(a_1^4\big(a_2^2(b_1+b_2) + b_1^2(a_2+b_2) + b_2^2(a_2+b_1)\big)\\
&\quad + a_2^4\big(a_1^2(b_1+b_2) + b_1^2(a_1+b_2) + b_2^2(a_1+b_1)\big)\\
&\quad + b_1^4\big(a_1^2(a_2+b_2) + a_2^2(a_1+b_2) + b_2^2(a_1+a_2)\big)\\
&\quad + b_2^4\big(a_1^2(a_2+b_1) + a_2^2(a_1+b_1) + b_1^2(a_1+a_2)\big)\Big)\\
D^{(7)}_{(4,1,1,1)} &= \frac{5}{1024}\big(a_1^4a_2b_1b_2 + a_1a_2^4b_1b_2 + a_1a_2b_1^4b_2 + a_1a_2b_1b_2^4\big)\\
D^{(7)}_{(3,3,1)} &= -\frac{5}{512}\big(a_1^3a_2^3(b_1+b_2) + a_1^3b_1^3(a_2+b_2) + a_1^3b_2^3(a_2+b_1)\\
&\quad + a_2^3b_1^3(a_1+b_2) + a_2^3b_2^3(a_1+b_1) + b_1^3b_2^3(a_1+a_2)\big)\\
D^{(7)}_{(3,2,2)} &= -\frac{1}{1024}\big(a_1^3(a_2^2b_1^2 + a_2^2b_2^2 + b_1^2b_2^2) + a_2^3(a_1^2b_1^2 + a_1^2b_2^2 + b_1^2b_2^2)\\
&\quad + b_1^3(a_1^2a_2^2 + a_1^2b_2^2 + a_2^2b_2^2) + b_2^3(a_1^2a_2^2 + a_1^2b_1^2 + a_2^2b_1^2)\big)\\
D^{(7)}_{(3,2,1,1)} &= \frac{1}{512}\big(a_1^3(a_2^2b_1b_2 + a_2b_1^2b_2 + a_2b_1b_2^2) + a_2^3(a_1^2b_1b_2 + a_1b_1^2b_2 + a_1b_1b_2^2)\\
&\qquad + b_1^3(a_1^2a_2b_2 + a_1a_2^2b_2 + a_1a_2b_2^2) + b_2^3(a_1^2a_2b_1 + a_1a_2^2b_1 + a_1a_2b_1^2)\big)\\
D^{(7)}_{(2,2,2,1)} &= -\frac{1}{1024}\big(a_1^2a_2^2b_1^2b_2 + a_1^2a_2^2b_1b_2^2 + a_1^2a_2b_1^2b_2^2 + a_1a_2^2b_1^2b_2^2\big)
\end{aligned}
$$

$$
\begin{aligned}
D^{(6)}_{(6)} &= -\frac{21}{1024}\big(a_1^6 + a_2^6 + b_1^6 + b_2^6\big)\\
D^{(6)}_{(5,1)} &= \frac{7}{512}\big(a_1^5(a_2+b_1+b_2) + a_2^5(a_1+b_1+b_2) + b_1^5(a_1+a_2+b_2) + b_2^5(a_1+a_2+b_1)\big)\\
D^{(6)}_{(4,2)} &= \frac{5}{1024}\big(a_1^4(a_2^2+b_1^2+b_2^2) + a_2^4(a_1^2+b_1^2+b_2^2) + b_1^4(a_1^2+a_2^2+b_2^2) + b_2^4(a_1^2+a_2^2+b_1^2)\big)\\
D^{(6)}_{(4,1,1)} &= -\frac{5}{512}\big(a_1^4(a_2b_1+a_2b_2+b_1b_2) + a_2^4(a_1b_1+a_1b_2+b_1b_2)\\
&\quad + b_1^4(a_1a_2+a_1b_2+a_2b_2) + b_2^4(a_1a_2+a_1b_1+a_2b_1)\big)\\
D^{(6)}_{(3,3)} &= \frac{1}{256}\big(a_1^3a_2^3 + a_1^3b_1^3 + a_1^3b_2^3 + a_2^3b_1^3 + a_2^3b_2^3 + b_1^3b_2^3\big)\\
D^{(6)}_{(3,2,1)} &= -\frac{1}{256}\Big(a_1^3\big(a_2^2(b_1+b_2) + b_1^2(a_2+b_2) + b_2^2(a_2+b_1)\big)\\
&\quad + a_2^3\big(a_1^2(b_1+b_2) + b_1^2(a_1+b_2) + b_2^2(a_1+b_1)\big)\\
&\quad + b_1^3\big(a_1^2(a_2+b_2) + a_2^2(a_1+b_2) + b_2^2(a_1+a_2)\big)\\
&\quad + b_2^3\big(a_1^2(a_2+b_1) + a_2^2(a_1+b_1) + b_1^2(a_1+a_2)\big)\Big)\\
D^{(6)}_{(3,1,1,1)} &= \frac{1}{128}(a_1^3a_2b_1b_2 + a_1a_2^3b_1b_2 + a_1a_2b_1^3b_2 + a_1a_2b_1b_2^3)\\
D^{(6)}_{(2,2,2)} &= -\frac{1}{8}\big(a_1^2a_2^2b_1^2 + a_1^2a_2^2b_2^2 + a_1^2b_1^2b_2^2 + a_2^2b_1^2b_2^2\big)\\
D^{(6)}_{(2,2,1,1)} &= \frac{1}{256}\big(a_1^2a_2^2b_1b_2 + a_1^2a_2b_1^2b_2 + a_1^2a_2b_1b_2^2 + a_1a_2^2b_1^2b_2 + a_1a_2^2b_1b_2^2 + a_1a_2b_1^2b_2^2\big)
\end{aligned}
$$

$$
\begin{aligned}
D^{(5)}_{(5)} &= -\frac{7}{256}\big(a_1^5 + a_2^5 + b_1^5 + b_2^5\big)\\
D^{(5)}_{(4,1)} &= \frac{5}{256}\big(a_1^4(a_2+b_1+b_2) + a_2^4(a_1+b_1+b_2) + b_1^4(a_1+a_2+b_2) + b_2^4(a_1+a_2+b_1)\big)\\
D^{(5)}_{(3,2)} &= \frac{1}{128}\big(a_1^3(a_2^2+b_1^2+b_2^2) + a_2^3(a_1^2+b_1^2+b_2^2) + b_1^3(a_1^2+a_2^2+b_2^2) + b_2^3(a_1^2+a_2^2+b_1^2)\big)\\
D^{(5)}_{(3,1,1)} &= -\frac{1}{64}\big(a_1^3(a_2b_1+a_2b_2+b_1b_2) + a_2^3(a_1b_1+a_1b_2+b_1b_2)\\
&\quad + b_1^3(a_1a_2+a_1b_2+a_2b_2) + b_2^3(a_1a_2+a_1b_1+a_2b_1)\big)\\
D^{(5)}_{(2,2,1)} &= -\frac{1}{128}\big(a_1^2a_2^2(b_1+b_2) + a_1^2b_1^2(a_2+b_2) + a_1^2b_2^2(a_2+b_1)\\
&\quad + a_2^2b_1^2(a_1+b_2) + a_2^2b_2^2(a_1+b_1) + b_1^2b_2^2(a_1+a_2)\big)\\
D^{(5)}_{(2,1,1,1)} &= \frac{1}{64}(a_1^2a_2b_1b_2 + a_1a_2^2b_1b_2 + a_1a_2b_1^2b_2 + a_1a_2b_1b_2^2)
\end{aligned}
$$

$$
\begin{aligned}
D^{(4)}_{(4)} &= -\frac{5}{128}\big(a_1^4 + a_2^4 + b_1^4 + b_2^4\big) \\
D^{(4)}_{(3,1)} &= \frac{1}{32}\big(a_1^3(a_2 + b_1 + b_2) + a_2^3(a_1 + b_1 + b_2) + b_1^3(a_1 + a_2 + b_2) + b_2^3(a_1 + a_2 + b_1)\big) \\
D^{(4)}_{(2,2)} &= \frac{1}{64}\big(a_1^2a_2^2 + a_1^2b_1^2 + a_1^2b_2^2 + a_2^2b_1^2 + a_2^2b_2^2 + b_1^2b_2^2\big) \\
D^{(4)}_{(2,1,1)} &= -\frac{1}{32}\big(a_1^2(a_2b_1 + a_2b_2 + b_1b_2) + a_2^2(a_1b_1 + a_1b_2 + b_1b_2) \\
&\quad + b_1^2(a_1a_2 + a_1b_2 + a_2b_2) + b_2^2(a_1a_2 + a_1b_1 + a_2b_1)\big) \\
D^{(4)}_{(1,1,1,1)} &= \frac{1}{16}a_1a_2b_1b_2
\end{aligned}
$$

Appendix E

Matrix solutions from Clifford modules

In the following, type 2 matrix solutions of Proposition 1 are built using Clifford modules.
Consider a $(p,0)$ Clifford module, i.e. a set of p Hermitian matrices γ^i such that $\{\gamma^i,\gamma^j\} = 2\delta^{ij}\mathbb{1}$. For even p, define v_1 to be proportional to an odd product of gamma matrices:

$$v_1 := \left(i^{\frac{|I|-1}{2} \bmod 2}\right) x \prod_{i\in I}\gamma^i, \quad I \subset \{1,\dots,p\},\ |I| \text{ odd},\ x \in \mathbb{R} \tag{E.1}$$

and v_2 a linear combination of the same gamma matrices:

$$v_2 := \sum_{i\in I} y_i\gamma^i, \quad y_i \in \mathbb{R}. \tag{E.2}$$

For concreteness, a simple example would be the following:

$$\begin{aligned} &p = 4\\ &I = \{1,2,3\}\\ &v_1 = ix\gamma^1\gamma^2\gamma^3\\ &v_2 = y_1\gamma^1 + y_2\gamma^2 + y_3\gamma^3. \end{aligned} \tag{E.3}$$

Matrices v_1 and v_2 as in (E.1) and (E.2) satisfy the conditions for a type 2 matrix solution of Proposition 1 with $y^2 := \sum_i y_i^2$. The proof goes as follows.
First of all, v_1 and v_2 have to be traceless and Hermitian. v_2 is a linear combination of Hermitian matrices with real coefficients and it is therefore Hermitian, while for v_1:

$$\begin{aligned} \left(\gamma^{i_1}\cdots\gamma^{i_{2k+1}}\right)^\dagger &= \gamma^{i_{2k+1}}\cdots\gamma^{i_1}\\ &= (-1)^{2k}\gamma^{2k}\cdots\gamma^1\gamma^{i_{2k+1}}\\ &= (-1)^{2k}(-1)^{2k-1}\dots(-1)\gamma^1\cdots\gamma^{i_{2k+1}}\\ &= (-1)^k\gamma^1\cdots\gamma^{i_{2k+1}}\\ &= (-1)^{\frac{|I|-1}{2}}\gamma^1\cdots\gamma^{i_{2k+1}} \end{aligned}$$

therefore the i factor in (E.1) compensates for the minus sign.
The tracelessness of v_2 follows from:

$$\operatorname{Tr}\gamma^i = \operatorname{Tr}\gamma^i\gamma^j\gamma^j = -\operatorname{Tr}\gamma^j\gamma^i\gamma^j = -\operatorname{Tr}\gamma^i\gamma^j\gamma^j = -\operatorname{Tr}\gamma^i$$

where the first equality comes from $\gamma^j\gamma^j = \mathbb{1}$, the second from the anti-commutation property and the third from the cyclicity of the trace. To prove it for v_1, first notice that for even p one can build a matrix γ (the chirality operator [8]) such that $\gamma^2 = \mathbb{1}$ and $\{\gamma, \gamma^i\} = 0$ for all i. Therefore:

$$\begin{aligned}\operatorname{Tr}\gamma^1\cdots\gamma^{i_{2k+1}} = \operatorname{Tr}\gamma^1\cdots\gamma^{i_{2k+1}}\gamma\gamma = -\operatorname{Tr}\gamma\gamma^1\cdots\gamma^{i_{2k+1}}\gamma = -\operatorname{Tr}\gamma^1\cdots\gamma^{i_{2k+1}}\gamma\gamma \\ = -\operatorname{Tr}\gamma^1\cdots\gamma^{i_{2k+1}}\end{aligned}$$

where again anti-commutation and cyclicity were used.
For the involutory property:

$$\begin{aligned}v_1^2 &= (-1)^k x^2\gamma^1\cdots\gamma^{i_{2k+1}}\gamma^1\cdots\gamma^{i_{2k+1}} \\ &= (-1)^k(-1)^{2k}(-1)^{2k-1}\ldots(-1)x^2\mathbb{1} \\ &= (-1)^k(-1)^k x^2\mathbb{1} \\ &= x^2\mathbb{1}\end{aligned}$$

$$\begin{aligned}v_2^2 &= \sum_{i,j} y_i y_j \gamma^i\gamma^j \\ &= \sum_{i,j} y_i y_j \left(\frac{\{\gamma^i,\gamma^j\} + [\gamma^i,\gamma^j]}{2}\right) \\ &= \sum_{i,j}\delta^{ij}y_i y_j\mathbb{1} := y^2\mathbb{1}\end{aligned}$$

For the commutation property:

$$\gamma^i\gamma^{i_1}\cdots\gamma^{i_{2k+1}} = \sum_j \delta_{ii_j}(-1)^{j-1}\gamma^{i_1}\cdots\gamma^{i_{j-1}}\gamma^{i_{j+1}}\cdots\gamma^{i_{2k+1}} \tag{E.4}$$

$$\gamma^{i_1}\cdots\gamma^{i_{2k+1}}\gamma^i = \sum_j \delta_{ii_j}(-1)^{2k+j-1}\gamma^{i_1}\cdots\gamma^{i_{j-1}}\gamma^{i_{j+1}}\cdots\gamma^{i_{2k+1}} \tag{E.5}$$

therefore $[\gamma^i, \gamma^{i_1}\cdots\gamma^{i_{2k+1}}] = 0$ and the conclusion follows by linearity in the first argument of the commutator.
Lastly, notice that from (E.4) or (E.5) it is clear that $\operatorname{Tr} v_1 v_2$ is a sum of traces of an even number of gamma matrices, but:

$$\operatorname{Tr}\gamma^1\cdots\gamma^{2k} = -\operatorname{Tr}\gamma^{2k}\gamma^1\cdots\gamma^{2k-1} = -\operatorname{Tr}\gamma^1\cdots\gamma^{2k}$$

where anti-commutation and cyclicity were used. Therefore $\operatorname{Tr} v_1 v_2 = 0$.

Appendix F

Products of Pauli matrices

When writing down the action of various Dirac operators, the product of a number of Pauli matrices is often needed. To this purpose, identify σ_0 with the identity matrix, and denote Pauli matrices and identity collectively as σ_α, for $\alpha = 0, 1, 2, 3$. If adopting the convention that Greek indices run from 0 to 3, while Latin indices run from 1 to 3, one can write:

$$\sigma_\alpha = \delta_{\alpha 0}\mathbb{1} + \delta_{\alpha a}\sigma_a$$

where sum over repeated indices is intended.
The two-product is also relatively straightforward to write in this notation:

$$\sigma_\alpha\sigma_\beta = \delta_{\alpha\beta}\mathbb{1} + (\delta_{\alpha 0}\delta_{\beta c} + \delta_{\alpha c}\delta_{\beta 0} + i\delta_{\alpha a}\delta_{\beta b}\epsilon_{abc})\sigma_c$$

or, condensing the bracket in a single symbol:

$$\sigma_\alpha\sigma_\beta = \delta_{\alpha\beta}\mathbb{1} + \eta_{\alpha\beta c}\sigma_c.$$

In order to write the three-product (which might be needed for example in the (0,3) Dirac operator) first compute:

$$\sigma_a\sigma_\beta = \delta_{\beta 0}\sigma_a + \delta_{\beta b}(\delta_{ab}\mathbb{1} + i\epsilon_{abc}\sigma_c)$$

which gives:

$$\begin{aligned}
\sigma_\alpha\sigma_\beta\sigma_\rho &= \delta_{\alpha\beta}\delta_{\rho 0}\mathbb{1} + \eta_{\alpha\beta c}\delta_{\rho r}\sigma_c\sigma_r + \text{traceless} \\
&= (\delta_{\alpha\beta}\delta_{\rho 0} + \eta_{\alpha\beta c}\delta_{\rho r}\delta_{cr})\mathbb{1} + \text{traceless} \\
&= (\delta_{\alpha\beta}\delta_{\rho 0} + \eta_{\alpha\beta c}\delta_{\rho c})\mathbb{1} + \text{traceless} \\
&= (\delta_{\alpha\beta}\delta_{\rho 0} + \delta_{\alpha 0}\delta_{\beta c}\delta_{\rho c} + \delta_{\alpha c}\delta_{\beta 0}\delta_{\rho c} + i\delta_{\alpha a}\delta_{\beta b}\delta_{\rho c}\epsilon_{abc})\mathbb{1} + \text{traceless}
\end{aligned}$$

or, in a more symmetric way:

$$\begin{aligned}
\sigma_\alpha\sigma_\beta\sigma_\rho = (&\delta_{\alpha 0}\delta_{\beta 0}\delta_{\rho 0} + \delta_{\alpha 0}\delta_{\beta c}\delta_{\rho c} + \delta_{\alpha c}\delta_{\beta 0}\delta_{\rho c} + \delta_{\alpha c}\delta_{\beta c}\delta_{\rho 0} \\
&+ i\delta_{\alpha a}\delta_{\beta b}\delta_{\rho c}\epsilon_{abc})\mathbb{1} + \text{traceless}.
\end{aligned}$$

The interpretation is clear: the terms with a non-vanishing trace are the ones in which all the matrices are the identity, or one is the identity and the other two are the same Pauli matrix, or all three are Pauli matrices but two of them combine in

a commutator to give the third one.
Similarly, the four-product expands to:

$$\begin{aligned}
\sigma_\alpha\sigma_\beta\sigma_\rho\sigma_\tau &= (\delta_{\alpha\beta}\mathbb{1} + \eta_{\alpha\beta c}\sigma_c)(\delta_{\rho\tau}\mathbb{1} + \eta_{\rho\tau d}\sigma_d) \\
&= \delta_{\alpha\beta}\delta_{\rho\tau}\mathbb{1} + \eta_{\alpha\beta c}\eta_{\rho\tau d}\sigma_c\sigma_d + \text{traceless} \\
&= (\delta_{\alpha\beta}\delta_{\rho\tau} + \eta_{\alpha\beta c}\eta_{\rho\tau d}\delta_{cd})\mathbb{1} + \text{traceless} \\
&= (\delta_{\alpha\beta}\delta_{\rho\tau} + \eta_{\alpha\beta c}\eta_{\rho\tau c})\mathbb{1} + \text{traceless} \\
&= \big[\delta_{\alpha\beta}\delta_{\rho\tau} + \delta_{\alpha 0}\delta_{\beta a}\delta_{\rho 0}\delta_{\tau a} + \delta_{\alpha 0}\delta_{\beta a}\delta_{\rho a}\delta_{\tau 0} + \delta_{\alpha a}\delta_{\beta 0}\delta_{\rho 0}\delta_{\tau a} + \delta_{\alpha a}\delta_{\beta 0}\delta_{\rho a}\delta_{\tau 0} \\
&\quad + i\epsilon_{abc}\left(\delta_{\alpha a}\delta_{\beta b}\delta_{\rho c}\delta_{\tau 0} + \delta_{\alpha a}\delta_{\beta b}\delta_{\rho 0}\delta_{\tau c} + \delta_{\alpha a}\delta_{\beta 0}\delta_{\rho b}\delta_{\tau c} + \delta_{\alpha 0}\delta_{\beta a}\delta_{\rho b}\delta_{\tau c}\right) \\
&\quad - \delta_{\alpha a}\delta_{\beta b}\delta_{\rho r}\delta_{\tau t}(\delta_{ar}\delta_{bt} - \delta_{at}\delta_{br})\big]\mathbb{1} + \text{traceless} \\
&= \big[\delta_{\alpha 0}\delta_{\beta 0}\delta_{\rho 0}\delta_{\tau 0} \\
&\quad + \delta_{\alpha 0}\delta_{\beta a}\delta_{\rho 0}\delta_{\tau a} + \delta_{\alpha a}\delta_{\beta 0}\delta_{\rho a}\delta_{\tau 0} \\
&\quad + \delta_{\alpha 0}\delta_{\beta 0}\delta_{\rho a}\delta_{\tau a} + \delta_{\alpha a}\delta_{\beta a}\delta_{\rho 0}\delta_{\tau 0} + \delta_{\alpha 0}\delta_{\beta a}\delta_{\rho a}\delta_{\tau 0} + \delta_{\alpha a}\delta_{\beta 0}\delta_{\rho 0}\delta_{\tau a} \\
&\quad + i\epsilon_{abc}\left(\delta_{\alpha a}\delta_{\beta b}\delta_{\rho c}\delta_{\tau 0} + \delta_{\alpha a}\delta_{\beta b}\delta_{\rho 0}\delta_{\tau c} + \delta_{\alpha a}\delta_{\beta 0}\delta_{\rho b}\delta_{\tau c} + \delta_{\alpha 0}\delta_{\beta a}\delta_{\rho b}\delta_{\tau c}\right) \\
&\quad + \delta_{\alpha a}\delta_{\beta a}\delta_{\rho b}\delta_{\tau b} + \delta_{\alpha a}\delta_{\beta b}\delta_{\rho b}\delta_{\tau a} - \delta_{\alpha a}\delta_{\beta b}\delta_{\rho a}\delta_{\tau b}\big]\mathbb{1} + \text{traceless}
\end{aligned}$$

where again it is easy to see why these are the only terms contributing: the first line means that all the matrices are the identity; in the second and third line two are the identity and the other two are the same Pauli matrix; in the fourth line one matrix is the identity and the other three are Pauli, but two of them combine in a commutator to give the third one; and in the last line all four are Pauli matrices combining in pairs to give the identity.

Appendix G

Commuting involutory matrix solutions

G.1 The $(3,0)$ and $(0,3)$ class: $|I| = 0$ and $|J| = 3$

The equations reduce to:

$$v_0) \quad x_0^2 \left(2x_0^2 + 3 \sum_{\dot{a} \in J - J_0} x_{\dot{a}}^2 + \frac{g_2}{4} \right) = 0 \tag{G.1}$$

$$v_{\dot{c}}) \quad x_{\dot{c}}^2 \left(\sum_{\dot{a} \in J - J_{\dot{c}}} x_{\dot{a}}^2 + 2 \sum_{\dot{a} \in J_{\dot{c}}} x_{\dot{a}}^2 + \frac{g_2}{4} \right) = 0, \quad \text{if } \dot{c} \in J_0 \tag{G.2}$$

$$v_{\dot{c}}) \quad x_{\dot{c}}^2 \left(3x_0^2 + \sum_{\dot{a} \in J - J_{\dot{c}}} x_{\dot{a}}^2 + 2 \sum_{\dot{a} \in J_{\dot{c}}} x_{\dot{a}}^2 + \frac{g_2}{4} \right) = 0, \quad \text{if } \dot{c} \notin J_0. \tag{G.3}$$

The solutions will be classified based on the cardinality of J_0.
If $|J_0| = 3$ the equations decouple in the variables x_0^2 and $\sum x_{\dot{a}}^2$, giving:

$$x_0^2 = -\frac{g_2}{8}, \quad \sum_{\dot{a} \in J} x_{\dot{a}}^2 = 0, \quad \text{or} \tag{G.4}$$

$$x_0^2 = 0, \quad \sum_{\dot{a} \in J} x_{\dot{a}}^2 = -\frac{g_2}{8}, \quad \text{or} \tag{G.5}$$

$$x_0^2 = -\frac{g_2}{8}, \quad \sum_{\dot{a} \in J} x_{\dot{a}}^2 = -\frac{g_2}{8}. \tag{G.6}$$

If $|J_0| = 2$ then call $\bar{c}$ the unique index which is not in J_0. The solution is one of the following:

$$\boxed{\begin{aligned}
&x_0^2 = -\frac{g_2}{8}, \quad x_{\bar{c}}^2 = 0, \quad \sum_{\dot{a}\in J_0} x_{\dot{a}}^2 = 0, \quad \text{or} && \text{(G.7)}\\
&x_0^2 = 0, \quad x_{\bar{c}}^2 = -\frac{g_2}{8}, \quad \sum_{\dot{a}\in J_0} x_{\dot{a}}^2 = 0, \quad \text{or} && \text{(G.8)}\\
&x_0^2 = 0, \quad x_{\bar{c}}^2 = 0, \quad \sum_{\dot{a}\in J_0} x_{\dot{a}}^2 = -\frac{g_2}{8}, \quad \text{or} && \text{(G.9)}\\
&x_0^2 = -\frac{g_2}{20}, \quad x_{\bar{c}}^2 = -\frac{g_2}{20}, \quad \sum_{\dot{a}\in J_0} x_{\dot{a}}^2 = 0, \quad \text{or} && \text{(G.10)}\\
&x_0^2 = -\frac{g_2}{8}, \quad x_{\bar{c}}^2 = 0, \quad \sum_{\dot{a}\in J_0} x_{\dot{a}}^2 = -\frac{g_2}{8}, \quad \text{or} && \text{(G.11)}\\
&x_0^2 = 0, \quad x_{\bar{c}}^2 = -\frac{g_2}{12}, \quad \sum_{\dot{a}\in J_0} x_{\dot{a}}^2 = -\frac{g_2}{12}. && \text{(G.12)}
\end{aligned}}$$

If $|J_0| = 1$, then there are two possibilities. Call $\hat{c}$ the only index in J_0 and $\bar{c}_1$ and $\bar{c}_2$ the two indices not in J_0, then either $v_{\bar{c}_1} \perp v_{\bar{c}_2}$ or not. If they are orthogonal, the solutions are:

$$\boxed{\begin{aligned}
&x_0^2 = -\frac{g_2}{8}, \quad x_{\hat{c}}^2 = x_{\bar{c}_1}^2 = x_{\bar{c}_2}^2 = 0, \quad \text{or} && \text{(G.13)}\\
&x_{\hat{c}}^2 = -\frac{g_2}{8}, \quad x_0^2 = x_{\bar{c}_1}^2 = x_{\bar{c}_2}^2 = 0, \quad \text{or} && \text{(G.14)}\\
&x_{\bar{c}_i}^2 = -\frac{g_2}{8}, \quad x_0^2 = x_{\hat{c}}^2 = x_{\bar{c}_j}^2 = 0 && \text{(G.15)}
\end{aligned}}$$

when only one variable is non-vanishing, or:

$$\boxed{\begin{aligned}
&x_0^2 = x_{\hat{c}}^2 = -\frac{g_2}{8}, \quad x_{\bar{c}_1}^2 = x_{\bar{c}_2}^2 = 0, \quad \text{or} && \text{(G.16)}\\
&x_0^2 = x_{\bar{c}_i}^2 = -\frac{g_2}{20}, \quad x_{\bar{c}_j}^2 = x_{\hat{c}}^2 = 0, \quad \text{or} && \text{(G.17)}\\
&x_0^2 = x_{\hat{c}}^2 = 0, \quad x_{\bar{c}_1}^2 = x_{\bar{c}_2}^2 = -\frac{g_2}{12}, \quad \text{or} && \text{(G.18)}\\
&x_0^2 = x_{\bar{c}_i}^2 = 0, \quad x_{\bar{c}_j}^2 = x_{\hat{c}}^2 = -\frac{g_2}{12} && \text{(G.19)}
\end{aligned}}$$

when two variables are non-vanishing, or:

$$\boxed{\begin{aligned}
&x_0^2 = -\frac{g_2}{16}, \quad x_{\bar{c}_1}^2 = x_{\bar{c}_2}^2 = -\frac{g_2}{48}, \quad x_{\hat{c}}^2 = 0, \quad \text{or} && \text{(G.20)}\\
&x_0^2 = 0, \quad x_{\bar{c}_1}^2 = x_{\bar{c}_2}^2 = x_{\hat{c}}^2 = -\frac{g_2}{16}, \quad \text{or} && \text{(G.21)}\\
&x_0^2 = -\frac{g_2}{56}, \quad x_{\bar{c}_1}^2 = x_{\bar{c}_2}^2 = -\frac{g_2}{28}, \quad x_{\hat{c}}^2 = -5\frac{g_2}{56} && \text{(G.22)}
\end{aligned}}$$

when at least three variables are non-vanishing.
If $v_{\bar{c}_1}$ and $v_{\bar{c}_2}$ instead are not orthogonal, the solutions are the same as (G.13) to

(G.19), except that instead of two separate variables $x^2_{\bar{c}_1}$ and $x^2_{\bar{c}_2}$, there is a unique variable $x^2_{\bar{c}_1} + x^2_{\bar{c}_2}$.
The last three cases to analyze are when $J_0 = \emptyset$. Either all three dotted matrices are proportional to each other, or two of them are proportional and orthogonal to the remaining one, or all three are orthogonal.
If all three dotted matrices are proportional to each other, the solutions are:

$$\boxed{\begin{aligned} x_0^2 &= -\frac{g_2}{8}, \quad \sum_{\dot{a}} x^2_{\dot{a}} = 0, \quad \text{or} && \text{(G.23)} \\ x_0^2 &= 0, \quad \sum_{\dot{a}} x^2_{\dot{a}} = -\frac{g_2}{8} \quad \text{or} && \text{(G.24)} \\ x_0^2 &= \sum_{\dot{a}} x^2_{\dot{a}} = -\frac{g_2}{20}. && \text{(G.25)} \end{aligned}}$$

In the second case, denote $\bar{c}_1$ and $\bar{c}_2$ the indices of the two matrices proportional to each other, and $\hat{c}$ the remaining one. The solutions are:

$$\boxed{\begin{aligned} x_0^2 &= -\frac{g_2}{20}, \quad x^2_{\bar{c}_1} + x^2_{\bar{c}_2} = -\frac{g_2}{20}, \quad x^2_{\hat{c}} = 0, \quad \text{or} && \text{(G.26)} \\ x_0^2 &= -\frac{g_2}{20}, \quad x^2_{\bar{c}_1} = x^2_{\bar{c}_2} = 0, \quad x^2_{\hat{c}} = -\frac{g_2}{20}, \quad \text{or} && \text{(G.27)} \\ x_0^2 &= -\frac{g_2}{16}, \quad x^2_{\bar{c}_1} + x^2_{\bar{c}_2} = -\frac{g_2}{48}, \quad x^2_{\hat{c}} = -\frac{g_2}{48} && \text{(G.28)} \end{aligned}}$$

in addition to (G.13) to (G.15).
Lastly, when all matrices are orthogonal to each other, the solutions are:

$$\boxed{\begin{aligned} x^2_\alpha &= -\frac{g_2}{8}, \quad x^2_\beta = 0 \quad \forall\ \beta \neq \alpha, \quad \text{or} && \text{(G.29)} \\ x_0^2 &= x_{\dot{c}_{i_1}} = -\frac{g_2}{20}, \quad x^2_{\dot{c}_{i_2}} = x^2_{\dot{c}_{i_3}} = 0, \quad \text{or} && \text{(G.30)} \\ x_0^2 &= x_{\dot{c}_{i_1}} = 0, \quad x^2_{\dot{c}_{i_2}} = x^2_{\dot{c}_{i_3}} = -\frac{g_2}{12}, \quad \text{or} && \text{(G.31)} \\ x_0^2 &= -\frac{g_2}{16}, \quad x^2_{\dot{c}_{i_1}} = x^2_{\dot{c}_{i_2}} = -\frac{g_2}{48}, \quad x^2_{\dot{c}_{i_3}} = 0, \quad \text{or} && \text{(G.32)} \\ x_0^2 &= 0, \quad x^2_{\dot{c}_{i_1}} = x^2_{\dot{c}_{i_2}} = x^2_{\dot{c}_{i_3}} = -\frac{g_2}{16}, \quad \text{or} && \text{(G.33)} \\ x_0^2 &= -5\frac{g_2}{76}, \quad x^2_{\dot{c}_{i_1}} = x^2_{\dot{c}_{i_2}} = x^2_{\dot{c}_{i_3}} = -\frac{g_2}{76}. && \text{(G.34)} \end{aligned}}$$

G.2 The $(1,2)$ and $(2,1)$ class: $|I| = 2$ and $|J| = 1$

The solutions will be classified based on the cardinality of I_0 being 2, 1 or 0. For each alternative, J_0 can either be empty or contain the only dotted index. This brings to eleven different cases in total.
When $|I_0| = 2$ and $|J_0| = 1$, all matrices are proportional to each other. The

equation for $v_{\dot{c}}$ decouples and the solutions are:

$$x_0^2 = -\frac{g_2}{8}, \quad \sum_{a\in I} x_a^2 = 0, \quad x_{\dot{c}}^2 = 0 \text{ or } -\frac{g_2}{8}, \quad \text{or} \tag{G.35}$$

$$x_0^2 = 0, \quad \sum_{a\in I} x_a^2 = -\frac{g_2}{8}, \quad x_{\dot{c}}^2 = 0 \text{ or } -\frac{g_2}{8}, \quad \text{or} \tag{G.36}$$

$$x_0^2 = -\frac{g_2}{32}, \quad \sum_{a\in I} x_a^2 = -\frac{g_2}{32}, \quad x_{\dot{c}}^2 = 0 \text{ or } -\frac{g_2}{8}. \tag{G.37}$$

When $|I_0| = 2$ and $|J_0| = 0$, all non-dotted matrices are proportional to each other and orthogonal to the dotted one. The solutions are:

$$x_0^2 = -\frac{g_2}{8}, \quad \sum_{a\in I} x_a^2 = 0, \quad x_{\dot{c}}^2 = 0, \quad \text{or} \tag{G.38}$$

$$x_0^2 = 0, \quad \sum_{a\in I} x_a^2 = -\frac{g_2}{8}, \quad x_{\dot{c}}^2 = 0, \quad \text{or} \tag{G.39}$$

$$x_0^2 = 0, \quad \sum_{a\in I} x_a^2 = 0, \quad x_{\dot{c}}^2 = -\frac{g_2}{8}, \quad \text{or} \tag{G.40}$$

$$x_0^2 = -\frac{g_2}{32}, \quad \sum_{a\in I} x_a^2 = -\frac{g_2}{32}, \quad x_{\dot{c}}^2 = 0, \quad \text{or} \tag{G.41}$$

$$x_0^2 = -\frac{g_2}{16}, \quad \sum_{a\in I} x_a^2 = 0, \quad x_{\dot{c}}^2 = -\frac{g_2}{8}, \quad \text{or} \tag{G.42}$$

$$x_0^2 = 0, \quad \sum_{a\in I} x_a^2 = -\frac{g_2}{12}, \quad x_{\dot{c}}^2 = -\frac{g_2}{12}, \quad \text{or} \tag{G.43}$$

$$x_0^2 = -\frac{g_2}{32}, \quad \sum_{a\in I} x_a^2 = -\frac{g_2}{24}, \quad x_{\dot{c}}^2 = -7\frac{g_2}{48}. \tag{G.44}$$

When $|I_0| = 1$ and $|J_0| = 1$, call c_1 the index in I_0 and c_2 the index in $I - I_0$. Solutions with one non-vanishing variable are:

$$x_0^2 = -\frac{g_2}{8}, \quad x_{c_1}^2 = x_{c_2}^2 = x_{\dot{c}}^2 = 0, \quad \text{or} \tag{G.45}$$

$$x_{c_i}^2 = -\frac{g_2}{8}, \quad x_0^2 = x_{c_j}^2 = x_{\dot{c}}^2 = 0, \quad \text{or} \tag{G.46}$$

$$x_{\dot{c}}^2 = -\frac{g_2}{8}, \quad x_0^2 = x_{c_i}^2 = 0. \tag{G.47}$$

Solutions with two non-vanishing variables are:

$$\boxed{\begin{aligned}
&x_0^2 = x_{c_1}^2 = -\frac{g_2}{32}, \quad x_{c_2}^2 = x_{\dot{c}}^2 = 0, \quad \text{or} && \text{(G.48)}\\
&x_0^2 = x_{c_2}^2 = -\frac{g_2}{20}, \quad x_{c_1}^2 = x_{\dot{c}}^2 = 0, \quad \text{or} && \text{(G.49)}\\
&x_0^2 = x_{\dot{c}}^2 = -\frac{g_2}{8}, \quad x_{c_1}^2 = x_{c_2}^2 = 0, \quad \text{or} && \text{(G.50)}\\
&x_{c_1}^2 = x_{c_2}^2 = -\frac{g_2}{12}, \quad x_0^2 = x_{\dot{c}}^2 = 0, \quad \text{or} && \text{(G.51)}\\
&x_{c_1}^2 = x_{\dot{c}}^2 = -\frac{g_2}{8}, \quad x_0^2 = x_{c_2}^2 = 0, \quad \text{or} && \text{(G.52)}\\
&x_{c_2}^2 = -\frac{g_2}{8}, \quad x_{\dot{c}}^2 = -\frac{g_2}{16}, \quad x_0^2 = x_{c_1}^2 = 0. && \text{(G.53)}
\end{aligned}}$$

Solutions with more than two non-vanishing variables are:

$$\boxed{\begin{aligned}
&x_0^2 = -\frac{g_2}{32}, \quad x_{c_1}^2 = -\frac{g_2}{96}, \quad x_{c_2}^2 = -\frac{g_2}{12}, \quad x_{\dot{c}}^2 = 0, \quad \text{or} && \text{(G.54)}\\
&x_0^2 = -\frac{g_2}{32}, \quad x_{c_1}^2 = -\frac{g_2}{32}, \quad x_{c_2}^2 = 0, \quad x_{\dot{c}}^2 = -\frac{g_2}{8}, \quad \text{or} && \text{(G.55)}\\
&x_0^2 = -\frac{g_2}{20}, \quad x_{c_1}^2 = 0, \quad x_{c_2}^2 = -\frac{g_2}{20}, \quad x_{\dot{c}}^2 = -\frac{g_2}{10}, \quad \text{or} && \text{(G.56)}\\
&x_0^2 = 0, \quad x_{c_1}^2 = x_{c_2}^2 = x_{\dot{c}}^2 = -\frac{g_2}{12}, \quad \text{or} && \text{(G.57)}\\
&x_0^2 = -\frac{g_2}{32}, \quad x_{c_1}^2 = -\frac{g_2}{96}, \quad x_{c_2}^2 = -\frac{g_2}{12}, \quad x_{\dot{c}}^2 = -\frac{g_2}{12}. && \text{(G.58)}
\end{aligned}}$$

When $|I_0| = 1$ and $|J_0| = 0$, call c_1 the index in I_0 and c_2 the index in $I - I_0$. There are two possibilities: either $v_{c_2} \propto v_{\dot{c}}$ or not. In the first case (G.45) to (G.49) as well as (G.51) and (G.54) are still solutions, in addition to:

$$\boxed{\begin{aligned}
&x_0^2 = x_{\dot{c}}^2 = -\frac{g_2}{20}, \quad x_{c_1}^2 = x_{c_2}^2 = 0, \quad \text{or} && \text{(G.59)}\\
&x_{c_1}^2 = x_{\dot{c}}^2 = -\frac{g_2}{12}, \quad x_0^2 = x_{c_2}^2 = 0, \quad \text{or} && \text{(G.60)}\\
&x_{c_2}^2 = x_{\dot{c}}^2 = -\frac{g_2}{8}, \quad x_0^2 = x_{c_1}^2 = 0 && \text{(G.61)}
\end{aligned}}$$

and:

$$\boxed{\begin{aligned}
&x_0^2 = -\frac{g_2}{32}, \quad x_{c_1}^2 = -\frac{g_2}{96}, \quad x_{c_2}^2 = -\frac{g_2}{12}, \quad x_{\dot{c}}^2 = 0, \quad \text{or} && \text{(G.62)}\\
&x_0^2 = -\frac{g_2}{32}, \quad x_{c_1}^2 = -\frac{g_2}{96}, \quad x_{c_2}^2 = 0, \quad x_{\dot{c}}^2 = -\frac{g_2}{12}, \quad \text{or} && \text{(G.63)}\\
&x_0^2 = -\frac{g_2}{14}, \quad x_{c_1}^2 = 0, \quad x_{c_2}^2 = -\frac{g_2}{56}, \quad x_{\dot{c}}^2 = -\frac{g_2}{56}, \quad \text{or} && \text{(G.64)}\\
&x_0^2 = 0, \quad x_{c_1}^2 = x_{c_2}^2 = x_{\dot{c}}^2 = -\frac{g_2}{12}, \quad \text{or} && \text{(G.65)}\\
&x_0^2 = -\frac{g_2}{32}, \quad x_{c_1}^2 = -3\frac{g_2}{32}, \quad x_{c_2}^2 = -\frac{g_2}{8}, \quad x_{\dot{c}}^2 = -\frac{g_2}{8}. && \text{(G.66)}
\end{aligned}}$$

If instead $v_{c_2} \perp v_{\dot{c}}$, again (G.45) to (G.49) are solutions, as well as (G.51), (G.59), (G.60), (G.63) and (G.54), in addition to:

$$\boxed{\begin{aligned}
&x_{c_2}^2 = x_{\dot{c}}^2 = -\frac{g_2}{12}, \quad x_0^2 = x_{c_1}^2 = 0, \quad \text{or} && \text{(G.67)}\\
&x_0^2 = -\frac{g_2}{16}, \quad x_{c_1}^2 = 0, \quad x_{c_2}^2 = -\frac{g_2}{48}, \quad x_{\dot{c}}^2 = -\frac{g_2}{48}, \quad \text{or} && \text{(G.68)}\\
&x_0^2 = 0, \quad x_{c_1}^2 = x_{c_2}^2 = x_{\dot{c}}^2 = -\frac{g_2}{16}, \quad \text{or} && \text{(G.69)}\\
&x_0^2 = -\frac{g_2}{32}, \quad x_{c_1}^2 = -3\frac{g_2}{32}, \quad x_{c_2}^2 = -\frac{g_2}{16}, \quad x_{\dot{c}}^2 = -\frac{g_2}{16}. && \text{(G.70)}
\end{aligned}}$$

When $|I_0| = 0$ and $|J_0| = 1$, either the two non-dotted matrices are proportional or orthogonal to each other. In the first case the solutions are:

$$\boxed{\begin{aligned}
&x_0^2 = -\frac{g_2}{8}, \quad \sum_{a\in I} x_a^2 = 0, \quad x_{\dot{c}}^2 = 0, \quad \text{or} && \text{(G.71)}\\
&x_0^2 = 0, \quad \sum_{a\in I} x_a^2 = -\frac{g_2}{8}, \quad x_{\dot{c}}^2 = 0, \quad \text{or} && \text{(G.72)}\\
&x_0^2 = 0, \quad \sum_{a\in I} x_a^2 = 0, \quad x_{\dot{c}}^2 = -\frac{g_2}{8}, \quad \text{or} && \text{(G.73)}\\
&x_0^2 = -\frac{g_2}{20}, \quad \sum_{a\in I} x_a^2 = -\frac{g_2}{20}, \quad x_{\dot{c}}^2 = 0, \quad \text{or} && \text{(G.74)}\\
&x_0^2 = -\frac{g_2}{8}, \quad \sum_{a\in I} x_a^2 = 0, \quad x_{\dot{c}}^2 = -\frac{g_2}{8}, \quad \text{or} && \text{(G.75)}\\
&x_0^2 = 0, \quad \sum_{a\in I} x_a^2 = -\frac{g_2}{12}, \quad x_{\dot{c}}^2 = -\frac{g_2}{12}. && \text{(G.76)}
\end{aligned}}$$

While in the second case one has (G.45), (G.46), (G.47) in addition to:

$$\boxed{\begin{aligned}
&x_0^2 = x_{c_i}^2 = -\frac{g_2}{20}, \quad x_{c_j}^2 = x_{\dot{c}}^2 = 0, \quad \text{or} && \text{(G.77)}\\
&x_0^2 = x_{\dot{c}}^2 = -\frac{g_2}{8}, \quad x_{c_1}^2 = x_{c_2}^2 = 0, \quad \text{or} && \text{(G.78)}\\
&x_{c_1}^2 = x_{c_2}^2 = -\frac{g_2}{12}, \quad x_0^2 = x_{\dot{c}}^2 = 0, \quad \text{or} && \text{(G.79)}\\
&x_{c_i}^2 = x_{\dot{c}}^2 = -\frac{g_2}{12}, \quad x_0^2 = x_{c_j}^2 = 0 && \text{(G.80)}
\end{aligned}}$$

and:

$$\boxed{\begin{aligned}
&x_0^2 = -\frac{g_2}{16}, \quad x_{c_1}^2 = x_{c_2}^2 = -\frac{g_2}{48}, \quad x_{\dot{c}}^2 = 0, \quad \text{or} && \text{(G.81)}\\
&x_0^2 = 0, \quad x_{c_1}^2 = x_{c_2}^2 = x_{\dot{c}}^2 = -\frac{g_2}{16}, \quad \text{or} && \text{(G.82)}\\
&x_0^2 = -\frac{g_2}{56}, \quad x_{c_1}^2 = x_{c_2}^2 = -\frac{g_2}{28}, \quad x_{\dot{c}}^2 = -5\frac{g_2}{56}. && \text{(G.83)}
\end{aligned}}$$

Finally, when $|I_0| = |J_0| = 0$, there are four possible cases. When all non-dotted and dotted matrices are proportional to each other, the solutions are:

$$x_0^2 = -\frac{g_2}{8}, \quad \sum_{a\in I} x_a^2 = 0, \quad x_{\dot{c}}^2 = 0, \quad \text{or} \tag{G.84}$$

$$x_0^2 = 0, \quad \sum_{a\in I} x_a^2 = -\frac{g_2}{8}, \quad x_{\dot{c}}^2 = 0, \quad \text{or} \tag{G.85}$$

$$x_0^2 = 0, \quad \sum_{a\in I} x_a^2 = 0, \quad x_{\dot{c}}^2 = -\frac{g_2}{8}, \quad \text{or} \tag{G.86}$$

$$x_0^2 = -\frac{g_2}{20}, \quad \sum_{a\in I} x_a^2 = -\frac{g_2}{20}, \quad x_{\dot{c}}^2 = 0, \quad \text{or} \tag{G.87}$$

$$x_0^2 = -\frac{g_2}{20}, \quad \sum_{a\in I} x_a^2 = 0, \quad x_{\dot{c}}^2 = -\frac{g_2}{20}, \quad \text{or} \tag{G.88}$$

$$x_0^2 = 0, \quad \sum_{a\in I} x_a^2 = -\frac{g_2}{8}, \quad x_{\dot{c}}^2 = -\frac{g_2}{8}, \quad \text{or} \tag{G.89}$$

$$x_0^2 = -\frac{g_2}{14}, \quad \sum_{a\in I} x_a^2 = -\frac{g_2}{56}, \quad x_{\dot{c}}^2 = -\frac{g_2}{56}. \tag{G.90}$$

When the non-dotted matrices are proportional to each other and orthogonal to the dotted matrix, the solutions are (G.84) to (G.88) and:

$$x_0^2 = 0, \quad \sum_{a\in I} x_a^2 = -\frac{g_2}{12}, \quad x_{\dot{c}}^2 = -\frac{g_2}{12}, \quad \text{or} \tag{G.91}$$

$$x_0^2 = -\frac{g_2}{16}, \quad \sum_{a\in I} x_a^2 = -\frac{g_2}{48}, \quad x_{\dot{c}}^2 = -\frac{g_2}{48}. \tag{G.92}$$

The penultimate case is when the dotted matrix is proportional to one of the non-dotted matrices, call it v_{c_1}, and orthogonal to the second non-dotted matrix, call it v_{c_2}. In this case the solutions are (G.45), (G.46), (G.47) in addition to:

$$x_0^2 = x_{c_i}^2 = -\frac{g_2}{20}, \quad x_{c_j}^2 = x_{\dot{c}}^2 = 0, \quad \text{or} \tag{G.93}$$

$$x_0^2 = x_{\dot{c}}^2 = -\frac{g_2}{20}, \quad x_{c_1}^2 = x_{c_2}^2 = 0, \quad \text{or} \tag{G.94}$$

$$x_{c_1}^2 = x_{c_2}^2 = -\frac{g_2}{12}, \quad x_0^2 = x_{\dot{c}}^2 = 0, \quad \text{or} \tag{G.95}$$

$$x_{c_1}^2 = x_{\dot{c}}^2 = -\frac{g_2}{8}, \quad x_0^2 = x_{c_2}^2 = 0, \quad \text{or} \tag{G.96}$$

$$x_{c_2}^2 = x_{\dot{c}}^2 = -\frac{g_2}{12}, \quad x_0^2 = x_{c_1}^2 = 0 \tag{G.97}$$

and:

$$x_0^2 = -\frac{g_2}{16}, \quad x_{c_1}^2 = x_{c_2}^2 = -\frac{g_2}{48}, \quad x_{\dot{c}}^2 = 0, \quad \text{or} \tag{G.98}$$

$$x_0^2 = -\frac{g_2}{14}, \quad x_{c_1}^2 = -\frac{g_2}{56}, \quad x_{c_2}^2 = 0, \quad x_{\dot{c}}^2 = -\frac{g_2}{56}, \quad \text{or} \tag{G.99}$$

$$x_0^2 = -\frac{g_2}{16}, \quad x_{c_1}^2 = 0, \quad x_{c_2}^2 = -\frac{g_2}{48}, \quad x_{\dot{c}}^2 = -\frac{g_2}{48}. \tag{G.100}$$

The very last case in when all matrices are orthogonal to each other, with solutions as in (G.29) to (G.34) upon relabeling the matrices.